Biosynthesis and characterization of Selenium and Tellurium nanoparticles by marine bacteria

Thesis submitted to Goa University for the
Award of the
Degree of

DOCTOR OF PHILOSOPHY

In

MICROBIOLOGY

By

Ms. Diviya Chandrakant Vaigankar

Department of Microbiology
Goa University
Taleigao- Goa

May, 2020

Biosynthesis and characterization of Selenium and Tellurium nanoparticles by marine bacteria

Thesis submitted to Goa University

For the Award of the Degree of

DOCTOR OF PHILOSOPHY

In

MICROBIOLOGY

By

Ms. Diviya Chandrakant Vaigankar

Under the guidance of

Prof. Santosh Kumar Dubey
(Research Guide)
Department of Microbiology,
Goa University, Goa, India

Prof. Sandeep Garg
(Co-Guide)
Department of Microbiology,
Goa University, Goa, India

2020

GOA UNIVERSITY

Goa- 403206, India

Department of Microbiology

Certificate

This is to certify that ***Miss Diviya Chandrakant Vaigankar*** *has worked on the thesis entitled* ***"Biosynthesis and Characterization of Selenium and tellurium nanoparticles by marine bacteria"****. This thesis, being submitted to the Goa University, Goa India, for the award of the degree of Doctor of philosophy in Microbiology is an original record of research work carried out by the candidate herself and has not been submitted for the award of any other degree or diploma of this or any other University in India or abroad.*

Prof. Santosh Kumar Dubey
Research Guide

Prof. Sandeep Garg
Co-Guide

STATEMENT

*As required under the Goa University Ordnance OA-19.8 (viii), I hereby state that the present thesis entitled "**Biosynthesis and characterization of Selenium and Tellurium nanoparticles by marine bacteria**" is my original contribution, and the same has not been previously submitted for the award of degree/diploma to any institute or University.*

To the best of my knowledge, the existing study is the first comprehensive work of its kind from this area. The literature related to the problem investigated has been cited. Due acknowledgement has been made wherever facilities and suggestions have been availed of.

Diviya Vaigankar

Department of Microbiology,

Goa University

2020

Acknowledgement

Every successful journey is always accomplished owing to the collective efforts and I am overwhelmed to receive it from number of people. I take this opportunity to sincerely thank each and every one who directly or indirectly landed helping hands in various disciplines in completing this thesis. First and foremost, my gratitude towards my guide and supervisor **Prof. Santosh Kumar Dubey** for your immense guidance during my Ph.D. work. You were instrumental in inculcating confidence and the thrust required to be an independent researcher. Your confidence in me and impetus has really helped to overcome all my shortcoming and to be what I am today. Thank you, sir, for all your efforts to bring the best in me. I am highly grateful and obliged for all the support I always acquired from you. Secondly, I would like to thank my Co-guide **Prof. Sandeep Garg** for his constant support and guidance and also for all the other academic assistance I received. I am thankful to you sir form bottom of my heart without your support it wouldn't have been a smooth ride.

I would like to thank **Prof. Varun Sahani, Vice Chancellor** Goa University, Prof. P.K. Sharma, Dean of Life Sciences and Environment and Prof. Sandeep Garg, Head of the Department of Microbiology for the infrastructures and funding provided during my research tenure. I highly acknowledge University Grants Commission New Delhi, for my research Grants. I also thank my V.C.'s nominee Prof. S.K. Shyama, Prof. Sanjeev Ghadi and Dr. Judith Gonsalves for their genuine critics and support which helped during my Ph.D. work to improve and come up with good research outcomes. I also thank HODs of Biotechnology, Chemistry and Zoology, Goa University for permitting me to use the laboratory facilities as and when required.

My big thank to all the faculty members of the Department of Microbiology Prof. Irene Furtado, Prof. Sarita Nazareth, Dr. Lakshangy, Dr. Milind, Dr. Priya, Dr. Trelita, Dr. Bhakti, Dr. Gauri, Dr. Meghnath, Dr.

Sanika, Dr. Shyamalina, Dr. Varadha, Dr. Trupti, Dr. Delicia, Ms. Snigdha and Dr. Pooja. I would like to specially mention and thank **Dr. Milind Mohan Naik, Dr. Shyamalina Haldar** and **Dr. Priya D'costa** for their all-time support and guidance throughout my research work. I also thank **Dr. Neha Prabhu** and **Dr. Bhakti Salgaonkar** for their support during my work.

It is always said that a better work environment generates the best work output. I was blessed and fortunate to have lively and efficient friends as my colleague. My heart is drenched with immense gratitude while I mention **Ms. Sajiya Mujawar** and **Mr. Sanket Gaonkar** for all their help and support which I received. I couldn't imagine this journey without you two for being there constantly with me during all ups and downs. I thank you people for all your professional and personal advices and motivations. I would highly acknowledge my colleagues and friends **Alisha, Sulochana, Ashwini, Aarti, Dviti, Komal, Aabha, Dr. Jaya, Dr. Neha, Dr. Kashif, Dr. Praveen, Dr. A. D'Costa, Kiran, Dr. Jyothi, Dr. Chandan, Rahul, Aniket, Joleen** and **Minisha** for their assistance and support.

I am grateful to Mr. Areef sardar and Mr. Girish Prabhu from National Institute of Oceanography, Goa for energy dispersive X-ray spectroscopic facility and XRD analysis respectively. I thank Mr. Rahul Kerkar from Department of Chemistry, Goa University for FTIR analysis. I also acknowledge Dr. Ashwani Kumar and Dr. Ajeet Mohanty from National Institute of Malaria Research, field unit Campal Goa for guidance and support in carrying out mosquito larvicidal activity and Director, IIT Mumbai, AIIMS New Delhi for TEM analysis. I thank Mr. M. G. Lanjewar from the University Science Instrumentation Centre, Goa University for scanning electron microscopy.

My sincere gratitude to Non-teaching staff: **Mrs. Saraswati, Ms. Deepashri, Mrs. Afra, Mr. Buddhaji, Mr. Dominic, Mr. Narayana, Mr. Tanu, Mr. Rajesh, Mr. Gajanan, Mr. Bhushan, Mrs. Prathana, Ms. Vandana** and **Mrs. Yojana.**

To the people whom 'Thank you' is not absolutely justified, I take this opportunity to express my deepest gratitude to my family my father **Mr.**

Chandrakant Vaigankar my loving mother late **Mrs. Amla Vaigankar**, my brother **Mr. Shounak Vaigankar** and my extended family member **Mr. Sunil H. Naik** for all their blessings, support in all fronts. I could complete this extensive journey certainly due to their constant blessings and love. I also thank my rest beloved family members **Mr. Kumar, Mrs. Krupa, Rohit, Sanak, Siya** and **Varad** for their support. I would also thank my best friends **Tanvi** and **Prajakta** for their backing.

Lastly to my lifeline 'God all mighty' for continuously bestowing all the blessing to me, thank you for getting this work done I dedicate this thesis at your lotus feet.

Diviya Vaigankar

Abbreviations

%	**- Percentage**
°C	**- Degree centigrade**
µg	**- Microgram**
µl	**- Microlitre**
2, 3-DAN	**- 2, 3-diaminonaphthalene**
AgNPs	**- Silver nanoparticles**
ANOVA	**- Analysis of variance**
As	**- Arsenic**
ATCC	**- American type culture collection**
BLAST	**- Basic local alignment search tool**
BSA	**- Bovine serum albumin**
CaPNPs	**- Calcium phosphate nanoparticles**
Cd	**- Cadmium**
CFE	**- Cell free extract**
CMV	**- Cowpea mosaic virus**
Co	**- Cobalt**
Cr	**- Cromium**
Cu	**- Copper**
DDTC	**- Diethyldithiocarbamate**
DMEM	**- Dulbecco's modified eagle medium**
DMSO	**- Dimethyl sulphoxide**

DPPH	**- 1, 1-diphenyl-2-picryllhydrazly**
DW	**- Distilled water**
E	**- Energy band gap**
EDS	**- Energy dispersive spectroscopy**
EDTA	**- Ethylenediaminetetraacetic acid**
EPS	**- Exopolysaccharides**
FBS	**- Fetal bovine serum**
FeONPs	**- Ferrous oxide nanoparticles**
FTIR	**- Fourier Transformed Infrared Spectroscopy**
FWHM	**- Full width half maximum**
gm	**- Gram**
GO	**- Gene ontology**
GSH	**- Glutathione**
h	**- Hour**
H_2O_2	**- Hydrogen peroxide**
H_2S	**- Hydrogen peroxide**
Hg	**- Mercury**
ICAR	**- Indian centre for agricultural research**
ICDD	**- International centre for diffraction data**
K_2TeO_3	**-Potassium tellurite**
KNO_3	**- Potassium nitrite**

KOH	**- Potassium hydroxide**
L	**- Litter**
MHA	**-Muller Hinton agar**
MIC	**- Minimum inhibitory concentration**
min	**- Minutes**
mL	**- Millilitre**
mM	**- Milli molar**
mm	**- Millimeter**
Mn	**-Manganese**
MT	**- Metallothionein**
MTT	**- 3-(4, 5-dimethylthiazol-2-yl)-2, 5 diphenyltetrazolium**
Na_2SeO_3	**- Sodium selenite**
NaCl	**- Sodium chloride**
NADH	**- Nicotinamide adenine dinucleotide**
NB	**- Nitrate broth**
NED	**- N-(1-naphthyl) ethylene diamine hydrochloride**
ng	**- Nanogram**
NH_4Cl	**- Ammonium chloride**
Ni	**- Nickel**
nm	**- Nanometer**
NP	**-SH- Non-protein thiols**
NPK	**- Nitrogen-Phosphorus-Potassium**

NPs	**- Nanoparticles**
NR	**- Nitrate reductase**
OH	**- Hydroxyl**
Pb	**- Lead**
PB	**-SH- Protein bound thiol**
PBS	**- Phosphate buffered saline**
PC	**- Phytochelatin**
PCR	**- Polymerase chain reaction**
PMSF	**- Phenyl methane sulphonyl fluoride**
QC	**- Quality check**
QDs	**- Quantum dots**
ROS	**- Reactive oxygen species**
Rpm	**- Revolution per minute**
RT	**- Room temperature**
SAED	**- Selected area electron diffraction**
SDS	**- Sodium dodecyl sulphate**
Se	**- Selenium**
SeNPs	**- Selenium nanoparticles**
Sp.	**- Specie**
Spp.	**- Species**
SPR	**- Surface plasmon resonance**
SR	**- Selenite reductase**
TEM	**- Transmission electron microscopy**
TeNPs	**- Tellurium nanoparticles**

TMV	**- Tobacco mosaic virus**
TR	**- Tellurite reductase**
UV	**- Ultraviolet**
Vis	**- Visible**
WHO	**- World health organization**
XRD	**- X-ray diffraction**
ZMA	**- Zobell marine agar**
ZMB	**- Zobell marine broth**
Zn	**- Zinc**
ZnCuFe-oxideNPs	**- Zinc, copper ferrous oxide nanoparticles**
ZnONPs	**- Znic oxide nanoparticles**
Λ	**- Wavelength**

List of tables

List of figures

Contents

Chapter I

Microbes as 'nano-factories' for synthesis of nanomaterials- recent trends and innovations

"What I want to talk about is the problem of manipulating and controlling things on a small scale''

-Richard P. Feynman

The ever-increasing interest of nanomaterial in markets worldwide has boosted the research in nanotechnology. Devising experimental methods for synthesis of composite size, shape and monodispersed nanomaterial with other appropriate desired characteristics still remains the challenging task. Green chemistry in nanoparticle synthesis is a relatively new emerging trend as far as sustainability is a concern. This chapter briefly elucidates the current worldwide research on biosynthesis, mechanisms and applications of nanoparticles using microorganisms.

1.1 Background

Nanotechnology is an interdisciplinary field awaiting to delve into the countless unique advantages of engineering the structure of materials at a scale as low as an atom, molecules or their aggregates. Nanotechnology deals with the formulation and exploitation of materials which has wide applications. The prefix ‘nano’ transcribes to a Greek word dwarf which is a billionth of a meter. Nanotechnology encompasses the synthesis and application of materials with at least one attribute in 1-100 nm dimension. Fig. 1.1 represents the relative size comparisons of different objects found in living world. The key thought of nanotechnology was addressed by Richard Feynman at American institute and technology in 1959 through his lecture “There's plenty of room at the bottom”. This concept was later propagated in well-known paper ‘Molecular engineering: An approach to the development of general capabilities for molecular manipulation’ by K. Eric Drexler in 1081(Drexler, 1981). Although Eric Drexler was known to pioneer this field, it was Professor Norio Taniguchi from Tokyo University who coined the term ‘nanotechnology’ in 1974 through his work on ultra-precise machining.

Later in 1986, the publication titled ‘Engines of Creation’ (Drexler, 1986) provided a breakthrough for molecular nanotechnology

and thus, began the field of nanotechnology. The term nanotechnology **2** | Page has ascended in the late 80's however, it has been actually produced and used by human's way back in the fourth century A.D. The dichroic Lycurgus cup used by Romans which is yellowish green in direct light and turns to translucent ruby colour when light falls upon the glass can be the classic example. This exclusive phenomenon of dichromatism is due to the presence of Silver and Gold nanoparticles in the glass structure.

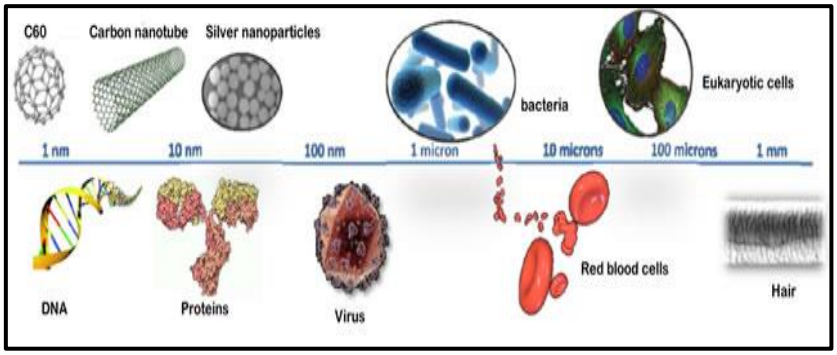

Fig. 1.1 Comparative size representation of various natural and man-made things (https://www.azonano.com/article.aspx?ArticleID=3012).

NPs are generally classified into inorganic and organic nanoparticles (Fig. 1.2). Organic types include carbon nanoparticles (fullerenes), polymeric nanoparticles and solid lipid nanoparticles (Liposomes). Inorganic NPs are magnetic nanoparticles (magnetite and greigite), metallic/ metalloid nanoparticles (copper, gold, silver, platinum, selenium and tellurium) and semiconductor nanoparticles (cadmium sulfide, zinc sulfide, titanium dioxide and zinc oxide).

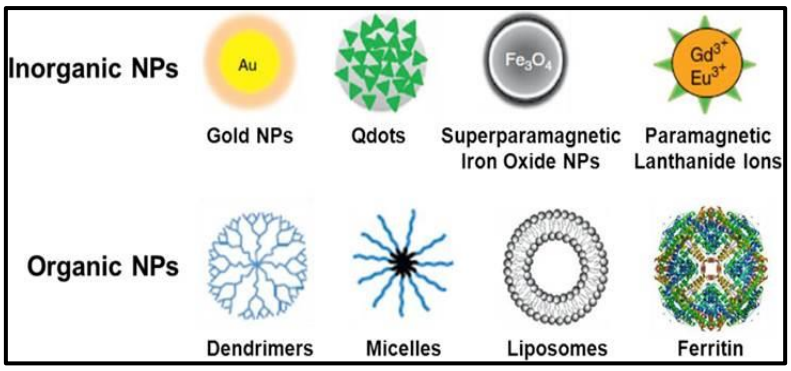

Fig. 1.2 General classification of nanoparticles (https://www.nanoshel.com/organic-and-inorganic-nanoparticles).

1.2 Characteristics of nanoparticles

Over the past several years, vigorous multidisciplinary and combined efforts involving various investigators have resulted in demonstration of nanoparticles with numerous applications in diverse areas. Unlike bulk materials, nanoparticles have unique physical, chemical, electronic, electrical, mechanical, magnetic, thermal, dielectric, optical and biological properties (Daniel et al., 2004). These properties of nanoparticles are mainly due to the larger area to volume ratio, reduced imperfections, comparatively larger surface energy and quantum confinement of electrons. The properties of nanoparticles enhance with decrease in size due to the shift in electronic structure from continuous bands to discrete electronic levels.

One of the unique properties of metal nanoparticles which is mainly attributed due to size reduction is Surface Plasmon Resonance (SPR). This optical effect in nano-dimension mainly arise due to the combined oscillations of electrons in the conduction band on excitation and thus giving rise to sharp peaks in its spectral extinction (Burda et al., 2005). Quantum confinement effect of nanoparticles is one of the widely known phenomena. Unlike bulk materials where the properties are solely dependent on the chemical composition of the particles, the nanoparticles possess mainly size and shape-dependent properties. In semiconductor materials, decrease in particle size below the Bhor

radius gives rise to electron confinement effect, thus broadening the band gap which gives rise to various fluorescent colours (Neikov et al., 2019). The semiconductor nanoparticles (NPs) particularly quantum dots (QDs) exhibits this 3-D quantum confinement properties which are size-dependent (Fig. 1.3).

Thus, these novel properties further broaden the spectrum of applications for these nanomaterials in detectors, sensors, bio imaging, drug delivery, LCD display screens, photo-catalysis, solar cells, photovoltaic cells and phosphors. Recent technological advances suggest that the surface properties of these nanomaterials can be manipulated to create multi-functional nanoparticles. It is interesting to note that these nanomaterials can be modified to obtain desired particles by merely changing its physical and chemical properties (Daniel et al., 2004).

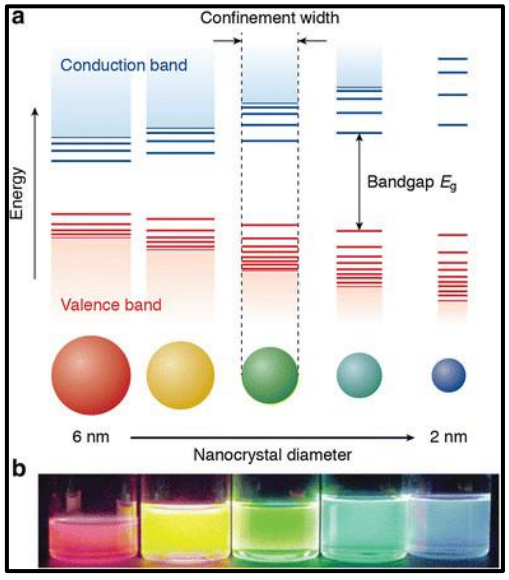

Fig. 1.3 Schematic representation of the quantum confinement effects (Rabouw de Mello Donega, 2017).

The process of synthesis is a deciding phase where the properties (shape and size) of the particles can be altered as required. Thus, the surface of the nanoparticle is prerequisite in designing

materials of desired properties where, NPs can be efficiently assembled by altering their surface chemistry or also by attaching specifically targeted materials (Fig. 1.4). In recent times, NPs are fabricated based on the applications by tailoring the different compositions. For example, NPs can be functionalized with antibodies, nucleic acids, protein/peptides and polymers thus, enabling its application in targeted drug delivery.

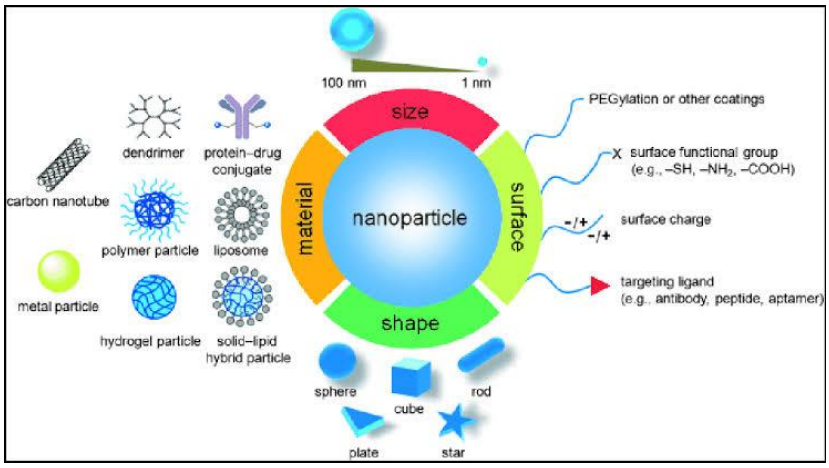

Fig. 1.4 Functional nanoparticles with its applications in the fields of biomedical research (Pardhiya and Paulraj 2014).

1.3 Synthesis of nanoparticles

Nanoparticles are broadly synthesized using two approaches viz. bottom-up and top-down (Figs. 1.5 & 1.6). In bottom-up approach, the atoms or molecules are assembled to get nano-dimensions which includes various chemical and biogenic methods. Whereas, in the top-down approach the bulk material is broken down externally using microscopic devices to get the desired shape and size.

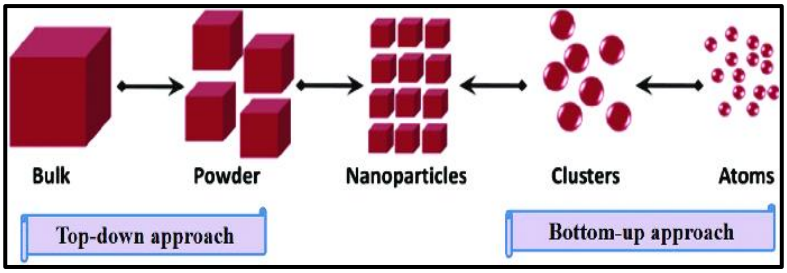

Fig. 1.5 Bottom-up and top-down approaches of nanoparticle synthesis (Pareek et al., 2017).

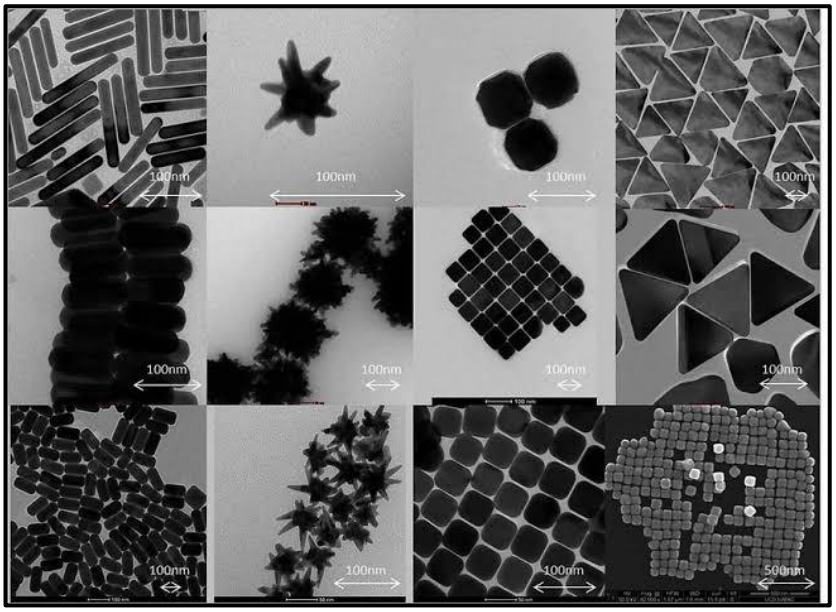

Fig. 1.6 Transmission electron microscopic images of various gold nanoparticles synthesized by bottom-up and top-down approaches (Bouloudenine and Bououdina, 2016).

1.3.1 Physical and chemical processes to synthesize NPs

Physical methods mainly encompass laser ablation, inert gas condensation, spray pyrolysis, electrospray, electron beam nanolithography and combustion flames (Kammler et al., 2001; Lamas et al., 2003; Amendola and Meneghetti, 2009; Adhikari et al., 2010; Kang et al., 2011; Pimpin and Srituravanich, 2012). Inert gas condesnation is the oldest and most coomonly used methods where, the

metals (gold/palladium) are evaporated in high vaccume chamers which are usually filled with inert gas. Subsequently the NPs are formed when the evaporated metals are condensed into small nanocrytals by colesence and Brownian motion.

Laser ablation (top-down approach) produces nanoparticles by dipping the bluk materials in a liquid solution upon which laser is focused. Thus, giving rise to plasma plumes due to ablation which condenses to yield nanoparticles. In the physical process, good size distribution of nanoparticles is achieved. However, some of these processes may require harmful precursors and the reactions are mostly multistep which may lead to the generation of particles with unfavourable surface chemistry. It also requires the use of high temperature and pressure devices and involves the generation of toxic by-products, thereby restricting its use.

The chemical methods mainly involve reduction, sol-gel, solvothermal, hydrothermal, reverse-micelles and co-precipitation (Adschiri et al., 2001; Nahar and Arachchige, 2013). Chemical reduction method mainly consists of a reducing agent (Sodium borohydride, sodium citrate, hydrazine, Polyethylene glycol and formaldehyde), metal/metalloid salt precursor and surfactant or stabilizers (SDS, PVP) to prevent its aggregation. Additionally, in order to speed up the reaction and synthesis process heat or catalyst can also be introduced and solvents are used for stabilizing the metal salts. Reduction ensure generation of large quantities of nanoparticles with control over size and shape. However, the process is associated with high cost, use of toxic precursors, reducing agents and capping agents. It also requires the use of high temperature equipment and also involve the generation of toxic by-products, thereby restricting its use. The use of toxic stabilizing agents reduces its potential to be used in the biomedical field due to reduced biocompatibility and high toxicity.

The second most widely used procedure for nanoparticle synthesis is sol-gel. Firstly, the monomers (sol) are synthesised from

the starting materials (colloidal material) this is followed by gel formation. The commonly used precursors are metal alkoxides and chlorides which are hydrolysed and polycondensed for colloids formation. Usually it involves the use of dopants in the sol like rare earth elements or organic dyes these mainly homogeneously distributes the nanoparticles formed. Since it's the gel state the materials can be moulded into complex metiers. High purity of products is obtained since the precursors used are dissolved in solvents for sol gel formation additionally, it promises good stability and size control. However, it has certain disadvantages viz. the temperature applied in the process usually ranges from 200- 600 °C, High permeability, weak bonding, hard porosity and low wear resistance restricts them to achieve its full industrial potential. Thermal mismatch, its surface- dependency and expensive raw materials are also the major drawbacks additionally, the process is usually time consuming since it involves multiple steps.

1.3.2. Biological processes to synthesize NPs

Even though the chemical and physical methods are widely preferred, the disadvantages associated with them restrict their usage consequently, raising the concern to develop desired approaches which are environment-friendly and safe.

The biological entity comprising of the structural components are in nano-dimensions. Entire biological system or its components may be used for biosynthesis of nanoparticles. Additionally, biological macromolecules viz. DNA, protein (ferritin, serrapeptase, phytochelatins and glutathiones), and viral particles (Tobacco mosaic virus) have also been studied for generation of nanoparticles (Douglas et al. 1995, Brelle et al. 1999, Shenton et al., 1999, Ravindra 2009, Anil Kumar et al. 2007).

Microbes possesses the inherent potential to synthesize several nanomaterials including nanoparticles. The microbial process involves the use of inorganic materials and its conversion into complex or

simpler forms either intracellularly (Baesman et al., 2007, Muthukannan and Karuppiah, 2011) or extracellularly (Oremland et al., 2004, Kathiresan et al., 2010). The cells are usually grown in the medium supplemented with metal/metalloid salts in order to achieve intracellular nanoparticle synthesis. Intracellular process involve the synthesis of NPs inside the cells hence these nanoparticles are usually isolated using either physical or chemical methods by cell wall disruption using Triton X-100, SDS or lysozymes and This is followed by centrifugation to remove the cell debris and subsequent purification of nanoparticles sonication (Kalimuthu et al., 2008, Nangia et al., 2009).

The rate in case of intracellular NPs formation can be easily manipulated. In Extracellular biosynthesis of NPs the factors involved for NPs generation are usually present outside the cells hence it doesn't involve the extraction procedures. Commonly, the supernatant of previously grown culture broth is centrifuged and thereafter the metal/ metalloid salts are added (Shahverdi et al., 2007) additionally, cell free extracts obtained after sonication of cells are also used for NPs synthesis (Singh et al. 2014).

The microbial synthesis of nanoparticles is advantageous since it's the integral metabolic process occurring at cellular levels at ambient conditions. Microbes are also important in the biogeochemical cycling of metals, metalloids and minerals. They are known to alleviate these metals and metalloids through various mechanisms including bioaccumulation, bioreduction, biosorption, efflux, precipitation and sequestration (Lovley, 1993; Nies, 1999; Rossbach et al., 2000). Additionally, microbial biosynthesis can be very flexible, highly organized, ordered and effective since it occurs under controlled conditions and size control can be easily achieved as the process usually takes place in special compartments i.e. in periplasmic space and vesicles. It doesn't require use of external toxic reducing, stabilizing/ capping or surfactants unlike in other physical or chemical processes. It's worth mentioning that most of the intended applications in the field

of biology or medicine are feasible only through specific biological synthesis.

Among various environments, the marine environment is a unique habitat which is characterized by extreme conditions and retains rich microbial diversity. These microbes are reported to have specific mechanisms to tolerate high salt concentrations, extreme pH, pressure and high levels of different toxic metals and metalloids. However, these marine microbes have not been studied extensively for nanoparticle biosynthesis.

1.3.3 Biosynthesis of nanoparticles mediated by marine microbes

Marine microorganism's viz. bacteria, actinobacteria, cyanobacteria, yeast and fungi are known to synthesize gold, silver, calcium, iron, gypsum, lead, cadmium, tellurium and selenium NPs (Table 1.1). These microbes are also reported to produce mineral crystals and metallic/ metalloid materials in nano-dimensions either intracellularly or extracellularly with the properties similar to chemically or physically synthesised nanomaterials (Asmathunisha et al., 2013).

Biosynthesis of silver NPs using *Pseudomonas stutzeri* AG259 isolated from silver mine has been reported for the first time by Klaus and co-workers (1999). Intracellular synthesis of gold NPs with size ranging from 20-100 nm was obtained when cells of *Pseudomonas* sp. ram bt-1 were incubated with silver nitrate solution (Ahmad et al., 2003). Similarly, in another study by Muthukannan and Karuppiah, (2011) intracellular polydispersed silver NPs with size (20-100 nm) was obtained using a novel strain of *Pseudomonas* sp. 591786. *Sulfurospirillum barnesii* has been reported to synthesize tellurium NPs intracellularly with size < 50 nm (Baesman et al., 2007). However, two strains of *Bacillus megaterium* (BSB6 and BSB12) were reported to synthesize selenium NPs both extracellularly as well as intracellularly with an average size of 200 nm (Mishra et al., 2011a). Extracellular pH-

dependent gold nanoparticle synthesis was achieved using *Halomomas salina* (Shah et al., 2012). A recent study reported *Citrobacter fruendii* strain KP6 isolated from Mandovi estuary of Goa, India to biosynthesize selenium NPs extracellularly (Samant et al., 2018).

Several multicellular and unicellular fungi have also been reported to resist and biosynthesize metallic nanoparticles (Table 1.1). *Pseudomonas fellutanum* isolated from coastal mangroves when challenged with silver nitrate were observed for the production of extracellular silver NPs with an average size of 2-5 nm (Kowshik et al., 2003) The cytosolic extracts of *C. albicans* was used to study the extracellular gold NP synthesis (Chauhan et al., 2011). Active biomass of *Pseudomonas chrysogenum* incubated with $HAuCl_4$ solution showed the intracellular synthesis of gold NPs after 72 h of incubation (Sheikhloo et al., 2011).

It has been reported that shape and size of nanoparticles can be manipulated by controlling various parameters viz. pH and temperature of the growth medium along with the concentration of metal/metalloid substrates (Gericke and Pinches, 2006). Additionally, to obtain homogenous sized and shaped NPs, it is mandatory to carefully control and monitor the above condition. Apart from cell-free supernatant and whole-cell biomass bacterial metabolites have also been used as reducing agents for biosynthesis which mainly includes polysaccharides, proteins, enzymes and pigments. For instance, *Bacillus subtilis* MSBN17 was reported to produce polysaccharide bio-flocculant which was responsible for the production of silver NPs in reverse micelles (Sathiyanarayanan et al., 2013).

Metal microbial interactions in some cases result in NPs synthesis which is governed by various factors viz. nature and solubility of metal/ metalloid ions and type of interactions involved (Haferburg and Kothe, 2007). The interactions of metal/metalloid are initiated by adsorption which is the attachment of these metals/metalloids on the bacterial surfaces. After adsorption, these metals/ metalloids are either

transported into the cells with the help of various transporters or are reduced/oxidised by various microbial components mainly enzymes, proteins or thiols and other microbial components. Thus, it is interesting and mandatory to study such interactions in order to delineate the process of microbial NPs synthesis.

Table 1.1: Marine microbes reported in the synthesis of various nanoparticles

Marine microbes	Strains	NPs	Size (nm)	Intra/ extracellular	References
Bacteria					
	Rhodococcus sp.	Au	5-7	I	Ahmad et al., 2003
	Bacillus selenitireducens	Se	300	E	Oremland et al., 2004
	Selenihalanaerobacter shriftii	Se	300	E	Oremland et al., 2004
	Bacillus selenitireducens	Te	10 x 200	I & E	Baesman et al., 2007
	Sulfurospirillum barnesii	Te	< 50	I	Baesman et al., 2007
	Sulfospirillum barnesii	Se	300	E	Oremland et al., 2004
	Escherichia coli	Ag	5-20	E	Kathiresan et al., 2010

	Pseudomonas sp.	Ag	10-100	I	Muthukannan and Karuppiah, 2011
	Bacillus megaterium BSB6 and BSB12	Se	200	I & E	Mishra et al., 2011a
	Marinobacter pelagius	Ag	2-6	E	Sharma et al., 2012
	Idiomarina sp. PR58-8	Ag	26	I	Seshadri et al., 2012
	Shewanella oneidensis	Te	100-200	I	Kim et al., 2012
	Halomomas salina	Au	-	E	Shah et al., 2012
	Bacillus sp.	Te	20 x 180	I	Zare et al., 2012
	Desulforibrio caledoiensis	ZnS	~ 30	E	Qi et al., 2013
	Vibrio alginolyticus	Ag	50-100	I & E	Rajeshkumar et al., 2014
	Rhodobacter capsulatus	Te	100	E	Borghese et al., 2010

	Enterococcus sp.	CdS	50-180	E	Rajeshkumar et al., 2014
	Ochrobactrum anhtropi	Ag	38-85	I	Thomas et al., 2014
	Saccharophagus degradans ATCC 43961 (Sde 2-40)	MnO_2	34	E	Salunke et al., 2015
	Rhodococcus aetherivorans	Te	148 ± 104	I	Presentato et al., 2016
	Idiomarina sp. PR58-8	Se	50-350	I	Srivastava and Kowshik, 2016
	Escherichia coli VM1	Ag	10-15	E	Maharani et al., 2016
	Citrobacter fruendii strain KP6	Se	45 -70	E	Samant et al., 2018
Actinobacteria					
	Streptomyces sp. Al-Dhabi-87	Ag	10-17	E	Al-Dhabi et al., 2018
Cyanobacteria					

	Plectonema boryanum UTEX 485	Ag	< 10	E	Lengke et al., 2007
	Spirulina platensis	Ag, Au & bime tallic	6-10, 7-16 & 17-25	E	Govindaraju et al., 2008
	Oscillatoria willei	Ag	100-200	E	Ali et al., 2011
	Phormidium tenue	CdS	5	E	MubarakAli et al., 2012
Fungi					
	Verticillium (AAT-TS-4)	Ag	12-25	I	Mukherjee et al., 2001
	Penicillium fellutanum	Ag	5-20	E	Kathiresan et al., 2009
	Aspergillus niger	Ag	5-35	E	Kathiresan et al., 2010
	Penicillium brevicompactum KCCM 60390	Au	25-60/ 20-50	I & E	Mishra et al, 2011b
	Aspergillus terreus	Ag	1-20	E	Li et al., 2012

	Pergillus sydowii	Au	8.7-15.6	E	Vala, 2015
Yeast					
	Yarrowia lipolytica NCIM3589	Au	-	I	Pimprikar et al., 2009
	Candida sp. VITDKGB	Ag	87	E	Kumar et al., 2011
	Magnusiomyces ingens LHF1	Au	10-80	E	Zhang et al., 2016
	Rhodosporidium diobovatum	Pb	2-5		Seshadri et al., 2011

Key: I: intracellular, E: extracellular

1.3.4 Mechanisms involved in the biosynthesis of nanoparticles

Mechanisms governing metal/metalloid nanoparticle synthesis by microorganisms is often regarded to be similar to that of metal resistance which includes biosorption, oxido-reduction, bioaccumulation, efflux and extracellular complexation or precipitation (Nies, 1999; Roane, 1999; Rossbach et al., 2000; Naik and Dubey, 2011). They also carry out various chemical reactions for their growth and survival commonly termed as bio-mineralization which is responsible for the production of nanoparticles. In chemolithotrophic organisms which mainly use inorganic substrates to obtain energy produces, various by-products which interact with metals to form NPs. The classic example is in sulphate-reducing bacteria where sulphate is

reduced to sulphide which in turns binds with metal ions ultimately precipitating metal sulphide. In contrast, some bacteria utilise inorganic materials in nano-range and make them the integral component to establish cell functions. For instance, magnetotactic bacteria use inorganic chains of magnetic crystals Fe_3O_4 or Fe_3S_4 which enables them to orient themselves in accordance with earth's geomagnetic field (Krumov et al., 2009). Although there exist numerous reports on the biosynthesis of nanoparticles, the exact mechanisms of synthesis are not well understood. Broadly, the mechanisms can be categorised as enzymatic and non- enzymatic for the biosynthesis of nanoparticles as described below.

1.3.4.1 Enzymatic nanoparticle biosynthesis

1.3.4.1.1 Bioreduction using oxidoreductase enzymes:

a) NADH-dependent reductases

In one of the studies by Mukherjee et al. (2001) it was hypothesized that the cell wall and cell membrane-bound enzymes are responsible for the synthesis of silver NPs. Later, the reduction of silver ions to silver hydrosols by NADH-dependent reductases was reported in *Fusarium oxysporum* by Ahmed et al. (2003). In *Rhodopseudomonas capsulata* the formation of gold nanoparticles via the transfer of electrons from NADH by NADH dependent reductase to gold ions which in turn gets reduced to gold NPs was studied (He et al., 2007) [Fig. 1.7]. *Thermus thermophilus* HB8 was reported to exhibit NADH dependent tellurite reductases activity and tellurite resistance (Chiong et al., 1988a). In another study carried out by Nangia et al. (2009) the possible mechanism of NADH-dependent enzymes in silver reduction using *Stenotrophomonas maltophilia* was demonstrated clearly.

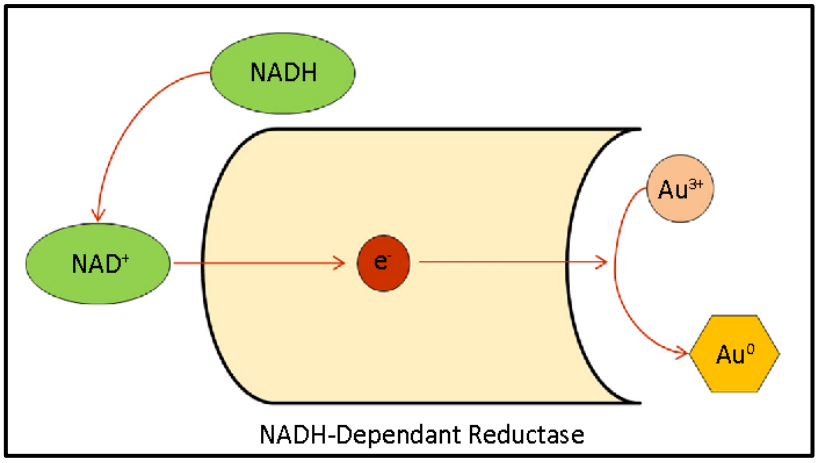

Fig. 1.7 NADH dependent biosynthesis of nanoparticle.

b) Nitrate reductase (NR)

There are various reports on the involvement of nitrate reductase in metal nanoparticle biosynthesis which includes, *Bacillus licheniformis*, *E. coli and H. salina* (Narayanan and Sakthivel, 2010; Vaidyanathan et al., 2010; Shah et al., 2012). Fig. 1.8 depicts the role of NR in silver NPs biosynthesis using *Streptomyces* sp. (Golinska et al. 2014). In *Fusarium oxysporum* NR is conjugated with a quinine (an electron donor), reducing the metal ion to elemental form (Moghaddam, 2010). In a study by Anil Kumar and co-workers (2007), reported synthesis of silver nanoparticles from purified NR from the culture *supernatant of F. oxysporum.*

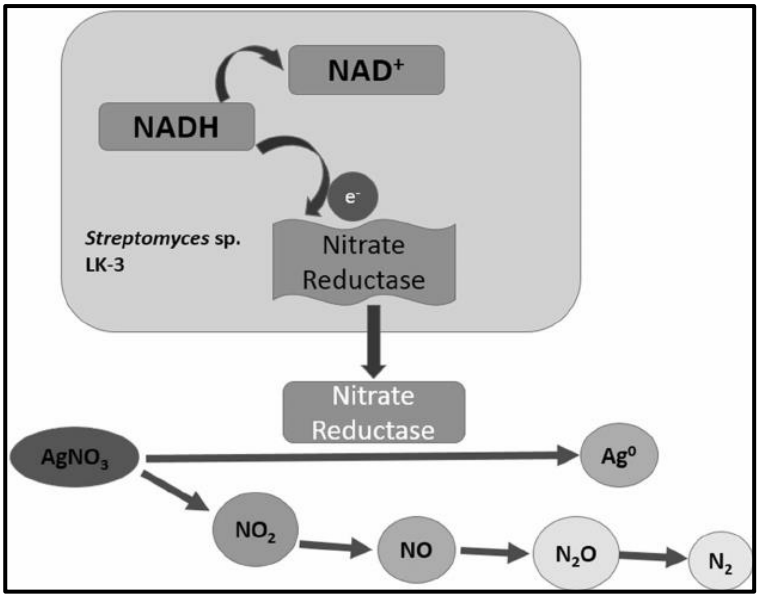

Fig. 1.8 The role of nitrate reductase in silver nanoparticle synthesis Golinska et al. (2014).

c) Sulphate and sulphite reductase

Formation of ZnS nanoparticles has been described in detail in *Rhodobacter sphaeroides* which involves a series of reductases starting from sulphate permease which facilitates the entry of soluble sulphate into the inner bacterial membrane. ATP sulfurylase and phosphoadenosine phosphosulfate reductase then reduce sulphate to sulphite which consequently is reduced to sulphide by sulphite reductase. This is followed by the formation of cysteine via O-acetylserine thiolyase (Holmes et al., 1997), later S^{2-} is formed using cysteine desulfhydrase in presence of zinc. Finally, the S^{2-} reacts with soluble zinc salt forming ZnS NPs.

1.3.4.2 Non- enzymatic biosynthesis of metallic nanoparticles

Glutathione (non-protein thiol- GSH) and two groups of metal-binding ligands viz. metallothioneins (protein-bound thiol- MT) and phytochelatins (protein-bound thiol-PC) are cysteine-rich metal-binding peptides which are very well studied for metal resistance and

synthesis of NPs. GSH has triple peptide and is known to detoxify various metals in *S. cerevisiae* and *C. glabrata* and is also known to be the structural unit of PCs. MTs are low molecular weight polypeptides while, PCs help in binding of calcium and are usually found to be induced by cadmium, lead, zinc, antimony, silver, nickel, mercury, copper, selenium, gold, bismuth and tellurium (Hulkoti and Taranath, 2014). In the presence of metal stress, microbes particularly the yeast cells increase the GSH and PCs which results in metal thiolate complex formation. These then traps the metal and metalloids inside the cell thus, reducing their toxicity. Additionally, PCs can incorporate inorganic sulphur, thus increasing its capacity to bind to cadmium. Sulphide ions are easily incorporated into cadmium–GSH complexes which result in the formation of NPs (Park et al., 2016).

1.4 Selenium nanoparticles (SeNPs)

Selenium (Se) is widely distributed metalloid belonging to Group XVI of the periodic table, sharing structural and chemical similarities with sulphur and tellurium. It occurs in the environment as inorganic, unstable selenide (Se^{2-}), water-soluble selenite (SeO_3^{2-}), selenate (SeO_4^{2-}) and elemental water-insoluble selenium (Se^0). Organic forms include selenocysteine and selenomethionine. Se is a significant trace element in all domains of life and it forms an important structural component of various selenoproteins like thioredoxin reductase and glutathione peroxidase (Allan et al., 1999). It is widely referred as ‘double-edged sword’ since in humans the nutritional dose of Se (i.e. 200-400 µg/day) boosts immunity and also promotes cell death (Arthur et al., 2003; Zeng and Combs 2008). Moreover, its deficiency leads to “Keshan disease” and excess of Se (<400 µg/mL) causes selenosis (Chen, 2012; Morris and Crane, 2013). However, 40 µg/mL of Se is regarded as safe in drinking water as per WHO guidelines (WHO, 2011).

Although selenium is toxic to various life forms at high concentrations, microorganisms including bacteria can tolerate and survive very high concentrations of selenite without any adverse effects on their cellular metabolism (Ghosh et al., 2008). Reduction of selenite to elemental selenium and methylation to volatile forms such as dimethyl selenide are widely studied mechanisms involved in selenite biotransformation (Ranjard et al., 2002; Hunter and Manter, 2009).

However, not much has been understood for instance, Nitrate reductase (NR) in *E. coli* was found to be involved in reduction of selenite to elemental selenium (Avazéri et al., 1997). Likewise, a study carried out by Hunter et al. (2007) and Hunter, (2007) reported SeNPs generation in *Rhizobium* sp. strain B1 and *Azospira oryzae* respectively which revealed the involvement of periplasmic nitrite reductase. In another study by Stolz (2006), it was found that respiratory arsenate reductase in *Bacillus selenitireducens* strain MLS10 was responsible for selenite reduction.

Selenium in nano-dimensions has gained tremendous attention due to its extensive applications (Fig. 1.8) in electronics, agriculture, food, feed, environmental bioremediation along with a special emphasis in the field of medicine due to its crucial biological role even at low concentration (Shirsat et al., 2015). Although SeNPs has numerous applications, studies on marine bacteria synthesising SeNPs are scanty (Table 1.1). The specificity, selectivity, bioavailability and low toxicity of SeNPs make them one of the most promising candidates to be used for biomedical applications.

1.5 Tellurium nanoparticles (TeNPs)

Tellurium (Te) is a metalloid present at 0.027 ppm concentration in the earth crust. In the environment it occurs as inorganic, unstable telluride [Te^{2-}], water-soluble, toxic tellurate [TeO_4^{2-}] and tellurite [TeO_3^{2-}]; organic form as dimethyl telluride (CH_3TeCH_3) and elemental tellurium (Te^0). Industrially Te and its compounds find applications in solar panels, glasses, rubber,

photocopying machine, metal alloys, rechargeable batteries, semiconductors in electronics, protein crystallographic analysis and as catalysts in various chemical processes (Chasteen et al., 2009; Naumov, 2010).

Tellurite is highly toxic to microorganisms at concentrations as low as 1 µg/mL (Taylor, 1999). The toxicity of tellurite is of great concern to prokaryotes as well as eukaryotes since its lethal concentration is several folds lower than that of other metals viz. Fe, Hg, Cd, Cu, Cr, Zn, Co and Se which is a metalloid (Chasteen et al., 2009; Presentato et al., 2016). Some microorganisms have evolved resistance mechanisms such as reduction of tellurite to black elemental tellurium, intracellular and extracellular accumulation of reduced tellurium and volatilization by methylation (Trutko et al., 2000; Basnayake et al., 2001; Fuentes et al., 2007; Chasteen et al., 2009).

There are few strains of bacteria which have been reported to synthesize TeNPs (Table 1.1). However, mechanisms involved in tellurite reduction/generation of elemental Te are not much explored. Plasmid-mediated Te resistance was reported in Gram-negative bacteria by Turner et al. (1995a). In *Thermus thermophilus* HB8, NADH-dependent reduction of K_2TeO_3 was reported conferring the tellurite reductase activity (Chiong et al., 1998a). In another study by Pugin et al. (2014), glutathione reductase-mediated synthesis of Te nanostructures was reported.

Te in nano-dimensions possesses unique properties such as high surface to volume ratio, piezo-thermoelectrical, photoconductivity, catalytic and non-linear optical characteristics which have attracted the attention of several researchers around the world (Liu et al., 2003; Kurimella et al., 2013). Various applications of Te nanoparticles are listed in Fig. 1.8. However, more recently, Te and Cd quantum dots have been studied to have great prospective in imaging and solar cells (Liu et al., 2003; Li et al., 2014). Te also possesses antibacterial and antibiofilm properties (Srivastava et al., 2015; Zonaro et al., 2015).

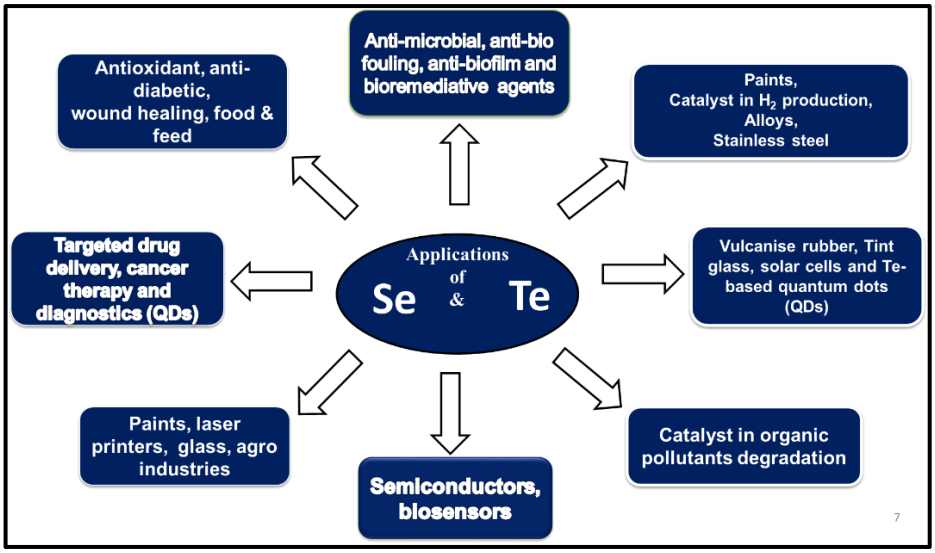

Fig. 1.9 Applications of Se and Te NPs.

Aims and Scope

- *Extensive research has been carried out in the area of metal and metalloid nanoparticles biosynthesis by microorganisms.*
- *However, there are few reports on the biosynthesis of Se and Te nanoparticles mediated by marine bacteria.*
- *Mechanism of biosynthesis of these metalloid nanoparticles mediated by marine bacteria is not much explored.*
- *Realizing the importance of Se and Te nanoparticles in various fields viz. biology, medicine and environment, it would be promising to exploit marine bacteria as a model organism for Se and Te nanoparticles biosynthesis.*

Keeping the above facts into consideration following objectives were postulated:

1. ***Screening and isolation of marine bacterial strains synthesizing Selenium and Tellurium nanoparticles.***
2. ***Identification of potential bacterial strains synthesizing Se and Te nanoparticles.***
3. ***Optimization of Selenium and Tellurium nanoparticles biosynthesis using selected bacterial isolates.***
4. ***Physico-chemical characterization of biosynthesized Selenium and Tellurium nanoparticles.***
5. ***Applications of biosynthesized Selenium and Tellurium nanoparticles.***

Chapter II

Materials and methods

2.1 Sampling of selenite and tellurite resistant marine bacteria

Surface water and sediment samples were collected from various marine habitats of Goa, India in a sterile polycarbonate bottle and zip lock bags respectively. Various physiological parameters like pH, temperature, latitude and longitude were also recorded.

2.2 Enrichment, isolation and screening of selenite and tellurite resistant marine bacteria

Enrichment of the samples were carried by adding 1mL of water sample and / or 1 gm of sediment sample to 50 mL Zobell Marine Broth (ZMB, Appendix A) supplemented with 0.5 mM sodium selenite (Na_2Se0_3) and potassium tellurite (K_2TeO_3) respectively, these were then incubated at 28 ± 2 °C on a shaker at 150 rpm for 48 h. Isolation of selenite and tellurite reducing bacteria was carried out by dilution plating of the enriched sample on Zobell marine agar (ZMA, Appendix A) plates amended with 2 mM Na_2Se0_3 and K_2TeO_3 respectively and plates were incubated at 28 ± 2 °C for 24 h. The isolates obtained were then re-streaked on ZMA plates without metalloid salts in order to ensure that colouration of the colonies was certainly due to reduction of metalloids and not because of bacterial pigment. Morphologically distinct tellurite and selenite reducing bacterial colonies were selected for further studies.

2.3 Determination of Minimum Inhibitory Concentration (MIC) of selenite and tellurite

Bacterial isolates were selected and spot inoculated on ZMA plates with increasing concentrations of Na_2Se0_3 (0-120 mM) and K_2TeO_3 (0-20 mM). These plates were incubated at for 24 h and were checked for the appearance of colonies. The minimum concentration of tellurite and selenite at which no visible colonies were obtained 28 ± 2

°C was designated as MIC. MIC in liquid medium was determined by inoculating the selected bacterial isolates in ZMB with various concentrations of Na_2Se0_3 (0-120 mM) and K_2TeO_3 (0-20 mM) and incubating at 28 ± 2 °C, 150 rpm for 24 h. The absorbance was recorded at 600 nm and the lowest concentration of selenite and tellurite which inhibited growth was considered as MIC.

2.4 Morphological and biochemical characterization

The selenite and tellurite resistant isolates were subjected to Gram staining and were observed using a microscope 1000X magnification (Nikon H600L, Japan). Moreover, the KOH string test was performed to confirm the Gram character of the bacterial isolates (Powers, 1995). Here, a drop of 3 % KOH (Appendix B) was placed on a clean glass slide and a loop full of bacterial culture was added and mixed thoroughly. After 60 sec the mixture was checked for the formation of strings and that organism was considered to be Gram-negative. Various biochemical tests were performed to tentatively identify the selected bacterial isolates based on Bergey's Manual of Systematic Bacteriology (Holt et al., 1994).

2.5 Molecular identification of selenite and tellurite resistant marine bacteria

2.5.1 Extraction of genomic DNA

Genomic DNA extraction of the selenite and tellurite reducing bacterial strains was carried out using Dneasy® Blood & Tissue Kit (Qiagen, Hilden, Germany), analysed using 0.8 % agarose gel electrophoresis (Appendix C) and was visualized by gel documentation system (Syngene G: BOX, UK). The extracted genomic DNA was quantified and was also checked for purity using nanodrop 2000c spectrophotometer (Thermofisher Scientific, USA).

2.5.2 PCR amplification and DNA sequencing of 16S rRNA gene

The 16S ribosomal RNA gene (16S rRNA) was amplified with 27F (5' AGAGTTTGATCMTGGCTCAG 3') and 1492R (5' TACGGYTACCTTGTTACGACTT 3') universal eubacterial primers using Nexus Gradient Mastercycler (Eppendorf, Germany). The reaction conditions are listed as used (Appendix C). The PCR amplicon was observed on 1% agarose gel (Appendix C) followed by purification using Wizard SVGel and PCR clean-up system (Promega, USA). The purified 16S rRNA gene amplicon was then sequenced at Eurofins Genomics Bangalore, India.

2.5.3 Bioinformatic analysis of amplified 16S r RNA gene

The DNA sequence was analysed by BLAST (Altschul et al., 1990) and submitted to GenBank. Neighbor-joining method was used for the construction of a phylogenetic dendrogram using the MEGA 7 package (Tamura et al., 2013).

2.6 Growth behaviour of selected marine bacteria in the presence of selenite and tellurite

The potential selenite and tellurite resistant bacterial strains GUSDM4 and GUSDZ9 were inoculated in ZMB supplemented with different concentrations of Na_2Se0_3 (0, 2, 4, 10, 50, 100 and 101 mM) and K_2TeO_3 (0, 1, 2, 3, 4, 5, 5.5 and 6 mM) under constant shaking at 150 rpm and temperature at 28 ± 2 °C for 48 h. The growth behaviour of the strain at various concentrations of K_2TeO_3 was monitored by recording the absorbance at 600 nm at specific time intervals using UV-Vis spectrophotometer (Shimadz-1601, Japan). Whereas that of selenite resistant strain was monitored by quantifying the proteins over time. The experiment was carried out in triplicates and the standard deviation was determined.

2.7 SEM-EDX analysis of selected bacterial strain

The selected bacterial isolates (GUSDM4 and GUSDZ9) were grown in ZMB supplemented with Na_2Se0_3 (0, 4 mM) and K_2TeO_3 (0, 3 mM) as control and test were kept for 48 h under constant shaking at 150 rpm and at 28 °C. The bacterial cells were centrifuged at 6000 rpm for 10 min (Eppendorf, Germany) and the resultant cell pellet was washed with 0.1 M phosphate-buffered saline (PBS) with pH 7.4 (Appendix B). A thin smear of bacterial cells were prepared on a coverslip and this was then fixed in 2.5 % glutaraldehyde. The cells were subjected to drying in acetone from 20 % to 100 % and viewed using scanning electron microscope coupled with electron dispersive spectroscopic analysis (JEOL JSM-6360 LV, USA).

2.8 X-ray diffraction analysis of selected bacterial strain

Bacterial cells grown in presence of Na_2Se0_3 (0 and 4 mM) and K_2TeO_3 (0 and 3 mM) respectively were centrifuged at 10,000 rpm for 10 min. The bacterial cells were washed subsequently with 0.1M PBS (pH 7.4). The obtained cell pellets were dried at 45 °C for 48 h and pulverized to fine powder. This was further used to make a film on a glass slide for XRD analysis using Rigaku Miniflex X-ray diffractometer (Panalytical X'pert-pro diffractometer, Japan) operated at 40 keV voltage, 20 mA of current, 1.541 Å of Cu Ka radiation and 2θ ranged from 10° to 80° by a step of 0.2°.

2.9 Fourier Transformed Infrared Spectroscopy (FTIR) of selected bacterial strains

Bacterial cells grown in presence or absence of Na_2Se0_3 (0 and 4 mM) and K_2TeO_3 (0 and 3 mM) respectively were centrifuged at 10,000 rpm for 5 min this was followed by washing with 0.1 M PBS (pH 7.4). The cell pellets obtained were dried in an incubator at 45 °C

for 48 h. The pellet was then fined with the help of agate mortar. The samples were then placed into a sample holder after grinding with excess KBr. The IR spectrum of 4000-400 cm^{-1} was displayed using instrument IR Prestige-21 (Shimadzu, Japan).

2.10 Selenite uptake by selected selenite resistant bacterial strain

Time course study of selenite uptake was done using a modified spectrophotometric method as described by Watkinson, (1996). Briefly, *Halomonas* sp. strain GUSDM4 was grown in presence of 2 and 4 mM Na_2SeO_3 and every 4 h, 0.5 mL aliquot was centrifuged at 10,000 rpm for 10 min. The supernatant (100 µL) was used to determine the selenite content. Appropriate controls such as un-inoculated medium with Na_2SeO_3 and inoculated medium without metal were kept and processed under similar conditions. For selenite estimation, 0.1 M HCl (5 mL), 0.1M NaF (0.25 mL) and 1M disodium oxalate (0.25 mL) were added and mixed in a test tube. Subsequently, 0.25 mL culture supernatant, 1.25 mL of 0.1 % of 2, 3 DAN (2, 3-diaminonathtalene) was added, mixed and incubated at 60 °C for 15 min. The above mixture was cooled at room temperature and 3 mL of cyclohexane was added to extract selenium - 2, 3 DAN complex with vigorous shaking. The solution was then centrifuged at 6000 rpm for 12 min and absorbance at 377 nm of the organic phase was determined using UV-Vis spectrophotometer (Shimadzu -1601, Japan). The experiments were performed in triplicates and the standard error was determined.

2.11 Tellurite uptake by selected tellurite resistant bacterial strain

Tellurite uptake was estimated by modified diethyldithiocarbamate (DDTC) colorimetric assay (Turner et al., 1992). The bacterial strain was grown in ZMB with 2 mM K_2TeO_3 and

after every 4 h, 0.5 mL culture aliquots were removed and centrifuged at 10000 rpm for 10 min. The supernatant (100 µL) was added to the tube containing 0.3 M Tris buffer (pH 7) and 2 mM DDTC and absorbance was recorded at 340 nm in order to determine unreduced tellurite remaining in the supernatant. The assay was carried out in triplicates and the standard deviation was determined.

2.12 Antibiotic susceptibility of selected selenite and tellurite resistant bacteria

The sensitivity of selected selenite and tellurite resistant bacterial isolates (GUSDM4 and GUSDZ9) to various antibiotics was determined on Muller Hinton agar (Appendix A) by Kirby-Bauer disc diffusion test (Bauer et al., 1966). Bacterial cultures grown overnight were spread placed on MHA plates to obtain uniform bacterial lawn subsequently, the antibiotic octa-disc (Himedia, India) were retained on them. The petriplates were then incubated for 24 h at 28 °C and zone of clearance due to antibiotics were recorded.

2.13 Cross tolerance of selected selenite and tellurite resistant bacteria

The bacterial isolates (GUSDM4 and GUSDZ9) were grown in ZMB medium with various concentrations of other metals and metalloid viz. cadmium (Cd), nickel (Ni), zinc (Zn), lead (Pb) and arsenic (As) along with selenite and tellurite respectively (Appendix B). The flasks were incubated at 28 ± 2 °C, 150 rpm for 24 h and growth was monitored by taking absorbance at 600 nm. The MIC of the selected isolates against various metals and metalloid in the presence of both selenite and tellurite was recorded individually.

2.14 Biosynthesis of Selenium Nanoparticles (SeNPs)

2.14.1 To determine the ability of *Halomonas* sp. strain GUSDM4 to biosynthesize SeNPs during its growth phase

The potential of the strain GUSDM4 to synthesize selenium nanoparticles (SeNPs) was studied by inoculating the culture inoculum (1% v/v) in ZMB supplemented with 2 mM Of Na_2SeO_3 and incubated at 28 °C ± 2 at 150 rpm for 24 h. The culture broth after incubation was centrifuged at 10,000 rpm, for 10min at 4 °C. The brick-red coloured cell biomass was then lysed in PBS (0.1 M) using a sonicator (Vibronics, 0.5 pulses for 10 min with 5 min interval) and centrifuged at 8000 rpm for 10 min. The resulting supernatant obtained was then scanned in the range of 200-800 nm in UV-Vis spectrophotometer. The flask containing culture without Na_2SeO_3 and uninoculated media served as controls.

2.14.2 To evaluate the ability of *Halomonas* sp. strain GUSDM4 to biosynthesize SeNPs using cell-free culture supernatant

The culture (1 % v/v) was inoculated into ZMB medium and incubated at 120 rpm, ambient temperature (25 °C), for 48 h. The fully grown culture was then centrifuged at 10,000 rpm, 4 °C for 10 min and the cell-free supernatant was collected into a fresh flask without disturbing the pellet. The supernatant was added to 2 mM of Na_2SeO_3 in 1:1 proportion and incubated at 25 °C for 48 h. Subsequently, the aliquot (1 mL) was withdrawn and scanned in the range of 200-800 nm using UV-Vis spectrophotometer.

2.15 Optimization of SeNPs biosynthesis during growth phase by *Halomonas* sp. strain GUSDM4

Optimization of SeNPs biosynthesis was carried out under different growth conditions of pH (5, 6, 7, 8, 9 and 10), temperature (18,

22, 25, 28, 30, 35, 37 and 40 °C) and Na_2SeO_3 concentration (1, 2, 3, 4, 5 and 6 mM). The culture was inoculated in ZMB flasks with varying pH, temperature and sodium selenite concentrations respectively. Nanoparticle containing supernatant was extracted and monitored at 265 nm using UV-Vis spectrophotometer.

2.16 Time course study of SeNPs biosynthesis during the growth phase of *Halomonas* sp. strain GUSDM4

SeNPs synthesis during the growth phase of *Halomonas* sp. was carried out under optimized conditions obtained from (2.15). The reaction mixture was withdrawn after a specific time interval and was monitored between 200-800 nm using UV-Vis spectrophotometer.

2.17 Harvesting of biosynthesized SeNPs

In order to obtain SeNPs, the culture containing SeNPs was harvested by centrifugation at 10,000 rpm for 10 min and the resultant brick red coloured pellet was washed thrice with 0.1M PBS. The cell pellet was re-suspended in methanol: chloroform (2:1 v/v) and sonicated (0.5 pulses for 10 min with 5 min interval). After cell lysis, the suspension was subjected to centrifugation at 6000 rpm for 10 min, the supernatant obtained was retained and the pellet containing cell debris was discarded. The brick-red colloidal suspension obtained was further harvested at 10,000 rpm for 30 min and the pellet obtained was subsequently washed twice with deionised water and ethanol. The pellet was dried at 80 °C using an oven in order to get SeNPs and pulverised to obtain the fine powder using agate mortar.

2.18 Characterization of biogenic SeNPs

2.18.1 UV-Vis spectroscopic analysis

The biogenic SeNPs were suspended in methanol: chloroform solvents (2:1 v/v) and absorbance were recorded in the range of 190 - 800 nm with methanol: chloroform (2:1 v/v) as blank.

2.18.2 Scanning electron microscopy (SEM) and Energy dispersive spectroscopy (EDS)

A thin layer of dried powder of SeNPs nanoparticles (1 µg) was placed on copper stubs and coated with gold using a high vacuum evaporator. It was then analysed by SEM coupled with EDS (JEOL JSM-5800LV).

2.18.3 X-ray diffraction analysis

X-ray diffraction pattern for biosynthesized SeNPs was obtained by scanning the dried powder of biogenic SeNPs using Rigaku Miniflex X-ray diffractometer (Philips, Netherlands) operated at 40 keV voltage, 20 mA of current and 1.541 Å of Cu Ka radiation. The data obtained were plotted in Origin 8 software and FWHM (Full Width Half Maxima) was obtained. The crystal size of the nanoparticle was calculated using Scherer's equation as follows: $D = K\lambda/\beta Cos\theta$ where D is the mean grain size, k is constant, λ is the X-ray wavelength for CuKa radiation, β is the FWHM of the diffraction peak (radians) and θ corresponds to the Bragg's angle.

2.18.4 Transmission Electron Microscopic analysis and SAED analysis

The TEM analysis of biogenic SeNPs was carried out by dispersing powdered SeNPs in methanol and mounting on a carbon-coated copper TEM grid (Philips, model- CM200) coupled with selected area electron diffraction (SAED). The machine was operated at an accelerating voltage of 190 keV and images were taken at a

resolution of 2.4 Å. The size of SeNPs was calculated using Image J software.

2.19 Biosynthesis of tellurium Nanoparticles (TeNPs)

2.19.1 To determine the ability of *Shewanella* sp. strain GUSDZ9 to biosynthesize TeNPs during its growth Phase

The tellurite reducing bacterial strain GUSDZ9 was inoculated in ZMB supplemented with 2 mM K_2TeO_3 and incubated at 28 ± 2 °C under constant shaking at 150 rpm for 24 h. The culture broth after incubation was centrifuged at 10,000 rpm, for 10 min at 4 °C. The black coloured cell biomass was then lysed in PBS (0.1 M) using a sonicator (0.5 pulses for 10 min with 5 min interval) and centrifuged at 8000 rpm for 10 min. The supernatant obtained was then scanned in the range of 200 - 800 nm in UV-Vis spectrophotometer. The flask containing culture without K_2TeO_3 and uninoculated media served as controls.

2.19.2 To evaluate the ability of *Shewanella* sp. to synthesize TeNPs using cell-free supernatant

The ability of *Halomonas* sp. to biosynthesize TeNPs using cell-free supernatant was evaluated as described in section (2.14.2).

2.20 Optimization and time course studies of TeNPs biosynthesis during growth phase by *Shewanella* sp. strain GUSDZ9

The optimum pH, temperature and tellurite concentrations for TeNPs biosynthesis was determined by inoculating overnight grown culture separately in ZMB containing different pH (5, 6, 7, 8, 9 and 10), concentrations of K_2TeO_3 (0.5, 1.0, 1.5, 2.0, 2.5 and 3.0 mM) and were incubated at various temperature (25, 28, 32, 37 and 42 °C)

respectively. One mL aliquot of culture suspension was withdrawn after 42 h and centrifuged at 10,000 rpm for 10 min. The pellet obtained was suspended in 0.1M phosphate buffer saline (PBS), sonicated and centrifuged at 8000 rpm for 10 min. The resulting supernatant was subjected to centrifuge at for 30 min at 10,000 rpm and pellet obtained was resuspended in methanol: chloroform (2:1 v/v). The suspension was monitored using UV-Vis spectrophotometer by recording the absorbance at 210 nm. These optimized conditions were maintained for subsequent time course study of TeNPs biosynthesis. Harvesting of the biogenic TeNPs was carried out the same protocol as described in section (2.17).

2.21 Characterization of biogenic TeNPs

Characterization of biosynthesized TeNPs by UV-Vis spectrophotometer, TEM-SAED, XRD and EDS was carried out as described in section (2.18).

2.22 Localization and mechanism of Se and Te NPs biosynthesis in *Halomonas* sp. strain GUSDM4 and *Shewanella* sp. strain GUSDZ9

2.22.1 Transmission electron microscopy (TEM) analysis

The selenite and tellurite reducing strains of *Halomonas* sp. and *Shewanella* sp. were grown in presence and absence of metalloid salts respectively. The cells were then harvested at 3000 rpm, followed by washing (0.1 M PBS pH 7.4) and were fixed with 2 % para-formaldehyde and 2.5 % glutaraldehyde prepared in PBS for 4 h at 4 °C. The bacterial cells were further centrifuged and the supernatant was discarded and 0.1 M PBS was added. The samples were then sectioned and analysed using TEM (Moragani 268D, Fei Electron Optics, USA).

2.22.2 Nitrate reductase (NR) assay

Halomonas sp. and *Shewanella* sp. were grown in nitrate broth (NB, Appendix A) with 0.2 and 2 mM of Na_2SeO_3 and K_2TeO_3 respectively for 2 days at 28 °C, 150 rpm. Un-inoculated medium with Na_2SeO_3 and K_2TeO_3 under similar conditions were kept as controls. The culture was harvested by centrifugation at 10,000 rpm for 10 min. The supernatant was collected and nitrite was estimated using Griess-Ilosvay's reagent. Griess Ilosvay's reagent (100 µL) was added to 300 µL of culture supernatant along with 2.6 mL of distilled water this was then incubated at room temperature for 30 min. For negative nitrite test, the presence of nitrate was checked by the addition of zinc dust.

Nitrite concentration was estimated by checking absorbance at 548 nm using UV-Vis spectrophotometer. $NaNO_2$ (0-0.5 µM) was used to prepare the standard curve. All the experiments were carried out in triplicates and standard deviation was calculated.

The NR activity in both the strains (GUSDM4 and GUSDZ9) were carried out using the protocol as described by Harley (1993) with slight modifications. The amount of nitrate reduced within 2 min by the cell-free extract, upon the adding substrate mix containing KNO_3 (10 mM), potassium phosphate buffer (25 mM) and ethylene diamine tetra acetic acid (EDTA, 0.05 mM, pH 7.3) was estimated.

Cell-free extracts (100 µL) of *Halomonas* sp. strain GUSDM4 and *Shewanella* sp. strain GUSDZ9 grown in presence of 0.2 mM and 2 mM of Na_2SeO_3 and K_2TeO_3 separately were added to the substrate mix with 0.2 mM β-nicotinamide adenine dinucleotide. Sulphanilamide solution (0.15 mM) in 3 mM HCl was added after 2 min in order to stop the reaction this was followed by addition by N-(1-naphthyl) ethylene diamine hydrochloride (NED, 0.19 mM) solution. The subsequent product was recorded at 540 nm using UV-Vis spectrophotometer. Appropriate positive and negative control consisting of 0.2 and 2 mM KNO_3 and inactivated (boiled for 15 min) cell-free extract respectively were used. The assays were performed in triplicates.

2.22.3 Preparation cell lysate, spheroplast and periplasmic fractions of *Halomonas* sp. and *Shewanella* sp.

The cells of *Halomonas* sp. GUSDM4 and *Shewanella* sp. strain GUSDZ9 were grown in ZMB containing 2 mM of Na_2SeO_3 and K_2TeO_3 respectively. The cells in their late log phase were centrifuged at 8000 rpm, 4 °C for 10 min. The cell pellet was then washed using washing buffer containing 20 mM Tris-HCl, 0.1 mM phenylmethylsulfonyl fluoride (PMSF), 0.6 mM EDTA with pH 8.4 and 0.9 % NaCl with pH 8.4 subsequently, the pellet was resuspended in 20 mM Tris buffer (0.6 mM PMSF and 0.6 mM EDTA). This was followed by addition of lysozyme (1 mg/mL) and incubation at 28 °C for 2 h. DNase (100 ng), RNase (10 ng), magnesium sulphate (20 mM) and magnesium acetate (100 mM) were added subsequently and incubated under similar condition. After incubation (30 min) the cell suspension was sonicated thrice (2 min) with 10 min cool-down intervals consequently, the suspension was incubated at 60 °C for 1 min this was then cooled on ice. The suspension was then centrifuged at 8000 rpm for 10 min and the resulting supernatant was collected in fresh centrifuge tube (Anderson et al., 1992).

For extraction of spheroplast and periplasm, the bacterial strains GUSDM4 and GUSDZ9 grown in ZMB were harvested by centrifugation (8000 rpm) for 10 min. The cells were suspended in Tris-HCl buffer (20 mM), PMSF (0.1 mM), and EDTA (10 mM), pH 8.4 and 20 % sucrose. The outer membrane was then lysed using lysozyme (0.5 mg/mL) for 40 min this was followed by centrifugation at 8000 rpm for 10 min. The resulting supernatant was collected in a centrifuge tube and the pellet obtained was washed thrice in Tris-HCl (20 mM), PMSF (0.1 mM), EDTA (10 mM, pH 8.4), 20 % sucrose and assayed for selenite and tellurite reductase activity.

2.22.4 Selenite and tellurite reductase activity

The selenite and tellurite reductase activity were determined in all three fractions viz. cell lysate, spheroplast and periplasmic by observing the accumulation of brick red Se and black TeNPs in presence of 10 mM Tris HCl, 1 mM Na_2SeO_3 / K_2TeO_3 and 1 mM NADH at 265 and 210 nm respectively. The selenite and tellurite activity were denoted by the extent of crude enzyme which lead to in a rise of 0.001 units of A265 and A210 (selenite and tellurite) / min/mL as 'One unit' of enzymatic activity. The assays were also conducted in the absence of NADH to know the requirement of NADH by the enzyme and the heat-killed enzyme served as a negative control. Protein estimation was carried out by Folin Lowry method (Lowry et al., 1951) using bovine serum albumin as standard.

2.23 Genetic determinants of *Shewanella* sp. GUSDZ9 in tellurite resistance/TeNPs biosynthesis

2.23.1 Whole-genome analysis of *Shewanella* sp. strain GUSDZ9 for determining the tellurite resistance

Genomic DNA of the isolate grown in ZMB was extracted using c-TAB and phenol: chloroform method followed by sequencing on an Illumina NextSeq 500 platform at Eurofins. The paired-end sequence libraries were prepared from the QC passed DNA samples using Illumina TruSeq Nano DNA Library Prep Kit. Covaris M220 was used to generate the 350 bps fragments of genomic DNA subsequently, the fragments were subjected to end-pair repair. The ligated products were then size selected using AMPure XP beads this was followed by PCR amplification of the fragments. PCR enriched libraries were analysed on 4200 tape station system for quantity and quality check. Subsequently, the Illumina libraries were loaded on Nexteq500 for cluster generation and sequencing.

The sequenced raw paired-end were subjected to quality filtration using FASTAQC tool to remove low-quality sequences using Trimmomatic v0.38. The filtered high-quality reads were assembled into scaffolds using SPAdes v3.11.1. The draft genome obtained was then compared with the reference (downloaded from NCBI) for reference-based scaffolding using MEDUSA (webserver). The total genes were predicted using Prokka v1.12 and Gene ontology (GO) terms were assigned to the predicted genes using Blast2GO platform. The genes involved in biological pathways were mapped to reference canonical pathways in KEGG orthology database using KAAS server. This was followed by identifying the genes involved in metal resistance using BacMet database.

2.24 Genotoxicity of biosynthesized Se and TeNPs

2.24.1 Isolation of lymphocytes

Blood sample (5 mL) was collected from a healthy human blood donor in a heparinized centrifuge tube and was centrifuged at 2000 rpm for 15 min. The white buffy coat at the interphase of the plasma layer and sedimentary blood cells were collected in a microcentrifuge tube. The blood cell pellet was washed with 0.5 mL of freshly prepared 0.85 % NH_4Cl (w/v) in order to remove contaminant red blood cells. Lymphocytes which appeared as white pellet after subsequent washes were re-suspended in PBS (pH 7) and stored at 4 °C.

2.24.2 Cell viability assay

Viability of the lymphocytes was ensured by determining the total cell count of lymphocytes using cell haemocytometer and trypan blue dye exclusion test prior to the comet assay. The lymphocyte suspension having a cell count of 10^4 -10^5 cells/mL were used to study the genotoxic effect of nanoparticles.

2.24.3 Exposure of Lymphocytes to nanoparticles

Lymphocyte samples were exposed to varying concentrations of Se (0, 20, 25, 50, 75 and 100 µg/mL) and Te (5, 10, 15, 20 and 25 µg/mL) nanoparticles to study genotoxicity of nanoparticles on lymphocytes. Incubation was carried out at 37 °C for 0, 2 and 4 h for Se and 0, 1 and 2 h for Te NPs.

2.24.4 Comet assay

The comet assay was performed using the protocol described by Bausinger and Speit, (2016) with modifications. The assay was performed in dark room with dim red light. The lymphocyte suspension exposed to different concentrations of Se and Te NPs was mixed with 150 µL of 0.5 % low melting agarose at 37 °C and was overlaid on a frosted slide pre-coated with 1 % normal melting agarose. This was gently covered with a coverslip and allowed to solidify at 0 °C. The coverslip was removed gently, followed by placing a layer of 0.5 % low melting agarose. After solidification of the final layer, the slide was immersed in freshly prepared lysing solution consisting of 2.5 M NaCl, 100 mM EDTA, 10 mM Tris-HCl, 10 % DMSO and 1 % Triton X-100 (pH 10) at 4 °C overnight. The slides were then immersed in electrophoresis buffer containing 300 mM NaOH and 1 mM EDTA, pH 10 for 20 min for DNA unwinding. Electrophoresis was carried out for 20 min at 25 V. After electrophoresis, the slides were placed in a cold neutralizing buffer comprising of 0.4 M Tris-HCl, pH 7.5 for 10 min.

The slides were then stained with 15 µg/mL ethidium bromide (Appendix C) and examined under a BX53 Olympus fluorescence microscope (Japan) at 200X magnification. The images of the comets were captured using ProgRes®Capture Pro 2.7. CASP image analysis software was used to analyse the percent tail DNA as an indicator of single-strand DNA damage. Two slides per specimen (500 comets) were selected for analysis. Lymphocytes exposed to H_2O_2, a known genotoxic agent served as a positive control.

2.24.5 Statistical analysis

Statistical analysis was performed using Graph pad prism 7 software. Data were analysed using Student t-test and one-way ANOVA. The significance of the data for each dose against that of the respective control was analysed by the Student t-test. Whereas one-way ANOVA was used to determine variation in the dose-response and time response of the biogenic Se and Te NPs on human lymphocytes. Data were considered statistically significant at $p < 0.05$.

2.25 Applications of biosynthesized selenium and tellurium nanoparticles

2.25.1 Biomedical applications of Se and Te NPs

2.25.1.1 Antimicrobial activity Se and Te NPs

Agar well diffusion method was employed to determine the antimicrobial action of synthesized Se and Te NPs against different clinical isolates namely *Staphylococcus aureus*, *Escherichia coli*, *Klebsiella pneumonia*, *Staphylococcus epidermidis*, *Salmonella typhimurium*, *Pseudomonas aeruginosa*, *Candida albicans* and *Shigella* spp. A stock solution of 25 mg/mL of Se and Te NPs in methanol was prepared and 100 µL of previously grown pathogenic cultures were spread plated on Muller-Hinton agar plates. Sterile cork borer of 10 mm was used to bore wells in the plates after half an hour of standing time. 100 µL of different concentrations (0-300 and 0-150 µg/mL) of suspended Se and Te NPs respectively were loaded on to the wells keeping appropriate controls (methanol and/ distilled water). This was followed by incubating plates at 37 ºC for 18 h and zone of inhibition was determined which was the measure of antimicrobial activity. The activity was carried out in triplicates and the standard deviation was determined. MIC for Se and TeNPs of all the pathogenic isolates were also determined. 12 h old pathogens were inoculated in nutrient broth

(Appendix A) with varying concentrations of Se and Te NPs (0-50 µg/mL) and were incubated at 37 °C for 48 h. The absorbance at 600 nm was checked and growth inhibition was recorded. The lowest concentration of Se and Te NPs were no growth was observed was regarded as respective MIC.

2.25.1.2 Antibiofilm potential of Se and Te NPs

The anti-biofilm activity of biogenic SeNPs and TeNPs against potential human pathogens procured from Goa Medical College, Goa, India was studied using modified crystal violet assay in a 96 well sterile polystyrene microtiter plate as described previously (Baygar and Ugur, 2017). Initially, 300 µL of nutrient broth was added into a sterile polystyrene microtiter plate to which 12 h old pathogenic bacterial cultures viz. *Streptococcus pyogenes, Staphylococcus aureu*s, *Klebsiella pneumoniae* and *Escherichia coli* were inoculated separately along with three different concentrations of biogenic SeNPs (20, 25 and 50 µg/mL) and TeNPs (5, 10 and 15 µg/mL). Un-inoculated nutrient broth and pathogens grown in nutrient broth without NPs were maintained as controls. The microtiter plate was incubated at 37 °C for 48 h under static conditions. Subsequently, the microtiter plate was drained, washed gently with sterile 0.1M PBS and distilled water to remove unbound cells, followed by drying for 30 min. Crystal violet (0.2 % w/v) was added (300 µL) to each well and incubated at 28 °C for 30 min., the excess dye was gently washed with sterile distilled water. Methanol (300 µL) was added to the dried wells of the microtiter plate and absorbance was measured at 660 nm keeping methanol as a blank. The anti-biofilm effect was estimated using the following formula:

% Anti-biofilm activity = [(Absorbance of control - absorbance of the sample)/absorbance of control] × 100; where Absorbance of control corresponds to the bacterial cells grown in nutrient broth without NPs. The anti-biofilm assay was carried out in triplicate and the standard deviation was determined.

2.25.1.3 Free-radical scavenging activity of Se and Te NPs

DPPH (1, 1-diphenyl-2-picryllhydrazly) radical scavenging activity of biogenic SeNPs and TeNPs was investigated using method described by Turlo et al. (2012) with minor modifications. In the presence of antioxidant purple DPPH changes into yellow stable compound and hydrogen donating capacity of antioxidant determines the extent of reaction (Niki et al., 2010).

Different concentrations of biogenic SeNPs (1-50 μg/mL) and TeNPs (1-35 μg/mL) were mixed with 1 mL of freshly prepared 0.2 mM DPPH. The tubes were mixed and incubated in dark for 30 min followed by measuring the absorbance at 570 nm using ascorbic acid as standard and methanol as blank. The percent of free radical scavenging activity was determined by the formula:

% Inhibition = [(Control OD−Sample OD)/ Control OD] ×100.

2.25.1.4 Anti-cancer potential of SeNPs

Biogenic SeNPs were evaluated for their cytotoxicity by MTT (3-(4, 5- dimethylthiazol-2-yl) -2, 5-diphenyltetrazolium bromide) assay. The dye is reduced by metabolically active human cells due to the action of various dehydrogenase enzymes to pink formazan dye. The adenocarcinomic human alveolar basal epithelial and normal human bronchial epithelial cells lines were used for this study. The cell lines were cultured in Dulbecco's modified Eagle medium with high glucose (DMEM-HG, DMEM-F12) supplemented with 10 % Foetal Bovine Serum (FBS). The cells cultured in T-25 flasks were trypsinized and aspirated into 5 mL centrifuge tubes. Subsequently, the cell pellet was obtained by harvesting cells at 2500 rpm and the cell suspension exhibiting a cell count of 2 X 10^4 was used for the assay. The 200 μL cell suspension was added to a 96 well microtiter plate and the plates were incubated in 5 % CO_2 incubator at 37 ˚C for 24 h. The cells were incubated with different concentrations of SeNPs for 24 h, followed by addition of MTT reagent (10 %) for 4 h. The media was aspirated

without disturbing the formazan crystals formed. Consequently, 100 µL of DMSO was added to the plate and absorbance at 570 and 630 nm was measured using UV-Visible spectrophotometer. Sodium selenite and positive control with cisplatin was also evaluated for their cytotoxicity. The experiment was carried out in triplicates and cell viability relative to unexposed cells (control) was calculated as follows:

$$\% \text{ cell viability} = [(A_{test})/ (A_{control})] \times 100$$

Where (A_{test}) is absorbance of the cells treated with SeNPs and ($A_{control}$) is absorbance of the cells without SeNPs treatment.

2.25.1.5 Genoprotective activity of biogenic SeNPs against UV - B damage

Alkaline comet assay was used to study the genoprotective activity of these biogenic SeNPs on human blood lymphocytes using the protocol described by Vaigankar et al. (2018) with minor modifications. Briefly, Blood samples from a healthy blood donor was collected in a heparinized centrifuge tube and was centrifuged at 2000 rpm for 15 min. the milky white precipitates which appears at the interphase of the plasma and sedimentary blood cells was collected into a microcentrifuge tube. The white precipitate was than washed with 0.5 mL of freshly prepared 0.85 % NH_4Cl (w/v), to remove red blood cells. Lymphocyte pellet after subsequent washes was re-suspended in PBS (pH 7) and stored at 4 °C. Prior to the comet assay viability of the lymphocytes was confirmed by determining the total cell count. The cell suspension having a cell count of 10^{4-5} cells/mL were used to study the genotoxicity.

Lymphocytes (25 µL) suspension was inoculated with 5 and 10 µg/mL of biogenic SeNPs separately in a 96 microtiter well plate and were exposed to UV-B light (319 nm) with UV dose (50 $mJcm^{-2}$) for 0, 60 and 120 sec. Comet assay was performed to monitor the DNA protective effect of SeNPs (Vaigankar et al., 2018).

2.25.2 Environmental applications of biogenic SeNPs and TeNPs

5.25.2.1 Photo-catalytic activity of biosynthesized SeNPs and TeNPs

The photocatalytic degradation of methylene blue dye using biosynthesized SeNPs and TeNPs was investigated in sunlight. Se and Te NPs (10 µg/mL) were added to methylene blue solution. This colloidal suspension was incubated in sunlight. The methylene blue solution without nanoparticles was also incubated under similar conditions as a control. The methylene blue degradation was monitored at different time intervals viz. 30, 60, 90, 120, 150, 180, 210 and 240 min by withdrawing 1 mL aliquots of the colloidal mixture followed by centrifugation. The supernatant obtained was scanned by UV-Vis spectrophotometer in the wavelength range of 190-800 nm. Absorbance maxima at 664 nm was considered as characteristic for methylene blue and was monitored at various time intervals. The extent of methylene blue dye degradation was calculated using the following formula:

% Decolourization= [(Initial absorbance - absorbance after treatment) /Initial absorbance] $_{X}$ 100

2.25.2.2 Larvicidal activity of biogenic Se and TeNPs

2.25.2.2.1 Source of immature for test mosquito species

The larvae of *Anopheles stephensi*, *Culex quinquefasciatus* and *Aedes aegypti* were obtained from National Institute of Malaria Research, Field Unit, Goa, insectary. The cultures of these species were retained at a temperature of 27±2 °C with a relative humidity of 70±5 % and a photoperiod: scotoperiod of 12:12 h (light: dark). Healthy 3rd instar larvae were utilised to conduct the bioassays.

2.25.2.2.2 Bioassay

All the three larvae of *Anopheles stephensi*, *Culex quinquefasciatus* and *Aedes aegypti* were used to carry our preliminary bioassay. Both Se and Te NPs were dissolved in methanol (1 mL) and 200 µL suspension was taken from stock and used for bioassay. Twenty healthy 3rd instar test larvae species were placed in a sterile bowl containing 250 mL of sterile water. Appropriate control with methanol were also maintained for each species. After 24 and 48 h of incubation the number of dead larvae were counted and percent mortality was calculated for each time interval. Abbott's formula was applied to calculate corrected mortality if the control mortality (%) was between 5 and 20 %. Probit analysis with SPSS PASW 18.0 was used to determine LC_{50}, mean and standard errors.

Abbott's formula for calculating Corrected mortality is as under

% Mortality = [(% mortality in the experiment) – (% mortality in the control)/ 100 – (% mortality in the control)] X 100

2.25.2.2.3 Larval Bioassays

Stock dilutions were prepared by dissolving Se and Te NPs in methanol and dilutions were made to attain an appropriate range of dosage. Third instar larvae (25) were transferred to autoclaved plastic containers in 250 mL of distilled water. These were then exposed to various concentrations of Se and Te NPs ranging from (3.15 to 100 ppm) for 24 and 48 h along with methanol control without addition of NPs suspension. The mortality and LC_{50} after 24 and 48 h were determined as described in the section above.

2.26 Agricultural Applications

2.26.1 Antiplant pathogen potential of Se ad Te NPs

Antifungal activity of Se and Te NPs against plant pathogens viz. *Fusarium oxysporum, Microphomina* sp. and *sclerotium* sp. procured from ICAR, Goa complex was studied using agar well method. A stock solution (50 mg/mL) of both Se and Te NPs were

prepared separately in methanol and various concentrations. The experiment was carried out as described in section **5.2.1.2**.

2.26.2 Effect of SeNPs on seed priming

The seed priming technology was employed to study the effect of SeNPs in presence of As (Arsenate) stress on rice crop var. *Jyoti*. Prior to seed priming, the equal number of seeds (20) were surface sterilized using 0.1 % mercuric chloride (w/v) solution (Appendix B) for 1 min followed by washing. The seeds were then dried and treated with various treatments of As (V), SeNPs, Na_2SeO_3 and distilled water for 24 h (Table 2.1). Treated seeds were then transferred to sterilized petri plates containing Whatman filter paper and incubated up to 10 days, regular amount of water was added on each day. After fifth and tenth day of incubation the seedlings were used to measure germination index, root length, shoot length, wet biomass, proline, and phenolics.

Table 2.1: Various treatments used for rice seed

S. N.	Treatments
1.	S+ Distilled water (Control)
2.	S+ SeNPs (0.8 mg/L)
3.	S+ SeNPs (1mg/L)
4.	S+Na_2SeO_3 (0.8 mg/L)
5.	S+Na_2SeO_3 (1 mg/L)
6.	S+As (V) (0.8 mg/L)
7.	S+As (V) (1 mg/L)

8.	S+As (V) +SeNPs (0.8 mg/L)
9.	S+As (V) +SeNPs (1 mg/L)
10.	S+As (V) +Na_2SeO_3 (0.8 mg/L)
11.	S+As (V) +Na_2SeO_3 (1 mg/L)

Key: S: - seed

2.26.2.1 Determination of final germination percentage, root and shoot length, and seedling wet biomass

The seedlings were kept on a clean glass plate and root length and shoot length were measured using the scale. The germination percent was measured using formula (Ellis and Robert, 1981). Wet biomass of the seedlings was also measured.

2.26.2.2 Determination of total phenolic and proline content

The phenolic contents of the seedlings were estimated using Folin- Ciocalteu colorimetric assay (Swain and Hillis, 1959). The seeds (100 mg) were grounded in a mortar pestle with 10 times volume of 80 % ethanol (10 mL). The mixture obtained was centrifuged (10,000 rpm for 20 min) the residues were re-extracted using 5 times the volume of ethanol (80 %). The residues were then dissolved in distilled water (5 mL). The above sample (100 µL) were taken and Folin- Ciocalteau reagent (0.5 mL) was added. This was followed by addition of 20 % Na_2C0_3 (2 mL) and were mixed thoroughly. The tubes were subjected to boiling in water bath for 1 min, cooled to RT and absorbance was measured at 650 nm using reagent as blank. In order to quantify the phenol in the test samples, the absorbance was compared with the standard catechol solution.

The proline in the samples was estimated using the spectrophotometric protocol described by Ábrahám et al. (2010). Briefly, seedlings (100 mg) were ground in presence of 3 % sulfosalicylic acid (5 µL/mg of seeds). The above homogenate was centrifuged (10,000 rpm for 5 min). The reaction mixture containing sulfosalicylic acid (100 µL), glacial acidic acid (200 µL) and acid ninhydrin (200 µL) were prepared to which plant extracts (100 µL) were added. The tubes were incubated at 96 °C for 60 min the reaction was later terminated on ice. The extracts were then separated using toluene (1 min) with vigorous shaking and the tubes were then allowed to stand till the organic and water phase was separated. The chromophore containing toluene was then read at 520 nm using toluene as reference. The proline contents in the seeds were quantified using the absorbance obtained in standard proline.

2.26.3 Role of SeNPs in plant growth promotion

SeNPs were studied for their plant growth promotion potential in the hydroponic system. Spinach (*Spinacia oleracea*) seeds were surface-sterilized using 0.1 % mercury chloride were placed in six 10 X plastic mesh pot net basket with cocopeat and pebbles and were placed onto a water-tray having essential nutrients (Nitrogen-Phosphorus-Potassium=NPK 2:1:1, pH 5). One set was maintained as control (without SeNPs) and other with SeNPs (0.5 mg/mL) in addition to NPK. The crop was allowed to grow for 45 days under sunlight at room temperature (27 to 31 °C). The plant characteristics including root length and shoot length were checked on the 15^{th} and 45^{th}

Chapter III

Results and Discussion-

Isolation, identification and characterization of potential selenite and tellurite resistant bacterial strains

3.1 Sampling, isolation and screening of selenite and tellurite resistant marine bacteria

Samples obtained from various marine and estuarine environments of Goa with respective codes (Fig. 3.1) were checked for various physiochemical parameters (Table 3.1). Discrete brick red coloured bacterial colonies were obtained after plating the enriched samples on ZMB with 2 mM Na_2SeO_3 (Fig. 3.2). Morphologically 50 dissimilar bacterial colonies were considered for further studies. These selected bacterial isolates did not show any brick red pigmentation upon streaking on ZMA plates without incorporation of Na_2SeO_3 which confirmed that the brick-red colouration was not due to bacterial pigment production. Moreover, the difference in the intensities of brick red colour was observed which clearly depicted the difference in the extent of the selenite reduction.

Similarly, plating of the enriched sample on ZMA plates containing 2 mM K_2TeO_3 resulted in the appearance of discrete metallic black colonies after incubation for 24 h (Fig. 3.3). Twenty morphologically diverse bacterial isolates were selected for further studies. These isolates did not show any black pigmentation upon streaking on ZMA plates without K_2TeO_3. Likewise, it was observed that the extent of tellurite reduction was also different in all twenty isolates which were evident from the difference in intensities of the black colour.

Mandovi and Zuary are the major estuaries situated in North and South Goa respectively and are mainly flanked by various electronic and other industries. Likewise, other marine habitats are also polluted due to the various anthropogenic activities. The marine environment is a unique habitat which is characterized by extreme conditions and possesses a rich microbial diversity. These marine microbes are reported to have specific mechanisms to tolerate high salt concentration, extreme pH and high levels of different toxic metal/metalloids. Adding to the above fact, these marine sites are also

considered to be heavily contaminated with various metals and metalloids. Selenite and tellurite are used in various agro, electrical and electronics industries. Furthermore, extensive shipping and other transport activities in the marine habitats have led to widespread metal or metalloid pollutions. Additionally, reports on various bacteria isolated from these sites demonstrating resistance as well as cross-resistance to different metals and metalloids viz. iron, manganese, cobalt, copper, zinc, lead chromium, mercury, selenium and organo-metal tributyltin are ascertained (Khanolkar et al., 2015; Sunitha et al., 2015; Naik and Dubey, 2017; Samant et al., 2018).

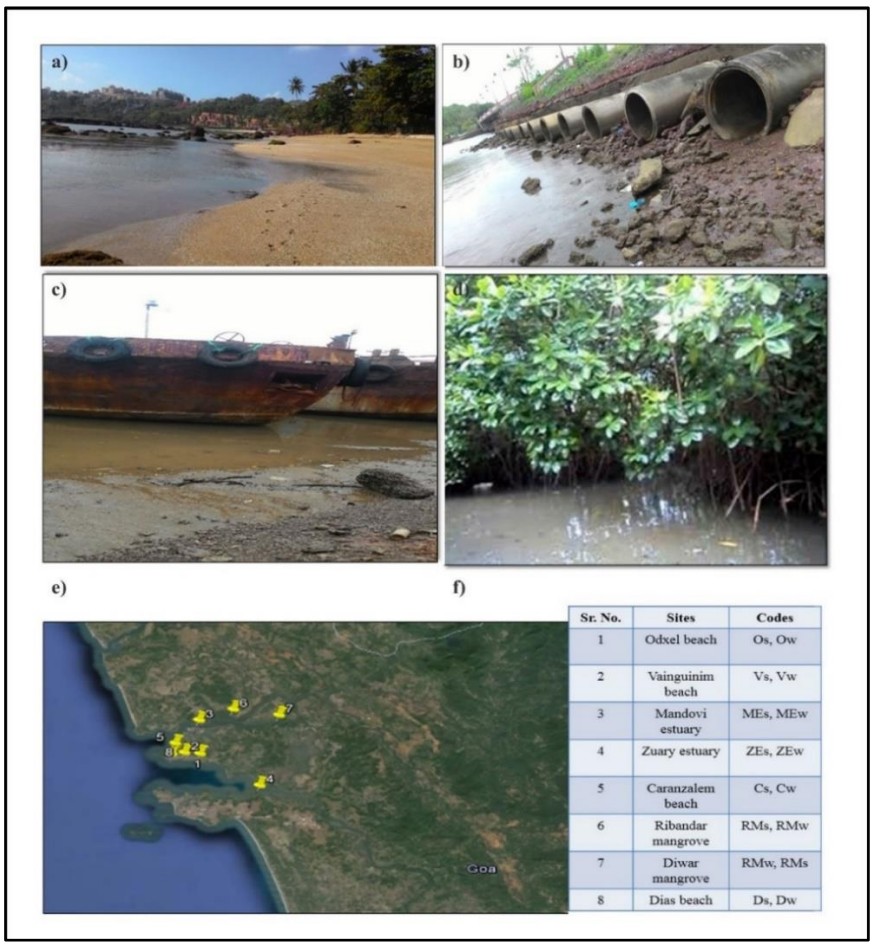

Sr. No.	Sites	Codes
1	Odxel beach	Os, Ow
2	Vainguinim beach	Vs, Vw
3	Mandovi estuary	MEs, MEw
4	Zuary estuary	ZEs, ZEw
5	Caranzalem beach	Cs, Cw
6	Ribandar mangrove	RMs, RMw
7	Diwar mangrove	RMw, RMs
8	Dias beach	Ds, Dw

Fig. 3.1 Sampling sites used for isolation of potential marine bacterial isolates: Dias beach (a); Zuary estuary (b) & (c); Ribandar mangroves (d); Marked locations along with codes used against the respective sites (e) & (f)

Table 3.1: Physicochemical parameters of various samples used

S. N.	Sampling sites	Samples	Temp-erature (°C)	pH	Latitude	Longitude
1.	Odxel beach	Sediment	30	7.7	15^0 27' 12.940'' N	73^0 49' 49.56" E
		Water	29.2	7.7		
2.	Vainguinim beach	Sediment	31	7.9	15^0 27'18.66'' N	$73^0$48'51.97''E
		Water	30	7.9		
3.	Mandovi estuary	Sediment	24.7	7.6	$15^0$30' 4.36''N	$73^0$49'46.17''E
		Water	23	7.6		
4.	Zuary estuary	Sediment	27	7.6	$15^0$24'31.03''N	$73^0$53'31.02''E
		Water	27	7.6		
5.	Caranzalem beach	Sediment	28	7.9	$15^0$28'5.76''N	$73^0$48'88.06''E
		Water	27.5	7.9		
6.	Ribander Mangrove	Sediment	28	7.9	$15^0$30'59.98''N	$73^0$51'52.91''E
		Water	27.6	7.6		
7.	Divar Mangrove	Sediment	26	7.6	$15^0$30'30.54''N	$73^0$54'42.67''E
		Water	25	7.5		
8.	Dias beach	Sediment	28	7.7	15^0 27'13.29'' N	$73^0$48'4.74''E
		Water	27.6	7.7		

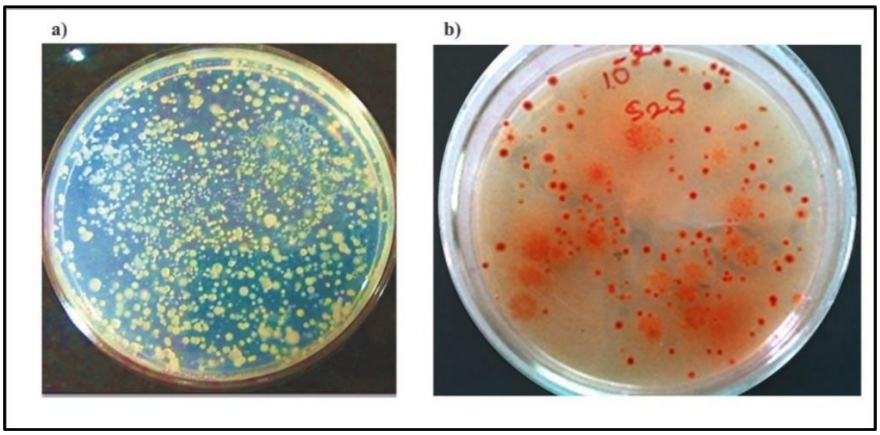

Fig. 3.2 ZMA plates: without Na_2SeO_3 (a), with (2 mM) Na_2SeO_3 showing brick red colonies (b).

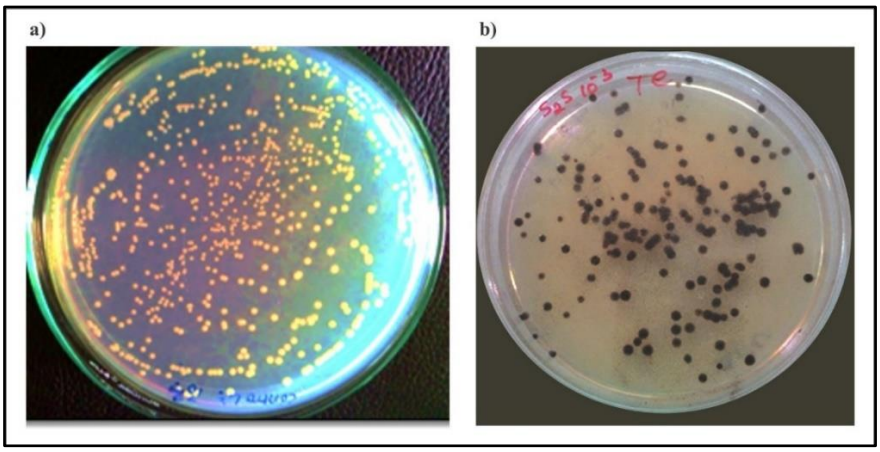

Fig. 3.3 ZMA plates: without K_2TeO_3 (a), with (2 mM) K_2TeO_3 showing metallic black colonies (b).

3.2 Determination of Minimum Inhibitory Concentration (MIC) of selenite and tellurite

Out of fifty selenite reducing bacterial isolates, 20 strains exhibiting MIC higher than 100 mM on ZMA were selected for further studies (Fig. 3.4). Among all the estuarine bacterial isolates the strain (designated as GUSDM4) showing the highest MIC was selected for further characterization. The bacterial strain GUSDM4 showed a MIC of 101 mM to Na_2SeO_3 in liquid medium with MTC of 100 mM which

is very high as compared to previously studied selenite resistant marine bacterial isolates although there are very few reports available. For instance, *Idiomarina* sp. isolated from the banks of Mandovi estuary Goa, India showed MIC of 10 mM for selenite which is 10 times lower than the present study (Srivastava and Kawshik, 2016). The above findings are highly substantial since the estuarine strain GUSDM4 also can be an ideal candidate for bioremediation of selenite contaminated sites.

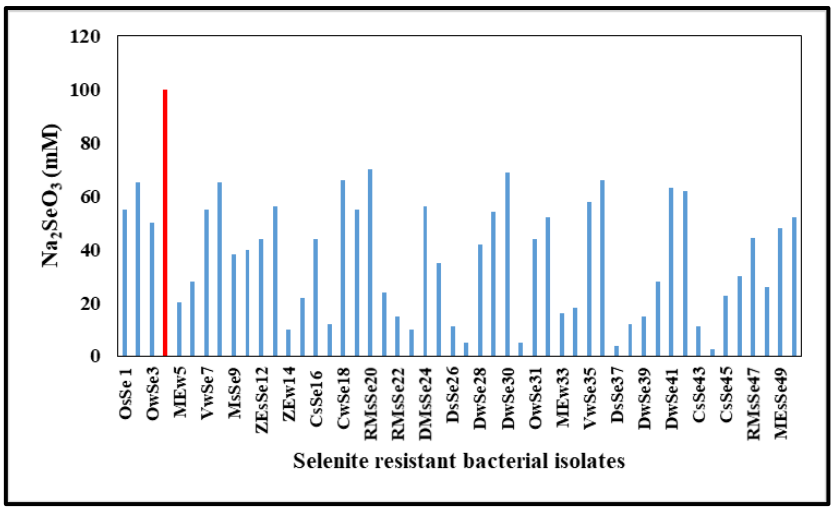

Fig. 3.4 MTC of selected potential selenite reducing bacterial isolates.

Whereas, in the case of tellurite, out of 20 isolates, 10 bacterial isolates exhibiting MIC higher than 15 mM on ZMA were chosen for further studies. In ZMB the estuarine bacterial strain GUSDZ9 showing highest MIC (i.e. 6 mM) was selected for further characterization (Fig. 3.5). The bacterial strain GUSDZ9 showed very high MIC as compared to previously isolated marine tellurite resistant bacterial isolates. For instance, bacteria isolated from the Caspian Sea exhibited MIC of 0.8 mM, whereas, marine bacterial strain 14B isolated from Rehoboth Beach, DE, United States was reported to tolerate 0.3 - 0.4 mM K_2TeO_3 (Ollivier et al., 2008; Zare et al., 2012). A recent study by Valdivia-

González et al. (2018) on *Shewanella* spp. has reported MIC values ranging from 0.05 - 1 mM. This is much lower as compared to MIC for strain GUSDZ9. Thus, estuarine strain GUSDZ9 with MIC 6 mM for K_2TeO_3 is a potential candidate which may be used for bioremediation of tellurite contaminated estuarine sites.

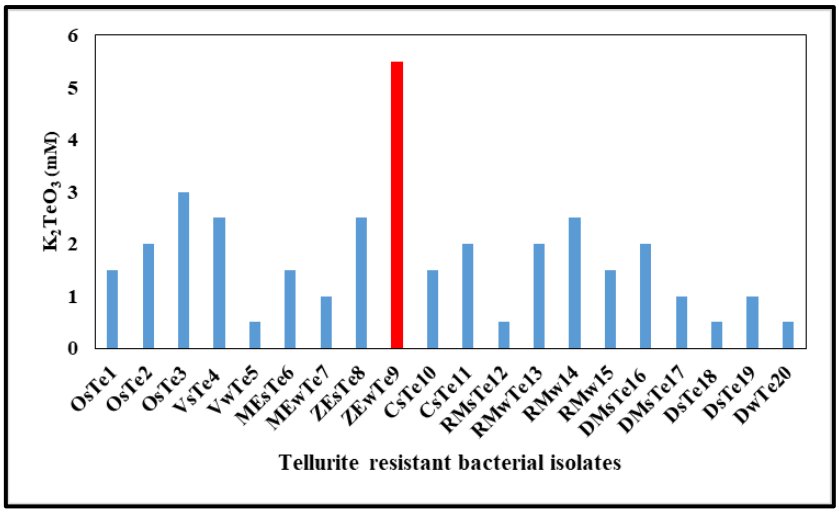

Fig. 3.5 MTC of selected potential tellurite reducing bacterial isolates.

3.3 Morphological and biochemical characterization

Selenite and tellurite resistant marine bacterial isolates were found to be Gram-negative rods which were further confirmed by KOH string test wherein the mixture containing cell culture and 3 % KOH turned viscous and resulted in the appearance of string. Based on biochemical tests, the selenite resistant strain was identified as *Halomonas* sp. and tellurite resistant as *Shewanella* sp. (Table 3.2).

Table 3.2 Biochemical characteristics of selenite (strain GUSDM4) and tellurite (strain GUSDZ9) resistant marine bacterial isolates

S. N.	Biochemical tests	GUSDM4	GUSDZ9
1.	Morphology	Rod (short)	Rod (long)
2.	Gram character	Gram -ve	Gram-ve
3.	Pigmentation	Yellow	Peach
4.	EPS	-	-
5.	Motility	+	+
6.	Salt range	5-20 %	0-6 %
7.	Oxidase	+	+
8.	Facultative anaerobe	-	+
9.	Catalase	+	+
10.	Lysine utilization	-	+
11.	Ornithine utilization	-	+
12.	Urease	+	+
13.	Phenylalanine deamination	-	-
14.	Nitrate reduction	+	+
15.	H_2S production	+	+
16.	Citrate utilization	+	+
17.	phosphatase	+	+
18.	ONPG	-	-
	Sugar fermentation tests		
19.	L-arabinose	-	-
20.	D-glucose	+	+
21.	D-galactose	+	+
22.	D-fructose	+	-
23.	Lactose	-	+
24.	Maltose	-	_
25.	Mannitol	+	_
26.	Mannose	-	_
27.	Rhemnose	-	_

28.	Sucrose	+	+
29.	Sorbitol	-	+
30.	Trehalose	-	+
	Hydrolysis of		
31.	Starch	-	+
32.	Gelatine	-	+
33.	Casein	-	+

Key: + Positive; - Negative

3.4 PCR amplification of 16S rRNA gene and DNA sequencing

Distinct genomic DNA bands of strains GUSDM4 and GUSDZ9 without RNA contamination were obtained (Fig. 3.6). PCR amplicons of the 16S rRNA gene were observed on 0.8 % agarose gel (Fig. 3.7). The 16S rRNA gene sequencing and sequence comparison against GenBank database using NCBI-BLAST search, the strain GUSDM4 showed the closest match to *Halomonas venusta*. The sequence has been deposited in Genbank as *Halomonas* sp. strain GUSDM4 with an accession number MG430411. The dendrogram analysis also clearly revealed phylogenetic relatedness with other species of *Halomonas* (Fig. 3.8).

The members belonging to family *Halomonadaceae* are characterized by having high salt tolerance (5 to 25 %) and also can survive at low to high temperatures (4 to 40 °C). Thus, making it a remarkable candidate for selenite bioremediation in varying habitats from estuaries to saline lakes and oceans. Reports on selenite reduction by the genus *Halomonas* are scanty. Moreover, this is the first detailed report on selenite reduction by *Halomonas* sp. isolated from Mandovi estuary showing the highest level of selenite resistance.

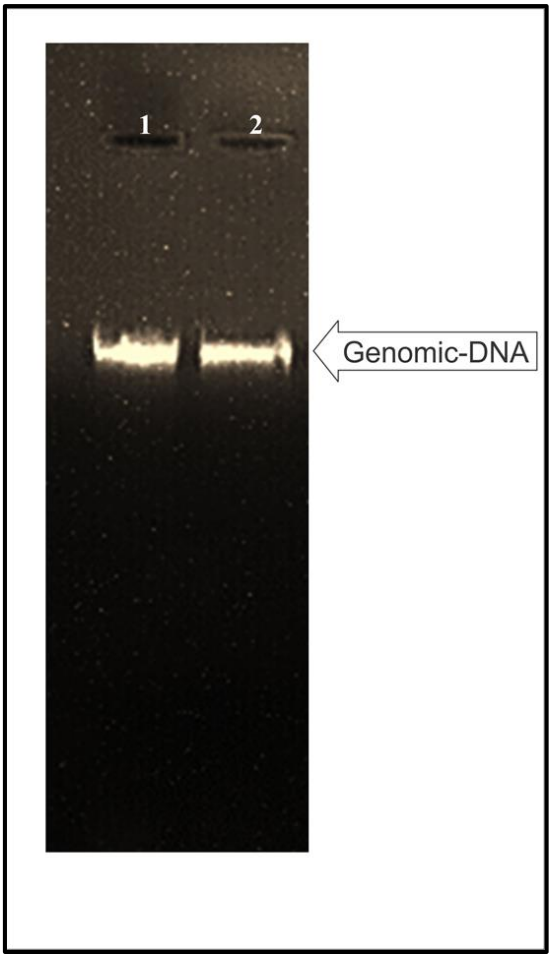

Fig. 3.6 Genomic DNA isolated from GUSDM4 and GUSDZ9

Lane1: GUSDM4

Lane 2: GUSDZ9

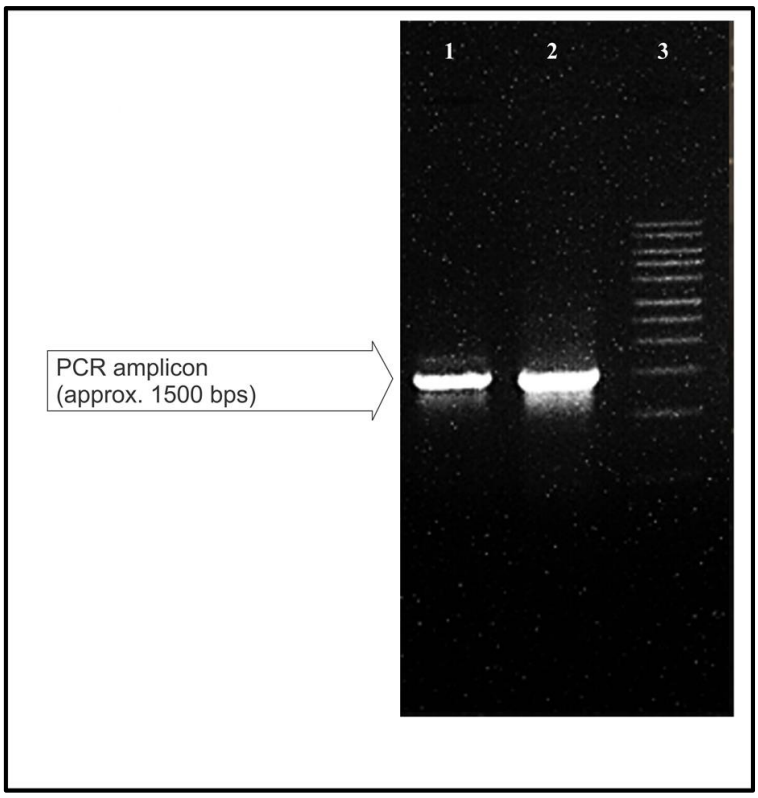

Fig. 3.7 16S rRNA gene amplicon of GUSDM4 and GUSDZ9

Lane1: GUSDM4

Lane 2: GUSDZ9

Lane 3: 100 bps DNA ladder

Similarly, BLAST analysis of 16S rDNA sequence of GUSDZ9 showed a match to *Shewanella baltica* and the sequence is now publicly available in Genbank with an accession number MF350629. The dendrogram analysis has clearly revealed the phylogenetic relatedness with other species of *Shewanella* (Fig. 3.9).

Bacteria belonging to the genus *Shewanella* are capable of anaerobic respiration using several electron acceptors. Moreover, family *Shewanellaceae* is considered to play a pivotal role in the bioremediation of sites contaminated with heavy metals and radioactive wastes (Fredrickson et al., 2008). Although few reports are available on tellurite reducing *Shewanella* spp. viz. *S. oneidensis, S. putrefaciens*

and *S. baltica* (Klonowska et al., 2005; Kim et al., 2012; 2013; 2014; Valdivia-González et al., 2018), but *Shewanella* sp. strain GUSDZ9 isolated from Zuary estuary showed a higher level of tellurite reduction as compared to previously reported spp. of *Shewanella*.

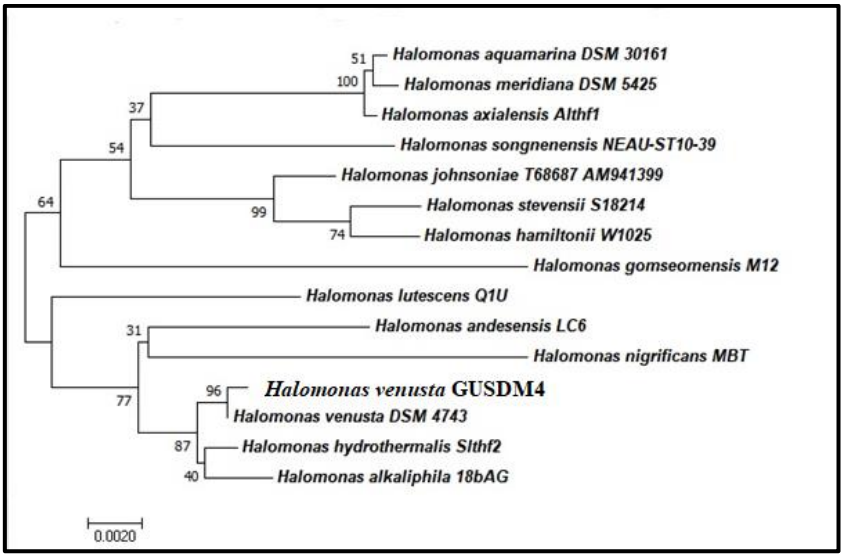

Fig. 3.8 Phylogenetic tree showing relatedness of *Halomonas* sp. strain GUSDM4 (accession number: MG430411) with other strains of *Halomonas*, constructed using neighbor joining method (Tamura et al., 2013). The bootstrap values are based on 1000 replicates.

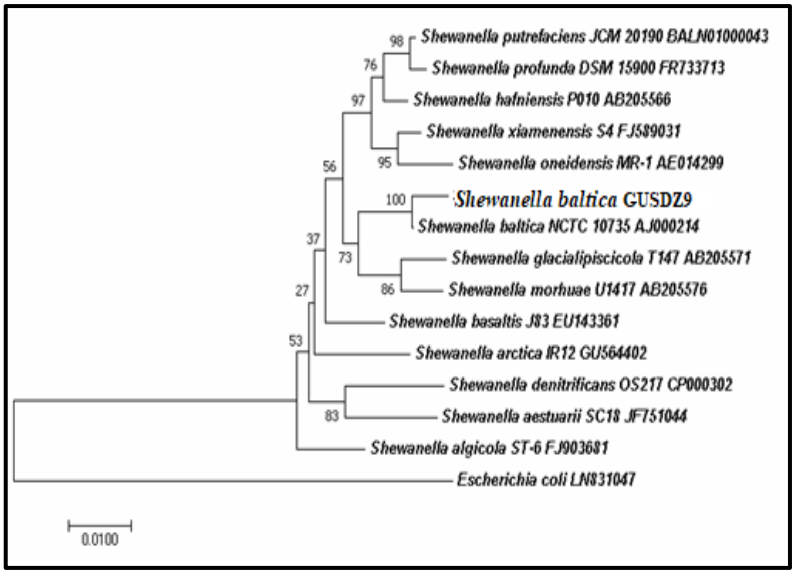

Fig. 3.9 Phylogenetic tree showing relatedness of *Shewanella* sp. strain GUDSZ9 (accession number: MF350629) with other strains of *Shewanella,* constructed using neighbor joining method (Tamura et al., 2013). The bootstrap values are based on 1000 replicates.

3.5 Growth pattern of *Halomonas* sp. strain GUSDM4 and *Shewanella* sp. strain GUSDZ9 in presence of various concentrations of respective salts

The growth pattern of *Shewanella* sp. strain GUSDZ9 in presence of different tellurite concentrations (0-6 mM) indicated that the growth of the isolate was adversely affected only at a higher concentration of tellurite (Fig. 3.10). This was evident by the extended lag phase at 4.0 and 5.5 mM K_2TeO_3 which is 6 h and 8 h respectively. Likewise, the growth pattern of *Halomonas* sp. strain GUSDM4 with various concentrations of selenite was found to be similar as compared to tellurite with only difference in the concentrations, since tellurite is known to be several-fold toxic as compared to selenite (Fig. 3.11). Additionally, the growth was inversely proportional to that of the increasing selenite but only at higher concentrations. However, the

MTC values in both the cases were less in liquid as compared to that in solid medium respectively due to the very fact that the bioavailability of both the metals/ metalloids increases by several folds in the liquid medium.

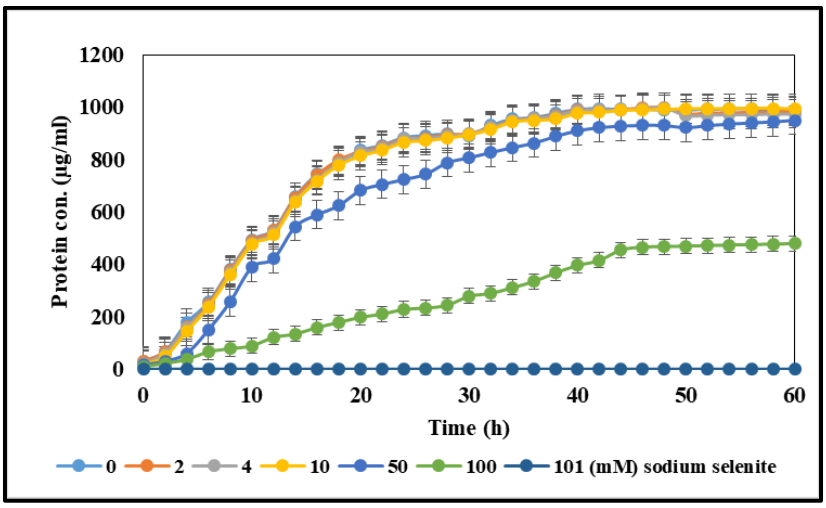

Fig. 3.10 Growth behaviour of strain GUSDM4 in various concentrations of sodium selenite.

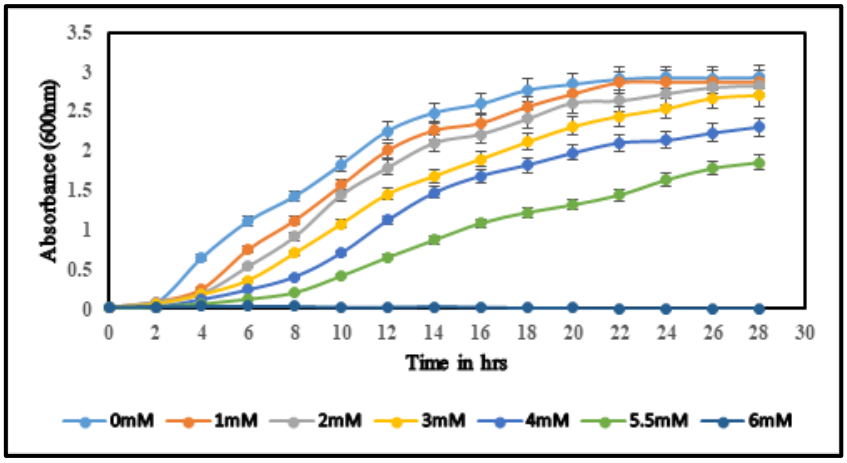

Fig. 3.11 Growth behaviour of strain GUSDZ9 in various concentrations of potassium tellurite.

3.6 SEM-EDX analysis of selected bacterial strains

The cells of *Halomonas* sp. strain GUSDM4 showed unique alteration pattern in the cell morphology due to selenite exposure. In the presence of 4 mM sodium selenite, the cells tend to aggregate and likely to stay in clusters to reduce the effect of metalloid (Fig. 3.12). A similar trend was also observed in the presence of 3 mM potassium tellurite (Fig. 3.14). These could be possible due to reducing the total surface area of the cells with respect to its volume which serves as an effective mechanism for the cells to overcome toxicity. The bacterial response to higher concentrations of toxic metal and metalloids to alleviate the toxicity are well documented (Sharma et al., 2017; Mujawar et al., 2019).

Electron dispersive X-ray spectroscopy did not show considerable adsorption of Se or Te on the bacterial cell surface (Fig. 3.13 & 3.15). This suggested that intracellular uptake of selenite and tellurite could be preferred in *Halomonas* sp. strain GUSDM4 and *Shewanella* sp. strain GUSDZ9 respectively.

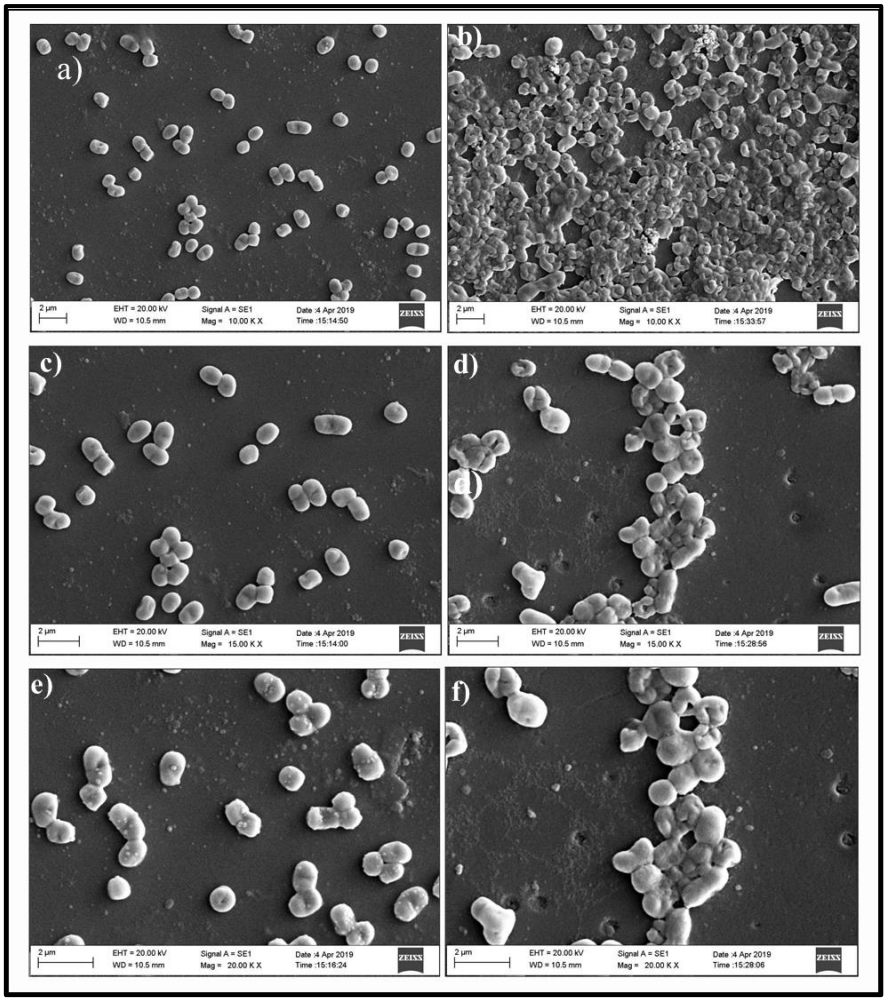

Fig. 3.12 Scanning electron micrographs of cells of *Halomonas* sp. strain GUSDM4

a) Bacterial cells without Na_2SeO_3 exposure (10X)

b) Bacterial cells with 4 mM Na_2SeO_3 exposure (10X)

c) Bacterial cells without Na_2SeO_3 exposure (15X)

d) Bacterial cells with 4 mM Na_2SeO_3 exposure (15X)

e) Bacterial cells without Na_2SeO_3 exposure (20X)

f) Bacterial cells with 4 mM Na_2SeO_3 exposure (20X)

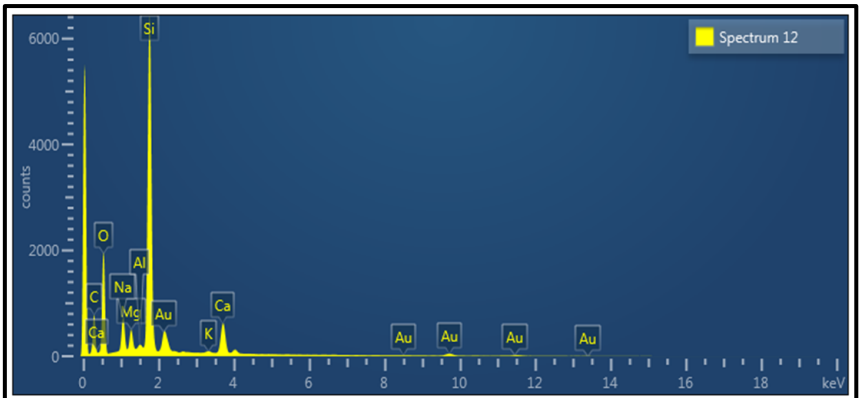

Spectrum		
Element	**Weight %**	**Atomic %**
O	**65.69**	**65.50**
Na	**2.13**	**1.48**
Si	**9.86**	**5.60**
Ca	**1.60**	**0.64**
C	**19.66**	**26.11**
Mg	**0.88**	**0.58**
K	**0.07**	**0.03**
Al	**0.11**	**0.07**
Total	**100.00**	**100.00**

Fig. 3.13 Electron dispersive X-ray spectrum of *Halomonas* sp. strain GUSDM4 cells exposed to 4 mM Na_2SeO_3 in ZMB.

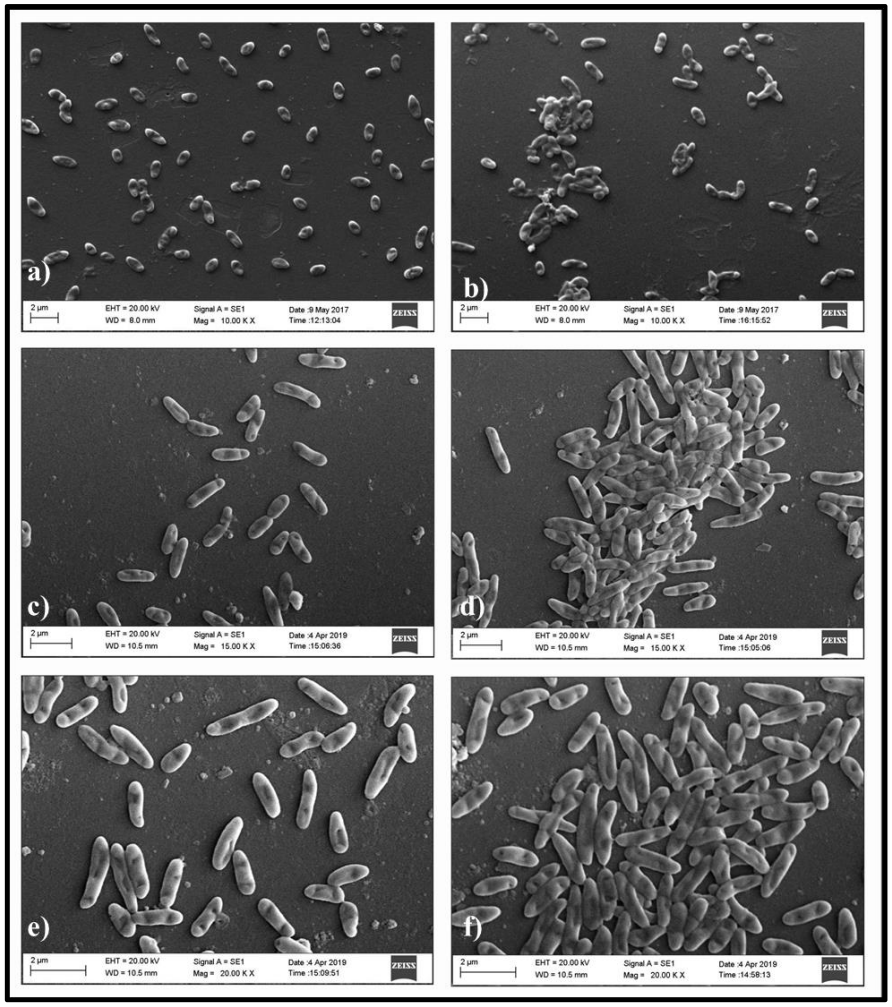

Fig. 3.14 Scanning electron micrographs of cells of *Shewanella* sp. strain GUSDZ9

a) **Bacterial cells without K_2TeO_3 exposure (10X)**
b) **Bacterial cells with 3 mM K_2TeO_3 exposure (10X)**
c) **Bacterial cells without K_2TeO_3 exposure (15X)**
d) **Bacterial cells with 3 mM K_2TeO_3 exposure (15X)**
e) **Bacterial cells without K_2TeO_3 exposure (20X)**
f) **Bacterial cells with 3 mM K_2TeO_3 exposure (20X)**

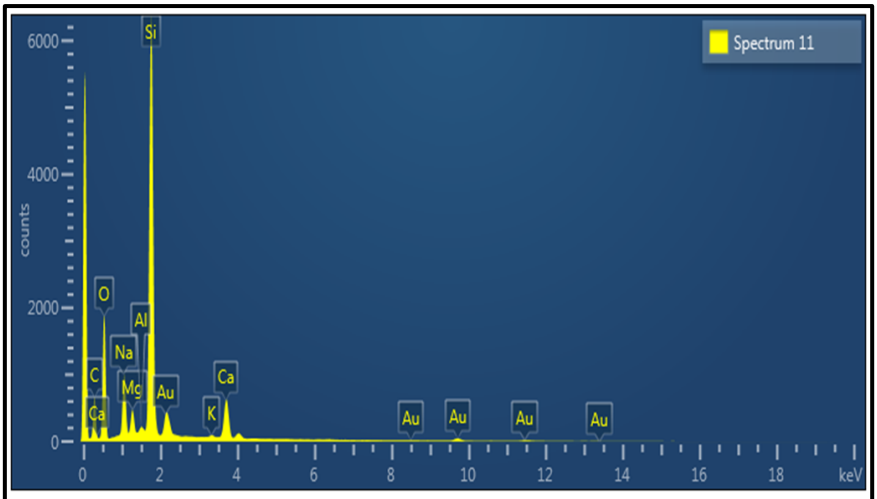

Spectrum		
Element	Weight %	Atomic %
O	64.56	65.07
Na	3.22	2.26
Si	10.61	6.09
Ca	1.76	0.71
Mg	0.88	0.58
C	18.75	25.17
K	0.09	0.04
Al	0.13	0.08
Total	100.00	100.00

Fig. 3.15 Electron dispersive X-ray spectrum of *Shewanella* sp. strain GUSDZ9 cells exposed to 3 mM K_2TeO_3 in ZMB.

3.7 X-ray diffraction analysis

X-ray data analysis using Origin 8 software showed certain peaks exclusively in the sample exposed to sodium selenite and potassium tellurite respectively (Fig. 3.16 & 3.17). The peaks were compared with that of the standards from the International Centre for Diffraction Data (ICDD). The peaks corresponding to 2θ value for the bacterial cells exposed to selenite were 23.46, 29.76, and 43.72 which clearly indicated the presence of elemental selenium (ICDD-card no.06-0362). This clearly confirmed that selenite is being biotransformed to elemental selenium by the cells of *Halomonas* sp. strain GUSDM4. Likewise, the XRD profile of the cells exposed to tellurite also revealed the presence of elemental tellurium. The observed Braggs peaks at 2θ

values of 23.02, 27.5, 38.2, 40.5, 47.0 and 49.65 indicted elemental tellurium. Thus, clearly indicating the bio transforming ability of *Shewanella* sp. strain GUSDZ9 from tellurite to elemental tellurium.

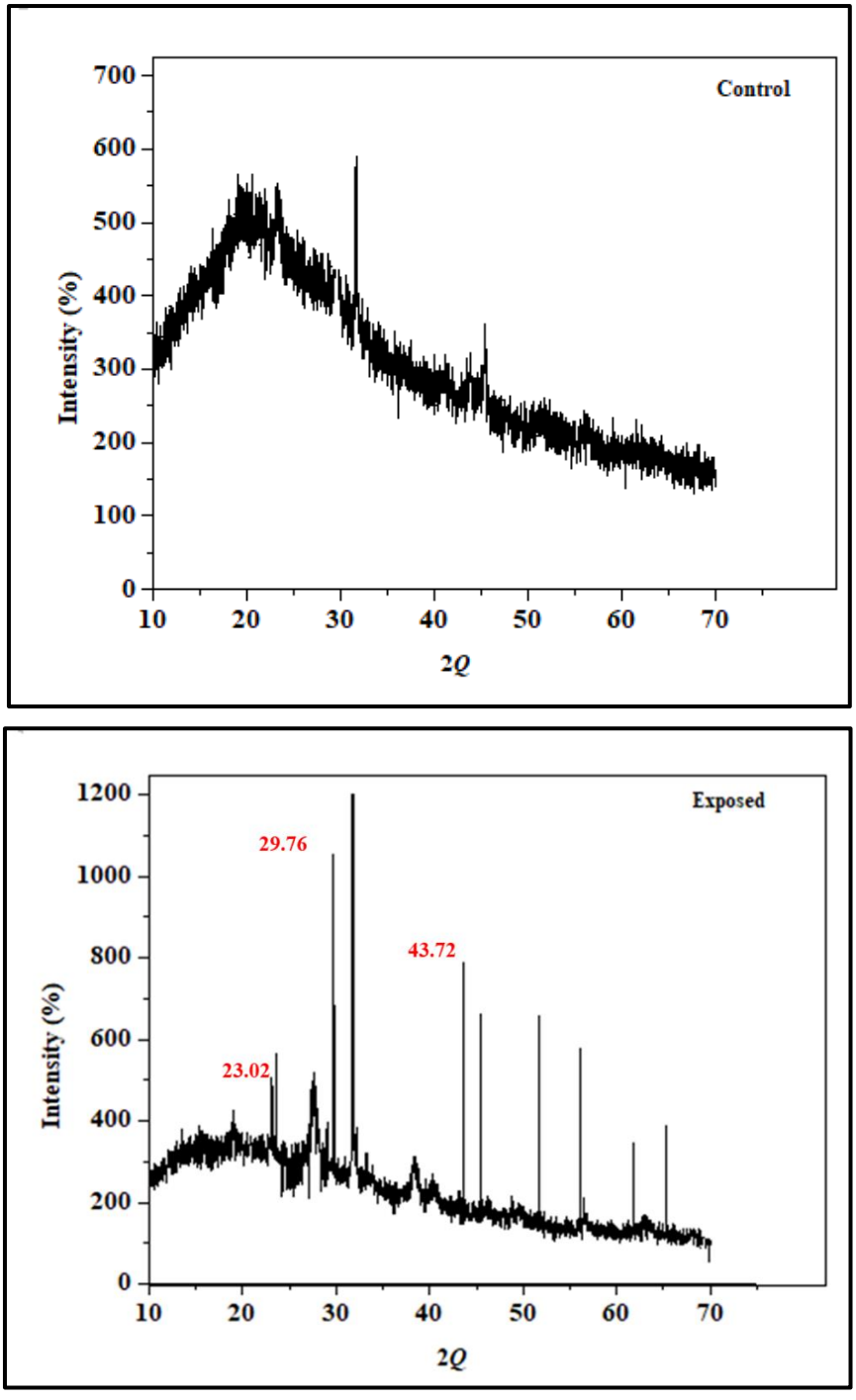

Fig. 3.16 X-ray diffraction profile of *Halomonas* sp. GUSDM4 exposed to 0 mM Na_2SeO_3 (Control) and 4 mM Na_2SeO_3 (Exposed).

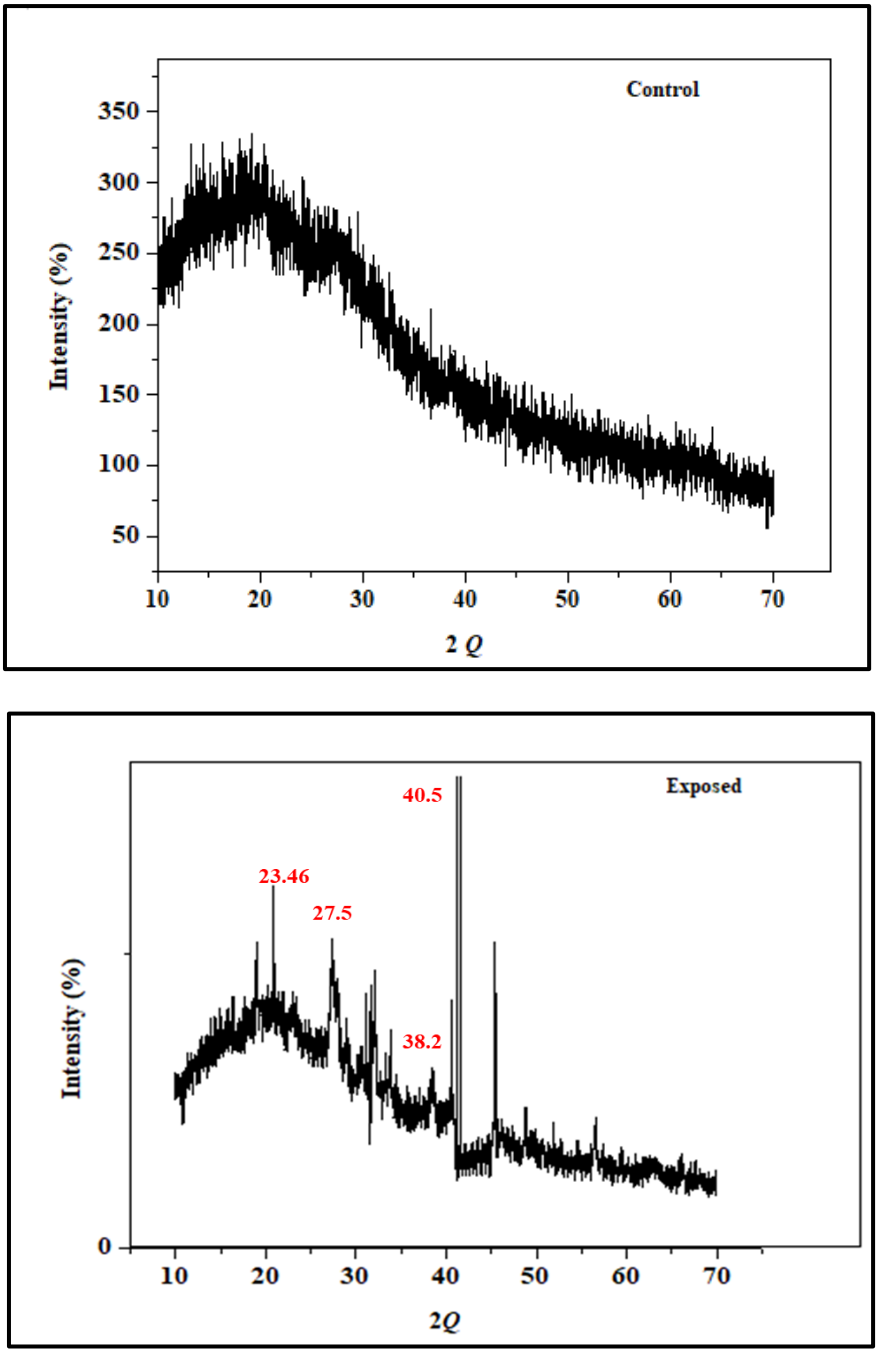

Fig. 3.17 X-ray diffraction profile of *Shewanella* sp. GUSDZ9 exposed to 0 mM (Control) and 3 mM K_2TeO_3 (Exposed).

3.8 Fourier Transformed Infrared Spectroscopy (FTIR)

Bacterial cells grown in presence or absence of sodium selenite (0 and 4 mM) and potassium tellurite (0 and 2 mM) when exposed to FTIR revealed various functional groups probably interacting with selenite and tellurite ions (Fig. 3.18). The spectra evidently indicated sharpening and shifting of various peaks which may be assigned to functional groups present on bacterial cells due to metalloid accumulation (Table 3.3). However, in a bacterial system, only few functional groups present on the cell surface are identified which are possibly responsible for interaction (Naumann et al., 1991). A significant shift of peak from 1734.20 to 1749.43 cm^1 and 1550.76 to 1544.43 cm^1 were observed indicating the interactions of amide bonds from proteins and peptides present in a cell membrane component of bacteria with metalloid.

A band shift from 1392.66 to 1401.77 cm^1 which is attributed to the proteins and fatty acids present on the bacterial cell wall was seen to be involved in selenite interaction (Naumann, 2001). However, shifts in peaks lower than 1000 cm^1 are not known to be involved in the bacterial cell interactions with metals and metalloids although observed. Thus, this study revealed that cell membrane components namely proteins, peptides and fatty acids are involved in Se accumulation.

Similarly, in case of tellurite a shift of peak from higher to lower energy level (i.e. 2943.37 to 2933.32 cm^1) which is assigned to fatty acids present on the membrane phospholipids interacting with Te was observed (Fig. 3.19). However, the shift of various peaks from 1739.79, 1668.42, 1550.76 cm^1 to 1745.57, 1670.35 and 1556.62 cm^1 respectively which are assigned to the amide bonds from proteins and peptides involving in Te accumulation were seen. A clear shift in peaks from 1450.34, 1388.74 to a lower energy 1444.68 cm^1 and 1377.77 cm^1 respectively (Table 3.4) which are known to be the mixed regions of

proteins and fatty acids were observed. Thus, conferring the functional group and metalloid interactions.

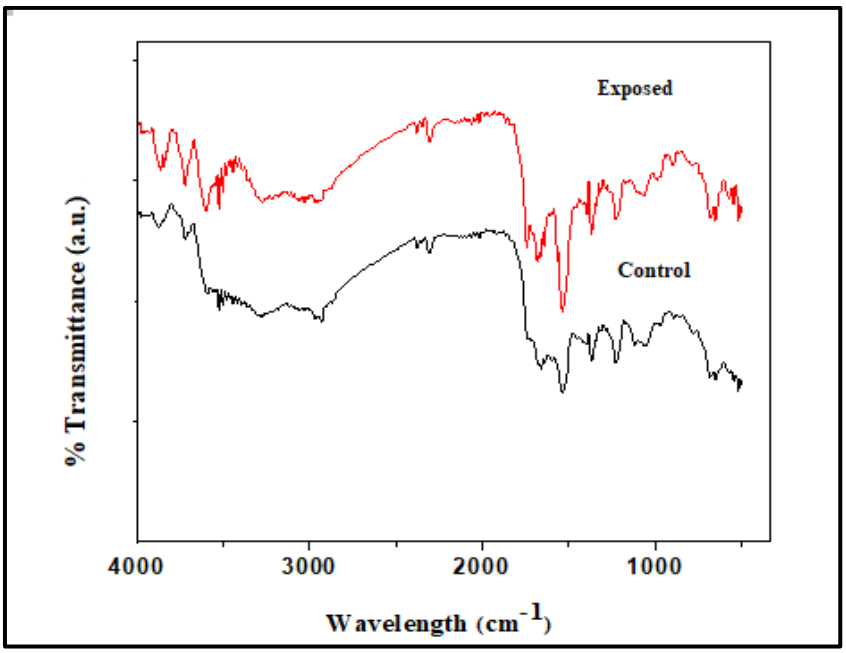

Fig. 3.18 IR profile of *Halomonas* sp. GUSDM4 exposed to 0 mM Na_2SeO_3 (Control) and 4 mM Na_2SeO_3 (Exposed).

Table 3.3: Characteristic IR absorption peaks indicating functional groups on the surface of *Halomonas* sp. strain GUSDM4

Control (cm^{-1})	Selenite exposed (cm^{-1})	Band assignment	Bacterial Interaction
3520.21	3518.16	OH stretch Primary or secondary, OH in-plane bend	ND

1734.20	1749.43	C=O stretch esters, saturated aliphatic	1*
-	1647.20	NH bend 1° alkanes	ND
1550.768	1544.98	N-O asymmetric stretch nitro compounds	1*
1392.66	1401.77	–OH bending vibrations	2*
893.64	898.82	C-H “oop” aromatics	ND
678.94	678.94	C-Br stretch alkyl halides	ND
659.66	659.66	C-Br stretch alkyl halides	ND
555.22	541.997	C-Br stretch alkyl halides	ND

1* Amide bonds from proteins and peptides present in a cell membrane component of bacteria.

2* proteins and fatty acids present on the bacterial cell wall.

ND Not defined

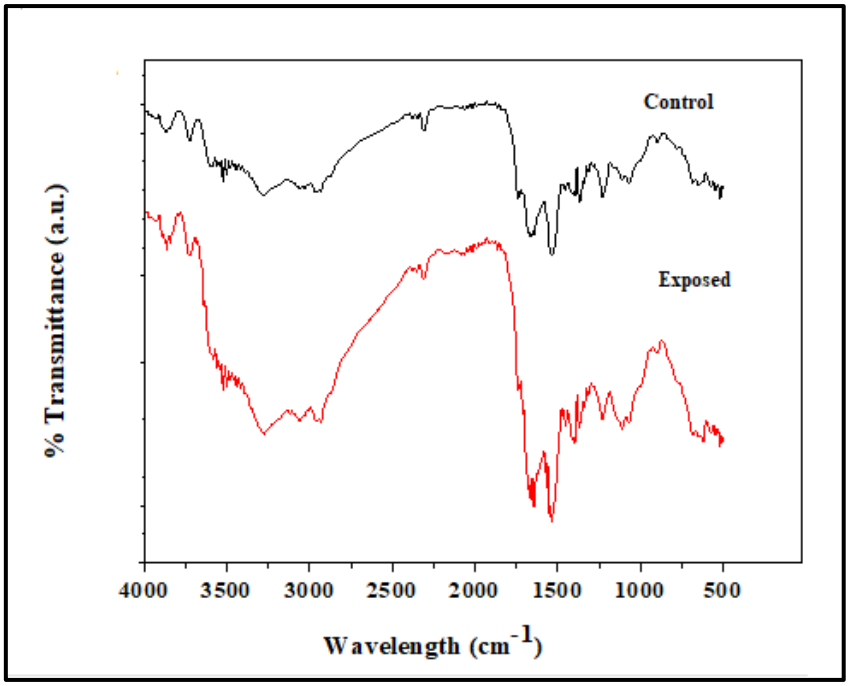

Fig. 3.19 IR profile of *Shewanella* sp. GUSDZ9 exposed to 0 mM (Control) and 3 mM K_2TeO_3 (Exposed).

Table 3.4: Characteristic IR absorption peaks indicating functional groups on the surface of *Shewanella* sp. strain GUSDZ9

Control (cm^{-1})	Tellurite exposed (cm^{-1})	Band assignment	Bacterial interaction
2943.37	2933.32	CH stretch alkanes	1*
1739.79	1745.57	C=O stretch esters, saturated aliphatic	2*
1668.42	1670.35	-C=C- stretch α B unsaturated aldehydes ketones and alkenes	2*

-	1641.42	-C=C- stretch α B unsaturated aldehydes ketones and alkenes	ND
-	1664.26	-C=C- stretch α B unsaturated aldehydes ketones and alkenes	ND
1550.76	1556.62	N-O asymmetric stretch nitro compounds	2*
1450.346	1444.68	C-H bend alkanes nitro compounds	3*
1388.74	1377.17	Methyl CH asym. /sym. Bend	3*

1* fatty acids present on the membrane phospholipids.

2* amide bonds from proteins and peptides on cell wall.

3* mixed regions of proteins and fatty acids on cell wall**.**

ND Not defined.

3.9 Selenite uptake by selected selenite resistant bacterial strain

Selenite uptake by *Halomonas* sp. strain GUSDM4 grown in ZMB with 2 and 4 mM Na_2SeO_3 was observed during early log phase of growth (i.e. 2 h) with an increase during mid-log phase (Fig. 3.20). At mid-log phase (26 h), 50 % reduction of selenite to elemental Se was observed. However, 96 % and 93 % uptake of selenite was achieved at the end of the stationary growth phase (58 h) at 2 and 4 mM respectively (Figs. 3.20 & 3.21). The previous study on *Rhodospirillum rubrum* showed selenite reduction at the beginning of stationary phase which is contradictory to the current study (Kessi et al., 1999). However, a similar reduction pattern was reported in *Idiomarina* sp. PR58-8 which was reported to initiate selenite reduction during early log phase with a maximum yield of 90 % at 38th h of bacterial growth (Srivastava and Kawshik, 2016).

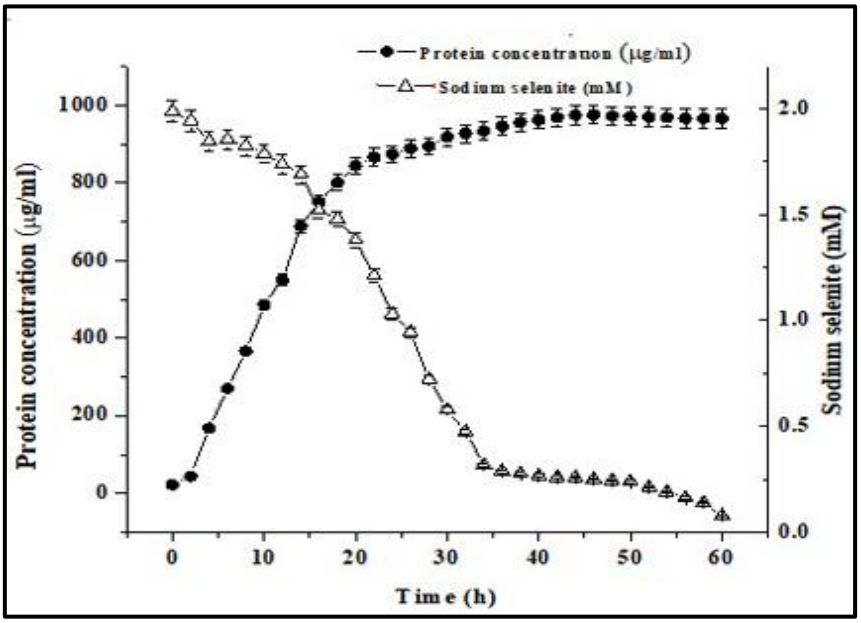

Fig. 3.20 Growth pattern and selenite uptake by *Halomonas* sp. strain GUSDM4 in presence of 2 mM of Na_2SeO_3.

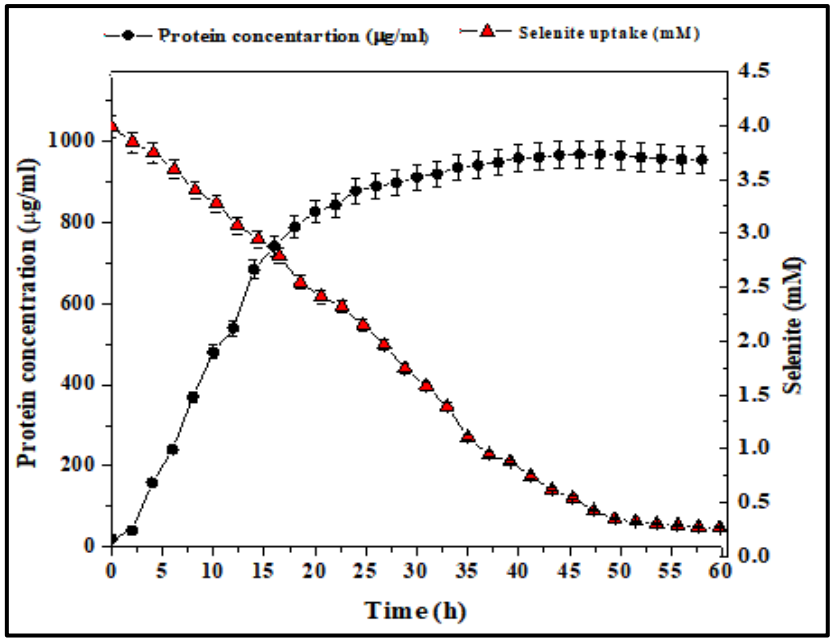

Fig. 3.21 Growth pattern and selenite uptake by *Halomonas* sp. strain GUSDM4 in presence of 4 mM of Na_2SeO_3.

3.10 Tellurite uptake by selected tellurite resistant bacterial strain

Tellurite uptake by *Shewanella* sp. strain GUSDZ9 grown in ZMB with 1 and 2 mM K_2TeO_3 was observed during early log phase of growth (2 h) with an increase during mid-log phase (Figs. 3.22 & 3.23). At mid-log phase (22 h), a 50 % reduction of tellurite was observed. However, complete utilization of tellurite was achieved at the end of the stationary growth phase (38 h). The previous study on *Salinococcus* sp. showed a 75 % reduction of tellurite after 72 h of bacterial growth supplemented with 0.4 mM K_2TeO_3 (Amoozegar et al., 2008). A similar reduction pattern was also reported in *Rhodococcus* sp. after 120 h while, *Bacillus* sp. BZ showed higher reduction rate (i.e. 80 %) after 48 h of bacterial growth (Zare et al., 2012; Presentato et al., 2016). Although, most of the studies pertaining to *Shewanella* spp. on tellurite-reduction have been reported to be more effective under anaerobic conditions, our study showed a higher reduction of tellurite under aerobic conditions. This is in agreement with one recent study which

has reported 70 to 80 % tellurite removal under aerobic conditions efficiently (Soda et al., 2018). Knowing the fact that *Shewanella* spp. are facultative anaerobes the bacterial strain GUSDZ9 may also be used for tellurite-reduction under anaerobic conditions. The present study holds considerable significance since 100 % reduction of 2 mM K_2TeO_3 was achieved at the end of the stationary growth phase (i.e. 38 h) which is the shortest time recorded so far.

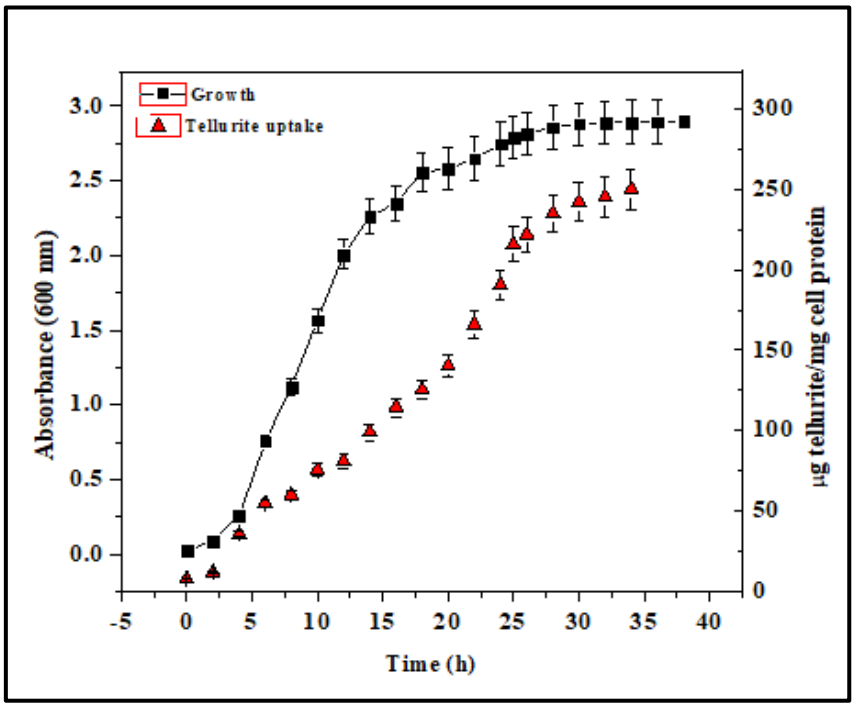

Fig. 3.22 Growth pattern and tellurite uptake by *Shewanella* sp. strain GUSDZ9 in presence of 1 mM of K_2TeO_3.

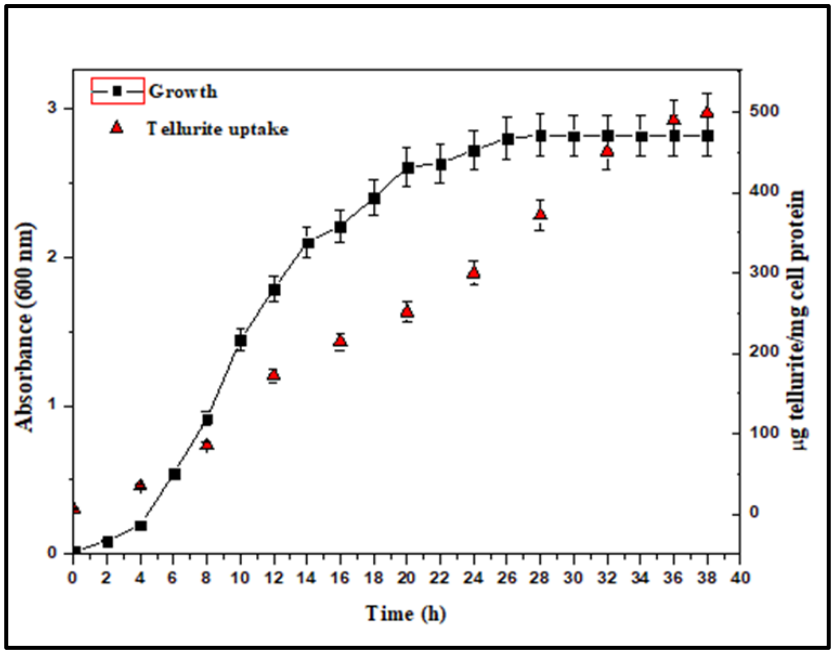

Fig. 3.23 Growth pattern and tellurite uptake by *Shewanella* sp. strain GUSDZ9 in presence of 2 mM of K_2TeO_3.

3.11 Antibiotic susceptibility

It was interesting to note that isolate GUSDM4 and GUSDZ9 were resistant to various antibiotics used namely Cephalothin (5µg), Gentamicin (10µg), Streptomycin (10µg), Tetracycline (30µg), Neomycin (30µg), Polymyxin-B (300 Units), Co-Trimoxazole (25µg), Chloramphenicol (30µg), Clindamycin (2µg), Oxytetracycline (30µg), Sulphatriad (200µg) and Kanamycin (30µg) which was evident from the zone of clearance. Additionally, the strain GUSDM4 was also found resistant to Sulphatriad (200µg), Carbenicillin (100µg) and Co-Trimazine (25µg) and strain GUSDZ9 showed resistance to Kanamycin (30µg) (Table 3.4). It has been well documented that genes encoding the metal and metalloid resistance to various antibiotics coexist on the chromosomal genome (Silver and Phung, 1996).

Table 3.5: Antibiotic susceptibility of *Halomonas* sp. strain GUSDM4 and *Shewanella* sp. strain GUSDZ9

Antibiotic	Concentration (per disc)	Response of isolates	
		GUSDM4	GUSDZ9
Ampicillin (AMP)	10µg	S	S
Cephalothin (CEP)	5µg	R	R
Colistin sulphate (CL)	25µg	S	S
Gentamicin (GEN)	10µg	R	R
Streptomycin (S)	10µg	R	R
Tetracycline (TE)	30µg	R	R
Neomycin (N)	30µg	R	R
Polymyxin-B (PB)	300 Units	R	R
Penicillin-G (P)	10 Units	S	S
Co-Trimoxazole (COT)	25µg	R	R
Chloramphenicol (C)	30µg	R	R
Bacitracin (B)	10 Units	S	S
Erythromycin (E)	15µg	S	S

Key: R resistant; S sensitive

3.12 Cross tolerance of selected selenite and tellurite resistant bacteria

The isolate GUSDM4 and GUSDZ9 showed tolerance to metals and metalloid in the presence of respective metalloids (Fig. 3.24). The isolate GUSDM4 tolerated the highest concentration of Mn (20 mM) followed by Cr (22 mM) and least was found to be for Pb (5 mM). Similar observations were recorded in case of GUSDZ9 which showed the highest tolerance to Mn (25 mM) and least for Pb (7.5 mM). The mechanism involving efflux pumps is usually present in prokaryotes to reduce the metal and metalloid toxicity. This mechanism is not very specific in nature for instance, *PbrA* can efflux Pb as well as Zn ions. Additionally, the structural analogy between various metals and metalloids is also responsible for cross-tolerance. Therefore, the feature of cross-tolerance can be a result of the operation of various such non-specific mechanisms in bacterial cells that govern metal and metalloid resistance (Naik et al., 2012).

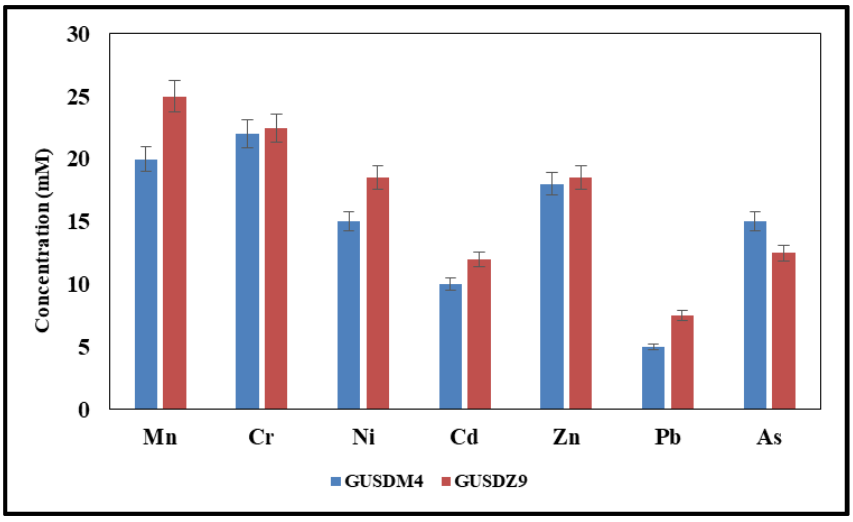

Fig. 3.24 Cross tolerance of *Halomonas* sp. strain GUSDM4 and *Shewanella* sp. strain GUSDZ9 to other metals and metalloid.

Summary

Morphologically **50** and **20** dissimilar bacterial colonies reducing selenite and tellurite respectively were isolated from different marine and estuarine habitats of Goa. The isolates namely GUSDM4 and GUSDZ9 exhibiting remarkably highest MTC of **100** and **5.5** mM towards Na_2SeO_3 and K_2TeO_3 respectively were selected for further studies. Bacterial strain GUSDM4 and GUSDZ9 were identified as ***Halomonas* sp.** and ***Shewanella* sp.** based on various biochemical tests and 16S rRNA gene sequencing.

SEM analysis of the bacterial cells exposed to selenite and tellurite revealed exclusive morphological alterations whereas, EDS analysis did not demonstrate surface adsorption of metalloids indicating internalization of metalloids. XRD analysis of the bacterial cells exposed to selenite and tellurite showed distinctive peaks which attributed to elemental Se and Te respectively. FTIR analysis also indicated the interactions of metals with the selective functional groups present on the bacterial cell wall.

The 2, 3-diaminonathtalene spectroscopic analysis evidently demonstrated **93** and **96 %** utilization of selenite at the end of the stationary growth phase (58 h) at **4** and **2** mM respectively. The Diethyl-dithiocarbamate based colorimetric analysis demonstrated complete reduction of **1** and **2** mM tellurite to elemental tellurium during the late stationary phase (34 & 38 h). Both the isolates showed resistance to a number of antibiotics and cross-tolerance to most of the metals and metalloid viz. Mn, Cr, Ni, Cd, Zn, Pb and As.

Chapter IV

Biosynthesis, Optimization and Characterization of Se and Te Nanoparticles by Halomonas sp. strain GUSDM4 and Shewanella sp. strain GUSDZ9

4.1 Biosynthesis of Selenium Nanoparticles (SeNPs)

4.1.1 To determine the ability of *Halomonas* sp. to biosynthesize SeNPs during its growth phase and using cell free culture supernatant

Selenite reduction to elemental Se using strain GUSDM4 was evident by the colour change in the medium from yellow to brick red in flask supplemented with 2 mM Na_2SeO_3. Whereas, control flask without Na_2SeO_3 did not show any brick red colouration (Fig. 4.1). The brick red colouration is reported to be the firm evidence for SeNPs formation which is due to surface Plasmon resonance effect (Srivastava and Mukhopadhyay, 2013). These small biosynthesised SeNPs further grow by aggregation of newly formed SeNPs by Ostwald ripening process (Huang et al., 2007). Thus, it is very important to optimize the whole biosynthesis process for best results.

There are numerous reports available on biosynthesis of SeNPs mediated by terrestrial bacteria however, reports on exploitation of marine bacteria are scarce (Forootanfar et al., 2015; Srivastava and Kawshik, 2016; Samant et al., 2018). The culture supernatant did not show any colour change after 48 h of incubation thus indicating intracellular biosynthesis of SeNP. This report is one of its kind demonstrating the intracellular biosynthesis of SeNPs by *Halomonas* sp.

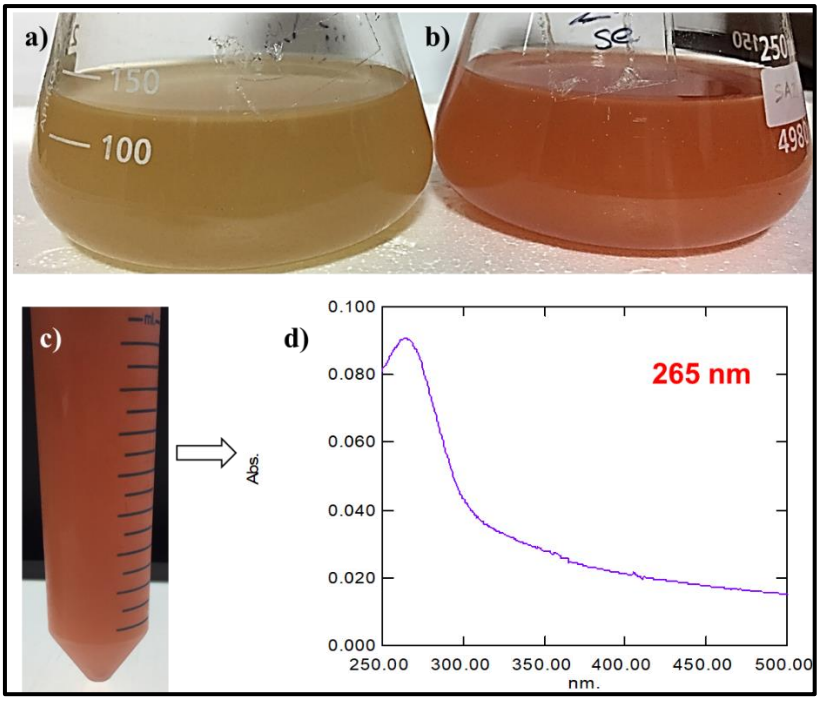

Fig. 4.1 Flasks showing (left to right) culture *Halomonas* sp. strain GUSDM4 grown in ZMB culture containing 0 mM Na_2SeO_3 (a), with 2 mM Na_2SeO_3 (b); Harvested SeNPs suspension (c); characteristic absorbance maxima of biogenic SeNPs using UV-Vis spectrophotometry (d).

SeNPs are of immense importance due to its diverse applications in medical, industrial and environmental fields. The properties of bulk selenium restrict its potential which are improved in nano-dimensions. These properties are usually associated with the varied size and shapes of nanomaterial thus, diversifying its applications. The researchers around the world are designing to develop economically viable and environmentally feasible methods for nanoparticle synthesis using biological approaches. The marine bacteria being robust are highly favourable since its takes place in ambient pressure and temperature conditions without the use of toxic chemicals.

4.1.2 Optimization of SeNPs biosynthesis during growth phase by *Halomonas* sp. strain GUSDM4

Optimization of SeNPs biosynthesis with respect to pH, temperature and Na_2SeO_3 was studied. The optimum pH, temperature and Na_2SeO_3 for SeNPs biosynthesis was found to be 7, 25 °C and 4 mM respectively (Fig. 4.2, 4.3 & 4.4). It was interesting to note that the estuarine strain GUSDM4 could synthesize SeNPs at broad temperature (25 to 40 °C) and pH (5 to 7) ranges. Although MTC for the strain GUSDM4 was recorded to be 100 the nanoparticle synthesis was not carried at such a high concentration since, it is a well-known fact that nanoparticles at high salt concentrations tends to aggregate forming particles with larger diameter which is undesirable. These reaction conditions including various experimental factors viz. pH, temperature and metalloid concentrations of the culture medium improves the chemical composition, shape, size distribution of NPs and allows maximum fabrication (Klaus et al., 1999).

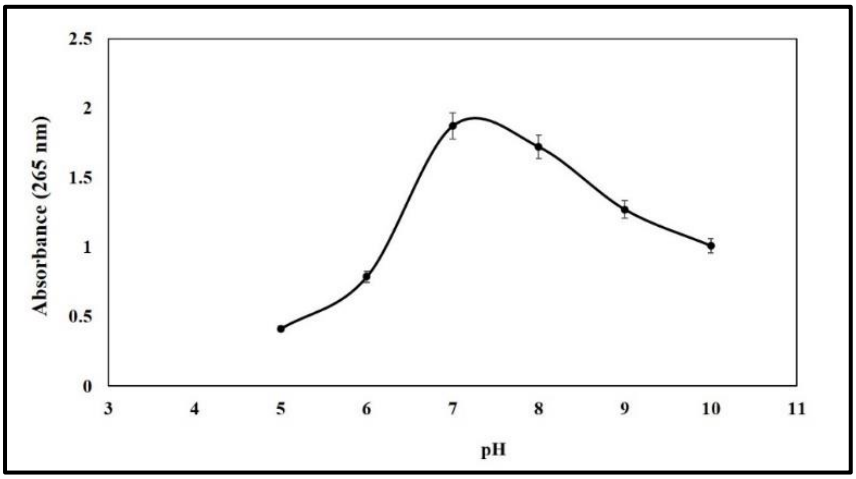

Fig. 4.2 Biosynthesis of SeNPs at different pH.

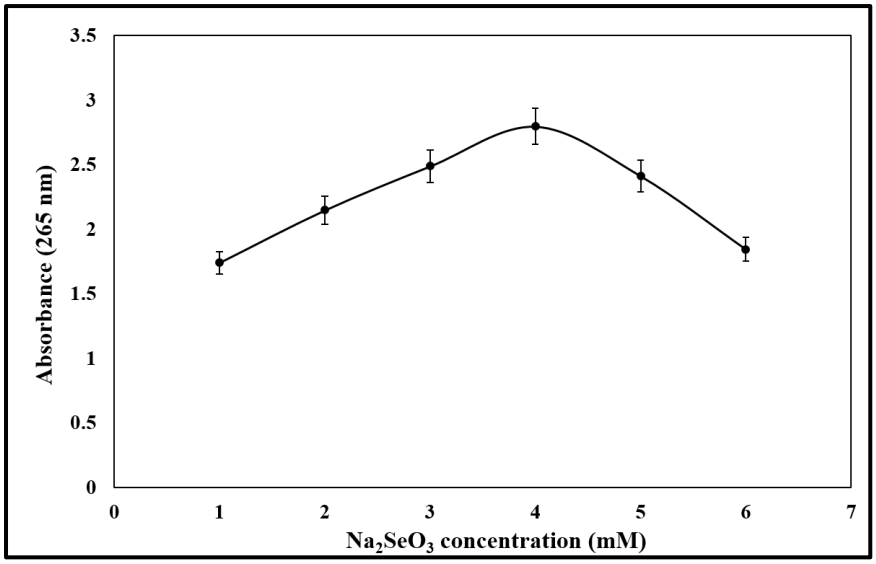

Fig. 4.3 Biosynthesis of SeNPs at different Na_2SeO_3 concentration.

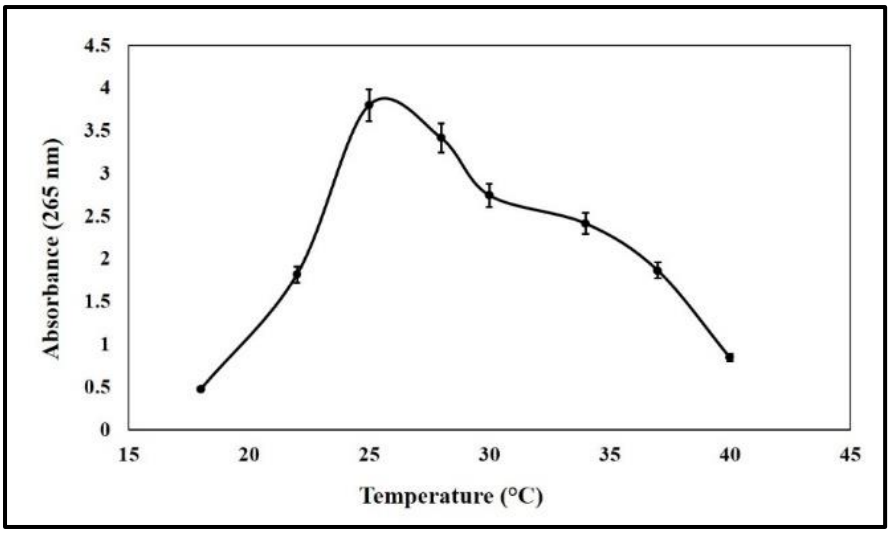

Fig. 4.4 Biosynthesis of SeNPs at different temperature.

4.1.3 Time course study of SeNPs biosynthesis during growth phase of *Halomonas* sp. strain GUSDM4

Time course study of SeNPs revealed that the biosynthesis was initiated during early bacterial log phase (4 h) which was evident from colour change in the media and a distinct peak at 265 nm (Fig. 4.5).

Biosynthesis of SeNPs was time dependent reaching maxima at 34 h of bacterial growth (Fig. 4.5). Previously, one of the studies on biosynthesis of SeNPs by marine strain of *Bacillus* sp. MSh-1 synthesized SeNPs after 14 h of incubation (Forootanfar et al., 2015). Additionally, in another study by Yazdi et al. (2013) the initiation of SeNPs biosynthesis was observed after 72 h of incubation. Keeping above facts into consideration our strain GUSDM4 is very efficient in biosynthesis of SeNPs.

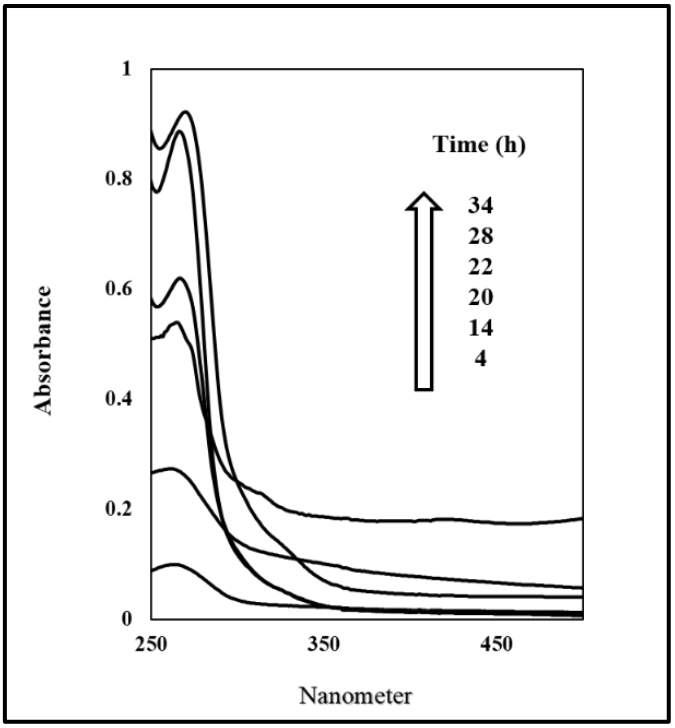

Fig. 4.5 Time course study of SeNPs biosynthesis under optimized conditions.

4.1.4 Harvesting of SeNPs

The SeNPs were harvested purified and made into powder using mortar and pestle and stored until used.

4.2. Characterization of biogenic SeNPs

4.2.1 UV-Vis spectroscopic analysis

An absorbance peak at 265 nm due to surface plasmon resonance was obtained of the brick red colloidal solution indicating the presence of SeNPs (Fig. 4.6) Similar findings conferring the biosynthesis of SeNPs have been published previously (Fesharaki et al., 2010; Srivastava et al., 2015).

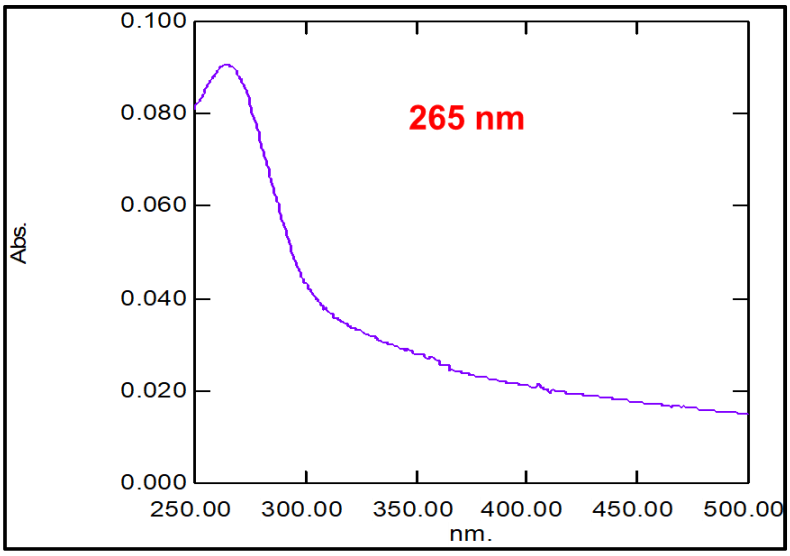

Fig. 4.6 Absorbance maxima for biosynthesized SeNPs at 265 nm.

4.2.2 Scanning electron microscopy (SEM) and Energy dispersive spectroscopy (EDS)

The EDS analysis depicted the presence of absorption bands at 1.5, 11.2 and 12.5 KeV further affirming the presence of elemental Se which is also conforming to previous reports (Fig. 4.7).

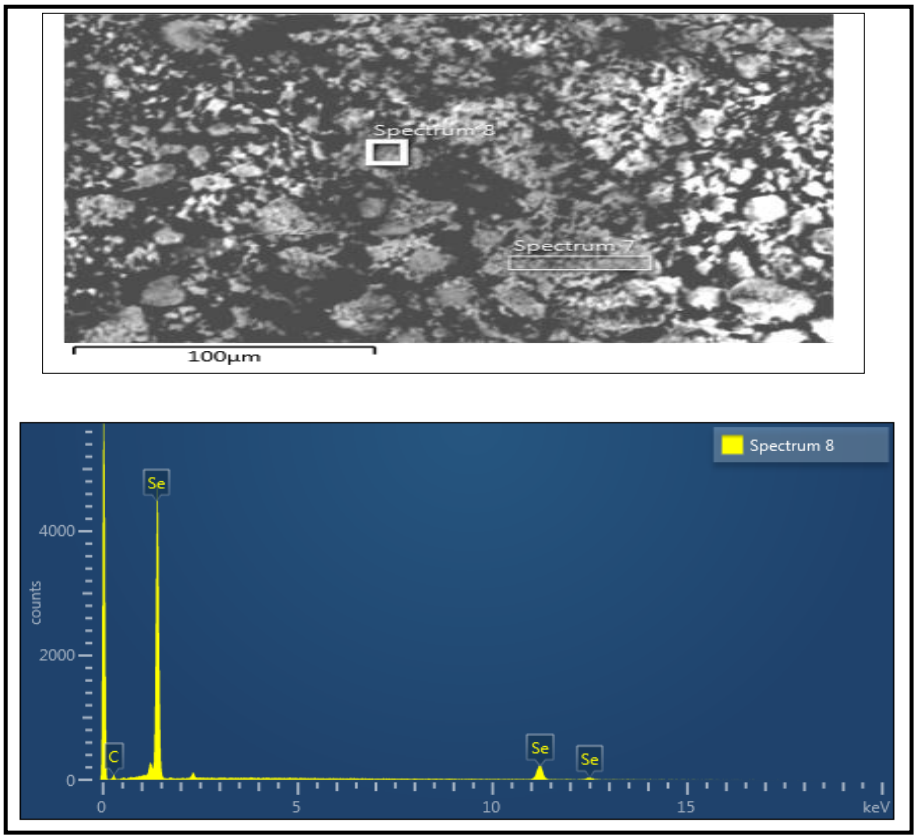

Fig. 4.7 SEM-EDS profile of biogenic SeNPs.

4.2.3 X-ray diffraction analysis

The XRD analysis revealed characteristic Bragg's peaks at 23.46, 29.76, and 43.72, conforming to [100], [101] and [110] lattices of hexagonal Se respectively (ICDD-card no.06-0362). The average particle size was found to be 37.27 nm (Fig. 4.8).

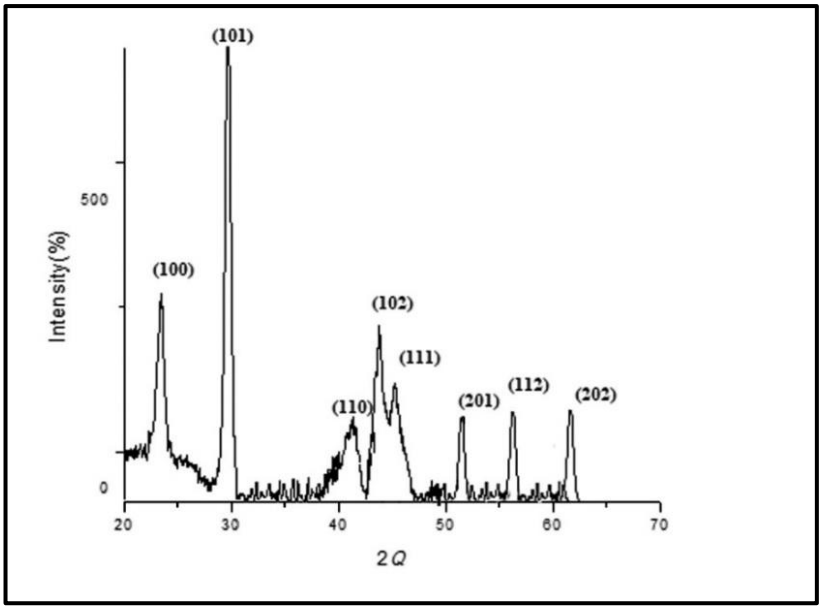

Fig. 4.8 XRD pattern for biosynthesized SeNPs exhibiting characteristics Bragg's peaks.

4.2.4 Transmission Electron Microscopic analysis and SAED analysis

TEM micrographs of SeNP revealed spherical morphology with size ranging from 20 nm to 60 nm diameter (Figs. 4.9 a, b, c & 4.10). Previously, biosynthesis of SeNPs using *Zooglea ramigera* reported the spherical shaped SeNPs ranging from 30-130 nm in diameter (Srivastava and Mukhopadhyay, 2013).

In yet another study size distribution of 200-400 nm was observed using the halophilic bacteria namely *B. selenitriducens, S. shriftii* and *S. barnesii* (Oremland et al., 2004). The SAED pattern further confirmed the crystalline nature of Se nanopheres exhibiting diffraction rings typical to hexagonal Se. Size play a major role in determining the functions of nanoparticles, smaller the size greater are the chances of enhancing its functionality and efficiency, the current study fulfils this criteria. Interestingly, our study is first evidence demonstrating SeNPs synthesis mediated by *Halomonas* sp. strain GUSDM.

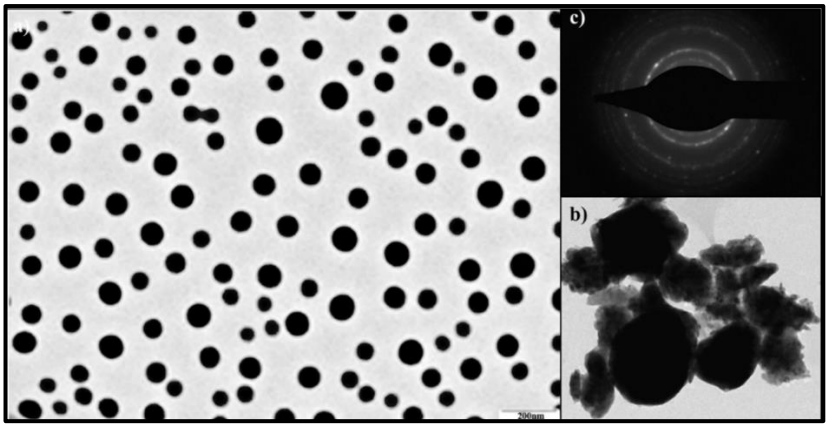

Fig. 4.9 TEM micrograph of biogenic SeNPs (a, b); SAED pattern of SeNPs corresponding to hexagonal crystal facets (c) (Inset).

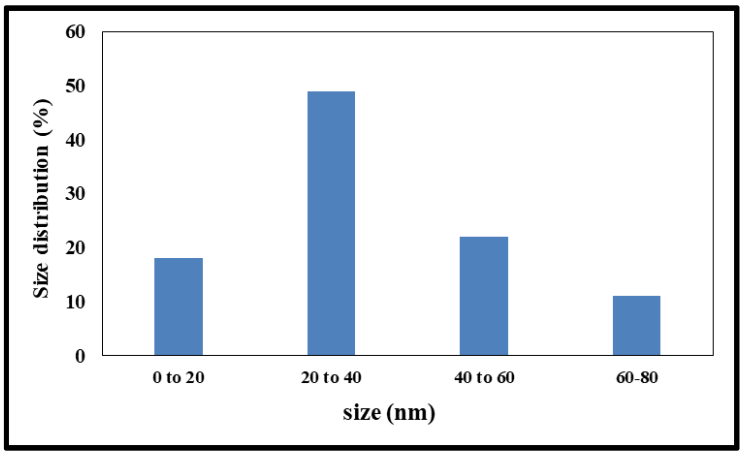

Fig. 4.10 Size distribution of biogenic SeNPs.

4.3 Biosynthesis of Tellurium Nanoparticles (TeNPs)

4.3.1 To determine the ability of *Shewanella* sp. strain GUSDZ9 to biosynthesize TeNPs during its growth phase and using cell free culture supernatant

Reduction of tellurite to elemental tellurium which is tentatively indicated by metallic black colouration was observed in culture supplemented with 2 mM K_2TeO_3. Control flasks without K_2TeO_3 and that of culture supernatant with 2 mM of K_2TeO_3 did not show any black colouration indicting that nanoparticle synthesis is growth

dependent and is intracellular (Fig. 4.11). Intracellular biosynthesis of TeNPs has been previously demonstrated in various bacteria viz. *Pseudomonas pseudoalcaligenes* KF707, *Shewanella oneidensis* and *Rhodococcus aetherivorans* (Di Tomaso et al., 2002; Kim et al., 2012; Presentato et al., 2016).

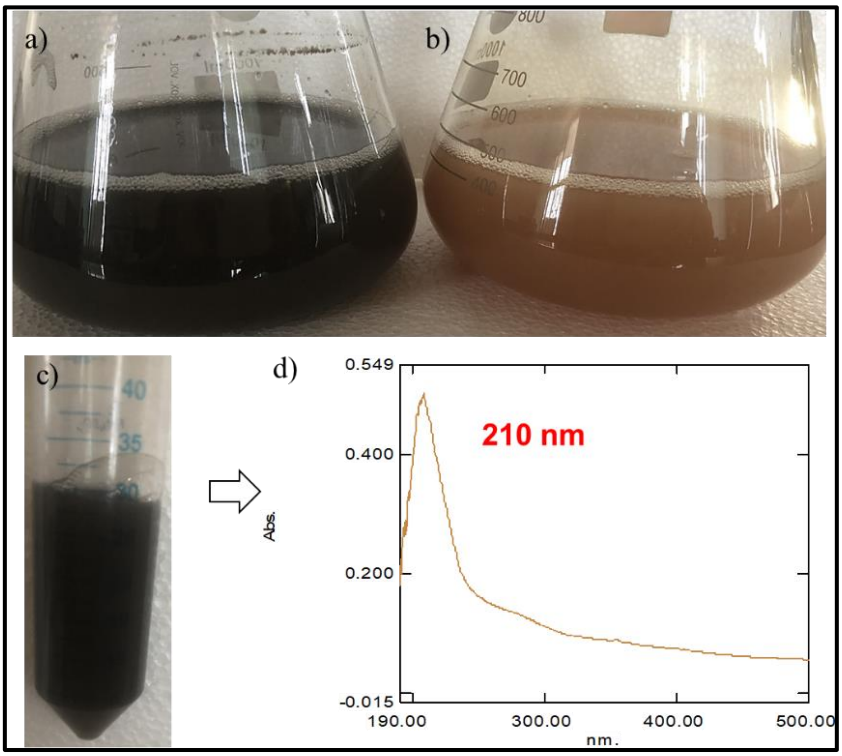

Fig. 4.11 Flasks showing (left to right) culture *Shewanella* sp. strain GUSDZ9 grown in ZMB containing 0 mM K_2TeO_3 (a), 2 mM K_2TeO_3 (b); Harvested TeNPs suspension (c); Characteristic absorbance maxima of biogenic TeNPs using UV- Vis spectrophotometry (d).

4.3.2 Optimization and time course studies of TeNPs biosynthesis during growth phase by *Shewanella* sp. strain GUSDZ9

Optimum K_2TeO_3 concentration and pH for TeNPs biosynthesis were found to be 2 mM and 7 respectively (Fig. 4.12, 4.13 & 4.14). It was interesting to note that the strain GUSDZ9 could synthesize TeNPs at broad pH range i.e. 6-10, tellurite concentrations from (0.5-3 mM) and at different temperature (25 to 37 °C). However, variation in the

intensity of black colouration was observed indicating differences in the extent of TeNPs biosynthesis at different pH and K_2TeO_3 concentrations.

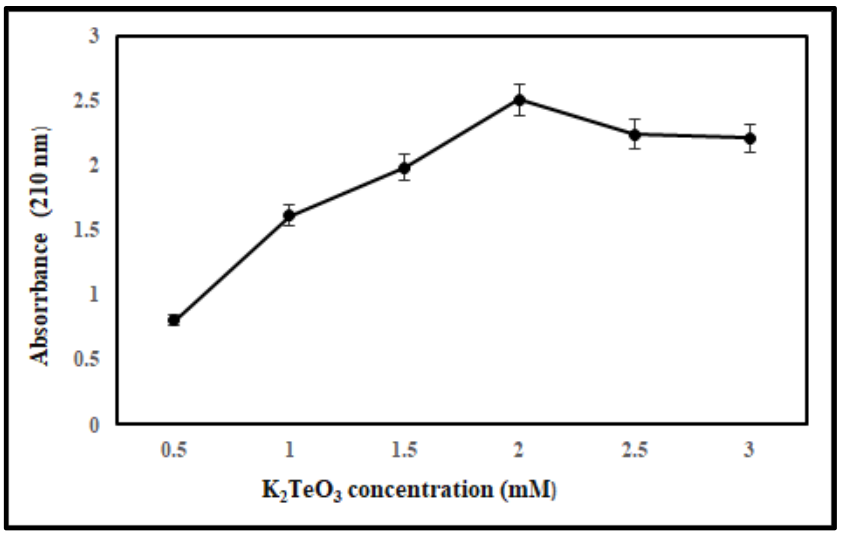

Fig. 4.12 Biosynthesis of TeNPs at different K_2TeO_3 concentrations.

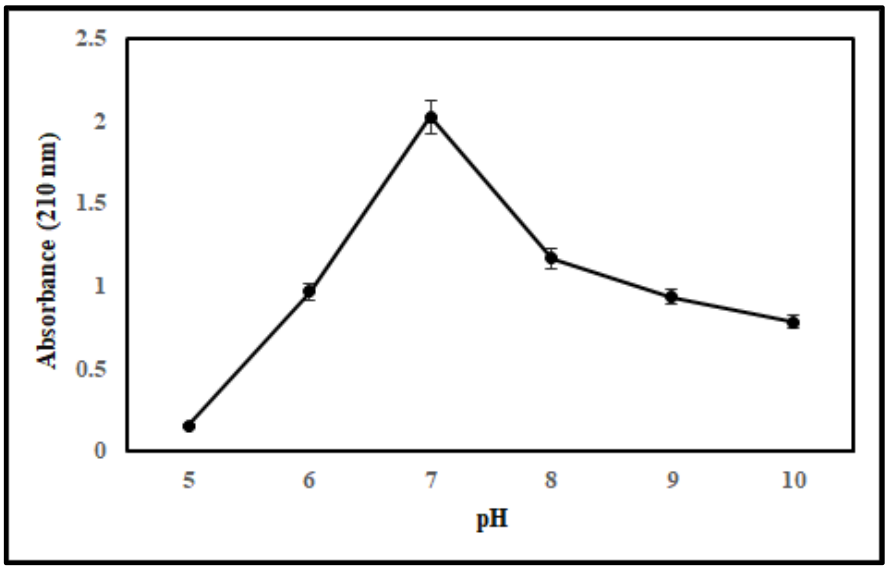

Fig. 4.13 Biosynthesis of TeNPs at different pH.

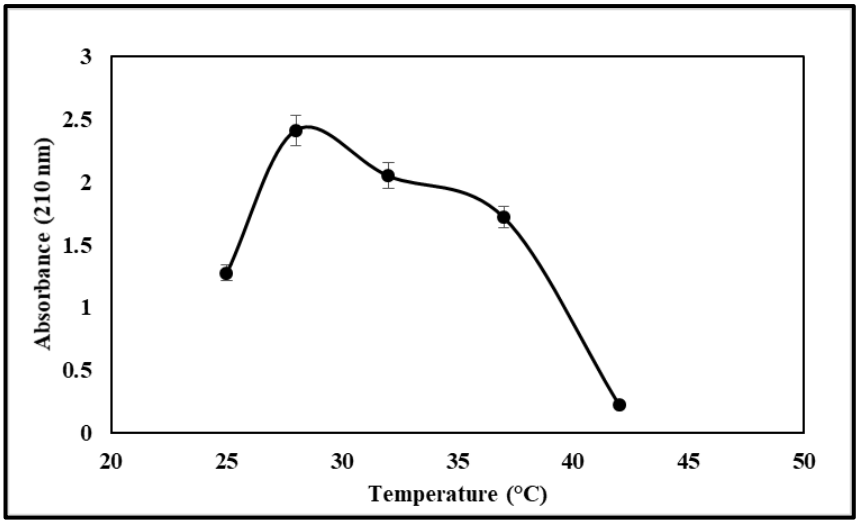

Fig. 4.14 Biosynthesis of TeNPs at different temperature.

4.3.3 Time course study

Biosynthesis of TeNPs was found to be time-dependent i.e. there was an increase in absorbance (210 nm) with time (Fig. 4.15). However, nanoparticle synthesis was found to be maximum during mid-log to early stationary phase. The optimum time for maximum nanoparticle synthesis was found to 28 h. Even though complete reduction of tellurite was observed at the end of the stationary phase there was a shift in surface plasmon resonance for TeNPs after early stationary phase indicating the formation of TeNPs with a larger diameter.

A similar shift in surface plasmon with the formation of larger diameter nanoparticles has been reported (Stoeva et al., 2002). Our strain synthesises TeNPs faster than the previously reported bacterial strain *Pseudomonas pseudoalcaligenes* KF707 (Di Tomaso et al., 2002) since the Te crystallites' synthesis began at the mid-exponential phase.

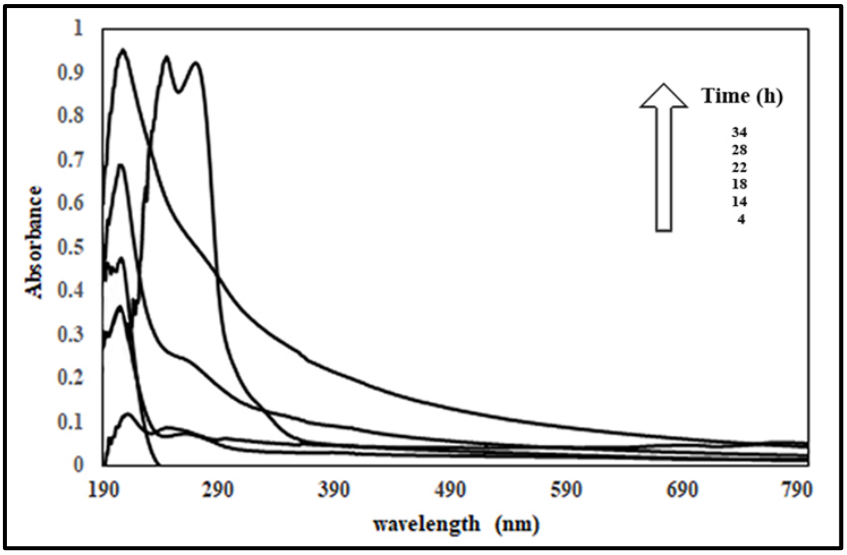

Fig. 4.15 Time course study for TeNPs under optimized conditions.

4.3.4 Characterization of biogenic TeNPs

4.3.4.1 UV-Vis analysis

An absorption peak at 210 nm by the black colloidal solution due to surface plasmon resonance clearly indicated the presence of TeNPs (Fig. 4.16). Similar findings have already been published confirming synthesis of TeNPs (Gautam and Rao, 2004; Zare et al., 2012; Forootanfar et al., 2015).

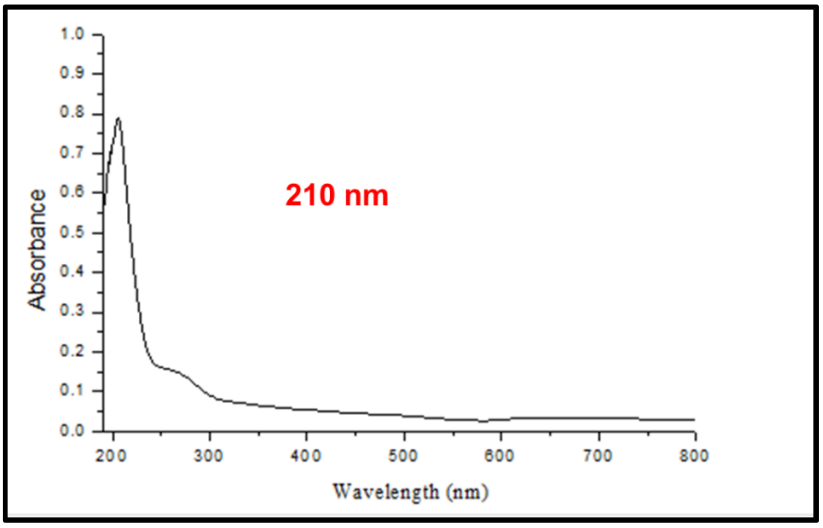

Fig. 4.16 Absorbance maxima for biosynthesized TeNPs at 210 nm using UV-Vis spectrophotometry.

4.3.4.2 XRD analysis

The XRD spectrum clearly illustrated characteristic Bragg's peaks at 23.02, 27.5, 38.2, 40.5, 47.0 and 49.65 which indiced to [100], [101], [102], [110], [200] and [201] of hexagonal phase of Te nanocrystals. (Fig. 4.17). The average grain size was found to be 57.7 nm. This was in accordance with a standard card of tellurium (ICDD card no. 36) and is also in agreement with the earlier report (Yuan et al., 2013; Manikandana et al., 2015; Srivastava et al., 2015).

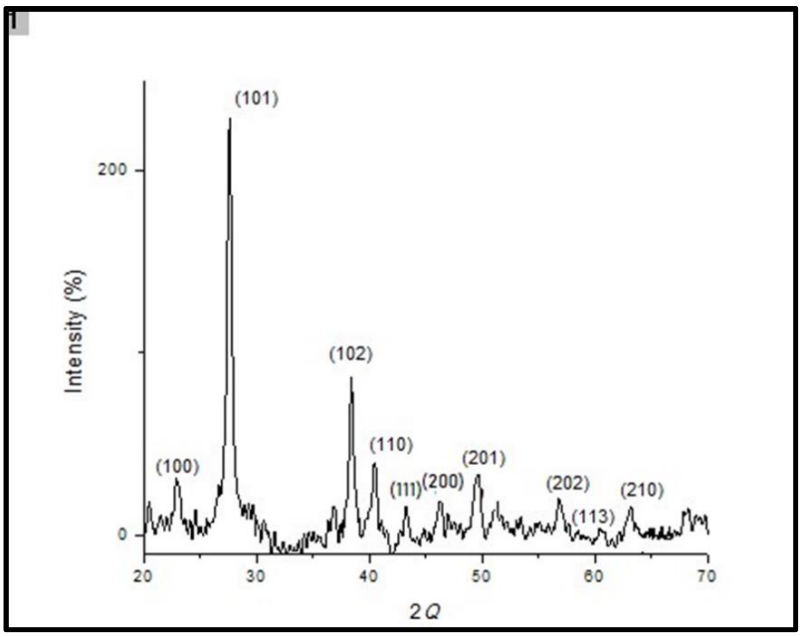

Fig. 4.17 XRD pattern for biosynthesized TeNPs exhibiting characteristics Bragg's peaks.

4.3.4.3 TEM and SAED analysis

TEM analysis of nanoparticles revealed unique nano-rod morphology for TeNPs with a diameter in the range of 8 to 75 nm (Fig. 4.18 & 4.19). Previously, various bacterial isolates have been reported to synthesize Te nano-rods viz. *Bacillus selenitireducens* (10 nm), *Shewanella oneidensis* MR-1 (10-20 nm), *Bacillus* sp. (20 nm), *Shewanella oneidensis* (10-20 nm) and *P. pseudoalcaligenes* (22 nm)

(Baesman et al., 2007; Kim et al., 2012; Zare et al., 2012; Mohanty et al., 2014; Forootanfar et al., 2015). However, nano-sphere and needle-shaped TeNPs have also been reported (Di Tommaso et al., 2002; Klonowska et al., 2005). Interestingly, our study is the first evidence demonstrating TeNPs biosynthesis by *Shewanella baltica*.

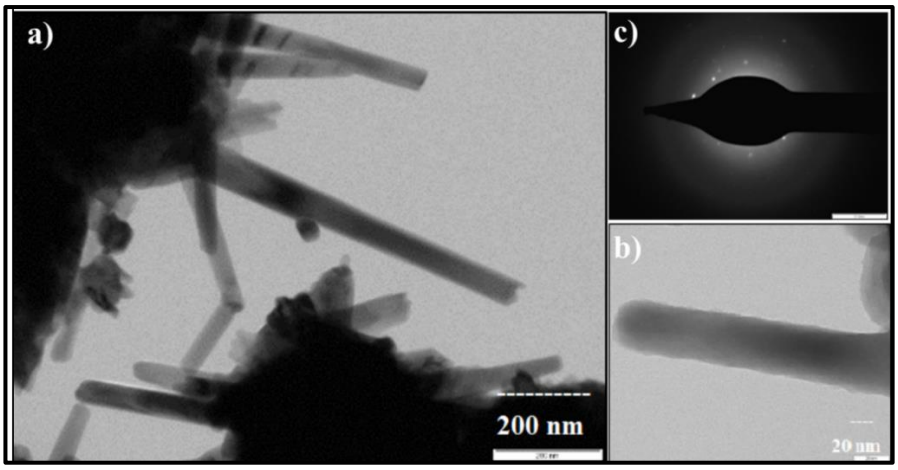

Fig. 4.18 TEM micrograph of biogenic TeNPs (a, b); SAED pattern of TeNPs corresponding to hexagonal crystal facets (c) (Inset).

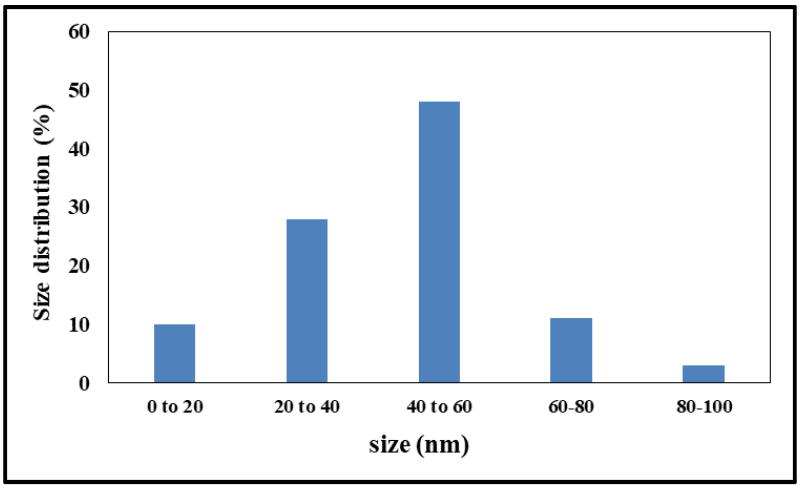

Fig. 4.19 Size distribution of biogenic TeNPs

4.3.4.4 Scanning electron microscopy (SEM) and Energy dispersive spectroscopy (EDS)

EDS analysis of TeNPs clearly revealed a prominent peak of elemental tellurium at 3.6 keV (Fig. 4.20) which gave the clear indication of presence of Te. However, the peak due to carbon may be attributed to the carbon taped sample holder as well as coating with carbon.

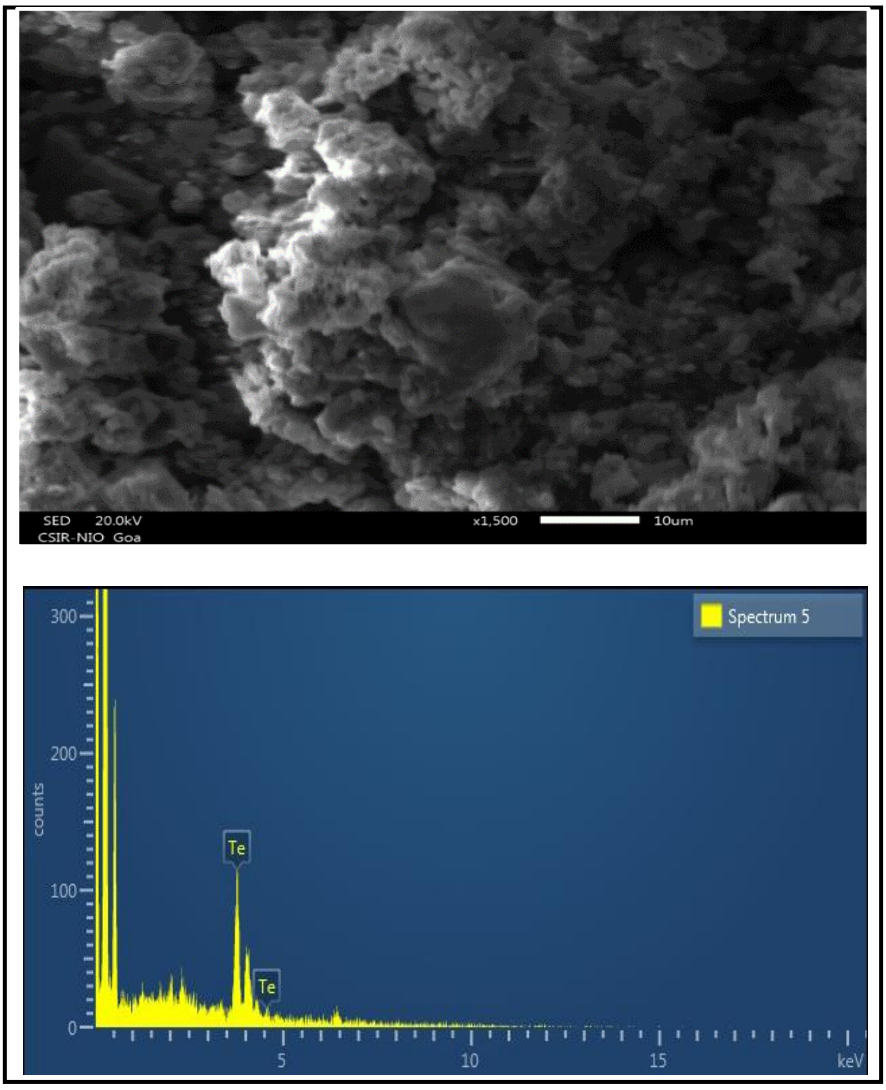

Fig. 4.20 SEM-EDS profile of TeNPs biosynthesized *by Shewanella* sp. strain GUSDZ9.

Summary

Biosynthesis of SeNPs initiated during early log phase (within 4 h) which was clearly evident from colour change and a characteristic peak at 265 nm due to surface plasmon resonance revealed by UV-Vis spectrophotometry. Optimum pH, salt concentrations, temperature and time was found to be 7, 4 mM, 25 °C and 34 h respectively for SeNPs biosynthesis. Characterization of SeNPs by X-ray crystallography, selected area electron diffraction and transmission electron micrography revealed spherical nanoparticles with hexagonal crystal lattice and diameter in the range from 20-80 nm. The energy dispersive X-ray analysis also confirmed presence of pure elemental selenium (Se^0).

TeNPs biosynthesis which initiated at early log phase (i.e. 4 h) was evidently monitored through colour change and a peak due to surface plasmon resonance at 210 nm using UV-Vis spectroscopic analysis. Optimum pH, salt concentrations temperature and time was found to be 7, 2 mM, 28 °C and 28 h respectively for TeNPs biosynthesis. X-ray crystallographic studies and transmission electron microscopy revealed unique nano-rods with a diameter ranging from 8-75 nm and average length of 80-300 nm. Energy dispersive X-ray analysis further confirmed presence of pure elemental tellurium.

Chapter V

Mechanism of Selenium and Tellurium Nanoparticles Biosynthesis

PART A

5.1. Localization of Se and Te NPs biosynthesis in *Halomonas* sp. strain GUSDM4 and *Shewanella* sp. strain GUSDZ9

5.1.1 Transmission electron microscopic (TEM) analysis

TEM analysis revealed electron dense deposits throughout the periplasm of *Halomonas* sp. on exposure to selenite but it was distinctly absent in the control cells (Figs. 5.1, 5.2). Moreover, intracellular spherical deposits of SeNPs were also visible within the bacterial periplasm. Similar intracellular selenium naospheres were also observed in *Bacillus cereus* (Dhanjal and Cameotra, 2010). Biosynthesis of spherical nano-Se in periplasmic space has also been reported in *Pseudoalteromonas* sp. strain Se-1-1 (Rathgeber et al., 2002). In yet another study similar intracellular biosynthesis of SeNPs have also been reported earlier in *Pantoea agglomerans* (Torres et al., 2012). These reports have further strengthened our findings that *Halomonas* sp. strain GUSDM4 is also capable of periplasmic synthesis and localization of SeNPs.

The cells of *Shewanella sp.* GUSDZ9 synthesized Te nanorods in the test culture on exposure to sodium tellurite, whereas no such distinct structures were observed in the control cultures which were not exposed to tellurite (Figs. 5.3, 5.4). However, unlike *Halomonas* sp. strain GUSDM4, cytoplasmic synthesis and localization of Te nanorods was observed in *Shewanella sp.* GUSDZ9. Intracellular deposition of Te nanorods has been also reported in *Bacillus* sp. BZ (Zare et al., 2012).

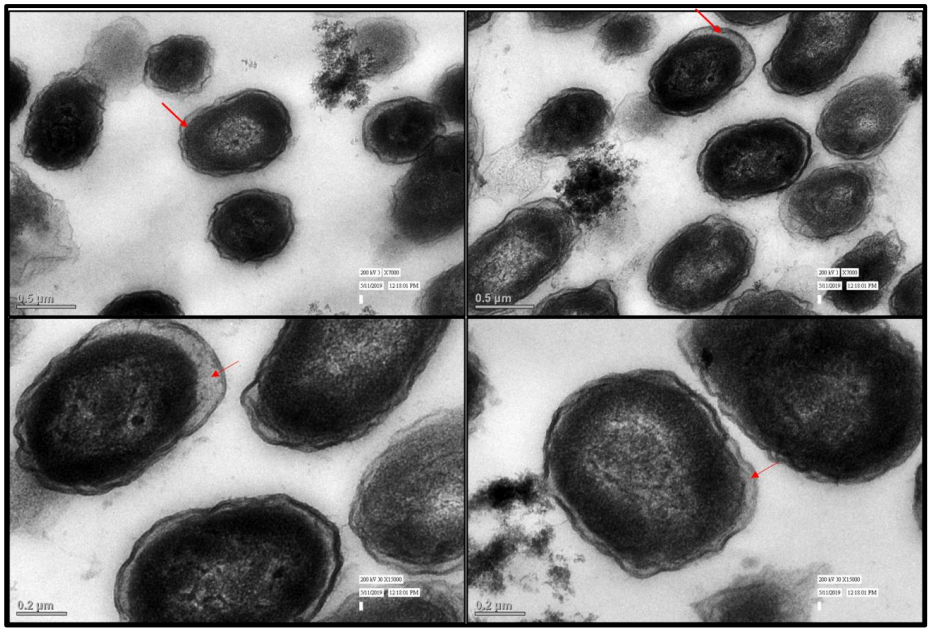

Fig. 5.1 Transmission electron micrographs of cells of *Halomonas* sp. strain GUSDM4: Bacterial cells without sodium selenite exposure showing clear periplasm (magnification, from left to right: 7000X, 7000X, 15000X and 15000X).

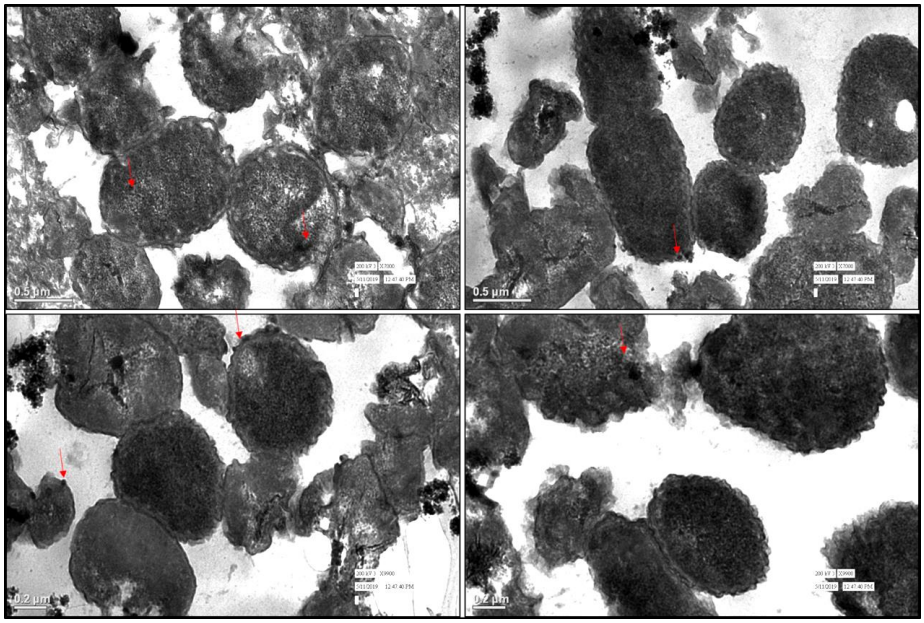

Fig. 5.2 Transmission electron micrographs of cells of *Halomonas* sp. strain GUSDM4: Bacterial cells exposed to 4 mM Na_2SeO_3 showing periplasm with dark granules of SeNPs. Red arrows indicate localization of Se nanospheres (Magnification from left to right: 7000 X, 7000X, 9900X and 9900X).

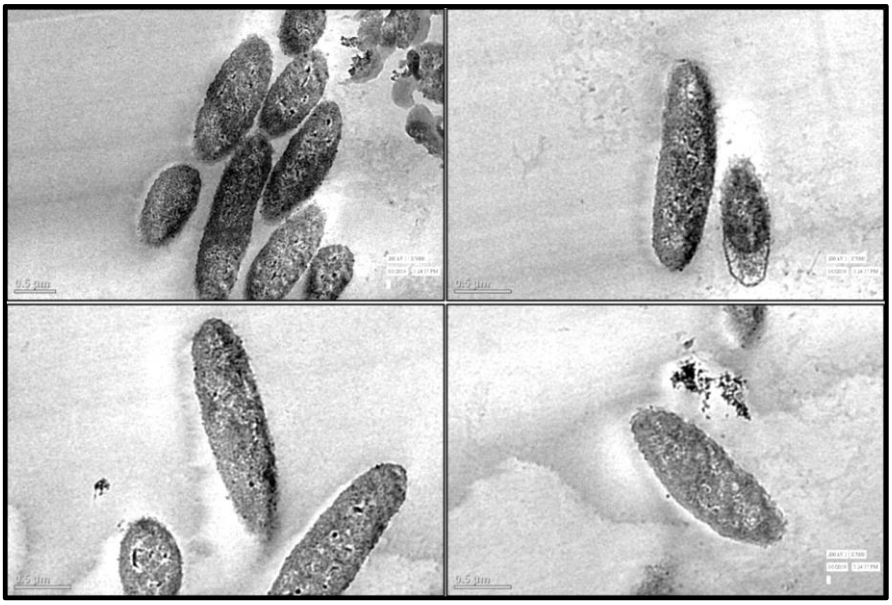

Fig. 5.3 Transmission electron micrographs of cells of *Shewanella* sp. strain GUSDZ9: Bacterial cells without K_2TeO_3 exposure. (Magnification from left to right: 5000X, 7000X, 15000X and 15000X).

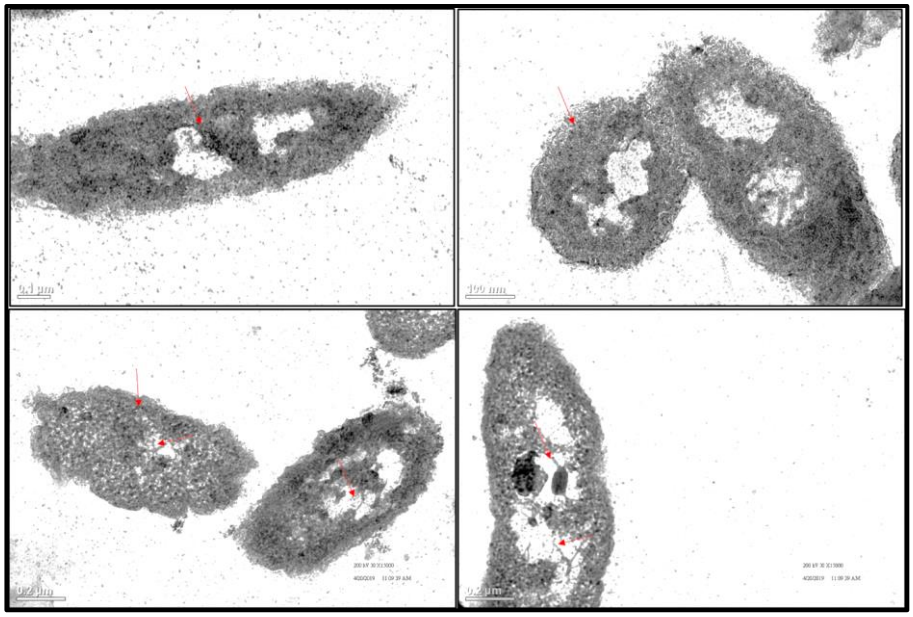

Fig. 5.4 Transmission electron micrographs of cells of *Shewanella* sp. strain GUSDZ9: Bacterial cells exposed to 2 mM K_2TeO_3. Red arrows indicate localization of Te nanorods (magnification from left to right: 15000X, 15000X, 15000X and 15000X).

5.2 Assessment of role of nitrate reductase in biosynthesis of Se and Te NPs

Addition of Griess-Ilosvay's reagent to the cell free supernatant showed pink colouration demonstrating nitrate reductase activity in both *Halomonas* sp. strain GUSDM4 and *Shewanella* sp. strain GUSDZ9. The concentration of nitrite formed in presence of 0.2 mM and 2 mM Na_2SeO_3 was similar (i.e. 33-34 nM) to that of the control (cells grown without Na_2SeO_3/KNO_3). However, due to the increase in substrate for NR higher nitrite content was observed in cell free extract of cells grown with 0.2 mM and 2 mM potassium nitrite (40 and 48 nM) respectively (Fig. 5.5). Likewise, the cell free extract of the cells with 0.2 mM and 2 mM sodium selenite exhibited similar NR activity (6.2 and 6.3 nM Nitrite/min/mL) as control (6.2 nM Nitrite/min/mL) [Fig. 5.7]. However, as compared to control higher NR activity of cell free extract from the cells grown with 0.2 mM and 2 mM KNO_3 was observed.

Similar trend was also observed in case of *Shewanella* sp. grown in presence of 0.2 mM and 2 mM potassium tellurite (Fig. 5.6). in this case, the nitrite content was 33 nM for both and NR activity was 6.34 and 6.39 nM Nitrite/min/mL respectively which was parallel to that of the control (6.24 nM Nitrite/min/mL) [Fig. 5.8]. Since nitrite content and NR activity in presence of selenite and tellurite was found to be comparable to that of the control cells, it may be inferred that NR may not be involved in Se and Te NPs biosynthesis. Even though we have successfully demonstrated the periplasmic localization of SeNPs but our observations suggest that NR being a periplasmic reductase, may not be involved in biosynthesis of SeNPs.

Microorganisms are known to tolerate high levels of these toxic metalloids, but the mechanisms are poorly understood. However, periplasmic NR and intracellular NR have been reported previously (Hunter and Kuykendall, 2007; Hunter, 2007).

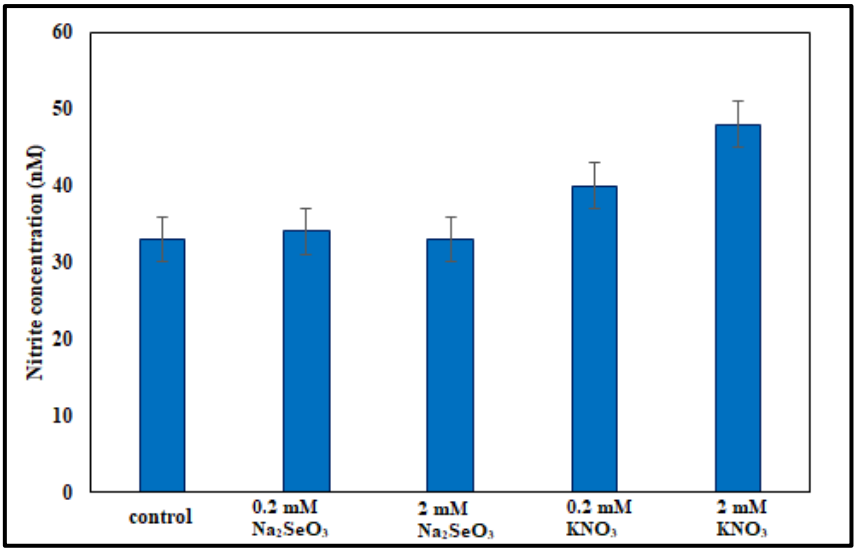

Fig. 5.5 Nitrite content in *Halomonas* sp. strain GUSDM4 grown in nitrate broth.

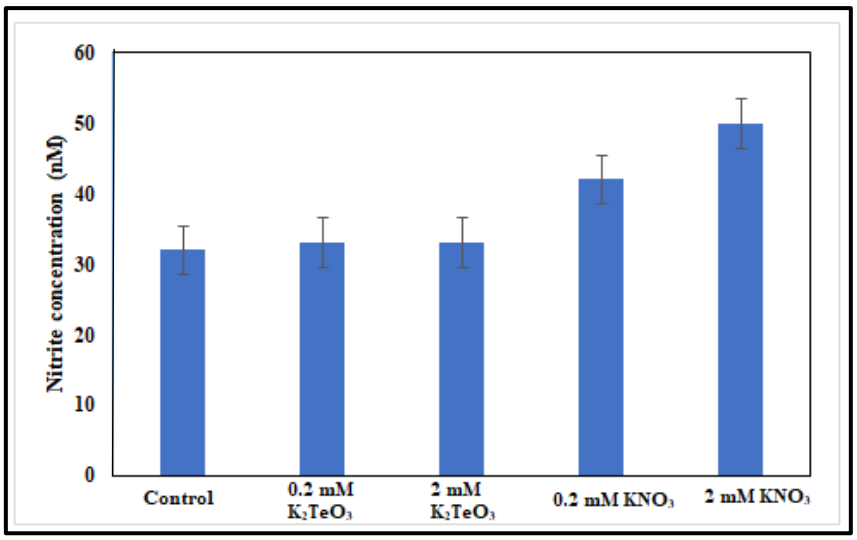

Fig. 5.6 Nitrite content in *Shewanella* sp. strain GUSDZ9 grown in nitrate broth.

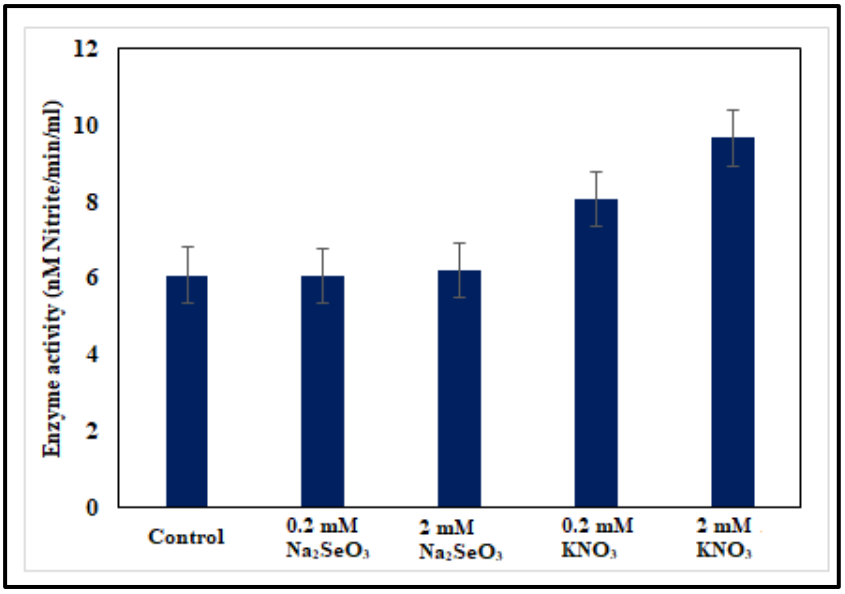

Fig. 5.7 Nitrate reductase activity of *Halomonas* sp. strain GUSDM4 grown in nitrate broth.

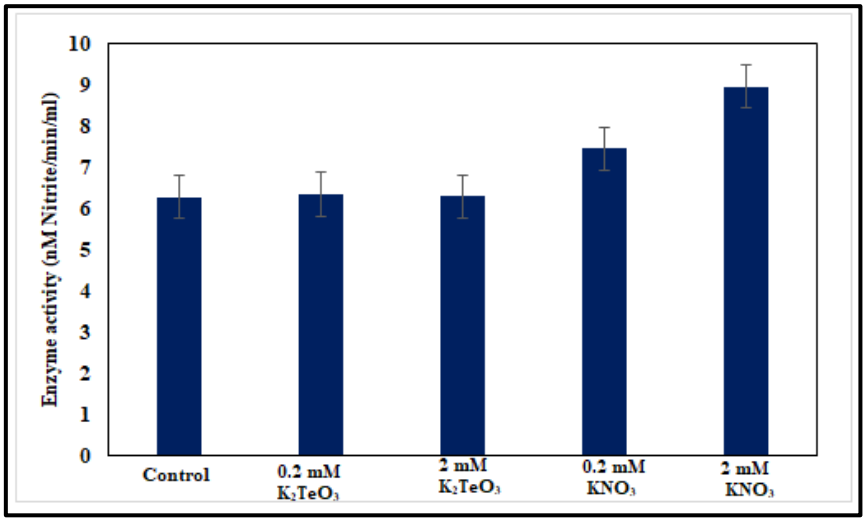

Fig. 5.8 Nitrate reductase activity in *Shewanella* sp. strain GUSDZ9 grown in nitrate broth.

5.3 Assessment of role of selenite reductase and tellurite reductase in biosynthesis of Se and Te NPs

5.3.1 Selenite and tellurite reductase activity

Selenite reductase has been reported in certain bacteria and actinobacteria viz. *Pseudomonas* sp. strain CA5, *Rhizobium selenitireducens, Streptomyces* sp. strain M10A65, *Streptomyces* sp. strain ES2-5 which catalyses selenite reduction and SeNPs biosynthesis (Hunter et al., 2009, 2014; Tan et al., 2016; Ramya et al., 2020). Increasing selenite reductase activity in presence of NADH demonstrates its significant role as a coenzyme of selenite reductase. It was interesting to note that selenite reductase (SR) activity was highest in periplasmic fraction (i.e. 20.25 U/mg protein) as compared to spheroplast (i.e. 10.56 U/mg protein) and cell lysate (i.e. 15.48 U/mg protein) fractions (Table 5.1). This also corroborate with our TEM analysis which evidently proved periplasmic synthesis of SeNPs. Thus, Selenite reductase activity of *Halomonas* sp. strain GUSDM4 is NADH dependent which is responsible for selenite reduction as well as SeNPs biosynthesis.

Tellurite reduction mediated by tellurite reductase (TR) has been reported in several bacteria viz. *E. coli, Mycobacterium avium, Thermus thermophiles HB8* and *Streptococcus faecalis* (Cooper and Few, 1952; Terai et al., 1958; Chiong et al., 1988b). Reduction of tellurite to elemental tellurium in presence and lack of NADH (Co-enzyme) was used to estimate tellurite reductase activity by measuring increase in absorbance at 210 nm. (Pearion and Jablonski, 1999). The specific enzyme activity of cells grown in presence of 2 mM tellurite was highest (i.e. 15.36 U/ mg protein) in cell lysate fraction as compared to spheroplast and periplasmic fractions (i.e. 5.89 and 9.54 U/mg protein respectively) [Table 5.2].

This further corroborate our TEM analysis which confirmed cytoplasmic biosynthesis of TeNPs by *Shewanella* sp. strain GUSDZ9. Therefore, we can infer that tellurite reductase, a NADH-dependent

reductase is involved in tellurite reduction and TeNPs biosynthesis. Although this study has clearly demonstrated involvement of TR activity in tellurite reduction but involvement of more mechanisms in tellurite reduction and TeNPs synthesis may not be ruled out (Zannoni et al., 2007).

From the above outcomes, the probable mechanism of biosynthesis of Se and Te NPs were explained. Once bacteria encounter these metalloids (namely selenite and tellurite) they are internalised via various influx pumps which are either specific or nonspecific to metals/ metalloids. For instance, in case of tellurite, influx pumps mainly *ActP* and *PitA* are reported to be responsible for uptake (Borghese and Zannoni, 2010; Elías et al., 2015). Upon internalization reductase (s) viz. selenite and tellurite reductase (s) present in the respective bacterial cell compartments are responsible for the reduction of selenite and tellurite into their elemental forms. The reduction process is initialized by transfer of electron from NADH to the metalloid ions by these enzymes. Subsequently, the electrostatic interactions of the positive charge present on these enzymes trap the negatively charged selenite (SeO_3^{2-}) and tellurite (TeO_3^{2-}) ions which results in the formation of Se and Te NPs respectively (Fig. 5.9 a, b).

Table 5.1: Selenite reductase activity of *Halomonas* sp. grown in presence of 2 mM Na_2SeO_3

S. N.	Fractions	Enzyme activity (U/mg protein)
1.	Cell lysate crude	15.48
2.	Periplasmic crude	20.25
3.	Spheroplast crude	10.56
4.	Periplasmic without NADH	0.01

Table 5.2: Tellurite reductase activity of *Shewanella* sp. grown in presence of 2 mM K_2TeO_3

S. N.	Fractions	Enzyme activity (U/mg protein)
1.	Cell lysate crude	15.36
2.	Periplasmic crude	5.89
3.	Spheroplast crude	9.54
4.	Cell lysate without NADH	0.01

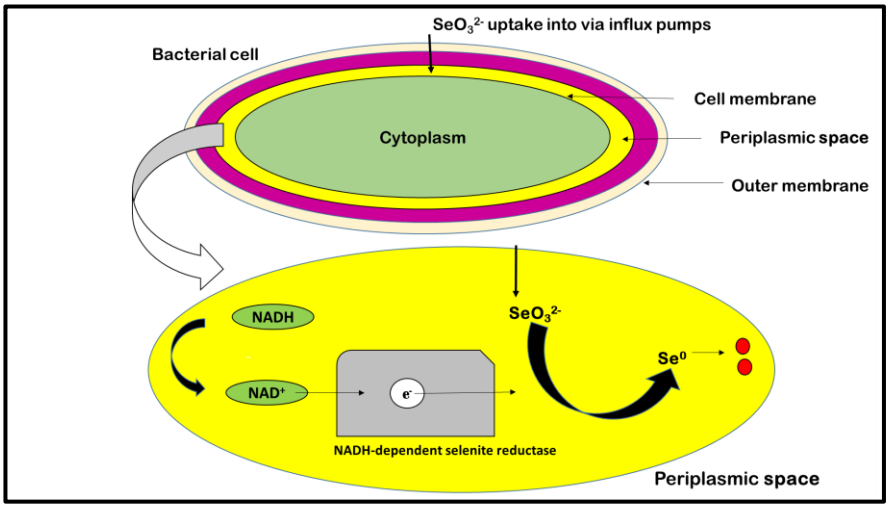

Fig. 5.9 a Schematic representation of probable mechanism involved in SeNPs biosynthesis by *Halomonas* sp. strain GUSDM4.

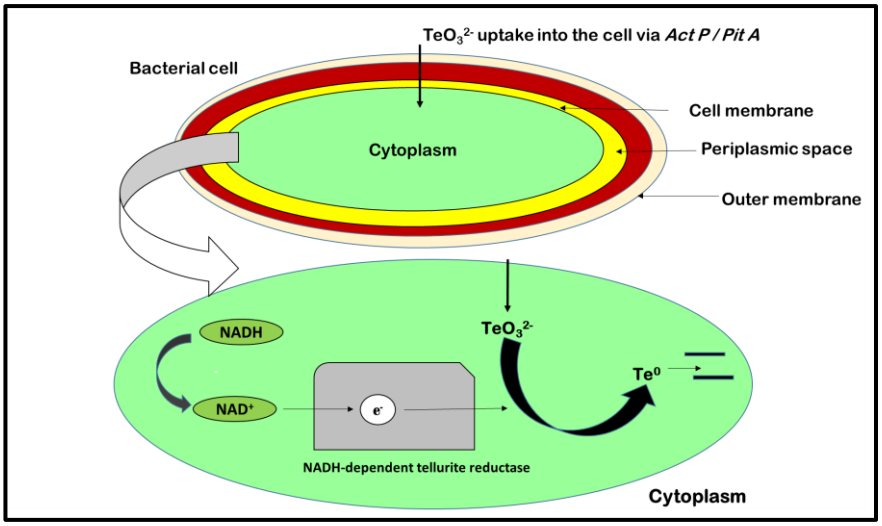

Fig. 5.9 b Schematic representation of probable mechanism involved in TeNPs biosynthesis by *Shewanella* sp. strain GUSDZ9.

PART B

5.4 Genetic determinants of *Shewanella* sp. GUSDZ9 in tellurite resistance/TeNPs biosynthesis

5.4.1 Whole genome sequence analysis of Tellurite reducing *Shewanella sp*. strain GUSDZ9

5.4.1.1 General characteristics of whole genome of *Shewanella* sp. GUSDZ9

The draft genome sequence of *Shewanella* sp. strain GUSDZ9 clearly revealed that its size is approximately 4.9 Mbps with average GC content of 46 % along with 4292 genes. Other general features of its genome have been enlisted in Table 5.3. Gene ontology studies using Blast2GO platform further grouped the predicted genes into three domains/categories based on biological processes, molecular functions and cellular components (Fig. 5.10). Out of 4292 genes, 1,702 genes have been annotated by KAAS and are categorized into 23 KEGG categories (Table 5.4). The highest percent distribution of genes was

observed in case of amino acid metabolism pathway (i.e. 11.86 %) followed by genes involved in carbohydrate metabolism (i.e. 10.3 %). The percent distribution in case of metabolism of cofactors and vitamins was 10.4. However, it was interesting to note that percent distribution of genes involved in membrane transport was 5.3 % whereas for signal transduction it was 9.6 %.

Table 5.3: General characteristics of whole genome of *Shewanella* sp. GUSDZ9

Molecular Characteristics	Value
Total number of Genes	4292
% G + C Content	46
Number of Protein coding genes (CDS)	4177
Number of rRNAs	5
Number of tRNAs	47
Average size of gene	970 bps
Maximum size of gene	8085
Minimum size of gene	59
Size of Draft genome	~ 4.9 Mbps

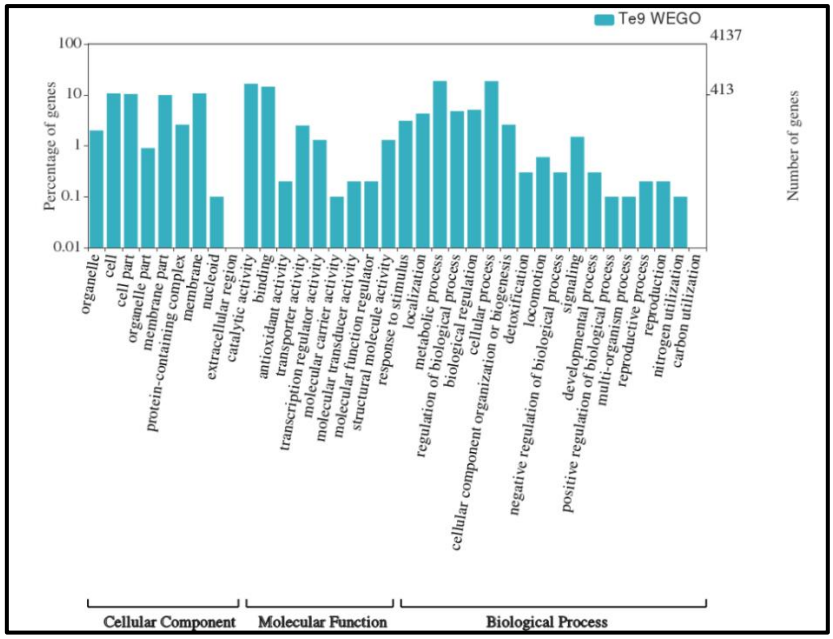

Fig. 5.10 Gene ontology of *Shewanella* sp. GUSDZ9 using WEGO.

Table 5.4: KEGG pathway classification of *Shewanella* sp. GUSDZ9

Pathways	No. of genes
Carbohydrate metabolism	177
Energy metabolism	139
Lipid metabolism	63
Nucleotide metabolism	82
Amino acid metabolism	202
Metabolism of other amino acids	61
Glycan biosynthesis and metabolism	39
Metabolism of cofactors and vitamins	176
Metabolism of terpenoids and polyketides	27
Biosynthesis of other secondary metabolites	45

Xenobiotics biodegradation and metabolism	**38**
Genetic information Processing	
Transcription	6
Translation	83
Folding, sorting and degradation	52
Replication and repair	53
Environmental information processing	
Membrane transport	90
Signal transduction	163
Cellular processes	
Transport and catabolism	16
Cell growth and death	28
Cellular community-eukaryotes	1
Cellular community-prokaryotes	77
Cell motility	65
Organismal system	
Environmental adaptation	**19**

5.4.1.2 Genes involved in tellurite resistance in *Shewanella* sp. strain GUSDZ9

The whole genome analysis of TeNPs biosynthesizing strain GUSDZ9 revealed various interesting tellurite determinants/genes (Table 5.5). Interestingly five genes conferring tellurite resistance viz. *tehB, pitA, terC, actP and trgB* were present in its genome. The *PitA* gene encoding phosphate transporter has also been reported in *Rhodobacter capsulatus* which actively participates in tellurite uptake (Borghese et al., 2008; Borghese and Zannoni, 2010). However, Elías

et al. (2015) reported involvement of *actP* in influx/uptake of tellurite in *E. coli* which was located upstream to *PitA* gene encoding phosphate transporter. In another study the operon *tehAB* involved in tellurite resistance has been reported in *R. sphaeroides* and *E. coli* where, *teh B* is the cytoplasmic protein involved in tellurite resistance (Taylor et al. 1994; Fleischmann et al. 1995; Turner et al., 1995b).

Liu and Taylor, (1999) reported that *tehB* alone has the ability to confer tellurite resistance in *Streptococcus* sp. However, despite of reports in various organisms its exact function is not clear. Tellurite determinant t*erC* is part of t*er* operon, t*erZABCDE* which is mainly responsible for tellurite reduction. However, in *Proteus mirabilis* a single transcript of *terC* was found to be induced (Toptchieva et al. 2003; Zannoni et al., 2007). Tellurite determinant, *trgB* has been reported in *R. sphaeroides* although its exact role is not clear yet (O'Gara et. al., 1997).

Table 5.5: Genes involved in tellurite resistance in *Shewanella* sp. strain GUSDZ9

S. N.	Gene ID	Resistance Gene	Uniprot Accession	Compound (resistant to)	Functions
1.	Te9_03387	*tehB*	P25397	Tellurium (Te)	Binding tellurite (Cytoplasmic)
2.	Te9_00863	*pitA*	P0AFJ7	Zinc (Zn), Tellurium (Te)	Influx of tellurite in bacteria
3.	Te9_01712	*terC*	P18780	Tellurium (Te)	Tellurite reduction (Membrane)
4.	Te9_02698	*actP*	D5AU53	Tellurium (Te)	Influx of tellurite into bacteria
5.	Te9_00759	*trgB*	O07841	Tellurium (Te)	ND

5.4.1.3 Resistance of *Shewanella* sp. GUSDZ9 to other metals and metalloids

It was interesting to note that the draft genome sequence of strain GUSDZ9 also contained genes conferring resistance to various metals and metalloids (Table 5.6). *Shewanella* is not only known for its multi-metal resistance but is also known for various robust properties viz. occurrence in extreme conditions of salt and fresh water, barometric pressure and temperature, utilization of diverse array of electrons as final acceptor in presence of oxygen (Hau and Gralnick,

2007). Therefore *Shewanella* sp. GUSDZ9 may serve as ideally potential candidate for metal and metalloid bioremediation along with TeNPs biosynthesis.

Table 5.6: Genes conferring resistance to other metalloids and metals in *Shewanella* sp. GUSDZ9

Gene ID	BacMet_ID	Resistance Gene	Uniprot Accession	Metal/metalloids (resistant to)
Te9_00007	BAC0168	*fptA*	P42512	Iron, Cobalt, Nickel, Gallium
Te9_01101	BAC0201	*kmtR*	O53838	Nickel, Cobalt
Te9_00088	BAC0125	*czcR*	Q44006	Cadmium, Zinc, Cobalt
Te9_01984	BAC0040	*baeS*	P30847	Zinc, Tungsten
Te9_00107	BAC0164	*fecE*	P15031	Nickel, Cobalt
Te9_00110	BAC0162	*fbpC*	P44513	Iron, Gallium
Te9_00120	BAC0190	*hmrR*	Q9X5X4	Copper
Te9_00132	BAC0452	*yqjH*	Q46871	Iron, Nickel
Te9_00140	BAC0710	*arrB*	AAQ01673	Arsenic
Te9_00173	BAC0497	*pfr*	P52093	Iron, Copper, Manganese
Te9_01647	BAC0089	*corR*	Q1D6V8	Copper

Te9_00320	BAC0468	*zraS/hydG*	P14377	Zinc, Lead
Te9_00779	BAC0609	*modA*	P37329	Tungsten, Molybdenum
Te9_01043	BAC0599	*modB*	Q72FN2	Tungsten, Molybdenum
Te9_00716	BAC0604	*wtpC*	Q8U4K3	Tungsten, Molybdenum
Te9_00348	BAC0719	*copR*	D4PBS0	Copper
Te9_00349	BAC0537	*copS*	Q02541	Copper
Te9_02458	BAC0356	*recG*	Q9HTL3	Chromium, Tellurium, Selenium
Te9_00459	BAC0003	*acn*	O53166	Iron
Te9_00498	BAC0035	*arsM*	Q6N3Y0	Arsenic
Te9_01106	BAC0299	*pbrB/pbrC*	Q58AJ7	Lead
Te9_00516	BAC0566	*actS*	Q52912	Cadmium, Zinc
Te9_00517	BAC0565	*actR*	A6UEL7	Cadmium, Zinc
Te9_00531	BAC0091	*corS*	Q1D6V7	Copper
Te9_02053	BAC0709	*arrA*	Q7WTU0	Arsenic
Te9_00632	BAC0400	*troB*	P96117	Zinc, Manganese, Iron
Te9_03527	BAC0169	*fpvA*	P48632	Manganese, Iron, Cobalt, Zinc,

				Nickel, Copper, Cadmium, Gallium
Te9_00777	BAC0611	*modC*	P09833	Tungsten, Molybdenum
Te9_00780	BAC0608	*modE*	P0A9G8	Tungsten, Molybdenum
Te9_03026	BAC0596	*baeR*	D0ZNE3	Copper, Zinc, Tungsten,
Te9_00843	BAC0465	*znuC/yebM*	P0A9X1	Zinc
Te9_00912	BAC0612	*perO*	D5AQ60	Molybdenum, Tungsten, Vanadium
Te9_00921	BAC0136	*dsbA*	P0AEG4	Cadmium, Zinc, Mercury
Te9_00929	BAC0316	*pstB*	P0AAH0	Arsenic
Te9_00996	BAC0163	*fecD*	P15029	Nickel, Cobalt
Te9_01025	BAC0644	*corD*	Q56017	Cobalt, Magnesium
Te9_04142	BAC0073	*cnrH*	P37978	Cobalt, Nickel
Te9_01151	BAC0161	*fbpB*	P71338	Iron, Gallium
Te9_01200	BAC0135	*dpsA*	Q8KR86	Iron
Te9_01220	BAC0115	*cutE/lnt*	P23930	Copper
Te9_01221	BAC0088	*corC*	P0A2L3	Cobalt, Magnesium

Te9_01301	BAC0022	*aioR/aoxR*	Q2VGB1	Arsenic
Te9_03405	BAC0138	*dsbC*	P0AEG6	Copper
Te9_01333	BAC0747	*copF*	F4ZBY1	Copper
Te9_01336	BAC0455	*ziaA*	Q59998	Zinc
Te9_02037	BAC0487	*pmrA*	Q70FH0	Iron
Te9_01338	BAC0126	*czcS*	Q44007	Cadmium, Zinc, Cobalt
Te9_01343	BAC0688	*merR2*	Q79B70	Mercury
Te9_01344	BAC0233	*merT*	P94185	Mercury
Te9_01345	BAC0675	*merP*	O07301	Mercury
Te9_01346	BAC0664	*merC*	O66048	Mercury
Te9_01347	BAC0653	*merA*	Q934S5	Mercury
Te9_03069	BAC0076	*comR/ycfQ*	P75952	Copper
Te9_01426	BAC0440	*yfeB*	Q56953	Iron, Manganese
Te9_01666	BAC0725	*copA*	Q59385	Copper
Te9_01681	BAC0607	*tupC*	Q93KD4	Tungsten
Te9_01692	BAC0317	*pstC*	P0AGH8	Arsenic

Te9_01693	BAC0315	*pstA*	P07654	Arsenic
Te9_01767	BAC0274	*nikE*	P33594	Nickel
Te9_01768	BAC0273	*nikD*	P33593	Nickel
Te9_01769	BAC0272	*nikC*	P0AFA9	Nickel
Te9_01770	BAC0271	*nikB*	P33591	Nickel
Te9_01771	BAC0270	*nikA*	P33590	Nickel
Te9_01827	BAC0095	*crdR*	O25918	Copper
Te9_01921	BAC0137	*dsbB*	P0A6M2	Cadmium, Mercury
Te9_01927	BAC0707	*sodB*	P0AGD3	Selenium
Te9_01935	BAC0583	*arsC*	P52147	Arsenic, Antimony
Te9_02038	BAC0488	*pmrB*	Q70FG9	Iron
Te9_02138	BAC0490	*G2alt*	B0FSM1	Aluminium
Te9_02211	BAC0102	*cueA*	Q8KWW2	Copper, Silver
Te9_03400	BAC0714	*arsT*	B7FB00	Arsenic
Te9_02364	BAC0355	*ruvB*	Q51426	Chromium, Tellurium, Selenium

Te9_02275	BAC0592	*arsR*	Q01256	Arsenic, Antimony, Bismuth
Te9_03794	BAC0036	*arsP*	B5LWZ8	Arsenic
Te9_02306	BAC0485	*pmrC*	Q70FH1	Iron
Te9_02309	BAC0482	*dmeF*	Q1MJL2	Cobalt, Nickel
Te9_02556	BAC0086	*corA*	P0ABI4	Magnesium (Mg), Cobalt, Nickel, Manganese
Te9_02912	BAC0116	*cutF/nlpE*	P40710	Copper
Te9_02945	BAC0572	*arsA*	P08690	Arsenic, Antimony
Te9_03025	BAC0289	*nrsS*	F7UKI4	Nickel
Te9_03147	BAC0682	*merR1*	P22853	Mercury
Te9_03213	BAC0643	*corB*	Q9X621	Cobalt, Magnesium
Te9_03225	BAC0555	*nccH*	Q44583	Nickel, Cobalt, Cadmium
Te9_03252	BAC0181	*glpF*	P0AER0	Antimony, Arsenic
Te9_03309	BAC0048	*bfrA*	P63697	Iron
Te9_03379	BAC0152	*srpC*	Q55027	Chromium
Te9_03406	BAC0601	*tunR*	Q72FN4	Tungsten, Molybdenum

Te9_03472	BAC0350	*sitB*	Q9XCS1	Manganese, Iron
Te9_03579	BAC0160	*fbpA*	P35755	Iron, Gallium
Te9_03634	BAC0229	*merG*	O07302	Mercury
Te9_03691	BAC0463	*znuA/yebL*	P39172	Zinc
Te9_03727	BAC0579	*arsB*	P74311	Arsenic, Antimony
Te9_03738	BAC0267	*nczA*	B8GZE9	Nickel, Cobalt, Zinc
Te9_03739	BAC0460	*zneB/hmxB*	Q1LCD7	Zinc
Te9_03795	BAC0462	*zntR/yhdM*	P0ACS5	Zinc
Te9_03867	BAC0484	*hupE2*	D2WPE1	Nickel
Te9_04084	BAC0568	*actP*	Q9X5V3	Copper
Te9_04085	BAC0108	*cusB*	P77239	Copper, Silver
Te9_04086	BAC0107	*cusA/ybdE*	P38054	Copper, Silver
Te9_04191	BAC0128	*cznB*	D3UHP9	Cadmium, Zinc, Nickel
Te9_04192	BAC0127	*cznA*	D3UHQ0	Cadmium, Zinc, Nickel
Te9_04203	BAC0605	*tupA*	Q93KD6	Tungsten
Te9_04204	BAC0606	*tupB*	Q93KD5	Tungsten

Te9_04228	BAC0065	*chrE*	Q5NUZ8	Chromium

The whole genome data evidently proved the probable involvement of different tellurite genetic determinants responsible for tellurite resistance and / TeNPs biosynthesis. Additionally, résistance to numerous other metals and metalloids also suggest that this strain could be also used for biosynthesis of the above-mentioned metals and metalloids as well.

Summary

Halomonas sp. strain GUSDM4 exposed to selenite (4 mM) clearly demonstrated intracellular depositions of SeNPs in the form of nano spheres. Whereas no spherical deposits were seen in control bacterial cells. *Shewanella* sp. strain GUSDZ9 exposed to tellurite (2mM) synthesized Te nanorods in the cytoplasm which was evident from nanorods deposits throughout the bacterial cell. Further characterization of these isolates confirmed that nitrate reductase is not involved in SeNPs and TeNPs biosynthesis. Enzyme studies additional revealed probable involvement of periplasmic selenite reductase in SeNPs biosynthesis and cytoplasmic tellurite reductase in TeNPs synthesis which was evident from enzyme activity.

The whole genome sequence analysis of *Shewanella* sp. strain GUSDZ9 revealed involvement of various tellurite resistance determinants (genes) viz. *tehB, pitA, terC, actP and trgB*. However, exact mechanisms involved in tellurium resistance is not yet understood. Additionally, several other genes of metallome involved in resistance to other metals and metalloids have also been found in *Shewanella* sp. strain GUSDZ9.

Chapter VI

Genotoxicity and Applications of Biogenic Selenium and Tellurium Nanoparticles

6.1Genotoxicity of biosynthesized Se and Te NPs

Genotoxicity of Se and Te NPs was determined using comet assay and are represented in Fig. 6.1 & 6.3. Presence of comet under fluorescence microscope was considered as the evidence of toxicity and the length of the comet was used to quantitate (Fig. 6.2, 6.4).

The genotoxicity of biogenic SeNPs at various concentrations (0, 25, 50, 75 and 100 µg/mL) and at various time interval (0, 2 and 4 h) are depicted (Fig. 6.1). However, DNA damage in all except positive control was found to be insignificant as compared to the control thus, indicating that SeNPs do not induce any toxicity on human lymphocytes. The percent (%) DNA damage induced by biogenic TeNPs at 15, 20, 25 and 50 µg/mL concentrations in the human lymphocytes at various time intervals (0, 1 and 2 h) are depicted in the Fig. 6.3. Interestingly, DNA damage observed at 15 µg/mL concentration of TeNPs with increasing time (1 and 2 h) was found to be insignificant compared to the control thus conferring that biogenic TeNPs do not induce any DNA damage in human cells at this concentration.

However, a significant dose-dependent increase in the mean % tail DNA, with respect to the control was observed with time which was proved by the student's t-test ($p= 0.0001$). Significant DNA damage was observed at 20 µg/mL (0 h) which increased in a time-dependent manner. A similar trend was also observed with 25 µg/mL concentration wherein 12.1 % tail DNA damage was recorded, reaching maxima (30 %) for 1 h whereas, at 2 h nearly 47 % damage was observed. The highest DNA damage for lymphocytes was recorded at the 50 µg/mL concentration wherein significant % tail DNA recorded was 16, 41 and 61 % at 0, 1 and 2 h of treatments respectively.

Increase in DNA damage at different concentrations of TeNPs (15, 20, 25 and 50 µg/mL) at all-time intervals (0, 1 and 2 h) was significant (except at 15 µg/mL) which was proved by one-way ANOVA ($F = 499.4$, $p< 0.0001$).

Even though TeNPs have been studied for various applications majorly in biomedical field but there are no reports as far as toxicity on human cells is concerned. Thus, these studies are of immense importance since this is the first ever report demonstrating the genotoxicity of biogenic TeNPs. Based on this study it is also advisable that utmost care must be taken in handling nano-wastes. TeNPs can be doped with SeNPs to reduce its toxicity.

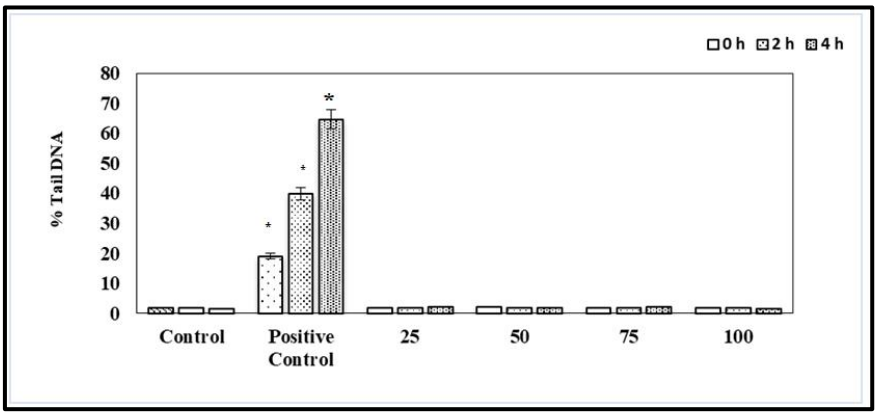

Fig. 6.1 Percent DNA damage in human lymphocytes exposed to different concentrations of SeNPs. Data are represented as mean ± SD (*p < 0.001).

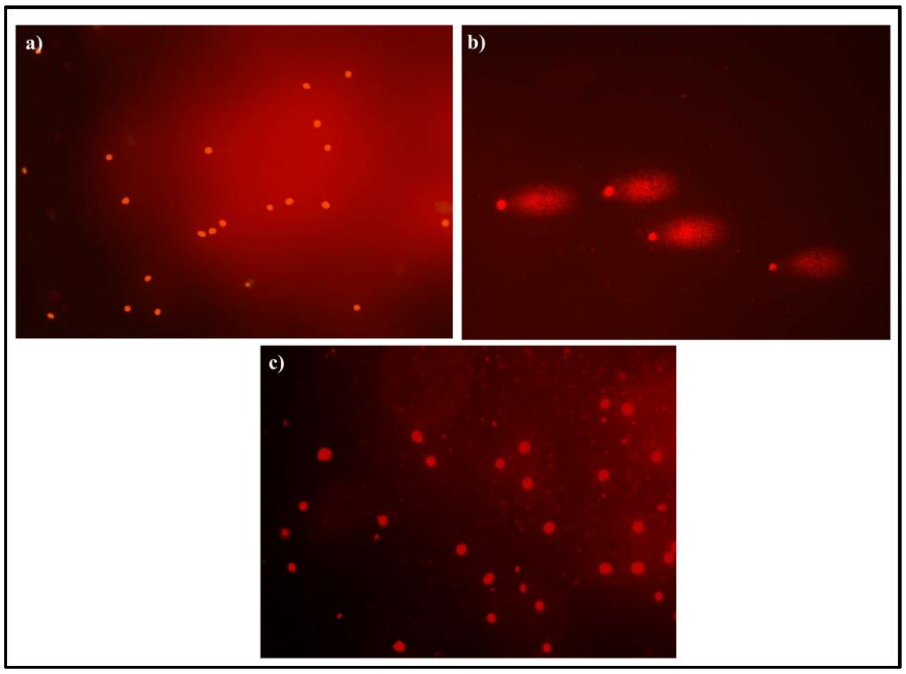

Fig. 6.2 Comet assay showing lymphocyte cells treated with: control: 0 µg/mL SeNPs (a); H_2O_2 (b); 100 µg/mL SeNPs (c).

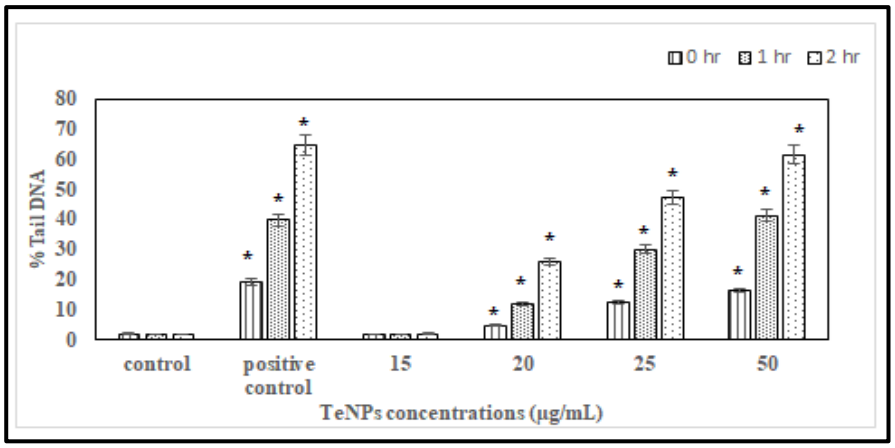

Fig. 6.3 Percent DNA damage in human lymphocytes exposed to different concentrations of TeNPs. Data are represented as mean ± SD (*p < 0.0001).

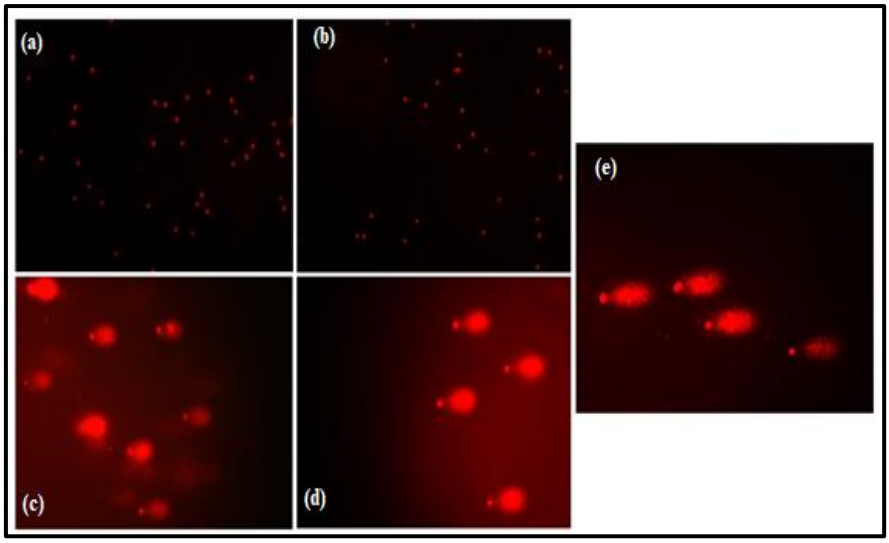

Fig. 6.4 Comet assay showing lymphocyte cells treated with: control: 0 µg/mL TeNPs (a); 15 µg/mL TeNPs (b); 20 µg/mL (c); 25 µg/mL (d); 50 µg/mL TeNPs (e).

6.1 Applications of biosynthesized selenium and tellurium nanoparticles

6.2.1 Biomedical applications of Se and Te NPs

6.2.1.1 Antimicrobial activity Se and Te NPs

Clinically potent isolates namely *Staphylococcus aureus*, *Escherichia coli*, *Staphylococcus epidermidis*, *Salmonella typhimurium*, *Pseudomonas aeruginosa*, *Shigella* sp., *Klebsiella pneumoniae and Candida albicans* obtained from Goa based Government Hospital were tested for their pathogenicity against biogenic Se and Te nanoparticles. It was observed SeNPs and TeNPs demonstrated excellent anti-microbial activity against all 8 isolates. An increase in zone of inhibition (mm) with increasing concentrations of nanoparticles were observed (Figs. 6.5 & 6.6). SeNPs were effective in inhibiting the growth of pathogens from concentrations in the range of 50 to 150 µg/mL. SeNPs were most effective against *E. coli* where, zone of inhibition (25.5, 33.35 and 44.5 mm) was recorded at 50, 75 and 100 µg/mL. This was followed by *S. typhimurium* which showed similar

trend at 50, 75 and 100 µg/mL where 22.5, 33.25 and 40.2 mm diameter of zone of inhibition was recorded respectively. Similar observations were also recorded in terms of *K. pneumoniae, P. aeruginosa*, and *Shigella* sp. In case of Gram-positive bacteria, the inhibitory concentration of SeNPs was much higher as compared to that for Gram negative microorganisms. For example, *S. aureus* (7.75 mm) and *S. epidermidis* (13.75 mm) required 75 µg/mL SeNPs for inhibition. The SeNPs also inhibited the growth of *C. albicans* (19.25 mm) at 200 µg/mL. Although there are few reports available on antimicrobial activity of SeNPs however, a report by Singh et al. (2014) showed antimicrobial activity against *Pseudomonas* sp. and *Staphylococcus aureus*, however, it did not show activity against *Klebsiella* sp. and *Escherichia coli.*

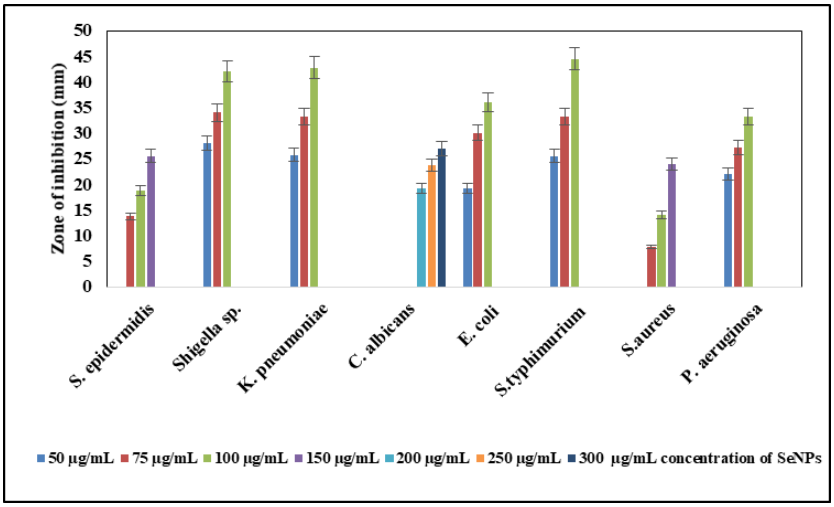

Fig. 6.5 Antimicrobial activity of SeNPs against human pathogens.

TeNPs were also found to be more effect against Gram negative bacteria as compared to Gram positive bacteria. For instance, *Staphylococcus aureus*, *Staphylococcus epidermidis* exhibited zone of inhibition (7.75, 4.25 mm) at concentration of 50 µg/mL respectively. Similarly, highest zone of inhibition was recorded for *E. coli* (28, 35

and 42 mm) followed by *Salmonella typhimurium* (22.5 33.25 and 40 mm) at 30, 50 and 75 µg/mL respectively. However, similar increasing zone of inhibition for increasing concentrations of TeNPs were obtained for *K. pneumoniae, P. aeruginosa* and *Shigella* sp. Previous report by Zare and co-workers have demonstrated antibacterial activity against *Staphylococcus aureus*, *Pseudomonas aeruginosa*, *Salmonella typhimurium* and *Klebsiella pneumoniae* with MIC of 250 µg/mL for *Staphylococcus aureus* and 125 µg/mL for rest 3 isolates respectively (Zare et al., 2012). TeNPs were also found to inhibit *C. albicans* exhibiting zone of inhibition at the concentration of 200 µg/mL thus, demonstrating anti-fungal activity. There is only one report demonstrating the antifungal activity of TeNPs against *C. albicans* at 1000 µg/mL (Zare et al., 2014).

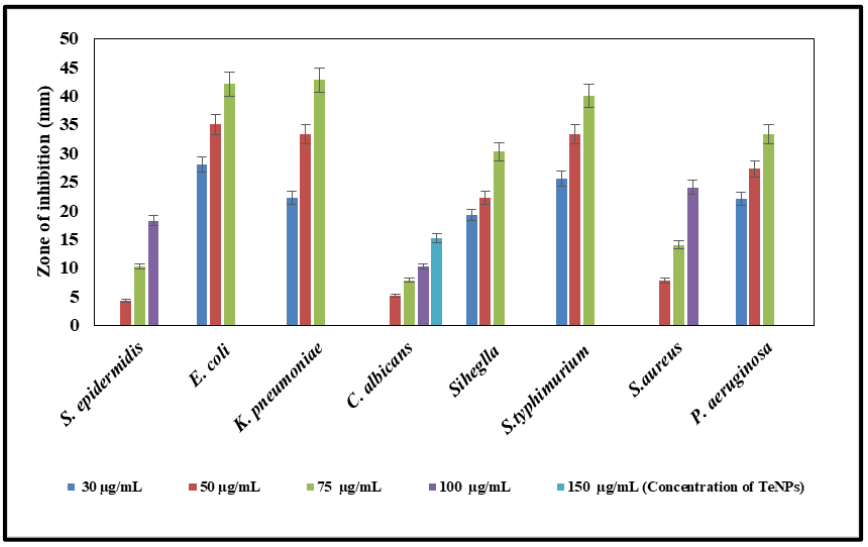

Fig. 6.6 Antimicrobial activity of TeNPs against human pathogens.

Fig. 6.7 depicts the MIC of Se and Te NPs for all the tested pathogenic strains of microorganisms. TeNPs showed MIC at much lower concentrations as compared to SeNPs. For instance, *S. aureus* exhibited MIC of 38.5 µg/mL for SeNPs whereas, in case of TeNPs it was found to be 28.5 µg/mL. MIC of Se and Te NPs for *E. coli* was

recorded to be 22.5 and 18.5 µg/mL respectively while, *C. albicans* showed MIC of 50.5 and 37.5 µg/mL of Se and Te NPs respectively.

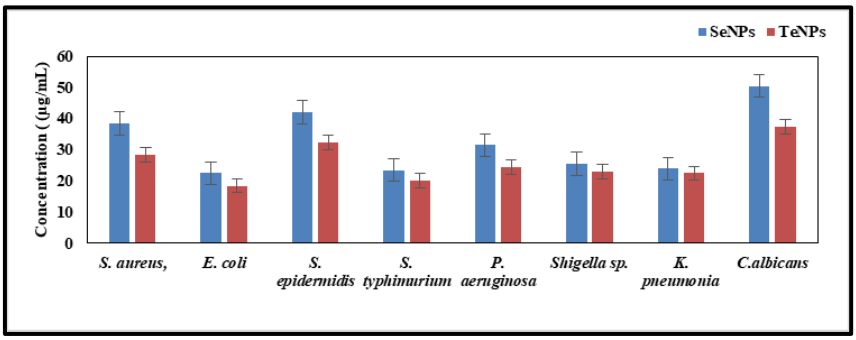

Fig. 6.7 MIC of Se and Te NPs for pathogenic strains.

Tellurium has been known historically for its biological activities in the treatment of microbial infections. The above findings are evidence of dose dependent antimicrobial activity of biogenic TeNPs and SeNPs against developing hospitalized pathogens viz. *Staphylococcus aureus*, *Escherichia coli*, *Staphylococcus epidermidis*, *Salmonella typhimurium*, *Pseudomonas aeruginosa*, *Shigella* sp., *Klebsiella pneumoniae and Candida albicans*. As most of the pathogens used for the study are known to be causative agents of various life-threatening infections viz. nosocomial infections, endocarditis, gastroenteritis, candidiasis, urinary tract infections, acute pneumonia and meningitis in host compromised patients or those using artificial assistances like catheters, shunts and prosthetic joints.

Nanoparticle based approach for antimicrobial activity is much more significant since many of these pathogens are developing resistance to many forefront antibiotics. Furthermore, various antimicrobial agents which find applications in diverse fields including food packaging, water disinfectants, paints, food feed and textiles are high in demands. Enormous and inappropriate use of these antimicrobial agents have led to the development of drug resistant bacterial species. Therefore, development of a novel antimicrobial

agent has become a prerequisite and thus, nanoparticle-based approach for fighting such infectious pathogens will be substantial.

6.2.1.2 Anti-biofilm potential of Se and TeNPs

SeNPs demonstrated dose-dependent antibiofilm activity against Gram positive and Gram-negative pathogens (Fig. 6.8). Highest antibiofilm activity was recorded against *K. pneumoniae* at 20 (39.45 %), 25 (55.89 %) and 50 (90.96 %) µg/mL. This was followed by *E. coli* in which 38.56, 48.58 and 78.26 % inhibition of biofilm was observed at 20, 25 and 50 µg/mL of SeNPs. In Gram positive *S. aureus* 18.89, 35.89 and 60.89 % inhibition were observed while in *S. pyogenes* inhibition recorded were 9.58, 18.56 and 55.89 % at 20, 25 and 50 µg/mL of SeNPs respectively. Previously, a similar % reduction of *S. aureus*, *P. aeruginosa* and *P. mirabilis* biofilms were reported (Shakibaie et al, 2015).

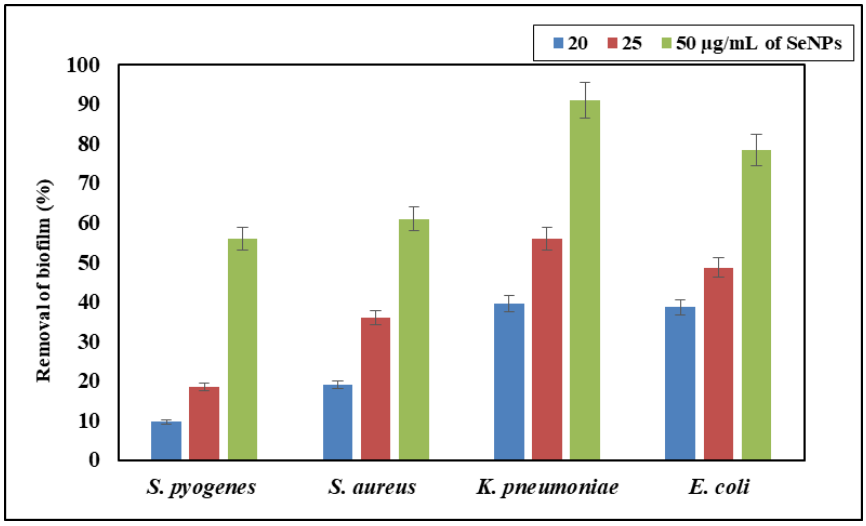

Fig. 6.8 Antibiofilm activity of SeNPs against human pathogen.

Anti-biofilm activity of biogenic TeNPs against clinically important microbial strains clearly demonstrated that these nanoparticles exhibited excellent anti-biofilm activity, which was dose-

dependent (Fig. 6.9). It was observed that TeNPs were very effective against *E. coli* wherein 92 % of biofilm eradication was achieved at 15 μg/mL, whereas 64 % was achieved at 10 μg/mL and 42 % at 5 μg/mL concentration of TeNPs. *K. pneumoniae* showed reduction in biofilm formation by 89 %, 47 % and 22 % when treated with 15, 10 and 5 μg/mL TeNPs respectively. In case of *S. aureus*, 81 % biofilm removal was recorded at 15 μg/mL which was followed by 51 % and 22 % at 10 and 5 μg/mL of TeNPs respectively. A similar pattern was observed in case of *Streptococcus pyogenes* which recorded 63 % biofilm removal at 15 μg/mL whereas, at 10 and 5 μg/mL concentrations, it was 20 and 9 % respectively (Fig. 6.9). There are few studies on antimicrobial potential of TeNPs (Lin et al., 2012; Zare et al., 2012; Mohanty et al., 2014; Pugin et al., 2014; Srivastava et al., 2015).

However, removal of planktonic and biofilm forming bacteria by biogenic TeNPs have also been reported which ensured biofilm eradication at much higher concentrations of TeNPs (Zonaro et al., 2015). Therefore, TeNPs biosynthesised by *Shewanella baltica* strain GUSDZ9 are comparatively more effective in inhibiting potential biofilm forming Gram-positive and Gram-negative human pathogens at very low concentrations.

The SEM analysis of the pathogenic bacterial cells also showed dose dependent inhibition of biofilm corroborating with the quantitative biofilm inhibition (Fig. 6.10 & 6.11). The control slides of *E. coli* and *K. pneumoniae* without Se and Te NPs treatment showed dense biofilm formations. In NPs-treated slides, dislodging of biofilm with increasing concentration of both Se and Te NPs was recorded. It was interesting to note that morphological alterations in forms of surface depression was prominently observed in all NPs treated cells. These observations further deep-rooted the anti-biofilm potential of Se and Te NPs.

This opens a new arena of applications for Se and Te NPs as coating agents in medical and health-related devices in order to prevent bacterial infections. Furthermore, these NPs may also have promising

applications in industrial sectors as potential tools to combat biofouling. Additionally, they can also serve as excellent candidates to eradicate biofilm formation in sewage tanks and other sewerage systems.

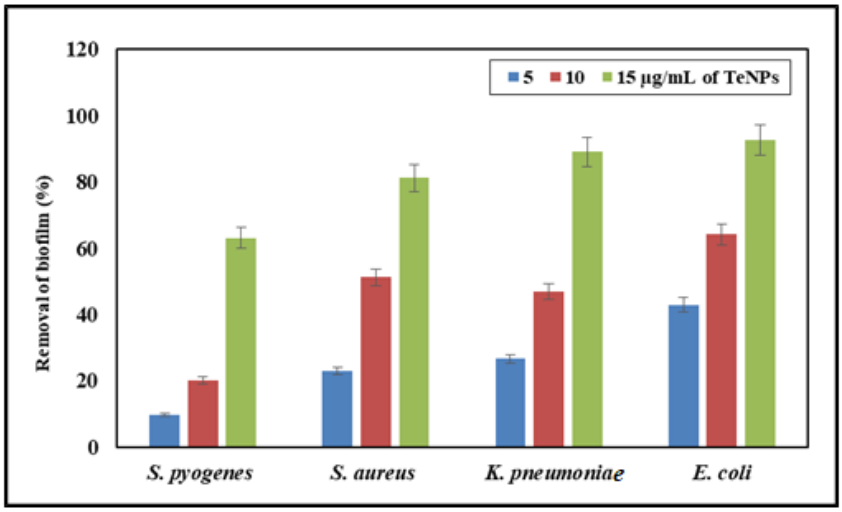

Fig. 6.9 Antibiofilm activity of TeNPs against human pathogens.

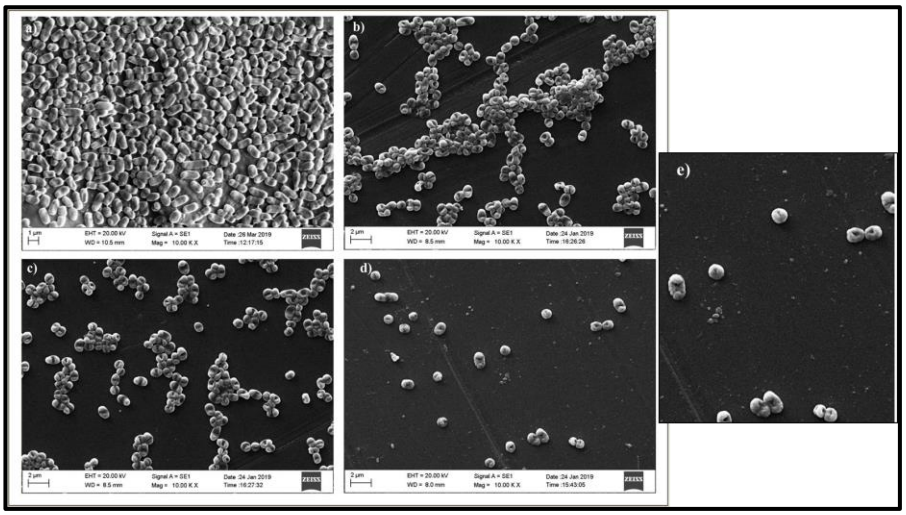

Fig. 6.10 Antibiofilm activity of SeNPs on *K. pneumoniae*: 0 µg/mL SeNPs (a); 20 µg/mL SeNPs (10X) (b); 25 µg/mL SeNPs (c); 50 µg/mL SeNPs (d); 50 SeNPs µg/mL (e).

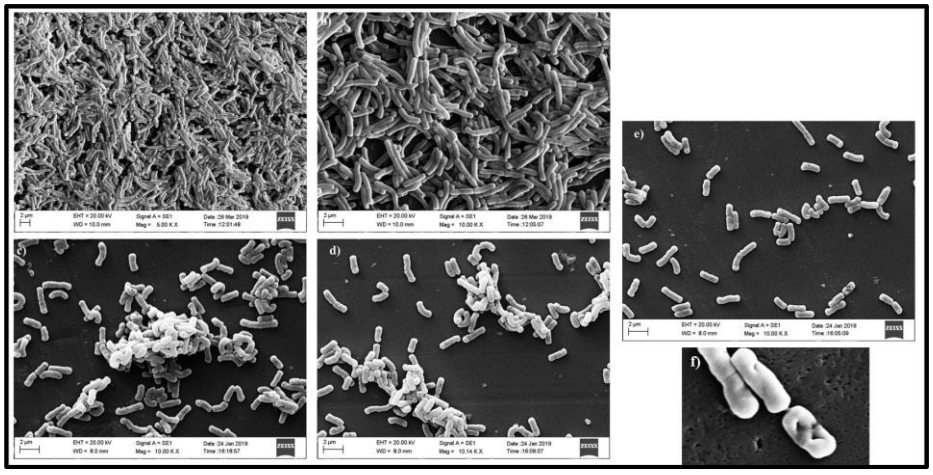

Fig. 6.11 Antibiofilm activity of TeNPs on *E. coli*: control: control: 0 µg/mL TeNPs (5X) (a); 0 µg/mL TeNPs (10X) (b); 5 µg/mL TeNPs (c); 10 µg/mL TeNPs (d); 15 TeNPs µg/mL (e).

6.2.1.3 Free-radical scavenging activity of Se and TeNPs

Biogenic SeNPs exhibited excellent dose dependent anti-oxidant potential. An increasing % radical scavenging activity with increasing concentrations of SeNPs was recorded. For instance, the percent scavenging activity at 25 µg/mL of biogenic SeNPs was found to be 50 % while, 90 % was recorded at 50 µg/mL (Fig. 6.12). Higher antioxidant properties of SeNPs is mainly due to the presence of seleno-enzyme viz. glutathione peroxidase (GPx) and thioredoxin reductase which are known to play a crucial role in scavenging free radicals.

Previous findings on anti-oxidant activity by biogenic SeNPs also showed a similar dose-dependent trend but at higher concentrations i.e. 100 to 1000 µg/mL (Ramya et al., 2015). Where, the percent scavenging activity at 100 µg/mL was 80 % while, at 1000 µg/mL the activity was found to be 100 %. However, current study exhibits around 90 % radical-scavenging potential at 50 µg/mL of SeNPs which is highly significant. Moreover, another study by Forootanfar et al. (2015) demonstrated 23.1 ± 3.4% radical scavenging activity at 200 µg/mL of SeNPs. Differences in the % scavenging activity may be attributed due to the difference in the size of biosynthesized nanoparticles with the fact

that smaller particles are known to exhibit greater scavenging activity as compared to larger aggregates (Torres et al., 2012).

TeNPs exhibited 55.6 % scavenging activity at 20 µg/mL and 83.96 % at 30 µg/mL. Reports showing involvement of biogenic TeNPs as antioxidants are very few. In one of the studies, the radical scavenging activity was demonstrated at 10-500 µg/mL of biogenic TeNPs synthesized by *P. pseudoalcaligenes* strain, the IC_{50} value was reported to be at 24.9 µg/mL of TeNPs (Shakibaie et al., 2017).

However, Andersson and coworkers, (1994) described for the first time the antioxidant potential of organotellurium compounds *in vitro*. Subsequently many tellurium containing compounds were studied for antioxidant potential. The common observation which was consistently noted was higher efficacy of tellurium derivatives in comparison to sulphur or selenium was noted (Cunha et al., 2009). Previously, antioxidant organo-Te also has been reported to be in inhibition of thioredoxin/thioredoxin reductase system (TrxR) and cancer cell growth by antioxidants (Urig and Becker, 2006).

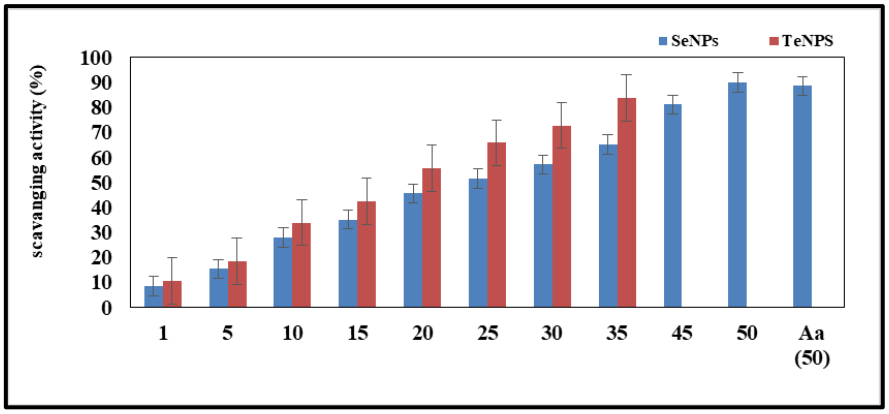

Fig. 6.12 Free radical scavenging activity of biogenic SeNPs and TeNPs (Ascorbic acid (Aa) served as a standard).

6.2.1.4 Anti-cancer potential of SeNPs

Although, selenium compounds viz. selenite, selenate, selenomethionine, selenocysteine and methyl-selenocysteine are known to be anti-carcinogenic but the concentrations at which these compounds are effective is very high and toxic (Zhang et al., 2007; Seng et al., 2012). SeNPs have attracted considerable attention due to its exceptional biological potential and reduced toxicity (Zheng et al., 2011). Biogenic SeNPs have been reported for its anti-cancer activity and are found to be effective against various cancer cell lines viz. MCF-7(breast adenocarcinoma), MDA-MB-231 (human breast carcinoma), A375 (human melanoma), LNcaP (prostrate), HK-2 (human kidney), HepG2 (liver hepatocellular carcinoma cell lines) and HeLa (human cervical carcinoma) (Chen et al., 2008; Kong et al., 2011; Zheng et al., 2011; Luo et al., 2012; Srivastava and Kowshik, 2016).

Dose dependent toxicity of SeNPs was very evident (Fig. 6.13). SeNPs were very effective in inhibiting the A549 cell lines at concentrations as low as 10 µg/mL while at 70 µg/mL complete mortality was observed. Interestingly, SeNPs were ineffective against normal human bronchial epithelial cells (BEAS-2B) making it extremely selective with respect to the type of cells. The high specificity of SeNPs only to the cancer cells may be due to the difference in anti-oxidant enzyme regulations which are over-expressed in case of cancer cells (Fang et al., 2005). Present chemotherapeutic treatments for cancer are nonspecific, less effective and additionally imparts numerous side effects to the patients. Under such circumstances highly specific Se-nano-therapeutics would be the best alternative so far as highly selective and targeted treatment is concerned.

We have clearly demonstrated the effect of SeNPs on cancer cell line (Fig. 6.14). The untreated A549 cells were highly dense, closely associated and abundant. However, after treatment with SeNPs, large cells have circularized and shrunken along with a decrease in density adherence of cells. Similar morphological alterations in Hela cells and

MDA-MB-231 cells have been reported earlier in presence of selenium nanoparticles by others (Luo et al., 2012).

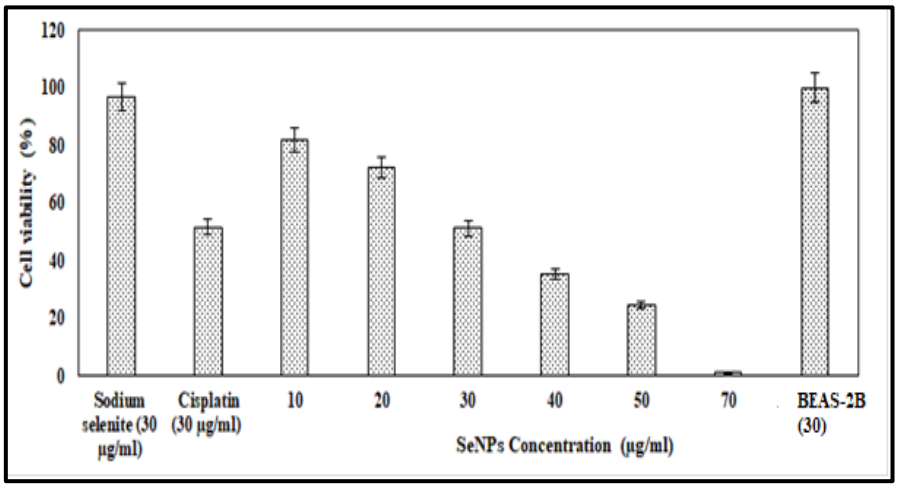

Fig. 6.13 Dose dependent anti-proliferative activity of biogenic SeNPs.

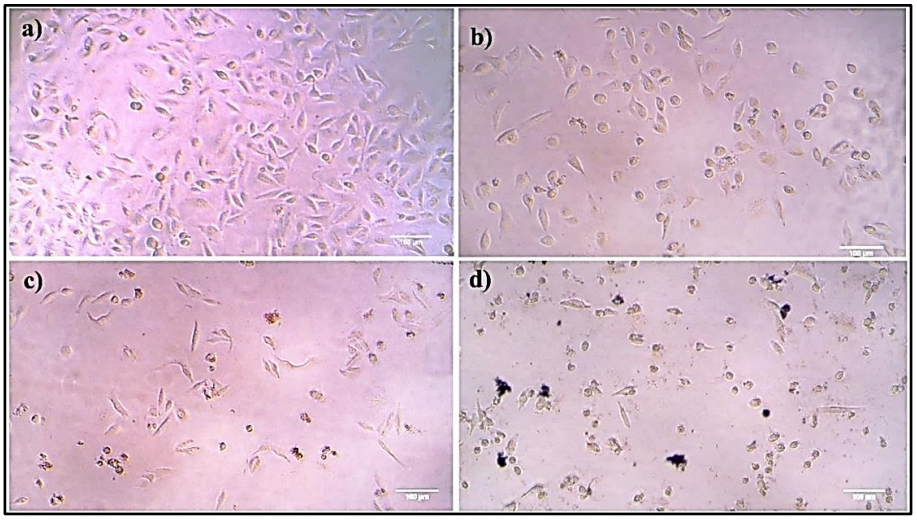

Fig. 6.14 Microscopic images of A549 cells: control without treatment (a); Cells treated with 30 µg/mL of cisplatin (b); Cells treated with 30 µg/ml SeNPs (c); Cells treated with 70 µg/ml SeNPs (d).

6.2.1.5 Genoprotective activity of biogenic SeNPs against UV-B damage

The percent tail DNA damage induced by UV exposure and protective effect induced by biogenic SeNPs in human lymphocytes at various time interval (0, 60 and 120 sec) have been clearly depicted in the Fig. 6.15. UV radiations causes DNA damage, apoptosis, cell cycle arrest, immunological depressions to name few. UV-B radiations causes formation of cyclobutane pyrimidine dimers (CPD) and photoproducts (6-4 PR) and also induces oxidative stress indirectly via ROS generation (Cadet et al., 2011). Comet assay or single cell gel electrophoresis has been used to study the UV-B damage on human lymphocytes (Cortés-Gutiérrez et al., 2011).

In the present study, lymphocytes exposed to UV-B light showed significant DNA damage with time, as compared to control which was proved by the student's t-test ($p= 0.001$). Percent DNA damage in untreated lymphocytes exposed to UV-B light was found to be 5 % followed by 30 and 47.2 % at 0, 60 and 120 sec time intervals respectively. However, unexposed lymphocytes did not reveal any % tail DNA damage.

Interestingly, SeNPs treated lymphocytes when exposed to UV-B light reduced the damage which was significant except at 10 μg/ml which was insignificant as compared to unexposed cells (Fig. 6.16).Thus, confirming the fact that SeNPs exhibits complete protection to human lymphocytes against UV-B damage. Increasing percent DNA damage with time of exposure to UV-B light (60 sec and 120 sec) was significant which was proved by one-way ANOVA ($F=477.6$, $p< 0.001$).

Previously, there exists only one report depicting similar UV protective effect of SeNPs synthesised using lemon leaf extracts (Prasad et al., 2013). Nevertheless, these studies are of immense importance since this the first ever report demonstrating the geno-protective potential of biogenic SeNPs biosynthesised using bacteria. Thus, these

biogenic SeNPs can be the best candidate for its effective application in sun ban creams and lotions.

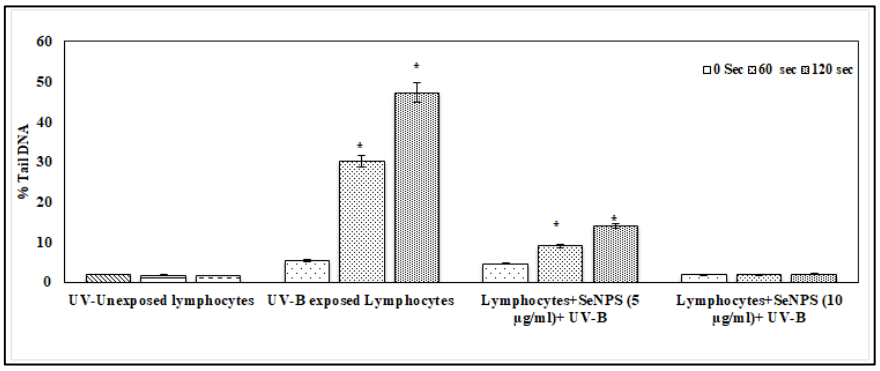

Fig. 6.15 Protective effect of different concentrations of SeNPs against UV induced DNA damage in human lymphocytes. (% DNA damage is expressed as % Tail DNA) Data are represented as mean ± SD (*p < 0.001).

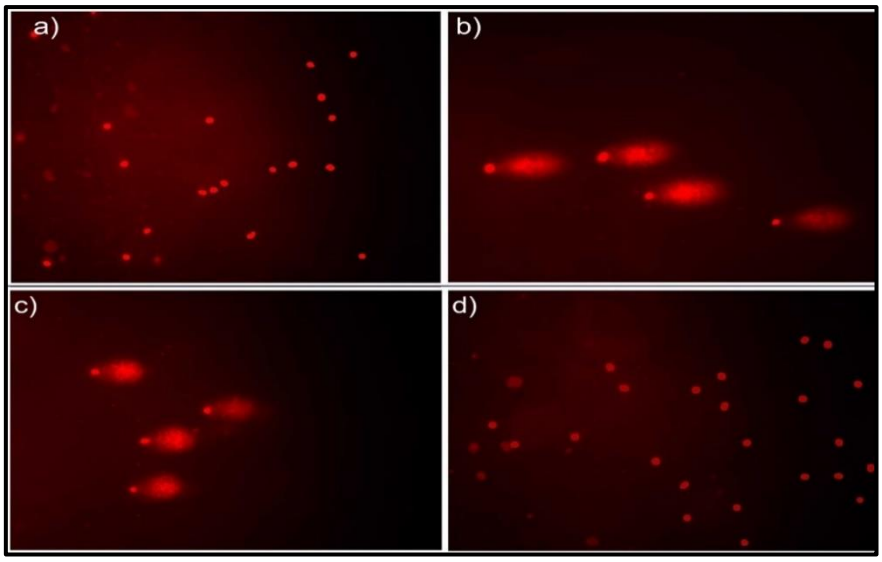

Fig. 6.16 Comet assay showing: unexposed cells (a); cells exposed to UV-B (b); UV-B exposed cells treated with 5 µg/mL SeNPs (c); UV exposed cells treated with 10 µg/mL SeNPs (d).

6.2.2 Environmental applications of biogenic SeNPs and TeNPs

6.2.2.1 Photo-catalytic activity of biosynthesized Se and TeNPs

Methylene blue reduction under sunlight demonstrated a gradual change in colour from blue to pale blue. In presence of SeNPs as catalyst, higher decrease in absorbance was observed. In control flask (without SeNPs) only 9.8 % methylene blue dye reduction was observed within 3.5 h, whereas, in presence of 10 µg/mL SeNPs 100 % reduction was observed (Fig. 6.17). In one of the reports by Ameri and co-workers (2015) SeNPs synthesized by *Streptomyces griseobrunneus* strain FSHH12 demonstrated 62.3 % reduction after 60 min in presence of 64 µg/mL Se NPs.

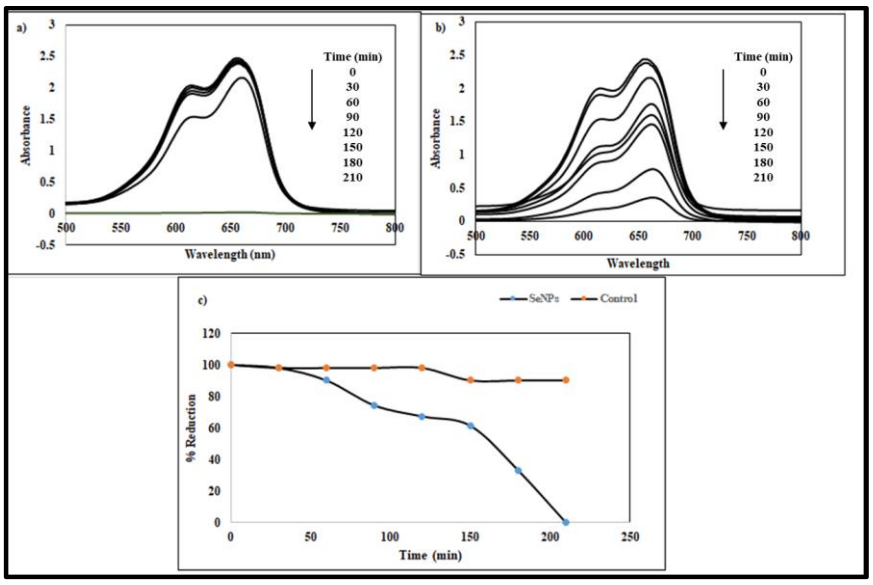

Fig. 6.17 UV-visible spectra of photo-catalytically reduced methylene blue dye: in absence of SeNPs (a); in presence of 10 µg/mL SeNPs (b); Percent reduction of methylene blue (c).

In presence of TeNPs as catalyst, an enhanced decrease in absorbance was observed. In control flask without Te nanorods, only 20 % reduction of methylene blue was observed within 4 h. Whereas, in presence of TeNPs 90 % reduction was observed which is very significant (Fig. 6.18). However, there are various drawbacks

associated with current physical and chemical methods employed viz. activation carbon adsorption, ultrafiltration, reverse osmosis and gas sparging for degradation of organic pollutants. However, chemically synthesized TeNPs have already been reported for photo-catalysis but there is no report on biogenic TeNPs - mediated photo-catalysis (Shanmugam et al., 2015). The use of nanoparticles in photo-catalytic degradation is advantageous since it is a reusable and recyclable process which does not require any additional step for disposal (Piella et al., 2013). Thus, biosynthesized SeNPs and TeNPs act as stable photo-catalysts to reduce and bioremediate methylene blue dye which is present in the effluents of textile industries. This is the first report showing photo-catalytic activity of biogenic TeNPs in methylene blue degradation through reduction.

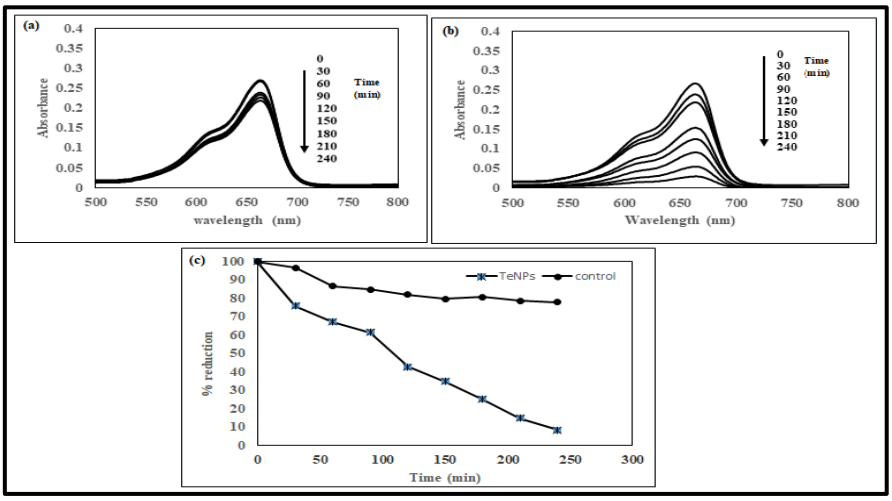

Fig. 6.18 UV-visible spectra of photo-catalytically reduced methylene blue dye: in absence of TeNPs (a); in presence of 10 µg/mL TeNPs (b); Percent reduction of methylene blue (c).

6.2.2.2 Larvicidal activity of biogenic Se and TeNPs

Both Se and Te NPs exhibited larvicidal activity against all three tested spp. of mosquito larvae. Tables 6.1 & 6.2 depicts the LC_{50} value against laboratory reared larvae of *Anopheles stephensi*, *Culex quinquefasciatus* and *Aedes aegypti.* TeNPs were found to be more effective against all 3 sp. of larvae as compared to SeNPs. For instance, LC_{50} against larvae of *Ae. aegypti* was found to be 6 and 8 folds lower as compared to SeNPs after 24 h and 48 h resypectively. Among all the larvae of different spp. highest % mortality was recorded for *Culex quinquefasciatus* followed by *Aedes aegypti* and *Anopheles stephensi.* The LC_{50} against *Culex quinquefasciatus* was in the range of 24.8 - 29.92 ppm SeNPs and in case of TeNPs it ranged from 4.23 to 5.32 ppm after 24 and 48 h of incubation respectively (Fig. 6.19).

Previously, SeNPs synthesized from leaf extract of *C. dentata* was reported to exhibit LC_{50} of 240.714 ppm, 104.13 ppm, and 99.602 ppm for *Anopheles stephensi*, *Aedes aegypti*, and *Culex quinquefasciatus* respectively (Sowndarya et al., 2017). However, we have reported lower values of LC_{50} for *Anopheles stephensi*, *Aedes aegypti*, and *Culex quinquefasciatus* which is almost 4, 2 and 3.3-fold lower than the earlier report. The microscopic images of the test and control larvae evidently revealed that Se and TeNPs might be developing toxicity once the nanoparticles are internalised by the larvae (Fig. 6.20).

Every year 70 million people are affected due mosquito borne diseases globally, among which 4 million is Indian population (Ghosh et al., 2012). Mosquito acts as a vector for most of the fatal and life-threatening diseases including malaria, dengue, yellow fever, filariasis, zika and chikungunya. These are global threats to both developing and developed countries due to its re-emergence and its tendency to spread outside the known geographic range causing epidemics (Ghosh et al., 2012).

The vector control strategies mainly target adults or larvae and largely involves the use of chemical insecticides. The repetitive use of these hazardous insecticides fosters various complications which include development of insecticide resistance, natural biological control system disruptions, outbursts of other insects and undesired effects on non-targeted spp. (Yang et al., 2002). The advantages associated with larval control include low moralities and effective coverage due to behaviour responses of immature mosquito (Benelli, 2015). Nanoparticle based approach is most desired due to its specificity and effectiveness even at low concentrations (Soni and Prakash 2012). Thus, use of biogenic Se and Te NPs as larvicidal agents would be much favourable.

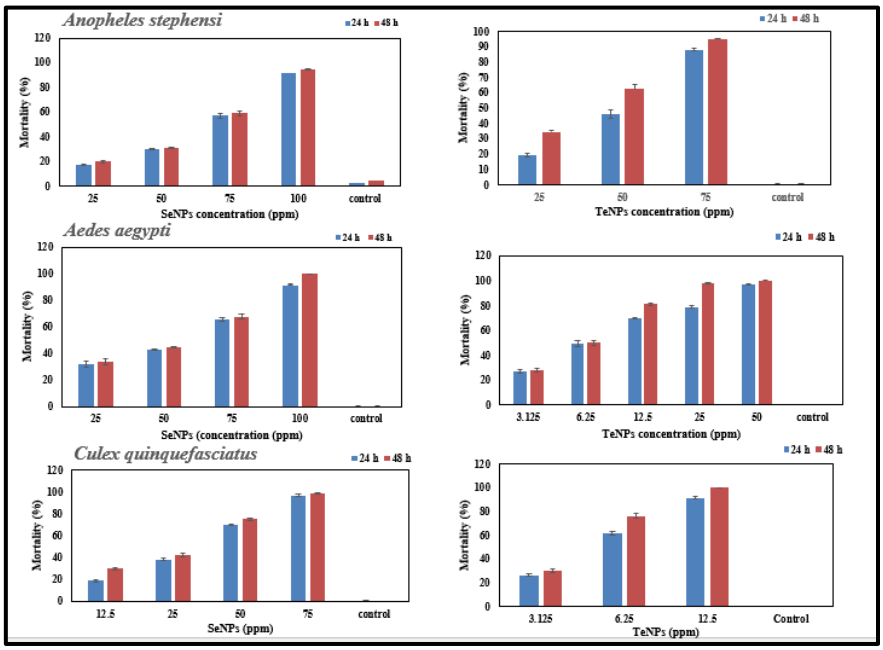

Fig. 6.19 Percent mortality of: *Anopheles stephensi* (a) & (d), *Aedes aegypti* (b) & (e), *Culex quinquefasciatus* (c) & f) treated with SeNPs and TeNPs respectively after 24 and 48 h.

Table 6.1: Larvicidal activity of biogenic SeNPs against *An. stephensi*, *Ae. aegypti* and *Cx. Quinquefasciatus*

SeNPs				
Mosquito spp.	**24 h**		**48 h**	
	LC_{50} (ppm) lower-upper limit	**LC_{90} (ppm) lower-upper limit**	**LC_{50} (ppm) lower-upper limit**	**LC_{90} (ppm) lower-upper limit**
Anopheles stephensi	**59.189** (44.753-78.282)	**141.163** (106.734-186.699)	**58.410** (44.156-77.265)	**140.500** (106.500-185.856)
Aedes aegypti	**50.378** (35.081-72.345)	**159.076** (110.773-228.441)	**44.506** (32.004-61.892)	**129.488** (93.114-180.079)
Culex quinquefasciatus	**29.925** (20.838-42.977)	**87.734** (61.091-125.997)	**24.800** (16.678-36.8790)	**82.383** (558.401-122.505)

Table 6.2: Larvicidal activity of biogenic TeNPs against *An. stephensi, Ae. aegypti* and *Cx. quinquefasciatus*.

TeNPs				
Mosquito spp.	**24 h**		**48 h**	
	LC_{50} (ppm) lower-upper limit	**LC_{90} (ppm) lower-upper limit**	**LC_{50} (ppm) lower-upper limit**	**LC_{90} (ppm) lower-upper limit**
Anopheles stephensi	**46.748** (34.904-62.610)	**99.982** (74.651-133.908)	**37.692** (26.725-53.159)	**93.511** (66.303-131.882)
Aedes Aegypti	**7.625** (4.341-13.395)	**51.102** (29.092-89.7655)	**5.974** (3.656-9.762)	**29.005** (17.750-47.397)
Culex quinquefasciatus	**5.325** (3.606-7.865)	**14.657** (9.925-21.646)	**4.367** (3.0789-6.194)	**10.265** (7.237-14.561)

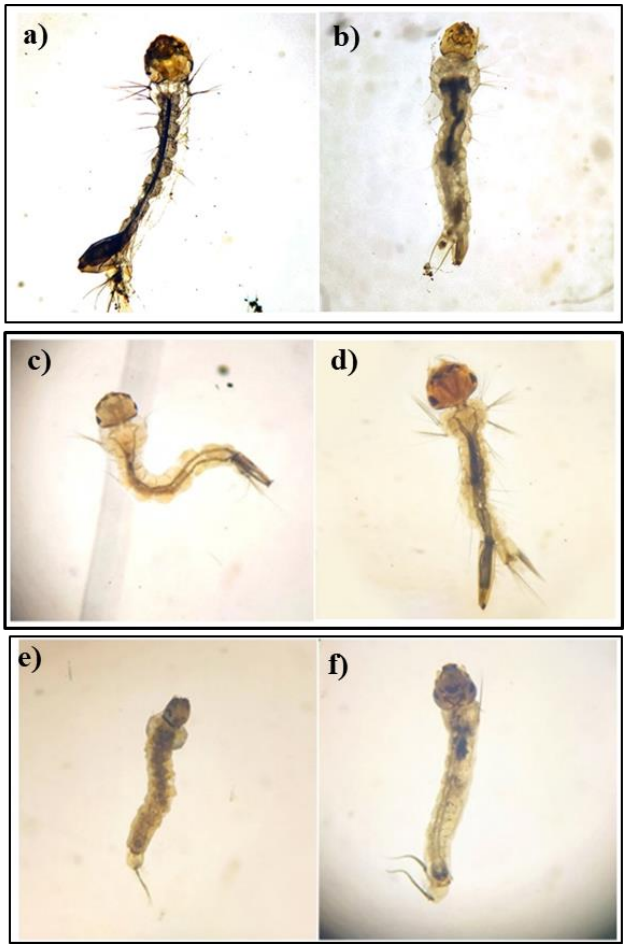

Fig. 6.20 Larvae of: *Aedes aegypti* (control) *(*a), *Aedes aegypti* (test) (b); *Culex quinquefasciatus* (control) (c), *Culex quinquefasciatus* (test) (d); *Anopheles stephensi* (control) (e), *Anopheles stephensi* (test) (f).

6.2.3 Agricultural applications of Se and Te NPs

6.2.3.1Anti-plant pathogen potential of Se and Te NPs

SeNPs and TeNPs demonstrated excellent anti-microbial activity against all the three plant pathogens. An increase in inhibition zone size with increasing concentrations of both Se and Te NPs was observed. Highest inhibition zone (5.2, 17.36 and 21.89 mm) was found to be for *F. oxysporum* at 25, 50 and 75 µg/mL SeNPs respectively whereas, smallest zone of inhibition (7.25, 12.58 and 18.25 mm) was noticed for *Sclerotium* sp. at 75, 100 and 125 µg/mL respectively (Fig.

6.21). TeNPs were effective in inhibiting the growth of plant pathogens at much lower concentrations as compared to SeNPs. For instance, highest zone of inhibition (7.2, 19.24, 28.56 and 33.25 mm) was observed for *Fusarium oxysporum* at 15, 30, 45 and 60 µg/mL respectively this was followed by *Microphomina* sp. and *sclerotium* sp. where 7.8, 12.85, 20.14 mm and 5.48, 10.59, 18.0 mm respectively (Fig. 6.22).

Thus, confirming the dose dependent antifungal activity of both Se and Te NPs. There are very few reports on antifungal activity of selenium nanoparticles (Ismail et al., 2016; Nandini et al., 2017). In one of the studies *A. solani* isolated from the leaves of the infected potato plants was reported to demonstrate 100 % inhibition of the pathogen in-vitro after 7 days of incubation (Ismail et al., 2016).

Interestingly, there are no reports available on anti-fungal properties of TeNPs. *F. oxysporum* although considered as a normal constituent of the fungal community in the rhizosphere of plants causes various diseases in various plant species (Gordon and Martyn, 1997). It causes Tracheomycosis (root rot) wherein the fungi penetrate into the roots and invade the vascular system, additionally they can also cause wilting causing damage to economically important species of plants (Gordon and Martyn, 1997).

Species belonging to genus *Fusarium* exhibits high level of host specificity and severe pathogenicity. *Macrophomina* spp. are among the most harmful ones which infect nearly 500 plants spp. in 100 or more families (Pratt et al., 1998). It affects fibrovascular system of roots and basal internodes of its hosts, thus impeding the transport of water and nutrients in the plant (Babu et al., 2007). It also causes collar rot, charcoal rot, damping off of seedling and blight (Babu et al., 2007; Khan et al., 2007). *Sclerotium* sp. are mainly known to cause white mold and southern blight (Inagaki and Makino 1977). The commonly used remedy to treat such pathogenic infections are various fungicides which mostly include toxic chemicals like methyl bromide causing

irreversible damage to the environment and additionally causing resistance. Ever increasing demands and use of these biocides are also reported to affect the non-target microorganisms which contribute synergistically to various plant and soil beneficiary process viz. nitrogen fixation, organic matter decomposition and nutrient release (Vyas, 1988; Edwards and Bater 1990).

It's worth mentioning that 90 % of these biocides are lost during or after application (Stephenson, 2003; Ghormade et al., 2011). Thus, it's mandatory to formulate high performing, cost effective biocides which are environmental friendly. Nanotechnology is being employed now to develop agricultural products which have added advantages to tackle aforementioned problems and includes, specificity, shelf life and toxicity.

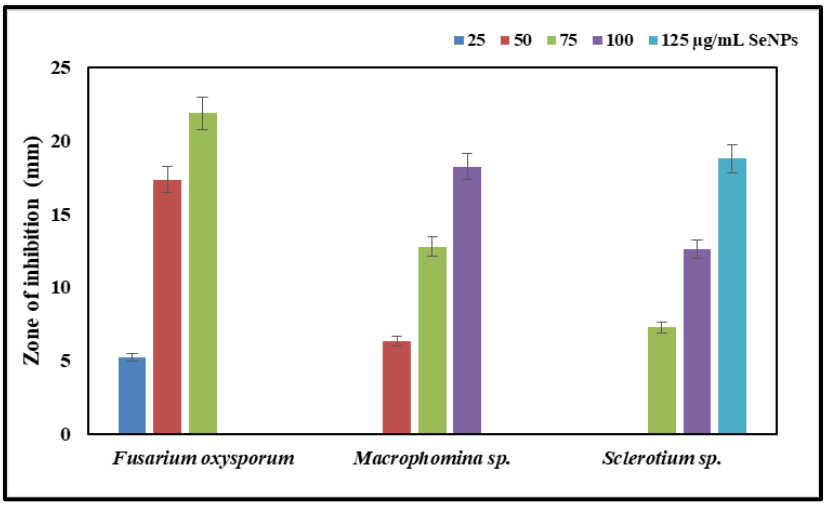

Fig. 6.21 Anti-plant pathogen potential of SeNPs.

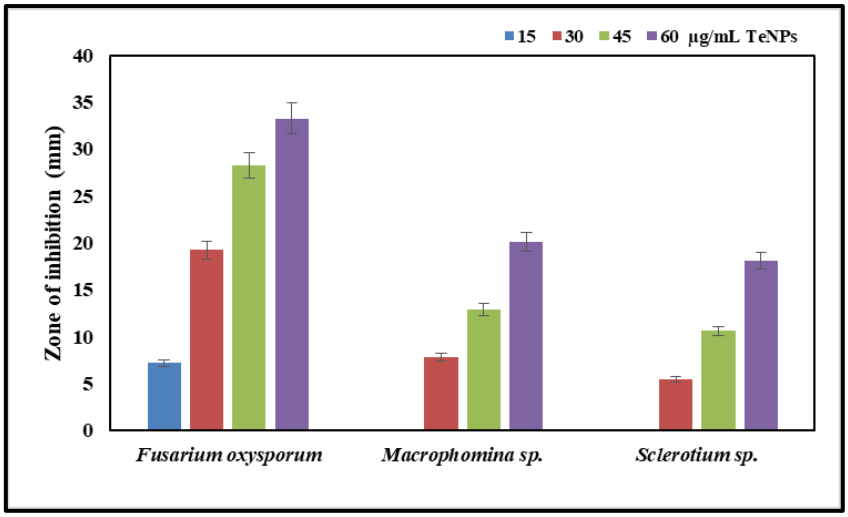

Fig. 6.22Anti-plant pathogen potential of TeNPs.

6.2.3.2 Effect of SeNPs on seed priming

6.2.3.2 Determination of final germination percentage, root and shoot length and seedling wet biomass

Although the % germination were found to be 100 % for all the treatments, the As (V) stress inhibited the growth of all the seedlings. While SeNPs supplemented seeds (var. *Jyoti*) via priming alone, enhanced the shoot length, root length and biomass accumulation by 1.2 and 1.4 and 1.2 folds respectively, as compared to seeds primed with DW (control). For instance, in presence of SeNPs (1 mg/L) the shoot length was found to be 7.1 cm whereas in control (Seeds+ DW) it was 6.1 cm after 10 days of incubation. It was observed that 1 mg/L of SeNPs were found to be more effective as compared to 0.8 mg/mL for all seeds. In presence of 1 mg/L arsenate the shoot length was found to be 5 cm whereas, in SeNPs (1 mg/L) primed seeds under As (V) stress it was calculated to be 6.9 cm after 10 days of incubation, indicating 1.38-fold increase (Fig. 6.23).

In case of root lengths, similar pattern was observed. For instance, in presence of (0.8 and 1 mg/L) of SeNPs alone, the root lengths were recorded to be 11.1 and 13.6 cm respectively after 10 day of incubation (Fig.6.24). Whereas, in control (seeds with DW) the root length was found to be 6.1 cm. The seeds under As (V) stress (0.8 and

1 mg/L) showed reduced root length (5.7 and 6.8 cm) respectively. While the root lengths of the seeds primed with SeNPs (0.8 and 1 mg/L) in presence of As (V) stress were found to be 7.5 and 10 cm respectively designating 1.5-fold increase. Selenite (1 mg/L) primed seeds also showed longer root length (10.3 cm) as compared to control (6.1 cm). Additionally, seeds primed with selenite (1 mg/L) under As stress also showed increase in root length and/or shoot length but not as effective as that of SeNPs. Figure 6.28 depicts the comparative growth of rice seedling under various treatments.

Similar observations were also recorded in case of wet biomass where 72 mg was recorded in case of control seeds while SeNPs primed (1 mg/L) seeds showed 81 mg of biomass after 10 days of incubation (Fig. 6.25). The biomass in case of seeds grown under As (V) stress was found to be 57 mg whereas, the seeds under As (V) stress treated with SeNPs (1 mg/L) were reported to retain biomass of 68 mg signifying 1.1-fold increase.

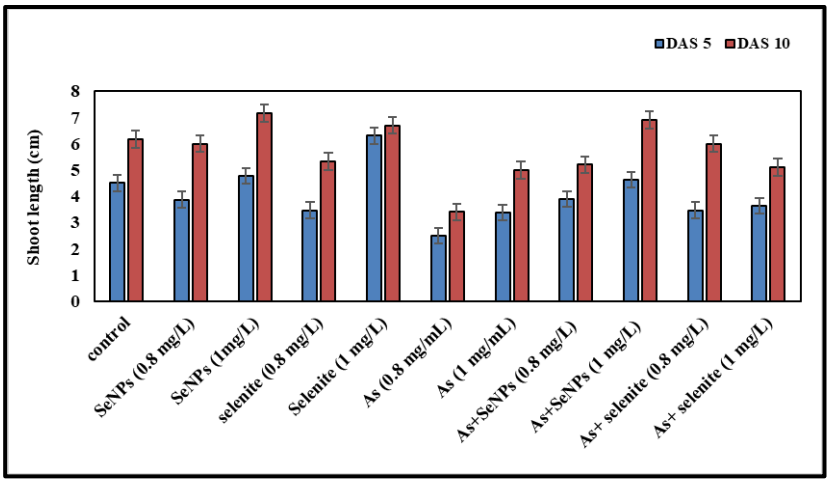

Fig. 6.23 Shoot length under various treatments after 5 and 10 days of germination.

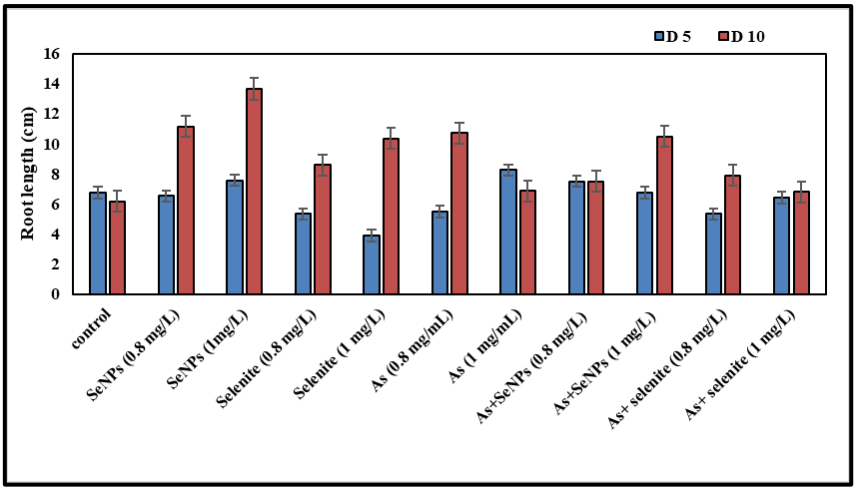

Fig. 6.24 Root length under various treatments after 5 and 10 days of germination.

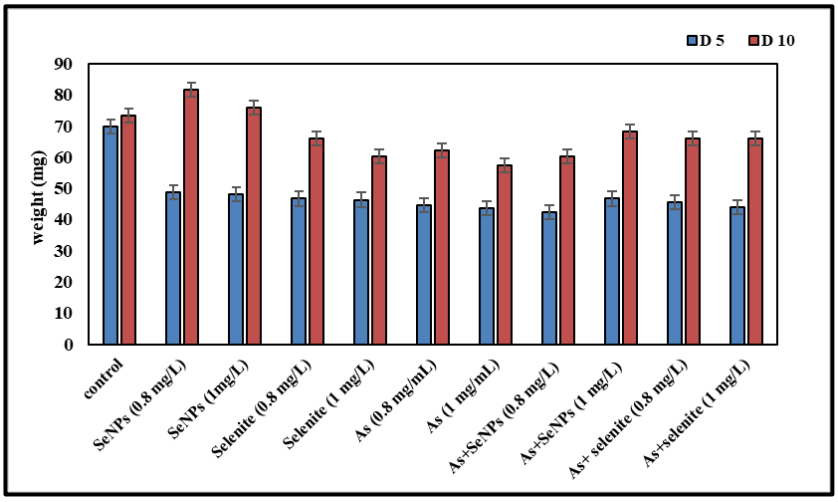

Fig. 6.25 Wet weight of rice seeds under various treatments after 5 and 10 days of germination.

6.2.3.2.2 Effect of seed priming on proline and phenolic contents of seeds

The proline content in control (Seeds with DW) was found to be 0.578 µmol/gm while in SeNPs (1mg/mL) primed seeds alone it was found to be 0.414 µmol/gm (Fig. 6.26). Under the stress of Arsenate (0.8 and 1 mg/L) the proline content were observed to be 0.9929 and 1.356

µmol/gm respectively. However, exceptional decrease of proline content in case of SeNPs (0.8 and 1 mg/mL) primed seeds under As (V) stress (0.745 and 0.822 77µmol/gm respectively) were observed. Whereas, in seeds primed with Na_2SeO_3 (0.8 and 1 mg/L) alone the proline was found to be 0.718 and 0.802 µmol/gm which was higher as compared to SeNPs primed seeds (0.6641 and 0.787 µmol/gm) after 10 days of incubation.

Similar trend in case of phenolic content was also observed. The control was recorded to exhibit the proline content of 5.125 mg/gm of seeds whereas seeds primed with SeNPs (0.8 and 1 mg/L) showed 5.25 and 6.15 mg/gm after 10 days (Fig. 7 A). The phenolic content in SeNPs primed seeds (0.8 and 1 mg/L) under As (V) stress was found to be 5.615 and 5.785 mg/gm respectively. Although seeds grown in selenite also showed decreased proline and/or phenolic contents but not as effective as observed in case of SeNPs (Fig 6.28).

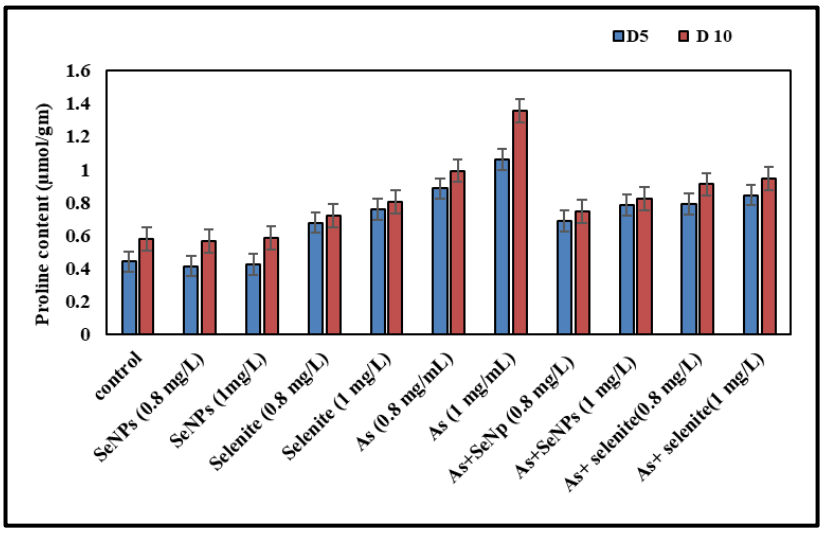

Fig. 6.26 Proline in rice plant with different treatments after 5 and 10 days of incubation.

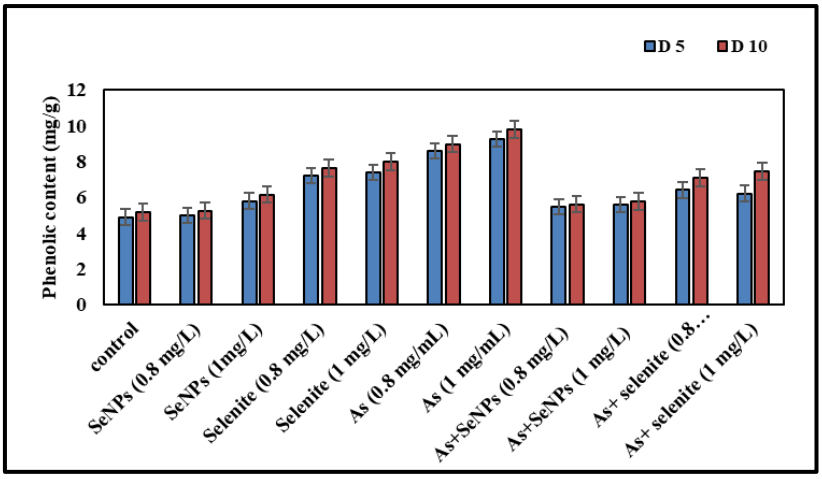

Fig. 6.27 Phenolic contents in rice plant with different treatments after 5 and 10 days of incubation.

Fig. 6.28 Rice plant under various treatment after 10 days of germination in presecen of 0.8 (A) and 1 mg/mL (B) SeNPs

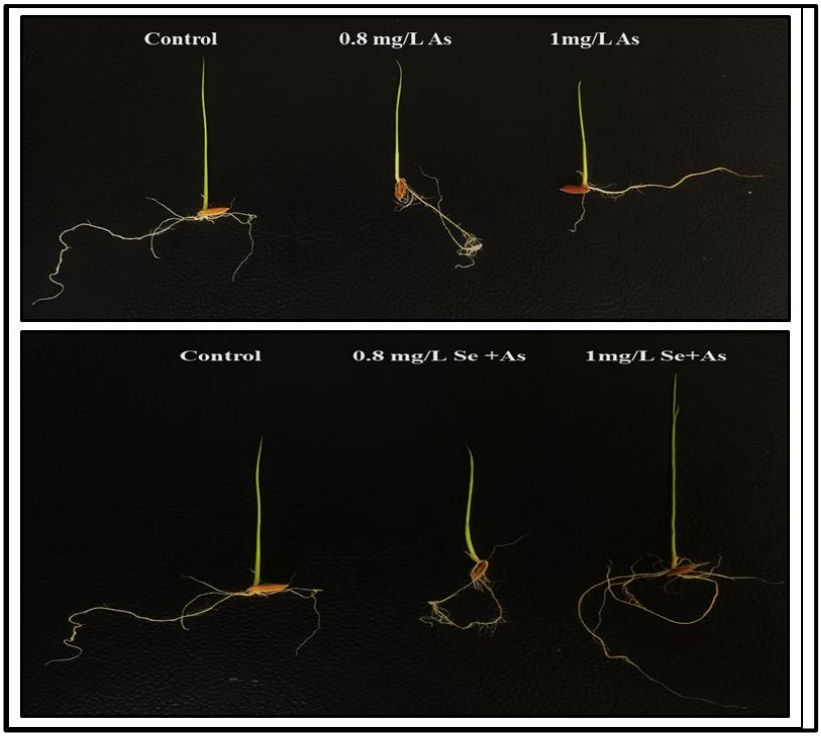

Fig. 6.29 Growth of rice seedlings under various treatments (after 10 days of germination).

Arsenic contamination in ground water is an alarming condition in south east Asian countries severely hampering the growth and development of crops. The sever concern for As contamination in irrigation or ground water is mainly because it shares common transport pathways with phosphates and silicates (Zhao et al., 2009). There are several methods which are reported to diminish the As stress in rice plants, like cultivation under aerobic conditions which reduce the As accumulation (Xu et al., 2008). However, newer methods encompassing use of latest technological advances like nanotechnology along with traditional ones are highly fascinating. Seed priming is one of the remarkably effective methods which involves the use of natural and/ or synthetic products to the seeds prior to germination.

Se at low concentration (1 mg/L) is known to be effective in enhancing the crop growth and also is known to behave antagonistically to As (Moulick et al., 2016). This study revealed that

SeNPs when supplemented in seeds and allowed to germinate under normal conditions exhibited excellent growth parameter viz. shoot length, root length and wet biomass thus, suggesting plant growth promoting ability. Previously, similar findings of using selenite in growth promotion was reported by Moulick and co-workers (2016) in rice crop of var. *Kranti* and *IR-36.* In yet another study by Cartes et al. (2011) beneficiary role of Se was reported in ryegrass cultivars. Se not only enhances the growth characters but also detoxifies the As stress.

Increased phenolic content with decrease in seedling growth indicated As toxicity to rice. Elevated phenolic contents are the indicator of various abiotic and biotic stress in plants (Khaliq et al., 2016). Interestingly, SeNPs primed seeds under As stress are known to alleviate the phenolic contents thus showing ameliorative effect of Se on the rice seeds.The increased proline content in As stressed seedlings also pointed the negative role of As. Proline is known as a cytoplasmic osmoticum and it also known to prevent protein denaturation (Moulick et al., 2016). It is mainly known as a stress marker for oxidative damage and it is well known fact that SeNPs can act as an excellent antioxidant agent. However, exact antagonistic mechanism of Se and As is not exactly known.

6.2.3.3. Role of SeNPs in plant growth promotion

With the advancement of nanotechnology in various fields it's now firmly anchoring its roots in the field of agriculture. Previously engineered nanoparticles viz. ZnONPs, FeONPs, ZnCuFe-oxideNPs, CaPNPs, AgNPs, had plant growth enhancing potential in various food crops when used as micronutrients (Mousavi Kouhi et al., 2014). Soil less farming widely known as hydroponics system used for plant cultivation is among the various methods for uptake of nanoparticles which have added advantages (Shankar et al., 2014).

The advantages of using nano-bio-formulations for plants include high growth rate, better food production with high

micronutrient levels, improved biomass, and artificial photosynthesis (Khodakovskaya et al., 2009). The plants grown in the presence of SeNPs showed enhanced growth in terms of root length, shoot length and total biomass as compared to the control. The root length of the test and control samples after 15 days was found to be (35 and 23 cm) respectively whereas, after 45 days it was 77 and 51.3 cm respectively. Similarly, the shoot length in control was found to be 6.4 and 17.2 cm after 15 and 45 days of incubation respectively while, test was reported to exhibit root length of 58.8 and 83.3 cm respectively (Fig. 6.30 & 6.31).

Se is essential as a micronutrient (1 mg/L) in plants however, SeNPs has added advantages as it can be easily taken up by the plants due its minute size. There are various applications of Se and its compounds in agriculture which include direct addition to soil, soaking seeds prior to sowing, hydroponics and aeroponics, as plant fortifying agents and foliar application of plants with Se solution (El-Batal et al., 2016). Se in nano dimensions has added advantages moreover, it also exhibits anti-plant pathogen potential along with antioxidants. It has been reported that nanoparticles regulate plant growth by limiting the reactive oxygen species (ROS) pathways (Mittler, 2017). Thus, novel nano-micronutrient fortified with anti-plant pathogen potential could be an ideal candidate in agro industries.

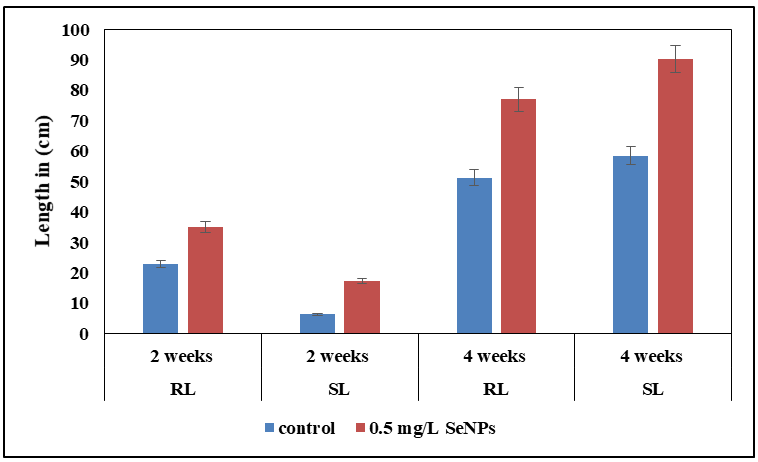

Fig. 6.30 Root and shoot length of radish crop after incubation with SeNPs.

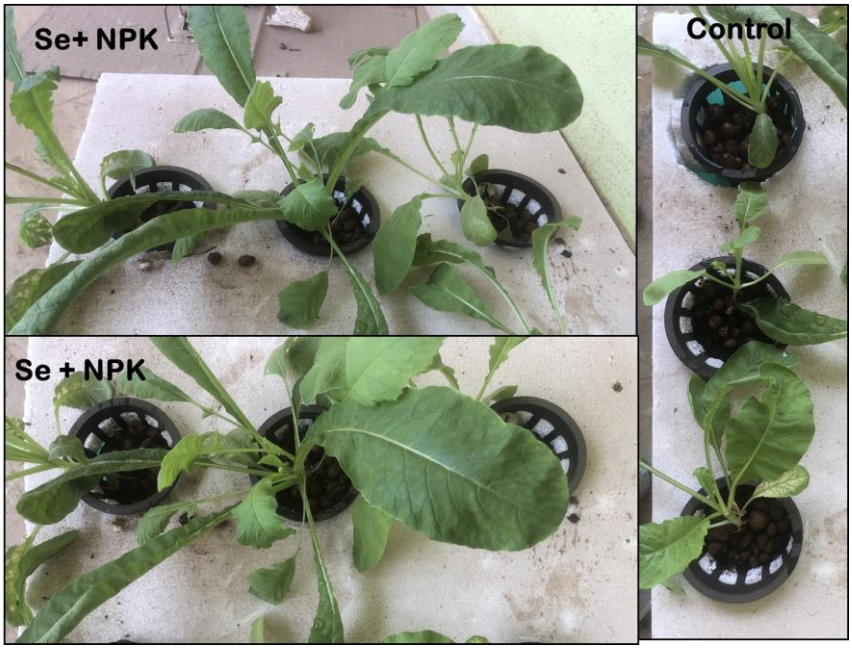

Fig. 6.31 Radish plant grown in NPK (2:1:1) supplemented with SeNPs (pH 5) with control: radish plant grown in NPK only.

Summary

SeNPs did not reveal any dose dependent genotoxicity on human blood lymphocytes whereas time and dose-dependent genotoxicity at concentrations higher than **15 µg/mL** of TeNPs was observed. SeNPs and TeNPs demonstrated excellent anti-microbial activities against all 8 pathogenic isolates. TeNPs were effective in inhibiting the pathogens at much lower concentrations as compared to SeNPs. It was observed that both Se and Te NPs were effective in inhibiting the biofilm formation at **20, 25** and **50 µg/mL** of Se and **5, 10** and **15 µg/mL** of TeNPs respectively. Dislodging of bacterial biofilm with increasing concentrations of NPs was clearly evident from the SEM images along with bacterial morphological alterations.

Biogenic SeNPs and TeNPs exhibited excellent dose dependent anti-oxidant potential at **50** and **36 µg/mL** respectively. SeNPs demonstrated exceptional dose-dependent and selective anti-proliferative activity against A549 adenocarcinomal human alveolar cell line where in complete mortality was observed at **70 µg/mL** of SeNPs.

The SeNPs treated cells also demonstrated morphological changes indicating anti-proliferation. The alkaline comet assay revealed geno-protective potential of these biogenic SeNPs **(10 µg/mL)** against UV-B induced DNA damage in human blood lymphocytes.

The biogenic Se and Te NPs at **5** and **10 µg/mL** evidently demonstrated **100** and **90 %** reduction of methylene blue dye respectively. TeNPs were more effective in inhibiting the mosquito larval population as compared to SeNPs at much lower concentrations. SeNPs and TeNPs demonstrated excellent anti-microbicity against all the three plant pathogens procured from ICAR, Goa.

It was observed that As stress inhibited the germination as well as the growth of the seedlings. In presence of SeNPs **(0.8 and 1 mg/L)** an increase in germination and seed growth was clearly seen. Moreover, increase in proline and phenolic content in As (V) treated seeds was prominent and it was found to be reduced in As (V) along with SeNPs

treated samples. Therefore, taken together, the results confirmed the role of SeNPs to ameliorate the seed potential under As stress.

The plants grown in hydroponics in the presence of SeNPs **(0.5 mg/L)** showed enhanced growth in terms of root length and shoot length as compared to the control. The alkaline comet assay also revealed geno-protective potential of these biogenic SeNPs against UV induced DNA damage in human blood lymphocytes. Se and Te NPs also demonstrated anti-plant pathogen activity.

Salient features of the research

- This is the first report of its kind on bioreductive detoxification of selenium biosynthesis by *Halomonas* sp. with highest MIC of 101 mM for Na_2SeO_3.
- We also report for the first-time biosynthesis of biogenic Te nanorods from *Shewanella* sp. exhibiting highest MIC of 6 mM for K_2TeO_3.
- 100 % reduction of 2 mM K_2TeO_3 was achieved at the end of the stationary growth phase (i.e. 38 h) which is the shortest time recorded so far.
- First ever report demonstrating geno-protective potential of biogenic SeNPs biosynthesised by bacteria.
- This is the first report showing photo-catalytic activity of biogenic TeNPs in methylene blue reduction.
- First ever report on mosquito larvicidal activity of TeNPs.
- First ever report demonstrating the genotoxicity of biogenic TeNPs.
- First to report use of SeNPs in ameliorating the effect of As (V) in rice crop and also in plant growth promotion in hydroponics.

Future prospects

- This study successfully demonstrated the biosynthesis of Se and Te nanoparticles thus, this method could be used for synthesis of various other metals, metalloid and semiconductor nanoparticles with desired shape and size.
- Biosynthesised Se and Te NPs confirmed various applications in medicine, environment and agriculture likewise, they also can be explored for additional applications viz. catalytic priorities for applications in industrial sectors.
- Protein profile of *Halomonas* sp. and *Sewanella* sp. in absence and presence of respective metalloid can be studied for better understanding the interactions of proteins with metalloids.
- Biogenic SeNPs also exhibited excellent selective anti-cancer potential against A549 adenocarcinomic human alveolar cells further, they can be studied for mechanism studies for better understanding the exact phase of arrest or oxidative damage and apoptosis additionally, immunological response studies also can be carried out.

\

Appendices

Appendix A

Media and Buffer composition

A.1 Zobell Marine Broth/ Agar 2216	g/L
Peptic digest of animal tissue	5
Yeast extract	1
Ferric citrate	0.1
Sodium chloride	19.45
Magnesium chloride	8.8
Sodium sulphate	3.24
Calcium chloride	1.8
Potassium chloride	0.55
Sodium bicarbonate	0.16
Potassium bromide	0.08
Strontium chloride	0.034
Boric acid	0.022
Sodium silicate	0.004
Sodium fluorate	0.0024
Ammonium nitrate	0.0016
Disodium phosphate	0.008
Agar	12

A.2 Mueller Hinton Agar	g/L
Meat infusion	2.0
Casein acid hydrolysate	17.5
Starch	1.5
Agar agar	17.0
pH	7.3±0.2

A.3 Nitrate Broth	g/L
Peptic digest of animal tissue	5.0
Meat extract	3.0
Potassium nitrate	1.0
Sodium chloride	30.0
pH (at 25 °C)	7.0±0.2

A.4 Nutrient Broth	g/L
Peptone	10.0
Beef extract	10.0
Sodium chloride	5.0
pH (at 25 °C)	7.3±0.1

Appendix-B

Other Chemicals

B.1 Prepare a stock solution of metals/ metalloids

1. Sodium selenite	17.29 g
DW	100 mL
2. Potassium tellurite	25.38 g
DW	100 mL
3. Zinc sulphite	28.75 g
DW	100 mL
4. Cadmium chloride	26.84 g
DW	100 mL
5. Lead nitrate	3.31 g
DW	100 mL
6. Arsenate	13.8g
DW	100 mL

Filter the solution through a 0.22-micron membrane and store.

B.2 KOH (3 %)

KOH	3.0 g
Distilled water	100 mL

B.3 Phosphate buffered saline (PBS)

137 mM NaCl

2.7 mM KCl

10 mM Na_2HPO_4

2 mM KH_2PO_4

Adjust the pH to 7.4

B.4 Reagents for Nitrate Reductase

B.4.1. 0.1 % N-(1-naphthyl) ethylenediamine dihydrochloride (ReagentA)

N-(1-naphthyl) ethylenediamine dihydrochloride 0.1 g

DW 100 mL

B.5 1 % Sulfanilic acid (Reagent B)

Sulfanilic acid 1 g

5 % phosphoric acid 100 mL

B.6 mercuric chloride (0.1 %)

Mercuric chloride 0.1 g

DW 100 mL

Appendix- C

C.1 PCR reaction mixture

Component	Concentration	Quantity
Template DNA	50 ng/µL	4 µL
Master mix	2X	25 µL
Forward primer	20 mM	2 µL
Reverse primer	20 mM	2 µL
Deionized water	-	17 µL
	Total volume	50 µL

C.2 Agarose Gel Electrophoresis

C.2.1 0.8 % and 1 % agarose

Weigh 0.8 g and 1.0 g and dissolve in 100 mL of 1X TAE buffer to prepare 0.8 % and 1 % agarose respectively. Melt the solution in microwave oven until clear, transparent solution is obtained. Add ethidium bromide to a final concentration of 0.5 µg/mL and cast the gel.

C.2.2 Ethidium Bromide

Add 1.0 g of ethidium bromide to 100 mL of deionized water. Stir on magnetic

stirrer for several hours to ensure that the dye has dissolved. Transfer the solution to amber coloured bottle and store at room temperature.

C.2.3 Gel Loading Buffer

0.05 % (w/v) Bromophenol blue

40 % (w/v) Sucrose

0.1M Ethylenediaminetetraaceticacid (EDTA) (pH 8.0)

0.5 % (w/v) Sodium dodecyl sulphate

C.2.4 10X Tris EDTA (TE) Buffer (pH 8.0)

Tris Chloride 100 mM

EDTA 10 mM

Sterilize for 20 min at 15 psi.

C.3 Reagents for comet assay

C.3.1 Normal Agarose

100 mg of normal agarose was mixed with 9 mL of DDW and heated till the agarose dissolves. 1 mL of 10X PBS was added and the final volume was made up to 10 mL with DDW.

C.3.2 Low Melting Agarose 0.5 %

0.5 % LMA was prepared by mixing 50 mg of low melting agarose with 9 mL of DDW and heated until just boiling. 1 mL of 10X PBS was added and the solution was made up to a final volume of 10 mL with DDW.

C.3.3 Lysing solution

73.01 g of NaCl, 18.7 g of EDTA and 0.6 g of Tris were dissolved in about 350 mL DDW. About 4 g of NaOH pellets were added and the mixture was allowed to dissolve. The pH was adjusted to 10 by HCl and to 445 with double DW. The remaining amount (55 mL) was adjusted by 10 % DMSO and 1 % Triton X which was added fresh according to the required amount.

10 mM Tris, pH 10

10 % DMSO

1 % TritonX-100

C.3.4. Electrophoresis buffer (pH > 13)

A. Stock solution

10 N NaOH: 200 g of NaOH pellets were dissolved in 500 mL DDW. This solution was dispersed in 27 mL aliquots in tightly capped tubes and was stored at ambient temperature (28-34 °C).

200 mM EDTA: 14.89 g of EDTA was dissolved in 200 mL DDW, the pH was adjusted to 10 and stored at ambient temperature (28-34 °C).

B. Working solution

The working solution was prepared by mixing 27 mL of 10 N NaOH, 4.5 mL of 200 mM EDTA and 1 mL of DMSO. The working solution was prepared fresh before each run.

C.3.5 Neutralization buffer (400 mM Tris, pH 7.5)

4.845 g of Tris base was added to 90 mL of DDW. The pH was adjusted to 7.5 and the volume was adjusted to 100 ml. the solution was stored at room temperature.

C.3.6 Stain

Ethidium bromide	15 µg
DW	1 mL

Standard curves

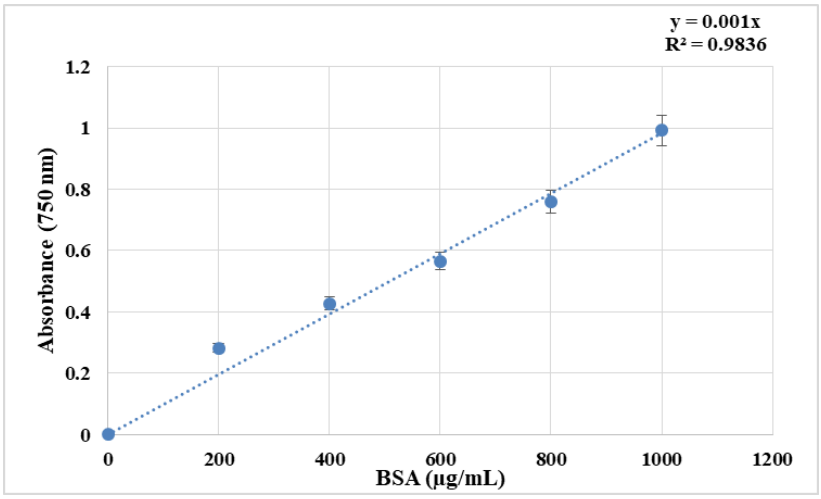

Fig. A standard curve for estimation of Proteins using Lowry's method. Values are mean ± (standard error) for three independent experiments.

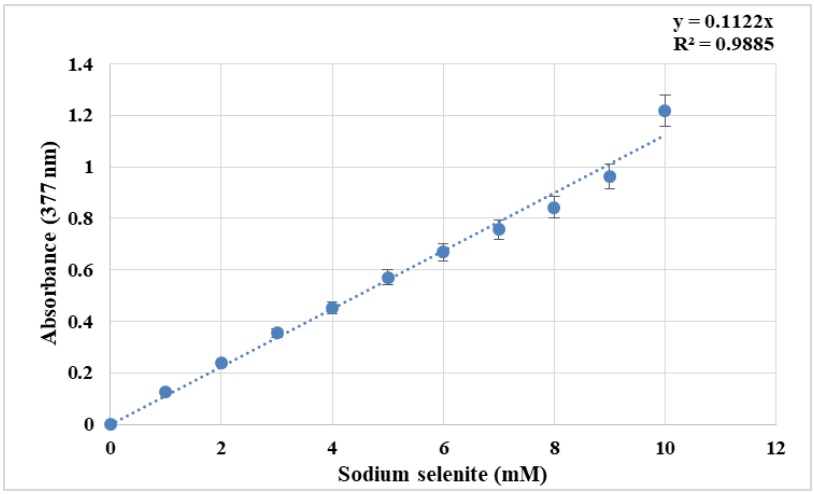

Fig. B Calibration curve of sodium selenite for estimation of selenite using 2,3-diaminonaphthalene (2,3-DAN).

Values are mean ± (standard error) for three independent experiments.

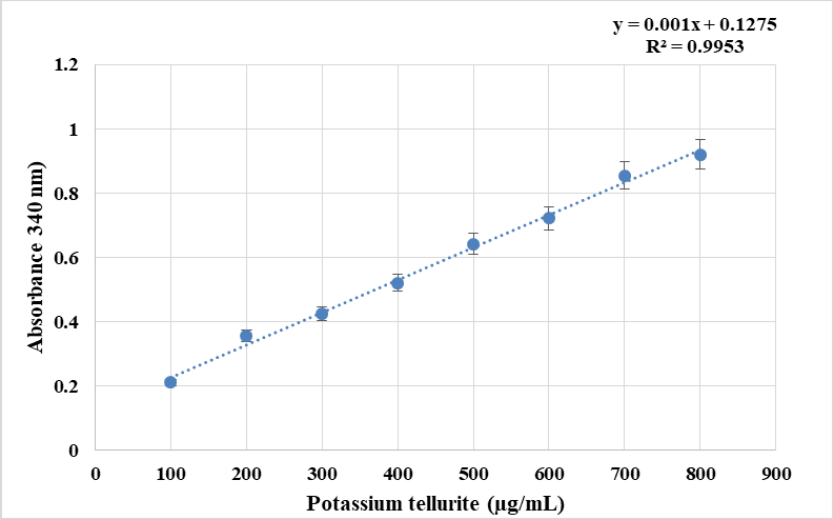

Fig. C Calibration curve of potassium tellurite (K2TeO3) for estimation of tellurite using diethyldithiocarbamate (DDTC).

Values are mean ± (standard error) for three independent experiments.

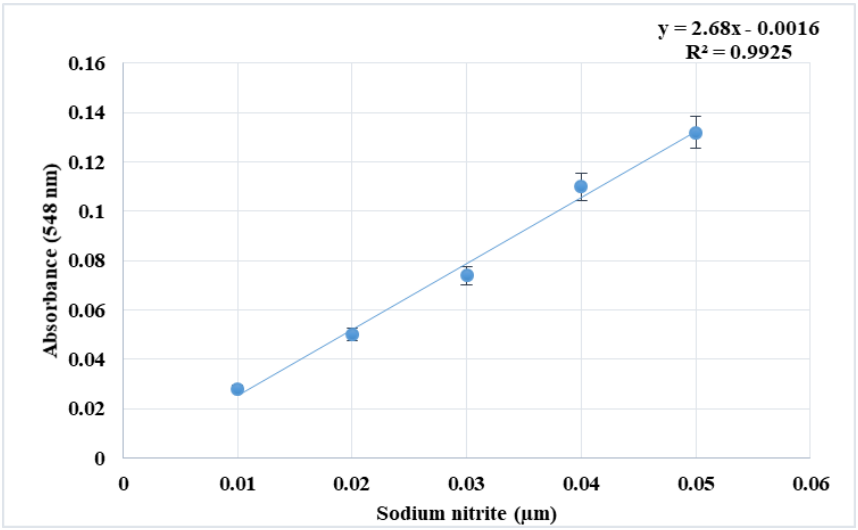

Fig. D Calibration curve of sodium nitrite for estimation of nitrite concentration.

Values are mean ± (standard error) for three independent experiments.

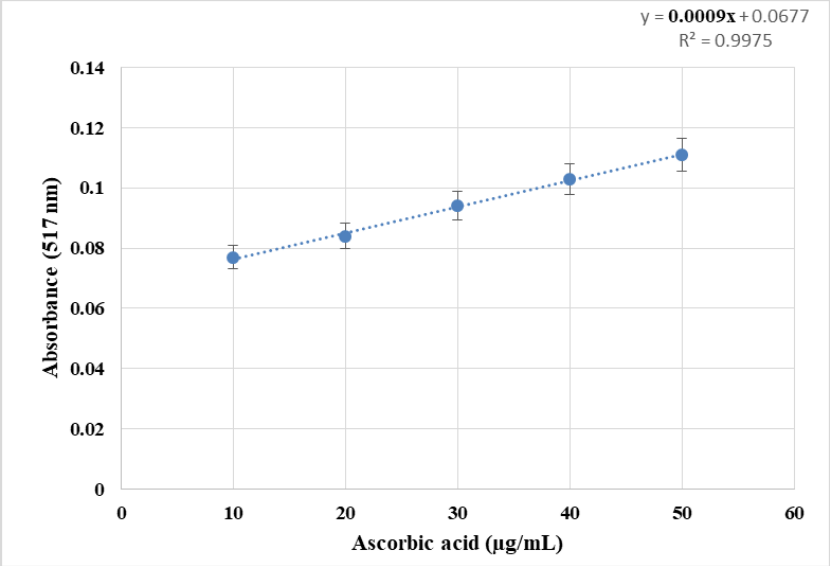

Fig. E Calibration curve of ascorbic acid for estimation of DPPH free radical scavenging activity.

Values are mean ± (standard error) for three independent experiments.

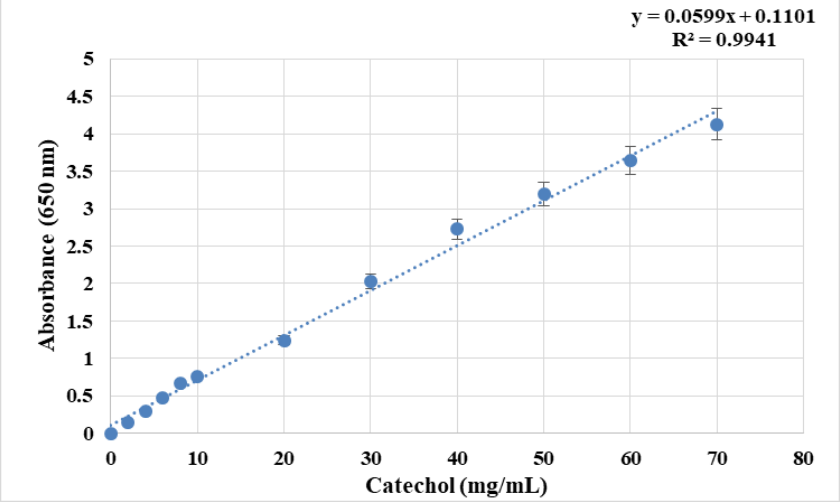

Fig. F Standard curve for estimation of phenol.

Values are mean ± (standard error) for three independent experiments.

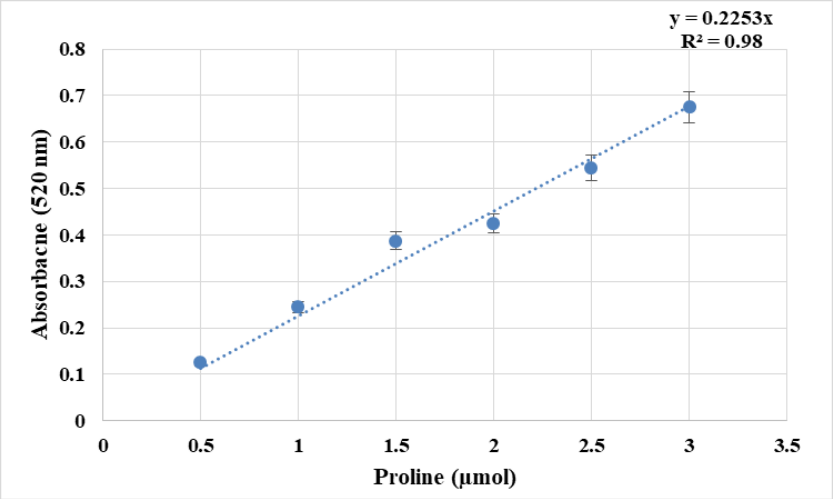

Fig. G Standard curve for estimation of proline.

Values are mean ± (standard error) for three independent experiments.

Bibliography

- Ábrahám, E., Hourton-Cabassa, C., Erdei, L. and Szabados, L., 2010. Methods for determination of proline in plants. In Plant Stress Tolerance. 317-331. Humana Press.
- Adhikari, B. and Banerjee, A., 2010. Facile synthesis of water-soluble fluorescent silver nanoclusters and HgII sensing. Chem. Mater. 22(15): 4364-4371.
- Adschiri, T., Hakuta, Y., Sue, K. and Arai, K., 2001. Hydrothermal synthesis of metal oxide nanoparticles at supercritical conditions. J. Nanopart. Res. 3(2-3): 227-235.
- Ahmad, A., Senapati, S., Khan, M.I., Kumar, R., Ramani, R., Srinivas, V. and Sastry, M., 2003. Intracellular synthesis of gold nanoparticles by a novel alkalotolerant actinomycete, *Rhodococcus* species. Nanotechnology, 14(7): 824.
- Al-Dhabi, N.A., Mohammed Ghilan, A.K. and Arasu, M.V., 2018. Characterization of silver nanomaterials derived from marine *Streptomyces* sp. al-dhabi-87 and its in vitro application against multidrug resistant and extended-spectrum beta-lactamase clinical pathogens. Nanomaterials, 8(5): 279.
- Ali, D.M., Sasikala, M., Gunasekaran, M. and Thajuddin, N., 2011. Biosynthesis and characterization of silver nanoparticles using marine cyanobacterium, *Oscillatoria willei* NTDM01. Dig. J. Nanomater. Biostruct. 6(2): 385-390.
- Allan, C.B., Lacourciere, G.M. and Stadtman, T.C., 1999. Responsiveness of selenoproteins to dietary selenium. Ann. Rev. Nutr. 19(1): 1-16.
- Altschul, S. F., Gish, W., Miller, W., Myers, E. W. and Lipman, D. J., 1990. Basic local alignment search tool. J. Mol. Biol. 215(3): 403-410.
- Amendola, V. and Meneghetti, M., 2009. Laser ablation synthesis in solution and size manipulation of noble metal nanoparticles. Phys. Chem. Phys. 11(20): 3805-3821.
- Amoozegar, M.A., Ashengroph, M., Malekzadeh, F., Razavi, M.R., Naddaf, S. and Kabiri, M., 2008. Isolation and initial

characterization of the tellurite reducing moderately halophilic bacterium, *Salinicoccus* sp. strain QW6. Microbiol. Res. 163(4): 456-465.

- Anderson, G.L., Williams, J. and Hille, R., 1992. The purification and characterization of arsenite oxidase from *Alcaligenes faecalis*, a molybdenum-containing hydroxylase. J. Biol. Chem. 267(33): 23674-23682.
- Andersson, C.M., Brattsand, R., Hallberg, A., Engman, L., Persson, J., Moldéus, P. and Cotgreave, I., 1994. Diaryl tellurides as inhibitors of lipid peroxidation in biological and chemical systems. Free Radic. Res. 20(6): 401-410.
- Anil Kumar, S., Abyaneh M.K., Gosavi, S.W., Kulkarni, S.K., Pasricha, R., Ahmad, A. and Khan, M.I., 2007. Nitrate reductase-mediated synthesis of silver nanoparticles from AgNO3. Biotechnol. Lett. 29:439-445.
- Arthur J.R., McKenzie R.C. and Beckett G.J., 2003. Selenium in the immune system. J. Nutr. 133, 1457S-1459S.
- Asmathunisha, N. and Kathiresan, K., 2013. A review on biosynthesis of nanoparticles by marine organisms. Colloids Surf. B. 103, 283-287.
- Avazéri, C., Turner, R.J., Pommier, J., Weiner, J.H., Giordano, G. and Verméglio, A., 1997. Tellurite reductase activity of nitrate reductase is responsible for the basal resistance of *Escherichia coli* to tellurite. Microbiol. 143(4): 1181-1189.
- Babu, B.K., Mesapogu, S., Sharma, A., Somasani, S.R. and Arora, D.K., 2011. Quantitative real-time PCR assay for rapid detection of plant and human pathogenic *Macrophomina phaseolina* from field and environmental samples. Mycologia 103(3): 466-473.
- Baesman, S.M., Bullen, T.D., Dewald, J., Zhang, D., Curran, S., Islam, F.S., Beveridge, T.J. and Oremland, R.S., 2007. Formation of tellurium nanocrystals during anaerobic growth of bacteria that use Te oxyanions as respiratory electron acceptors. Appl. Environ. Microbiol. 73(7): 2135-2143.

- Basnayake, R.S.T., Bius, J.H., Akpolat, O.M. and Chasteen, T.G., 2001. Production of dimethyl telluride and elemental tellurium by bacteria amended with tellurite or tellurate. Appl. Organomet. Chem. 15(6): 499-510.
- Bauer A., Kirby W., Sherris J. and Turck M., 1966. Antibiotic susceptibility testing by a standardized single disc method. Am. J. Clin. Pathol. 45, 493-49.
- Bausinger, J. and Speit, G., 2016. The impact of lymphocyte isolation on induced DNA damage in human blood samples measured by the comet assay. Mutagenesis 31, (5): 567-572.
- Baygar, T. and Ugur, A., 2017. In vitro evaluation of antimicrobial and antibiofilm potentials of silver nanoparticles biosynthesised by *Streptomyces griseorubens*. IET Nanobiotechnol. 677-681.
- Benelli, G., 2015. Research in mosquito control: current challenges for a brighter future. Parasitol. Res. 114(8): 2801-2805.
- Borghese, R. and Zannoni, D., 2010. Acetate permease (ActP) is responsible for tellurite (TeO_3^{2-}) uptake and resistance in cells of the facultative phototroph *Rhodobacter capsulatus*. Appl. Environ. Microbiol. 76(3): 942-944.
- Borghese, R., Marchetti, D. and Zannoni, D., 2008. The highly toxic oxyanion tellurite (TeO_3^{2-}) enters the phototrophic bacterium *Rhodobacter capsulatus* via an as yet uncharacterized monocarboxylate transport system. Arch. Microbiol. 189(2): 93-100.
- Bouloudenine, M. and Bououdina, M., 2016. Toxic effects of engineered nanoparticles on living cells. In Emerging Research on Bioinspired Materials Engineering. IGI Global. 35-68.
- Brelle, M., Zhang, J., Nguyen, L. and Mehra, R., 1999. Synthesis and ultrafast study of cysteineand glutathione-capped Ag2S semiconductor colloidal nanoparticles. J. Phy Chem. 103:10194-10201.

- Burda, C., Chen, X., Narayanan, R. and El-Sayed, M.A., 2005. Chemistry and properties of nanocrystals of different shapes. Chem. Rev. 105(4): 1025-1102.
- Cadet, J. and Douki, T., 2011. Oxidatively generated damage to DNA by UVA radiation in cells and human skin. J. Invest. Dermatol. 131(5): 1005-1007.
- Cartes, P., Gianfreda, L., Paredes, C. and Mora, M.L., 2011. Selenium uptake and its antioxidant role in ryegrass cultivars as affected by selenite seed pelletization. J. Soil Sci. Plant Nutr. 11(4): 1-14.
- Chasteen, T., Fuentes, D., Tantaleán, J. and Vásquez, C., 2009. Tellurite: history, oxidative stress, and molecular mechanisms of resistance. FEMS Microbiol. Rev. 33(4): 820-832.
- Chauhan, A., Zubair, S., Tufail, S., Sherwani, A., Sajid, M., Raman, S.C., Azam, A. and Owais, M., 2011. Fungus-mediated biological synthesis of gold nanoparticles: potential in detection of liver cancer. Int. J. Nanomed. 6, 2305.
- Chen, J.S., 2012. An original discovery: selenium deficiency and Keshan disease (an endemic heart disease). Asia. Pac. J. Clin. Nutr. 21(3): 320-326.
- Chen, T., Wong, Y.S., Zheng, W., Bai, Y. and Huang, L., 2008. Selenium nanoparticles fabricated in *Undaria pinnatifida* polysaccharide solutions induce mitochondria-mediated apoptosis in A375 human melanoma cells. Colloids Surf. B. 67(1): 26-31.
- Chiong, M., Barra, R., González, E. and Vásquez, C., 1988a. Resistance of *Thermus* spp. to potassium tellurite. Appl. Environ. Microbiol. 54(2): 610-612.
- Chiong, M., González, E., Barra, R. and Vásquez, C., 1988b. Purification and biochemical characterization of tellurite-reducing activities from *Thermus thermophilus* HB8. J. Bacteriol. 170(7): 3269-3273.
- Cooper, P.D. and Few, A.V., 1952. Uptake of potassium tellurite by a sensitive strain of *Escherichia coli*. Biochem. J. 51(4): 552.

- Cortés-Gutiérrez, E., Dávila-Rodríguez, M., Fernández, J., López-Fernández, C., Gosálbez, A. and Gosálvez, J., 2011. New application of the comet assay: chromosome-comet assay. J. Histochem. Cytochem. 59(7): 655-660.
- Cunha, R., Gouvea, I. and Juliano, L., 2009. A glimpse on biological activities of tellurium compounds. Ana. Acad. Bras. 81(3): 393-407.
- Daniel, M. and Astruc, D., 2004. Gold nanoparticles: assembly, supramolecular chemistry, quantum-size-related properties, and applications toward biology, catalysis, and nanotechnology. Chem. Rev. 104(1): 293-346.
- Dhanjal, S. and Cameotra, S., 2010. Aerobic biogenesis of selenium nanospheres by *Bacillus cereus* isolated from coalmine soil. Microb. Cell Fact. 9(1): 52.
- Di Tomaso, G., Fedi, S., Carnevali, M., Manegatti, M., Taddei, C. and Zannoni, D., 2002. The membrane-bound respiratory chain of *Pseudomonas pseudoalcaligenes* KF707 cells grown in the presence or absence of potassium tellurite. Microbiology 148(6): 1699-1708.
- Drexler, K.E., 1981. Molecular engineering: An approach to the development of general capabilities for molecular manipulation. Proc. Natl. Acad. Sci. 78(9): 5275-5278.
- Drexler, K.E., 1986. Engines of creation. Anchor.
- Douglas, T., Dickson, D,P., Betteridge, S., Charnock, J., Garner, C.D., and Mann, S., 1995. Synthesis and structure of an iron (iii) sulphide-ferritin bioinorganic nanocomposite. Science 269:54- 57
- Edition, F., 2011. Guidelines for drinking-water quality. WHO Chron. 38(4): 104-8.
- Edwards, C.A. and Bater, J.E., 1990. An evaluation of laboratory and field studies for the assessment of the environmental effects of pesticides. In Proceedings of the Brighton Crop Protection Conference, Pests and Diseases. BCPC 3, 963-968.

- El-Batal, A., Sidkey, N., Ismail, A., Arafa, R. and Fathy, R., 2016. Impact of silver and selenium nanoparticles synthesized by gamma irradiation and their physiological response on early blight disease of potato. J. Chem. Pharm. Res. 8(4): 934-951.
- Elías, A., Díaz-Vásquez, W., Abarca-Lagunas, M.J., Chasteen, T.G., Arenas, F. and Vásquez, C.C., 2015. The *ActP* acetate transporter acts prior to the *PitA* phosphate carrier in tellurite uptake by *Escherichia coli*. Microbiol. Res. 177, 15-21.
- Ellis, R. and Roberts, E., 1981. The quantification of ageing and survival in orthodox seeds. Seed Sci. Technol. 9, 373-409.
- Fang, J., Lu, J. and Holmgren, A., 2005. Thioredoxin reductase is irreversibly modified by curcumin a novel molecular mechanism for its anticancer activity. J. Biol. Chem. 280(26): 25284-25290.
- Fesharaki, P.J., Nazari, P., Shakibaie, M., Rezaie, S., Banoee, M., Abdollahi, M. and Shahverdi, A.R., 2010. Biosynthesis of selenium nanoparticles using *Klebsiella pneumoniae* and their recovery by a simple sterilization process. Braz. J. Microbiol. 41(2): 461-466.
- Fleischmann, R., Adams, M., White, O., Clayton, R., Kirkness, E., Kerlavage, A., Bult, C., Tomb, J., Dougherty, B. and Merrick, J., 1995. Whole-genome random sequencing and assembly of *Haemophilus influenzae* Rd. Science 269(5223): 496-512.
- Forootanfar, H., Amirpour-Rostami, S., Jafari, M., Forootanfar, A., Yousefizadeh, Z. and Shakibaie, M., 2015. Microbial-assisted synthesis and evaluation the cytotoxic effect of tellurium nanorods. Mater. Sci. Eng. 4, 183-189.
- Fredrickson, J., Romine, M.F., Beliaev, A., Jennifer, M., Osterman, L., Pinchuk, G., Reed, J., Rodionov, D. and Jorge, L.M., 2008. Towards environmental systems biology of *Shewanella*. Nat. Rev. Microbiol. 6(8): 592.
- Fuentes, D., Fuentes, E., Castro, M., Pérez, J., Araya, M., Chasteen, T., Pichuantes, S. and Vâsquez, C., 2007. Cysteine metabolism-related genes and bacterial resistance to potassium tellurite. J. Bacteriol. 189(24): 8953-8960.

- Gautam, U. K. and Rao, C. N. R., 2004. Controlled synthesis of crystalline tellurium nanorods, nanowires, nanobelts and related structures by a self-seeding solution process. J. Mater. Chem. 14(16): 2530-2535.
- Gericke, M. and Pinches, A., 2006. Biological synthesis of metal nanoparticles. Hydrometallurgy 83(1-4): 132-140.
- Ghormade, V., Deshpande, M.V. and Paknikar, K.M., 2011. Perspectives for nano-biotechnology enabled protection and nutrition of plants. Biotechnol. Adv. 29(6): 792-803.
- Ghosh, A., Chowdhury, N. and Chandra, G., 2012. Plant extracts as potential mosquito larvicides. IJMR 135(5): 581.
- Ghosh, A., Mohod, A.M., Paknikar, K.M. and Jain, R.K., 2008. Isolation and characterization of selenite-and selenate-tolerant microorganisms from selenium-contaminated sites. World J. Microbiol. Biotechnol. 24(8): 1607-1611.

- Golinska, P., Wypij, M., Ingle, A.P., Gupta, I., Dahm, H. and Rai, M., 2014. Biogenic synthesis of metal nanoparticles from actinomycetes: biomedical applications and cytotoxicity. Appl. Microbiol. Biotechnol. 98(19): 8083-8097.
- Gordon, T. N. and Martyn, R., 1997. The evolutionary biology of *Fusarium oxysporum*. Ann. Rev. phytophathol. 35(1): 111-128.
- Govindaraju, K., Basha, S.K., Kumar, V.G. and Singaravelu, G., 2008. Silver, gold and bimetallic nanoparticles production using single-cell protein (*Spirulina platensis*) Geitler. J. Mat. Sci. 43(15): 5115-5122.
- Haferburg, G. and Kothe, E., 2007. Microbes and metals: interactions in the environment. J. Basic Microbiol. 47(6): 453-467.
- Harley, S.M., 1993. Use of a Simple, Colorimetric Assay to Demonstrate Conditions for Induction of Nitrate Reductase in Plants. Am. Biol. Teach. 55(3): 162-64.
- Hau, H. and Gralnick, J., 2007. Ecology and biotechnology of the genus *Shewanella*. Annu. Rev. Microbiol., 61, 237-258.

- He, S., Guo, Z., Zhang, Y., Zhang, S., Wang, J. and Gu, N., 2007. Biosynthesis of gold nanoparticles using the bacteria *Rhodopseudomonas capsulata***.** Materials Lett. 61(18): 3984-3987.
- Holmes, J., Richardson, D., Saed, S., Evans-Gowing, R., Russell, D. and Sodeau, J., 1997. Cadmium-specific formation of metal sulfide 'Q-particles' by *Klebsiella pneumoniae*. Microbiol. 143(8): 2521-2530.
- Holt, J., Krieg, N., Sneath, P., Staley, J. and Williams, S., 1994. Bergey's manual of determinative microbiology. Williams and Wilkins, Maryland.
- Huang, J., Li, Q., Sun, D., Lu, Y., Su, Y. and Yang, X., 2007 Biosynthesis of silver and gold nanoparticles by novel sundried *Cinnamomum camphora* leaf, Nanotechnology 18(10): 5104–105115.
- Hulkoti, N.I. and Taranath, T.C., 2014. Biosynthesis of nanoparticles using microbes—a review. Coll. Surf. B. 121, 474-483.
- Hunter, W.J., 2007. An *Azospira oryzae* (syn *Dechlorosoma suillum*) strain that reduces selenate and selenite to elemental red selenium. Curr. Microbiol. 54(5): 376-381.
- Hunter, W.J., 2014. A *Rhizobium selenitireducens* protein showing selenite reductase activity. Curr. Microbiol. 68(3): 311-316.
- Hunter, W.J., Kuykendall, L.D. and Manter, D.K., 2007. *Rhizobium selenireducens* sp. nov.: a selenite-reducing α-Proteobacteria isolated from a bioreactor. Curr. Microbiol. 55(5): 455-460.
- Hunter, W. and Manter, D., 2009. Reduction of selenite to elemental red selenium by *Pseudomonas* sp. strain CA5. Curr. Microbiol. 58(5): 493-498.
- Inagaki, K. and Makino, M., 1977. Pseudo sheath blight of rice caused by *Sclerotium* sp. and' small sclerotial disease of Italian millet due to *Sclerotium orizicola* Nakata et Kawamura. Gakujutsu hokoku. Sci. Rep. 519.

- Ismail, A., Sidkey, N., Arafa, R., Fathy, R. and El-Batal, A., 2016. Evaluation of in vitro antifungal activity of silver and selenium nanoparticles against *Alternaria solani* caused early blight disease on potato. Biotechnol. J. Inter. 1-11.
- Kalimuthu, K., Babu, R.S., Venkataraman, D., Bilal, M., and Gurunathan, S. 2008. Biosynthesis of silver nanocrystals by *Bacillus licheniformis*. Colloid Surf. B 65: 150- 153.
- Kammler, H., Mädler, L. and Pratsinis, S., 2001. Flame synthesis of nanoparticles. Chem. Eng. Technol. 24(6): 583-596.
- Kang, I., Kang, M., Lee, E., Seo, H. and Ahn, C., 2011. Facile, hetero-sized nanocluster array fabrication for investigating the nanostructure-dependence of nonvolatile memory characteristics. Nanotechnology 22(25): 254018.
- Kathiresan, K., Manivannan, S., Nabeel, M. and Dhivya, B., 2009. Studies on silver nanoparticles synthesized by a marine fungus, *Penicillium fellutanum* isolated from coastal mangrove sediment. Colloid Surf. B. 71(1): 133-137.
- Kathiresan, K., Alikunhi, N., Pathmanaban, S., Nabikhan, A. and Kandasamy, S., 2010. Analysis of antimicrobial silver nanoparticles synthesized by coastal strains of *Escherichia coli* and *Aspergillus niger*. Can. J. Microbiol. 56(12): 1050-1059.
- Kessi, J., Ramuz, M., Wehrli, E., Spycher, M. and Bachofen, R., 1999. Reduction of selenite and detoxification of elemental selenium by the Phototrophic Bacterium *Rhodospirillum rubrum*. Appl. Environ. Microbiol. 65(11): 4734-4740.
- Khaliq, A., Ali, S., Hameed, A., Farooq, M., Farid, M., Shakoor, M., Mahmood, K., Ishaque, W. and Rizwan, M., 2016. Silicon alleviates nickel toxicity in cotton seedlings through enhancing growth, photosynthesis, and suppressing Ni uptake and oxidative stress. Arch. Agron. Soil Sci. 62(5): 633-647.
- Khan, S.N., 2007. *Macrophomina phaseolina* as causal agent for charcoal rot of sunflower. Mycopath. 5(2): 111-118.

- Khanolkar, D., Dubey, S. K. and Naik, M., 2015. Biotransformation of tributyltin chloride to less toxic dibutyltin dichloride and monobutyltin trichloride by *Klebsiella pneumoniae* strain SD9. Int. Biodeter. Biodegr. 104, 212-218.
- Klaus T., Joerger R., Olsson E., Granqvist C., 1999. Silver-based crystalline nanoparticles, microbially fabricated. PNAS (US) 96(24):13611– 13614.
- Khodakovskaya, M., Dervishi, E., Mahmood, M., Xu, Y., Li, Z., Watanabe, F. and Biris, A.S., 2009. Carbon nanotubes are able to penetrate plant seed coat and dramatically affect seed germination and plant growth. ACS Nano. 3(10): 3221-3227.
- Kim, D., Kanaly, R. and Hur, H., 2012. Biological accumulation of tellurium nanorod structures via reduction of tellurite by *Shewanella oneidensis* MR-1. Bioresour. Technol. 125,127-131.
- Kim, D., Kim, M., Jiang, S., Lee, J. and Hur, H., 2013. Promoted reduction of tellurite and formation of extracellular tellurium nanorods by concerted reaction between iron and *Shewanella oneidensis* MR-1. Environ. Sci. Technol. 47(15): 8709-8715.
- Kim, D., Park, S., Kim, M. and Hur, H., 2014. Accumulation of amorphous Cr (III)-Te (IV) nanoparticles on the Surface of *Shewanella oneidensis* MR-1 through reduction of Cr (VI). Environ. Sci. Technol. 48(24): 14599-14606.
- Klonowska, A., Heulin, T. and Vermeglio, A., 2005. Selenite and tellurite reduction by *Shewanella oneidensis*. Appl. Environ. Microbiol. 71(9): 5607-5609.
- Kong, L., Yuan, Q., Zhu, H., Li, Y., Guo, Q., Wang, Q., Bi, X. and Gao, X., 2011. The suppression of prostate LNCaP cancer cells growth by Selenium nanoparticles through Akt/Mdm2/AR controlled apoptosis. Biomaterials 32(27): 6515-6522.
- Krumov, N., Perner-Nochta, I., Oder, S., Gotcheva, V., Angelov, A. and Posten, C., 2009. Production of inorganic nanoparticles by microorganisms. Chem. Eng. Tech. 32(7): 1026-1035.

- Kumar, D., Karthik, L., Kumar, G. and Rao, K.B., 2011. Biosynthesis of silver nanoparticles from marine yeast and their antimicrobial activity against multidrug resistant pathogens. Pharmaco. Logyonline. 3, 1100-1111.
- Kumar, S., Abyaneh, M., Gosavi, S., Kulkarni, S., Pasricha, R., Ahmad, A. and Khan, M., 2007. Nitrate reductase-mediated synthesis of silver nanoparticles from $AgNO_3$. Biotechnol. Lett. 29(3): 439-445.
- Kurimella, V., Kumar, K. and Sanasi, P., 2013. A novel synthesis of tellurium nanoparticles using iron (II) as a reductant. Int. J. Nanosci. Nanotech. 4, 209-221.
- Lamas, D., Lascalea, G., Juárez, R., Djurado, E., Pérez, L. and de Reca, N., 2003. Metastable forms of the tetragonal phase in compositionally homogeneous, nanocrystalline zirconia–ceria powders synthesised by gel-combustion. J. Mat. Chem. 13(4): 904-910.
- Lengke, M., Fleet, M. and Southam, G., 2007. Biosynthesis of silver nanoparticles by filamentous cyanobacteria from a silver (I) nitrate complex. Langmuir 23(5): 2694-2699.
- Li, G., He, D., Qian, Y., Guan, B., Gao, S. and Cui, Y., Yokoyama, K. and Wang, L., 2012. Fungus-mediated green synthesis of silver nanoparticles *using Aspergillus terreus*. Int. J. Mol. Sci. 13(1): 466-476.
- Li, Z., Sun, Q., Zhu, Y., Tan, B., Xu, Z. and Dou, S., 2014. Ultra-small fluorescent inorganic nanoparticles for bioimaging. J. Mater. Chem. B. 2(19): 2793-2818.
- Lin, Z.H., Lee, C.H., Chang, H.Y. and Chang, H.T., 2012. Antibacterial activities of tellurium nanomaterials. Chem. - An Asian J. 7(5): 930-934.
- Liu, M. and Taylor, D.E., 1999. Characterization of gram-positive tellurite resistance encoded by the *Streptococcus pneumoniae tehB* gene. FEMS Microbiol. Lett. 174(2): 385-392.

- Liu, Z., Hu, Z., Xie, Q., Yang, B. and Qian, Y., 2003. Surfactant-assisted growth of uniform nanorods of crystalline tellurium. J. Mater. Chem. 13(1): 159-162.
- Lovley, D.R., 1993. Dissimilatory metal reduction. Annu. Rev. Microbiol. 47(1): 263-290.
- Lowry, O., Rosebrough, N., Farr, A. and Randall, R., 1951. Protein measurement with the Folin phenol reagent. J. Biol. Chem. 193: 265-275.
- Luo, H., Wang, F., Bai, Y., Chen, T. and Zheng, W., 2012. Selenium nanoparticles inhibit the growth of HeLa and MDA-MB-231 cells through induction of S phase arrest. Colloid Surf. B. 94: 304-308.
- Kowshik, M., Ashtaoutre, S., Kharrazi, S., Vogel, W., Urban, J., Kulkarni, S.K. and Paknikar, K.M., 2003. Extracellular synthesis of silver nanoparticles by a silver-tolerant yeast strains MKY3, Nanotechnology 14, 95-100.
- Maharani, V., Sundaramanickam, A. and Balasubramanian, T., 2016. In vitro anticancer activity of silver nanoparticle synthesized by *Escherichia coli* VM1 isolated from marine sediments of Ennore southeast coast of India. Enzyme Microb. Technol. 95, 146-154.
- Manikandana, M., Dhanuskodia, S., Mathewb, S. and Nampoorib, V. P. N., 2015. Nonlinear Optical Property of Tellurium Nanoparticles (Conference paper).
- Mishra, R.R., Prajapati, S., Das, J., Dangar, T.K., Das, N. and Thatoi, H., 2011a. Reduction of selenite to red elemental selenium by moderately halotolerant *Bacillus megaterium* strains isolated from Bhitarkanika mangrove soil and characterization of reduced product. Chemosphere, 84(9): 1231-1237.
- Mishra, A., Tripathy, S.K., Wahab, R., Jeong, S.H., Hwang, I., Yang, Y.B., Kim, Y.S., Shin, H.S. and Yun, S.I., 2011b. Microbial synthesis of gold nanoparticles using the fungus *Penicillium brevicompactum* and their cytotoxic effects against mouse mayo blast cancer C 2 C 12 cells. Appl. Microbiol. Biotechnol. 92(3): 617-630

- Mittler, R., 2017. ROS are good. Trends Plant Sci. 22(1): 11-19.
- Moghaddam, K., 2010. An Introduction to microbial metal nanoparticle preparation method. J. Young Investig. 19(1).
- Mohanty, A., Kathawala, M.H., Zhang, J., Chen, W.N., Loo, J.S.C., Kjelleberg, S., Yang, L. and Cao, B., 2014. Biogenic tellurium nanorods as a novel antivirulence agent inhibiting pyoverdine production in *Pseudomonas aeruginosa*. Biotechnol. Bioeng. 111(5): 858-865.
- Morris, J. and Crane, S., 2013. Selenium toxicity from a misformulated dietary supplement, adverse health effects, and the temporal response in the nail biologic monitor. Nutrients 5(4), 1024-1057.
- Moulick, D., Ghosh, D. and Santra, S.C., 2016. Evaluation of effectiveness of seed priming with selenium in rice during germination under arsenic stress. Plant Physiol. Biochem. 109, 571-578.
- Mousavi Kouhi, S.M., Lahouti, M., Ganjeali, A. and Entezari, M.H., 2014. Comparative phytotoxicity of ZnO nanoparticles, ZnO microparticles, and Zn^{2+} on rapeseed (*Brassica napus* L.): investigating a wide range of concentrations. Toxicol. Environ. Chem. 96(6): 861-868.
- MubarakAli, D., Gopinath, V., Rameshbabu, N. and Thajuddin, N., 2012. Synthesis and characterization of CdS nanoparticles using C-phycoerythrin from the marine cyanobacteria. Mater. Lett. 74, 8-11.
- Mujawar, S., Shamim, K., Vaigankar, D. and Dubey, S.K., 2019. Arsenite biotransformation and bioaccumulation by *Klebsiella pneumoniae* strain SSSW7 possessing arsenite oxidase (*aioA*) gene. BioMetals 32(1): 65-76.
- Mukherjee, P., Ahmad, A., Mandal, D., Senapati, S., Sainkar, S., Khan, M., Parishcha, R., Ajaykumar, P.V., Alam, M., Kumar, R. and Sastry, M., 2001. Fungus-mediated synthesis of silver nanoparticles and their immobilization in the mycelial matrix: a

novel biological approach to nanoparticle synthesis. Nano Lett. 1(10): 515-519.

- Muthukannan, R. and Karuppiah, B. 2011. Rapid synthesis and characterization of silver nanoparticles by novel *Pseudomonas* sp. "ram bt-1". J. Eco. Biotechnol. 3, 24-28.
- Nangia, Y., Wangoo, N., Goyal, N., Shekhawat, G. and Suri, C.R. 2009. A novel bacterial isolate *Stenotrophomonas maltophilia* as living factory for synthesis of gold nanoparticles. Microb. Cell Fact. 8:39.
- Nahar, L. and Arachchige, I., 2013. Sol-Gel methods for the assembly of metal and semiconductor nanoparticles. JSM Nanotechnol. Nanomed. 1, 1104.
- Naik, M., Shamim, K. and Dubey. S.K. 2012. Bacterial characterization of lead- resistant bacteria to explore role of bacterial metallothionein in lead resistance. Curr. Sci. 103(4): 426-429.
- Naik, M. and Dubey, S. K., 2017. Marine Pollution and Microbial Remediation. Springer.
- Naik, M. and Dubey, S.K., 2011. Lead-enhanced siderophore production and alteration in cell morphology in a Pb-resistant *Pseudomonas aeruginosa* strain 4EA. Cur. Microbiol. 62, 409-414.
- Nandini, B., Hariprasad, P., Prakash, H.S., Shetty, H.S. and Geetha, N., 2017. Trichogenic-selenium nanoparticles enhance disease suppressive ability of *Trichoderma* against downy mildew disease caused by *Sclerospora graminicola* in pearl millet. Sci. Rep. 7(1): 1-11.
- Nangia, Y., Wangoo, N., Goyal, N., Shekhawat, G. and Suri, C.R., 2009. A novel bacterial isolate *Stenotrophomonas maltophilia* as living factory for synthesis of gold nanoparticles. Microbial Cell Fact. 8(1): 39.
- Naumov, A. V., 2010. Selenium and tellurium: State of the markets, the crisis, and its consequences. Metallurgist 54(3): 197-200.

- Narayanan, K.B. and Sakthivel, N., 2010. Biological synthesis of metal nanoparticles by microbes. Adv. Colloid Interfac. 156(1-2): 1-13.
- Naumann D., 2000. Infrared spectroscopy in microbiology. In: Meyers RA (ed.) Encyclopedia of Analytical Chemistry, John Wiley and Sons Ltd. Chichester, UK, 102-131.
- Naumann, D., Helm, D. and Labischinski, H., 1991. Microbiological characterizations by FT-IR spectroscopy. Nature 351(6321): 81-82.
- Neikov, O.D., 2019. Chapter 13-Powders for Additive Manufacturing Processing. Handbook of Non-Ferrous Metal Powders. 373-399.
- Nies, D.H., 1999. Microbial heavy-metal resistance. Appl. Microbiol. Biotechnol. 51(6): 730-750.
- Niki, E., 2010. Assessment of antioxidant capacity in vitro and in vivo. Free Radic. Biol. Med. 49(4): 503-515.
- O'Gara, J.P., Gomelsky, M. and Kaplan, S., 1997. Identification and molecular genetic analysis of multiple loci contributing to high-level tellurite resistance in *Rhodobacter sphaeroides* 2.4. 1. Appl. Environ. Microbiol. 63(12): 4713-4720.
- Ollivier, P.R.L., Bahrou, A.S., Marcus, S., Cox, T., Church, T.M. and H anson, T.E., 2008. Volatilization and precipitation of tellurium by aerobic, tellurite-resistant marine microbes. Appl. Environ. Microbiol. 74(23): 7163-7173.
- Oremland, R., Herbel, M., Blum, J., Langley, S., Beveridge, T., Ajayan, P., Sutto, T., Ellis, A. and Curran, S., 2004. Structural and spectral features of selenium nanospheres produced by Se-respiring bacteria. Appl. Environ. Microbial. 70(1): 52-60.
- Pardhiya, S. and Paulraj, R., 2014. Role of nanoparticles in targeted drug delivery system. Nanotechnology in drug delivery 21-51.
- Pearion, C.T. and Jablonski, P.E., 1999. High level, intrinsic resistance of *Natronococcus occultus* to potassium tellurite. FEMS Microbiol. Lett. 174(1): 19-23.

- Pareek, V., Bhargava, A., Gupta, R., Jain, N. and Panwar, J., 2017. Synthesis and applications of noble metal nanoparticles: a review. ASEM 99(7): 527-544.
- Park, T.J., Lee, K.G. and Lee, S.Y., 2016. Advances in microbial biosynthesis of metal nanoparticles. Appl. Microbiol. Biotechnol. 100(2): 521-534.
- Piella, J., Bastús, N.G., Casals, E. and Puntes, V., 2013. Characterizing nanoparticles reactivity: Structure-photocatalytic activity relationship. J. Phys. Conf. Ser. 429(1): 012040. IOP Publishing.
- Pimpin, A. and Srituravanich, W., 2012. Review on micro-and nanolithography techniques and their applications. Eng. J. 16(1): 37-56.
- Pimprikar, P., Joshi, S.S., Kumar, A., Zinjarde, S. and Kulkarni, S., 2009. Influence of biomass and gold salt concentration on nanoparticle synthesis by the tropical marine yeast *Yarrowia lipolytica* NCIM 3589. Colloid Surf. B. 74(1): 309-316.
- Powers, EM., 1995. Efficacy of the Ryu non-staining KOH technique for rapidly determining gram reactions of food-borne and waterborne bacteria and yeasts. Appl. Environ. Microbiol. 61(10): 3756-8.
- Pratt, R., McLaughlin, M., Pederson, G. and Rowe, D., 1998. Pathogenicity of *Macrophomina phaseolina* to mature plant tissues of alfalfa and white clover. Plant Dis. 82(9): 1033-1038.
- Presentato, A., Piacenza, E., Anikovskiy, M., Cappelletti, M., Zannoni, D. and Turner, R.J., 2016. *Rhodococcus aetherivorans* BCP1 as cell factory for the production of intracellular tellurium nanorods under aerobic conditions. Microb. Cell Fact. 15(1): 204.
- Pugin, B., Cornejo, F., Muñoz-Díaz, P., Muñoz-Villagrán, C., Vargas-Pérez, J., Arenas, F. and Vásquez, C., 2014. Glutathione reductase-mediated synthesis of tellurium-containing nanostructures exhibiting antibacterial properties. Appl. Environ. Microbiol. 80, 7061-7070.

- Qi, P., Zhang, D. and Wan, Y., 2013. Sulfate-reducing bacteria detection based on the photocatalytic property of microbial synthesized ZnS nanoparticles. Analytica. chimica. Acta. 800, 65-70.
- Rabouw, F.T. and de Mello Donega, C., 2017. Excited-State Dynamics in Colloidal Semiconductor Nanocrystals. In Photoactive Semiconductor Nanocrystal Quantum Dots 1-30. Springer, Cham.
- Rajeshkumar, S., Ponnanikajamideen, M., Malarkodi, C., Malini, M. and Annadurai, G., 2014. Microbe-mediated synthesis of antimicrobial semiconductor nanoparticles by marine bacteria. J. Nanostruct. Chem., 4(2): 96.
- Ramya, S., Shanmugasundaram, T. and Balagurunathan, R., 2020. Actinobacterial enzyme mediated synthesis of selenium nanoparticles for antibacterial, mosquito larvicidal and anthelminthic applications. Particule. Sci. Technol. 38(1): 63-72.
- Ramya, S., Shanmugasundaram, T. and Balagurunathan, R., 2015. Biomedical potential of actinobacterially synthesized selenium nanoparticles with special reference to anti-biofilm, anti-oxidant, wound healing, cytotoxic and anti-viral activities. J. Trace Elem. Med. Bio. 32: 30-39.
- Ranjard, L., Prigent-Combaret, C., Nazaret, S. and Cournoyer, B., 2002. Methylation of inorganic and organic selenium by the bacterial thiopurine methyltransferase. J. Bacteriol. 184(11): 3146-3149.
- Rathgeber, C., Yurkova, N., Stackebrandt, E., Beatty, J.T. and Yurkov, V., 2002. Isolation of tellurite-and selenite-resistant bacteria from hydrothermal vents of the Juan de Fuca Ridge in the Pacific Ocean. Appl. Environ. Microbiol. 68(9): 4613-4622.
- Ravindra P., 2009. Protein-mediated synthesis of gold nanoparticles. Mat. Sci. Eng. B 163:93- 98.
- Roane, T.M., 1999. Lead resistance in two bacterial isolates from heavy metal–contaminated soils. Microb. Ecol. 37(3): 218-224.

- Rossbach, S., Wilson, T., Kukuk, M.L. and Carty, H., 2000. Elevated zinc induces siderophore biosynthesis genes and a zntA-like gene in *Pseudomonas fluorescens*. FEMS Microbiol. Let. 191(1): 61-70.
- Salunke, B., Sawant, S., Lee, S. and Kim, B., 2015. Comparative study of MnO_2 nanoparticle synthesis by marine bacterium *Saccharophagus degradans* and yeast *Saccharomyces cerevisiae.* Appl. Microbial. Biotechnol. 99(13): 5419-5427.
- Samant, S., Naik, M., Parulekar, K., Charya, L. and Vaigankar, D., 2018. Selenium reducing *Citrobacter fruendii* strain KP6 from Mandovi estuary and its potential application in selenium nanoparticle synthesis. Proc. Natl. Acad. Sci., India Section B: Biol. Sci. 88(2): 747-754.
- Sathiyanarayanan, G., Kiran, G. and Selvin, J., 2013. Synthesis of silver nanoparticles by polysaccharide bioflocculant produced from marine *Bacillus subtilis* MSBN17. Colloid Surf. B. 102, 13-20.
- Seng, H.L. and Tiekink, E.R., 2012. Anti-cancer potential of selenium-and tellurium-containing species: opportunities abound!. Appl. Organomet. Chem. 26(12): 655-662.
- Seshadri, S., Prakash, A. and Kowshik, M., 2012. Biosynthesis of silver nanoparticles by marine bacterium, *Idiomarina* sp. PR58-8. Bull. Mater. Sci. 35(7): 1201-1205.
- Seshadri, S., Saranya, K. and Kowshik, M., 2011. Green synthesis of lead sulfide nanoparticles by the lead resistant marine yeast, *Rhodosporidium diobovatum*. Biotechnol. Prog. 27(5): 1464-1469.
- Shah, R., Oza, G., Pandey, S. and Sharon, M., 2012. Biogenic fabrication of gold nanoparticles using *Halomonas salina*. J. Microbiol. Biotechnol. Res. 2(4): 485-492.
- Shahverdi, A.R., Minaeian, S., Shahverdi, H.R., Jamalifar, H. and Nohi, A. 2007. Rapid synthesis of silver nanoparticles using culture supernatants of *Enterobacteria*: A novel biological approach. Process Biochem. 42: 919–923.

- Shakibaie, M., Forootanfar, H., Golkari, Y., Mohammadi-Khorsand, T. and Shakibaie, M.R., 2015. Anti-biofilm activity of biogenic selenium nanoparticles and selenium dioxide against clinical isolates of *Staphylococcus aureus*, *Pseudomonas aeruginosa*, and *Proteus mirabilis*. J. Trace Elem. Med. Bio. 29, 235-241.
- Shakibaie, M., Adeli-Sardou, M., Mohammadi-Khorsand, T., ZeydabadiNejad, M., Amirafzali, E., Amirpour-Rostami, S., Ameri, A. and Forootanfar, H., 2017. Antimicrobial and antioxidant activity of the biologically synthesized tellurium nanorods; a preliminary in vitro study. Iran. J. Biotechnol. 15(4): 268.
- Shankar, A., Sadana, U. and Sekhon, N., 2014. Contribution of post-anthesis growth and manganese dynamics to differential grain yield in different wheat species. J. plant Nutr. 37(11): 1770-1781.
- Shanmugam, N., Suthakaran, S., Kannadasan, N. and Sathishkumar, K., 2015. Synthesis and characterization of Te doped ZnO nanosheets for photocatalytic application. JO Heterocyclics, 105, 15-20.
- Sharma, N., Pinnaka, K., Raje, M., Ashish, F., Bhattacharyya, M. and Choudhury, A. 2012. Exploitation of marine bacteria for production of gold nanoparticles. Microb. Cell Fact. 11(86), 1-6.
- Sharma, J., Shamim, K., Dubey, S.K. and Meena, R., 2017. Metallothionein assisted periplasmic lead sequestration as lead sulfite by *Providencia vermicola* strain SJ2A. Sci. Total Environ. 579, 359-365.
- Sheikhloo, Z. and Salouti, M., 2011. Intracellular biosynthesis of gold nanoparticles by the fungus *Penicillium chrysogenum*. Int. J. Nanosci. Nanotechnol. 7(2): 102-105.
- Shirsat, S., Kadam, A., Naushad, M. and Mane, R.S., 2015. Selenium nanostructures: microbial synthesis and applications. RSC Adv. 5(112): 92799-92811.

- Shenton, W., Douglas, T., Young, M., Stubbs, G. and Mann, S. 1999. Inorganic–organic nanotube composites from template mineralization of Tobacco mosaic virus. Adv. Mater. 11:253- 256.
- Silver, S. and Phung LT., 1996. Bacterial heavy metal resistance-New Surprises. Annu. Rev. Microbiol. 50, 753-789.
- Singh, G., Babele, P.K., Shahi, S.K., Sinha, R.P., Tyagi, M.B. and Kumar, A. 2014. Green synthesis of silver nanoparticles using cell extracts of *Anabaena doliolum* and screening of its antibacterial and antitumor activity. J. Microbiol. Biotechnol. 24(10): 1366-1379.
- Singh, N., Saha, P., Rajkumar, K. and Abraham, J., 2014. Biosynthesis of silver and selenium nanoparticles by *Bacillus* sp. JAPSK2 and evaluation of antimicrobial activity. Der. Pharm. Lett. 6(6): 175-181.
- Soda, S., Ma, W., Kuroda, M., Nishikawa, H., Zhang, Y. and Ike, M., 2018. Characterization of moderately halotolerant selenate-and tellurite-reducing bacteria isolated from brackish areas in Osaka. Biosci. Biotech. Bioch. 82(1): 173-181.
- Soni, N. and Prakash, S., 2012. Synthesis of gold nanoparticles by the fungus *Aspergillus niger* and its efficacy against mosquito larvae. Rep. Parasitol. 2, 1-7.
- Sowndarya, P., Ramkumar, G. and Shivakumar, M.S., 2017. Green synthesis of selenium nanoparticles conjugated *Clausena dentata* plant leaf extract and their insecticidal potential against mosquito vectors. Artif. Cell Nanomed. B. 45(8): 1490-1495.
- Srivastava, N. and Mukhopadhyay, M., 2013. Biosynthesis and structural characterization of selenium nanoparticles mediated by *Zooglea ramigera*. Powder Technol. 244, 26-29.
- Srivastava, P. and Kowshik, M., 2016. Anti-neoplastic selenium nanoparticles from *Idiomarina* sp. PR58-8. Enzyme Microb. Technol. 95, 192-200.
- Srivastava, P., Nikhil, E.V.R., Bragança, J.M. and Kowshik, M., 2015. Anti-bacterial TeNPs biosynthesized by haloarcheaon *Halococcus salifodinae* BK3. Extremophiles 19(4): 875-884.

- Stephenson, G., 2003. Pesticide use and world food production: risks and benefits. In: Coats, J., Yamamoto, H., editors. Environmental fate and effects of pesticides. ACS Symposium Series, Washington, 853, 261–70.
- Stoeva, S., Klabunde, K.J. and Sorensen, C.M., 2002. Gram-scale synthesis of monodisperse gold colloids by the solvated metal atom dispersion method and digestive ripening and their organization into two- and three-dimensional structures. J. Am. Chem. Soc. 124(10): 2305-2311.
- Stolz, J.F., Basu, P., Santini, J.M. and Oremland, R.S., 2006. Arsenic and selenium in microbial metabolism. Annu. Rev. Microbiol. 60, 107-130.
- Sunitha, M. S. L., Prashanth, S. and Kishor, P. K., 2015. Characterization of Arsenic-Resistant Bacteria and their ars Genotype for Metal Bioremediation. Int. J. Sci. Eng. Res. 6 (2): 304-309.
- Swain, T. and Hillis, W.E., 1959. The phenolic constituents of *Prunus domestica.* I- The quantitative analysis of phenolic constituents. J. Sci. Food Agr. 10(1): 63-68.
- Tamura, K., Stecher, G., Peterson, D., Filipski, A. and Kumar, S., 2013. MEGA6: molecular evolutionary genetics analysis version 6.0. Mol. Biol. and Evol. 30(12): 2725-2729.
- Tan, Y., Yao, R., Wang, R., Wang, D., Wang, G. and Zheng, S., 2016. Reduction of selenite to Se (0) nanoparticles by filamentous bacterium *Streptomyces* sp. ES2-5 isolated from a selenium mining soil. Microbi. Cell Facts. 15(1): 157.
- Taylor, D.E., 1999. Bacterial tellurite resistance. Trends Microbiol. 7(3): 111-115.
- Taylor, D.E., Hou, Y., Turner, R.J. and Weiner, J.H., 1994. Location of a potassium tellurite resistance operon (*tehA tehB*) within the terminus of *Escherichia coli* K-12. J. Bacteriol. 176(9): 2740-2742.
- T

- Terai, T., Kamahora, T. and Yamamura, Y., 1958. Tellurite reductase from *Mycobacterium avium*. J. Bacteriol. 75(5): 535.
- Thomas, R., Janardhanan, A., Varghese, R., Soniya, E., Mathew, J. and Radhakrishnan, E.K., 2014. Antibacterial properties of silver nanoparticles synthesized by marine *Ochrobactrum* sp. Braz. J. Microbiol. 45(4): 1221-1227.
- Toptchieva, A., Sisson, G., Bryden, L. and Taylor, D.E. and Hoffman, P., 2003. An inducible tellurite-resistance operon in *Proteus mirabilis*. Microbiol. 149(5): 1285-1295.
- Torres, S., Campos, V., León, C., Rodríguez-Llamazares, S., Rojas, S., Gonzalez, M., Smith, C. and Mondaca, M., 2012. Biosynthesis of selenium nanoparticles by *Pantoea agglomerans* and their antioxidant activity. J. Nanoparticle Res. 14(11):1236.
- Turlo, J., Gutkowska, B. and Herold, F., 2010. Effect of selenium enrichment on antioxidant activities and chemical composition of *Lentinula edodes* (Berk.) Pegl. mycelial extracts. Food Chem. Toxicol. 48(4): 1085-1091.
- Trutko, S., Akimenko, V., Suzina, N., Anisimova, L., Shlyapnikov, M., Baskunov, B., Duda, V. and Boronin, A., 2000. Involvement of the respiratory chain of Gram-negative bacteria in the reduction of tellurite. Arch. Microbiol. 173(3): 178-186.
- Turner, R., Weiner, J. and Taylor, D., 1995a. Neither reduced uptake nor increased efflux is encoded by tellurite resistance determinants expressed in Escherichia coli. Can. J. Microbiol. 41(1): 92-98.
- Turner, R., Weiner, J. and Taylor, D., 1995b. The tellurite-resistance determinants *tehA, tehB* and *klaA, klaB, telB* have different biochemical requirements. Microbiol. 141(12): 3133-3140.
- Turner, R., Weiner, J. and Taylor, D., 1992. Use of diethyldithiocarbamate for quantitative determination of tellurite uptake by bacteria. Anal. Biochem. 204(2): 292-295.

- Urig, S. and Becker K., 2006. On the potential of thioredoxin reductase inhibitors for cancer therapy. Seminar Cancer Biol. 16, 452–465.Academic Press.
- Vaidyanathan, R., Gopalram, S., Kalishwaralal, K., Deepak, V., Pandian, S.R.K. and Gurunathan, S., 2010. Enhanced silver nanoparticle synthesis by optimization of nitrate reductase activity. Colloids Surf. B. *75*(1): 335-341.
- Vaigankar, D., Dubey, S.K., Mujawar, S., D'Costa, A. and Shyama, S.K., 2018. Tellurite biotransformation and detoxification by *Shewanella baltica* with simultaneous synthesis of tellurium nanorods exhibiting photo-catalytic and anti-biofilm activity. Ecotox. Environ. Safe. 165, 516-526.
- Vala, A., 2015. Exploration on green synthesis of gold nanoparticles by a marine-derived fungus *Aspergillus sydowii*. Environ. Prog. Sustainable Energy 34(1): 194-197.
- Valdivia-González, M., Díaz-Vásquez, W., Ruiz-León, D., Becerra, A., Aguayo, D. R., Pérez-Donoso, J. and Vásquez, C., 2018. A comparative analysis of tellurite detoxification by members of the genus *Shewanella*. Arch. Microbiol. 200(2): 267-273.
- Vyas, S.C., 1988. Nontarget effects of agricultural fungicides. CRC Press, Inc.
- Watkinson, J.H., 1966. Fluorimetric determination of selenium in bio- logical material with 2,3-diaminonaphtalene. Anal. Chem. 38, 92-97.
- World Health Organization (WHO) (2011) Guidelines for drinking-water quality, 4th edn. WHO, Geneva
- Xu, X., McGrath, S., Meharg, A. and Zhao, F., 2008. Growing rice aerobically markedly decreases arsenic accumulation. Environ. Sci. Technol. 42(15): 5574-5579.
- Yang, Y., Lee, S., Lee, H., Kim, M., Lee, S. and Lee, H., 2002. A piperidine amide extracted from Piper longum L. fruit shows activity against *Aedes aegypti* mosquito larvae. J. Agric. Food Chem. 50(13): 3765-3767.

- Yazdi, M., Mahdavi, M., Setayesh, N., Esfandyar, M. and Shahverdi, A., 2013. Selenium nanoparticle-enriched *Lactobacillus brevis* causes more efficient immune responses in vivo and reduces the liver metastasis in metastatic form of mouse breast cancer. DARU. 21(1): 33.
- Yuan, Q., Yin, H. and Nie, Q., 2013. Nanostructured tellurium semiconductor: from nanoparticles to nanorods. J. Exp. Nanosci. 8(7-8): 931-936.
- Zannoni, D., Borsetti, F., Harrison, J. and Turner, R., 2007. The bacterial response to the chalcogen metalloids Se and Te.Adv. Microbe. Physiol. 53, 1-312.
- Zare, B., Sepehrizadeh, Z., Faramarzi, M.A., Soltany-Rezaee-Rad, M., Rezaie, S. and Shahverdi, A.R., 2014. Antifungal activity of biogenic tellurium nanoparticles against *Candida albicans* and its effects on squalene monooxygenase gene expression. Biotechol. Appl. Biochem., 61(4): 395-400.
- Zare, B., Faramarzi, M.A., Sepehrizadeh, Z., Shakibaie, M., Rezaie, S. and Shahverdi, A.R., 2012. Biosynthesis and recovery of rod-shaped tellurium nanoparticles and their bactericidal activities. Mater. Res. Bull. 47(11): 3719-3725.
- Zeng, H. and Combs Jr, G.F., 2008. Selenium as an anticancer nutrient: roles in cell proliferation and tumor cell invasion. J. Nutr. Biochem. 19(1): 1-7.
- Zhang, J., Wang, X. and Xu, T., 2007. Elemental selenium at nano size (Nano-Se) as a potential chemopreventive agent with reduced risk of selenium toxicity: comparison with se-methylselenocysteine in mice. Toxicol. Sci. 101(1): 22-31.
- Zhang, X., Qu, Y., Shen, W., Wang, J., Li, H., Zhang, Z., Li, S. and Zhou, J., 2016. Biogenic synthesis of gold nanoparticles by yeast *Magnusiomyces ingens* LH-F1 for catalytic reduction of nitrophenols. Colloid Surf. A 497, 280-285.
- Zhao, F., Ma, J., Meharg, A. and McGrath, S., 2009. Arsenic uptake and metabolism in plants. New Phytologist. 181(4): 777-794.

- Zheng, J., Zheng, S., Zhang, Y, Yu, B., Zheng, W., Yang, F. and Chen, T., 2011. Sialic acid surface decoration enhances cellular uptake and apoptosis-inducing activity of selenium nanoparticles. Colloids Surf. B. 83(1): 183-187.
- Zonaro, E., Lampis, S., Turner, R.J., Junaid, S. and Vallini, G., 2015. Biogenic selenium and tellurium nanoparticles synthesized by environmental microbial isolates efficaciously inhibit bacterial planktonic cultures and biofilms. Front. Microbiol. 6, 584.

Research publications

1. **Vaigankar, D.C.**, Dubey, S.K., Mujawar, S.Y., D'Costa, A. and Shyama, S.K., 2018. Tellurite biotransformation and detoxification by *Shewanella baltica* with simultaneous synthesis of tellurium nanorods exhibiting photo-catalytic and anti-biofilm activity. Ecotox. Environ. Safe. 165, 516-526 **IF: 4.527.**
2. **Vaigankar, D.C.**, Mujawar, S.M., Mohanty A. and Dubey, S.K. *Halomonas venusta* mediated detoxification and biotransformation of selenite into selenium nanoparticles exhibiting various biological activities (Communicated).
3. **Vaigankar, D.C.**, Mujawar, S.M. and Dubey, S.K. Biogenic nano selenium exhibiting promising agricultural and environmental applications. (under preparation).
4. **Vaigankar, D.C.**, Mujawar, S.M., Naik M.N. and Dubey, S.K. Whole genome analysis of *Shewanella baltica* strain GUSDZ9 isolated from Zuari eatuary Goa, India. (under preparation).

Other research publications

1. Samant, S., Naik, M., Parulekar, K., Charya, L. and **Vaigankar, D.,** 2018. Selenium reducing *Citrobacter fruendii* strain KP6 from Mandovi estuary and its potential application in selenium nanoparticle synthesis. Proc. Natl. Sci. India Sect. B: Bio. sci. 88(2): 747-754. **IF: 0.396**.
2. Naik, M. M., Naik, D., Charya, L., Mujawar, S. and **Vaigankar, D.,** 2018. Application of Marine Bacteria Associated with Seaweed, *Ulva lactuca*, for Degradation of Algal Waste. Proc. Natl. Sci. India Sect. B: Bio. sci. 88(2): 747-754. **IF: 0.396**.
3. Mujawar, S. Y., Shamim, K., **Vaigankar, D. C**. and Dubey, S. K., 2019. Arsenite biotransformation and bioaccumulation by

Klebsiella pneumoniae strain SSSW7 possessing arsenite oxidase (*aioA*) gene. BioMetals 32(1): 65-76. **IF: 2.455**.

Book chapter published

1. Samant, S., Naik, M.M., **Vaigankar, D.C.,** Mujawar. S.Y., Parab, P. and Meena, S.N., 2019. Biodegradation of seafood waste by seaweed-associated bacteria and application of seafood waste for ethanol production. In Advances in Biological Science Research (pp. 149-159). Academic press.

Research papers presented in National and International conferences

1. **Vaigankar, D.** and Dubey, S. K. Isolation and characterization of selenite reducing bacteria from Mandovi estuary Goa, India. In International conference on Microbial technology for better tomorrow (17-19th February 2018) held at Dr D. Y. Patil Arts, Commerce & Science College, Pimpri, Pune- Maharashtra.
2. **Vaigankar, D.** and Dubey, S. K. Biogenic selenium nanoparticles exhibiting capability to protect human lymphocytes against UV induced damage**.** In International conference on Materials and Environmental Science (7-8th December 2018) held at Shivaji University, Kolhapur-Maharashtra.

Workshops and symposia attended

- Attended one day seminar on "Advances in Microbiology and Marine Microbiology" held on 13th March 2015 at Dept. of Microbiology Goa University.

- 56th Annual Conference of Association of Microbiologists of India and International symposium on "Emerging Discoveries in Microbiology" 7-10 December 2015, JNU Delhi.
- Attended one day seminar on "New Perspectives in Biosciences" (7th December 2017) organised by Department of Microbiology, Goa University.
- National Conference of Young Researchers 2017 on "New Frontiers in Life Sciences and Environment" at Goa University.
- Participated in workshop on "Novel Sanitation Approaches and Emerging Trends In Waste Water Treatment Technology" organised by BITS Pilani, K K Birla Goa campus (19-21st December 2017).
- Attended one day seminar on "Biosafety and Intellectual Property rights" organized by Dept. of Biotechnology, Goa University.
- One-day seminar cum workshop on "BioTechniques" (29th November 2018) at Department of Biotechnology, Goa University.
- Participated in hands-on workshop on "Modern Laboratory Techniques" (11th -14th February 2020) organised by Dept. of Zoology, Goa University.
- Attended 2-day National seminar on "Effective Use of Nanotechnology and Nanomaterials for Sustainable Agriculture" (28th-19th February 2020) organised by Dept. of Microbiology, PESRSN College of Arts and Science Ponda, Goa.
- Participated in hands on training in "Molecular Phylogenetics" (7th - 9th February 2020) organised by Dept. of Zoology, Goa Univ

Ecotoxicology and Environmental Safety 165 (2018) 516–526

Contents lists available at ScienceDirect

Ecotoxicology and Environmental Safety

journal homepage: www.elsevier.com/locate/ecoenv

Tellurite biotransformation and detoxification by *Shewanella baltica* with simultaneous synthesis of tellurium nanorods exhibiting photo-catalytic and anti-biofilm activity

Diviya Chandrakant Vaigankar[a], Santosh Kumar Dubey[b,*], Sajiya Yusuf Mujawar[a], Avelyno D'Costa[c], Shyama S.K.[c]

[a] Laboratory of Bacterial Genetics and Environmental Biotechnology, Department of Microbiology, Goa University, Taleigao Plateau, Goa 403206, India
[b] Centre of Advanced Study in Botany, Banaras Hindu University, Varanasi, Uttar Pradesh 221005, India
[c] Genetic Toxicology Laboratory, Department of Zoology, Goa University, Taleigao Plateau, Goa 403206, India

ARTICLE INFO

Keywords:
Anti-biofilm
Bioremediation
Estuary
Genotoxicity
Shewanella baltica
Tellurium nanoparticles

ABSTRACT

Tellurite reducing bacterial strain was isolated from Zuari estuary, Goa India which could tolerate 5.5 mM potassium tellurite with a minimum inhibitory concentration of 6 mM. This strain was designated as GUSDZ9 and was identified as *Shewanella baltica* (accession number: MF350629) based on 16S rRNA gene sequencing and BLAST analysis. The Diethyl-dithiocarbamate based colorimetric analysis clearly demonstrated a complete reduction of 2 mM tellurite to elemental tellurium during the late stationary phase. Te Nanoparticles (TeNPs) biosynthesis which initiated at early log phase (i.e. 4 h) was evidently monitored through colour change and a peak due to surface plasmon resonance at 210 nm using UV–Vis spectroscopic analysis. X-ray crystallographic studies and transmission electron microscopy revealed unique nano-rods with a diameter ranging from 8 to 75 nm. Energy dispersive X-ray analysis further confirmed the presence of pure tellurium. The biogenic TeNPs at 10 and 5 μg/mL evidently demonstrated 90% degradation of methylene blue dye and anti-biofilm activity against potential Gram-positive and Gram-negative human pathogens respectively. The alkaline comet assay revealed time and dose-dependent genotoxicity at concentrations higher than 15 μg/mL of TeNPs. This study clearly demonstrated the potential of *Shewanella baltica* strain GUSDZ9 in bioremediation of toxic tellurite through bio-reduction into elemental tellurium and involvement of biogenic TeNPs in the photo-catalytic reduction of methylene blue and anti-biofilm activity. This is the first report of its kind on the synthesis of biogenic TeNPs from *Shewanella baltica* demonstrating photo-catalytic, anti-biofilm activity as well as genotoxicity.

1. Introduction

Estuarine environment is the most common dumping site for industrial, electronic and mining wastes. Consequently, estuaries are heavily contaminated with various persistent toxic metals viz. Cu, Hg, Cd, Pb and metalloids viz. Se, Te, As posing a serious threat to aquatic biota including microorganisms (Tchounwou et al., 2012). During the last several decades, metal and metalloid bioremediation of polluted sites using metal/metalloid resistant microorganisms have been studied extensively (Satyanarayana et al., 2012; Khalilian et al., 2015; Gupta et al., 2016). Tellurium (Te) is a metalloid present at 0.027 ppm concentration in the earth crust. It occurs in the environment as inorganic, unstable telluride [Te^{2-}], water-soluble, toxic tellurate [TeO_4^{2-}] and tellurite [TeO_3^{2-}]; organic form as dimethyl telluride (CH_3TeCH_3) and elemental tellurium (Te°). Industrially Te and its compounds find applications in solar panels, glasses, rubber, photocopying machine, metal alloys, rechargeable batteries, semiconductors in electronics, protein crystallographic analysis and as catalysts in various chemical processes (Chasteen et al., 2009; Naumov, 2010).

Tellurite is highly toxic to microorganisms at concentrations as low as 1 μg/mL (Taylor, 1999). The toxicity of tellurite is of great concern to prokaryotes as well as eukaryotes since its lethal concentration is several folds lower than that of other metals viz. Fe, Hg, Cd, Cu, Cr, Zn, Co and Se which is a metalloid (Chasteen et al., 2009; Presentato et al., 2016). Some microorganisms have evolved resistance mechanisms such as reduction of tellurite to black elemental tellurium, intracellular and extracellular accumulation of reduced tellurium and volatilization by methylation (Trutko et al., 2000; Basnayake et al., 2001; Fuentes et al.,

* Corresponding author.
E-mail address: santosh.dubey@bhu.ac.in (S.K. Dubey).

https://doi.org/10.1016/j.ecoenv.2018.08.111
Received 3 May 2018; Received in revised form 7 August 2018; Accepted 31 August 2018

2007; Chasteen et al., 2009). Few tellurite resistant marine bacteria have already been reported for their possible role in tellurite bioremediation (Rathgeber et al., 2002; Csotonyi et al., 2006; Amoozegar et al., 2008; Ollivier et al., 2008; Kim et al., 2012; Arenas et al., 2014; Borghese et al., 2014; Soda et al., 2018; Valdivia-González et al., 2018).

Bioreduction of soluble tellurite to insoluble elemental tellurium by microorganisms can occur with the formation of nanostructured particles. Since reductive biotransformation and synthesis of nanostructures proceed contextually, the use of estuarine microbes for simultaneous tellurite bioreduction in polluted environments and biogenesis of nanomaterials appears highly promising and economically attractive. Microbially-mediated strategies for nanoparticle synthesis are environment-friendly because they occur in mild reaction conditions avoiding energy-intensive procedures as well as the use of highly toxic stabilizing reagents, which are usually associated with physical and chemical approaches (Xi et al., 2005; Kaushik et al., 2010). There are few strains of bacteria which have been reported to synthesize TeNPs and include *Bacillus* sp., *Rhodococcus aetherivorans, Rhodobacter capsulatus, Bacillus selenitireducens, Sulfurospirillum barnesii* and *Shewanella oneidensis* (Klonowska et al., 2005; Baesman et al., 2007; Kim et al., 2012; Zare et al., 2012; Borghese et al., 2014; Presentato et al., 2016).

Nanoparticles are in high demand in various fields viz. medicine, electronic, catalyst, biosensors, paint, glass, alloy and battery industries (Li et al., 2011). Te in nano-dimensions possesses unique properties such as high surface to volume ratio, piezo-thermoelectrical, photoconductivity, catalytic and non-linear optical characteristics which have attracted the attention of several researchers around the world (Liu et al., 2003; Kurimella et al., 2013). More recently, Te and Cd quantum dots have been reported to have great potential in solar cells and imaging (Liu et al., 2003; Li et al., 2014). Application of nanoparticles in photo-catalytic degradation of toxic and hazardous effluents containing dyes, phenols and pesticides from textile, paper and agro-industries has drawn a lot of attention from environmental scientists. Since current methods employed for the degradation of organic pollutants are laborious and expensive, there is a pressing need for safe, efficient and eco-friendly methods to treat these organic pollutants. Thus, the use of nanoparticles in photo-catalytic degradation of organic pollutants may prove to be a better alternative.

Nanoparticles also find applications in medicine as antimicrobial agents to treat bacterial infections resistant to multiple antibiotics. Over the last few decades, the effectiveness of antibiotic treatment has decreased significantly due to the emergence of bacterial resistance to multiple antibiotics in hospital and community settings. The problem is particularly more serious in the treatment of biofilm-associated microbial infections. Therefore, there is an urgent need to develop novel nanomaterial-based antimicrobials possessing high bactericidal activity against biofilm forming pathogenic microorganisms.

However, with the profound use of nanoparticles in biomedical applications viz. antibacterial therapy and drug delivery, along with enhanced exposure to nanomaterials in everyday life, it is mandatory to investigate the toxicity of these nanoparticles. Under these circumstances, the genotoxicity of nanomaterials is a burgeoning issue in the area of nanotechnology. Although the genotoxicity of chemically-synthesized nanoparticles has been studied extensively, the genotoxicity of biologically-synthesized nanomaterials is scarcely reported (Foldbjerg et al., 2011; Ghosh et al., 2012; De Lima et al., 2013; Lebedová et al., 2017). Moreover, there are no reports on the genotoxicity of TeNPs even though they have been already studied for their antimicrobial and anti-biofilm applications (Lin et al., 2012; Zare et al., 2012; Mohanty et al., 2014; Pugin et al., 2014; Srivastava et al., 2015; Zonaro et al., 2015). Thus, it is highly imperative to study the genotoxic effect of biogenic TeNPs, intended for biomedical and environmental applications.

In the present study, the tellurite reduction potential of *Shewanella baltica* strain GUDSZ9 from Zuari estuary Goa, India, is discussed along with the simultaneous synthesis of TeNPs. We have also studied the potential application of these biogenic TeNPs in photo-catalytic degradation of methylene blue dye, anti-biofilm activity and genotoxicity against human lymphocytes.

2. Materials and methods

2.1. Materials

All the chemicals used for the present study were of certified analytical grade and were procured from Himedia (Mumbai, India) unless specified otherwise.

2.2. Enrichment and isolation of tellurite reducing estuarine bacteria from Zuari estuary, Goa, India

Estuarine surface water was collected from the Zuari estuary Goa, India (Latitude: 15°24'31.03''N, Longitude: 73°53'31.02''E and temperature: 27 °C) using a sterile polycarbonate bottle. One mL of water sample was added to 50 mL Zobell Marine Broth (ZMB) supplemented with 0.5 mM potassium tellurite (K_2TeO_3) and was incubated at 28 ± 2 °C on a shaker at 150 rpm for 48 h. Isolation of tellurite reducing bacteria was done by dilution plating of the enriched sample on Zobell marine agar (ZMA) plates amended with 2 mM K_2TeO_3 and plates were incubated at 28 ± 2 °C for 24 h. Discrete black coloured colonies were re-streaked on ZMA plates without K_2TeO_3 in order to ensure that blackening of the colonies was certainly due to the reduction of K_2TeO_3 to elemental tellurium and not because of bacterial pigment. Morphologically distinct tellurite reducing bacterial colonies were selected for further studies.

2.3. Determination of minimum inhibitory concentration (MIC) of tellurite

Total 20 bacterial isolates were selected and spot inoculated on ZMA plates with increasing concentrations of K_2TeO_3 (0–20 mM). These plates were incubated at 28 ± 2 °C for 24 h and were checked for the appearance of metallic black coloured colonies. The minimum concentration of tellurite at which no visible colonies were obtained was designated as MIC. Ten bacterial isolates with the high MIC on ZMA plates were selected for determining the MIC in ZMB. MIC in liquid medium was determined by inoculating the selected bacterial isolates in ZMB with various concentrations of K_2TeO_3 (0–20 mM). The flasks were incubated at 28 ± 2 °C for 24 h and absorbance at 600 nm was recorded. The lowest concentration of tellurite which inhibited growth was considered as MIC. Out of ten isolates, the bacterial strain exhibiting the highest MIC in ZMB for K_2TeO_3 was considered for further characterization.

2.4. Identification of potential tellurite reducing bacterial strain

The selected tellurite-resistant strain was characterized morphologically and biochemically followed by molecular identification. DNA extraction of the tellurite reducing bacterial strain was carried out using Dneasy® Blood & Tissue Kit (Qiagen, Hilden, Germany). The 16S ribosomal RNA gene (16 S rRNA) was amplified with 27 F (5' AGAGTTTG ATCMTGGCTCAG 3') and 1492R (5' TACGGYTACCTTGTTACGACTT 3') universal eubacterial primers using Nexus Gradient Mastercycler (Eppendorf, Germany). The PCR amplicon was analysed on 1% agarose gel followed by purification using Wizard SVGel and PCR clean-up system (Promega, USA). The 16S rRNA gene was sequenced at Eurofins Genomics Bangalore, India. The DNA sequence was analysed by BLAST (Altschul et al., 1990) and submitted to GenBank. Neighbor-joining method was used for the construction of a phylogenetic dendrogram using MEGA 7 package (Tamura et al., 2013).

2.5. Growth behaviour of potential tellurite reducing bacterial strain

The potential tellurite reducing bacterial strain GUSDZ9 was inoculated in ZMB supplemented with different concentrations (0–6 mM) of K_2TeO_3 under constant shaking at 150 rpm and temperature at 28 ± 2 °C for 48 h. The growth behaviour of the strain at various concentrations of K_2TeO_3 was monitored by recording the absorbance at 600 nm at specific time intervals using UV–Vis spectrophotometer (Shimadzu model-1601, Japan). The experiment was carried out in triplicates and the standard deviation was determined.

2.6. Tellurite uptake studies using selected tellurite reducing bacterial strain

Tellurite uptake was estimated by modified diethyldithiocarbamate (DDTC) colorimetric assay (Turner et al., 1992). The bacterial strain was grown in ZMB with 2 mM K_2TeO_3 and after every 4 h, 0.5 mL culture aliquots were removed and centrifuged at 9727 × g for 10 min. The supernatant (100 µL) was added to the tube containing 0.3 M Tris buffer (pH 7) and 2 mM DDTC and absorbance was recorded at 340 nm in order to determine unreduced tellurite remaining in the supernatant. The assay was carried out in triplicates and the standard deviation was determined.

2.7. TeNPs biosynthesis

The tellurite reducing bacterial strain GUSDZ9 was inoculated in ZMB supplemented with 2 mM K_2TeO_3 and incubated at 28 ± 2 °C under constant shaking at 150 rpm for 24 h. Reduction of K_2TeO_3 by the strain was confirmed by visual observation of black colour which is an indication of tellurite reduction to black elemental Te. Un-inoculated medium with K_2TeO_3 and culture supernatant with K_2TeO_3 were kept as appropriate controls.

2.8. Optimization and time course study of TeNPs biosynthesis using strain GUSDZ9

The tellurite and pH optima for TeNPs biosynthesis was determined at different concentrations of K_2TeO_3 and pH by inoculating overnight grown culture separately in ZMB containing different concentrations of K_2TeO_3 (0.5, 1.0, 1.5, 2.0, 2.5 and 3.0 mM) and pH (5, 6, 7, 8, 9 and 10) respectively. One mL aliquot of culture suspension was withdrawn after 42 h and centrifuged at 9727 × g for 10 min. The pellet obtained was suspended in phosphate buffered saline (PBS), sonicated and centrifuged at 7782 × g for 10 min. The resulting supernatant was centrifuged again at 9727 × g for 30 min and pellet obtained was re-suspended in methanol: chloroform (2:1 v/v). The suspension was monitored using UV–Vis spectrophotometer by recording absorbance at 210 nm which is characteristic for elemental Te. These optimized conditions were maintained for subsequent time course study of TeNPs biosynthesis.

In order to obtain TeNPs, the culture containing TeNPs was harvested by centrifugation at 9727 X g for 10 min and the resultant black coloured pellet was washed thrice with PBS. The cell pellet was re-suspended in methanol: chloroform (2:1 v/v) and sonicated (0.5 pulses for 10 min with 5 min interval). After cell lysis, the suspension was centrifuged at 3502 × g for 10 min, the supernatant was retained and the pellet containing cell debris was discarded. The black colloidal suspension obtained was further harvested at 9727 × g for 30 min and the pellet obtained was subsequently washed twice with deionised water and ethanol. The pellet was dried at 80 °C using an oven in order to get TeNPs.

2.9. Characterization of biogenic TeNPs

2.9.1. UV–Vis spectroscopic analysis

The biogenic TeNPs were suspended in methanol: chloroform solvents (2:1 v/v) and absorbance was recorded in the range of 190–800 nm with methanol: chloroform (2:1 v/v) as blank.

2.9.2. X-ray diffraction analysis

X-ray diffraction pattern for biosynthesized TeNPs was obtained using Rigaku Miniflex X-ray diffractometer operated at 40 keV voltage, 20 mA of current and 1.541 Å of Cu Ka radiation. The data obtained was plotted in Origin 8 software and FWHM (Full Width Half Maxima) was obtained. The crystal size of the nanoparticle was calculated using Scherer's equation as follows: $D = K\lambda/\beta Cos\theta$ where D is the mean grain size, k is constant, λ is the X-ray wavelength for CuKa radiation, β is the FWHM of the diffraction peak in radians and θ is the Bragg's angle.

2.9.3. Transmission electron microscopic analysis

TEM analysis of biogenic TeNPs was carried out by dispersing powdered TeNPs in methanol and mounting on a carbon-coated copper TEM grid (Philips, model- CM200). The machine was operated at an accelerating voltage of 190 keV and images were taken at a resolution of 2.4 Å. The size of TeNPs was calculated using Image J software.

2.9.4. Energy dispersive X-ray analysis

A thin film of powdered TeNPs was placed on a carbon-taped sample holder followed by coating the TeNPs with carbon. The energy dispersive X-ray analysis of the coated sample was carried out using scanning electron microscope (JSM 5800 LV, model- JEOL, Japan) equipped with energy dispersive X-ray analysis operated at 20 keV to determine the elemental composition of the biogenic TeNPs.

2.10. Applications of biogenic TeNPs

2.10.1. Photo-catalytic activity of biosynthesized TeNPs

The photo-catalytic degradation of methylene blue dye using biosynthesized TeNPs was investigated in sunlight. TeNPs (10 µg/mL) was added to a methylene blue solution. This colloidal suspension was incubated in sunlight. The methylene blue solution without nanoparticles was also incubated under similar conditions as a control. The methylene blue degradation was monitored at different time intervals viz. 30, 60, 90, 120, 150, 180, 210 and 240 min by withdrawing 1 mL aliquots of colloidal mixture followed by centrifugation. The supernatant obtained was scanned by UV–Vis spectrophotometer in the wavelength range of 190–800 nm. Absorbance maxima at 664 nm was considered as characteristic for methylene blue and was monitored at various time intervals. The extent of methylene blue dye degradation was calculated using the following formula:

$$\%\text{Decolourization} = (\text{Initial absorbance} - \text{absorbance after treatment}) / \text{Initial absorbance} \times 100$$

2.10.2. Anti-biofilm activity assay of biosynthesised TeNPs

The anti-biofilm activity of biogenic TeNPs against potential human pathogens procured from Goa Medical College, Goa, India was studied using modified crystal violet assay in a 96 well sterile polystyrene microtiter plate as described previously (Baygar and Ugur, 2017). Initially, 300 µL of nutrient broth was added into a sterile polystyrene microtiter plate to which 12 h old pathogenic bacterial cultures viz. *Streptococcus pyogenes, Staphylococcus aureus*, *Klebsiella pneumoniae* and *Escherichia coli* were inoculated separately along with three different concentrations of biogenic TeNPs (5, 10 and 15 µg/mL). Un-inoculated nutrient broth and pathogens grown in nutrient broth without TeNPs were maintained as controls. The microtitre plate was incubated at 37 °C for 48 h under static conditions. Subsequently, the microtiter plate was drained, washed gently with sterile PBS and distilled water to remove unbound cells, followed by drying for 30 min. Crystal violet (0.2% w/v) was added (300 µL) to each well and incubated at 28 °C for 30 min, excess dye was gently washed with sterile distilled water.

Methanol (300 μL) was added to the dried wells of the microtitre plate and absorbance was measured at 660 nm keeping methanol as a blank. The anti-biofilm effect was estimated using the following formula:

% Anti-biofilm activity = (Absorbance of control–absorbance of sample)/absorbance of control × 100; where Absorbance of control corresponds to the bacterial cells grown in nutrient broth without TeNPs. The anti-biofilm assay was carried out in triplicate and the standard deviation was determined.

2.11. Genotoxicity of biogenic TeNPs using comet assay

Genotoxicity of the biogenic TeNPs against human lymphocytes was studied using comet assay. Blood sample (5 mL) was collected from a healthy human blood donor in a heparinized centrifuge tube and was centrifuged at 1953 × g for 15 min. The white buffy coat at the interphase of plasma layer and sedimentary blood cells were collected in a microcentrifuge tube. The blood cell pellet was washed with 0.5 mL of freshly prepared 0.85% NH_4Cl (w/v) in order to remove contaminant red blood cells. Lymphocytes which appeared as a white pellet after subsequent washes were re-suspended in PBS (pH 7) and stored at 4 °C.

The viability of the lymphocytes was ensured by determining the total cell count of lymphocytes prior to the comet assay. The lymphocyte suspension having a cell count of 10^4–10^5 cells/mL were used to study the genotoxic effect of nanoparticles.

Tubes containing lymphocytes (25 μL) were suspended with 15, 20, 25 and 50 μg/mL of biogenic TeNPs separately and were incubated at 37 °C for 0, 1 and 2 h. DNA damage was monitored in the lymphocytes by employing the comet assay (Bausinger and Speit, 2016; D'Costa et al., 2017). Briefly, the lymphocyte suspension exposed to different concentrations of TeNPs was mixed with 150 μL of 0.5% low melting agarose at 37 °C and was overlaid on a frosted slide pre-coated with 1% normal melting agarose. This was gently covered with a coverslip and allowed to solidify at 0 °C. The coverslip was removed gently, followed by placing a layer of 0.5% low melting agarose. After solidification of the final layer, the slide was immersed in freshly prepared lysing solution consisting of 2.5 M NaCl, 100 mM EDTA, 10 mM Tris-HCl, 10% DMSO and 1% Triton X-100 (pH 10) at 4 °C overnight. The slides were then immersed in electrophoresis buffer containing 300 mM NaOH and 1 mM EDTA, pH 10 for 20 min for DNA unwinding. Electrophoresis was carried out for 20 min at 25 V. After electrophoresis, the slides were placed in a cold neutralizing buffer comprising of 0.4 M Tris-HCl, pH 7.5 for 10 min. The slides were then stained with 15 μg/mL ethidium bromide and examined under a BX53 Olympus fluorescence microscope (Japan) at 200× magnification. The images of the comets were captured using ProgRes®Capture Pro 2.7. CASP image analysis software was used to analyse the percent tail DNA as an indicator of single-strand DNA damage. Two slides per specimen (500 comets) were selected for analysis. Lymphocytes exposed to H_2O_2, a known genotoxic agent served as a positive control.

2.12. Statistical analysis

Statistical analysis was performed using graph pad prism 7 software. Data was analysed using the Student *t*-test and one way ANOVA. The significance of the data for each dose against that of the respective controls were analysed by the Student *t*-test. Whereas, one way ANOVA was used to determine variation in the dose-response and time response of the biogenic TeNPs on human lymphocytes. Data were considered as statistically significant at $p < 0.05$.

3. Results and discussion

3.1. Enrichment and isolation of tellurite reducing estuarine bacterial strains

After enrichment of estuarine water sample in ZMB containing 0.5 mM K_2TeO_3, black colouration was observed in the flask indicating the reduction of tellurite to black coloured elemental tellurium. Subsequently, plating the enriched sample on ZMA plates containing 2 mM K_2TeO_3 resulted in the appearance of discrete metallic black colonies after incubation for 24 h (Supplementary Fig. 1). Twenty morphologically diverse bacterial isolates were selected for further studies. These isolates did not show any black pigmentation upon streaking on ZMA plates without K_2TeO_3 (Supplementary Fig. 2). However, it was observed that extent of tellurite reduction was also different in all twenty isolates which was evident from the difference in intensities of the black colour.

The Zuari estuary of Goa is polluted with several metal and metalloids due to extensive shipping and other industrial activities. Interestingly, bacteria from Zuari estuary have already been reported to tolerate high levels of various metal, organo-metal and metalloid pollutants (Khanolkar et al., 2015; Pereira, 2017; Samant et al., 2018; Sunitha et al., 2015). Zuari estuary is also flanked by various electronic and electrical industries. In the present communication, we have confirmed that the bacterial isolates from Zuari estuary are resistant to tellurite, which may be due to exposure of these bacterial isolates to tellurite.

3.2. Determination of MIC of tellurite using selected estuarine bacterial strains

Out of 20 isolates, 10 bacterial isolates exhibiting MIC higher than 15 mM on ZMA were chosen for further studies. In ZMB the estuarine bacterial strain GUSDZ9 showing highest MIC (i.e. 6 mM) was selected for further characterization. The bacterial strain GUSDZ9 showed very high MIC as compared to previously isolated marine tellurite resistant bacterial isolates for instance, bacteria isolated from the Caspian Sea exhibited MIC of 0.8 mM, whereas, marine bacterial strain 14 B isolated from Rehoboth beach, DE, United States was reported to tolerate 0.3–0.4 mM K_2TeO_3 (Ollivier et al., 2008; Zare et al., 2012). A recent study by Valdivia-González et al. (2018) on *Shewanella* spp. has reported MIC values ranging from 0.05 to 1 mM. This is much lower as compared to MIC for strain GUSDZ9. Thus, estuarine strain GUSDZ9 with MIC 6 mM for K_2TeO_3 is a potential candidate which may be used for bioremediation of tellurite contaminated estuarine sites.

3.3. Identification of tellurite reducing estuarine bacterial strain GUSDZ9

The bacterial strain GUSDZ9 was found to be Gram-negative, motile, rod-shaped, oxidase and catalase positive, H_2S producing and facultative anaerobic bacteria. Based on 16 S rRNA gene sequence and comparison of the sequence against GenBank database using NCBI-BLAST search, the strain GUSDZ9 was identified as *Shewanella baltica* (accession number MF350629). The dendrogram analysis has clearly revealed phylogenetic relatedness with other species of *Shewanella* (Fig. 1). Bacteria belonging to genus Shewanella are capable of anaerobic respiration using several electron acceptors. Moreover, the family Shewanellaceae is considered to play a pivotal role in bioremediation of sites contaminated with heavy metals and radioactive wastes (Fredrickson et al., 2008). Although few reports are available on tellurite reducing *Shewanella* spp. viz. *S. oneidensis, S. putrefaciens* and *S. baltica* (Klonowska et al., 2005; Kim et al., 2012, 2013, 2014; Valdivia-González et al., 2018), but *Shewanella baltica* strain GUSDZ9 isolated from Zuari estuary showed a higher level of tellurite reduction as compared to previously reported spp. of *Shewanella*.

3.4. Growth behaviour of tellurite-reducing Shewanella baltica strain GUSDZ9

Growth pattern of *Shewanella baltica* strain GUSDZ9 in presence of different tellurite concentrations (0–6 mM) indicated that the growth of the isolate was adversely affected only at a higher concentration of tellurite (Supplementary Fig. 3). This was evident by the extended lag

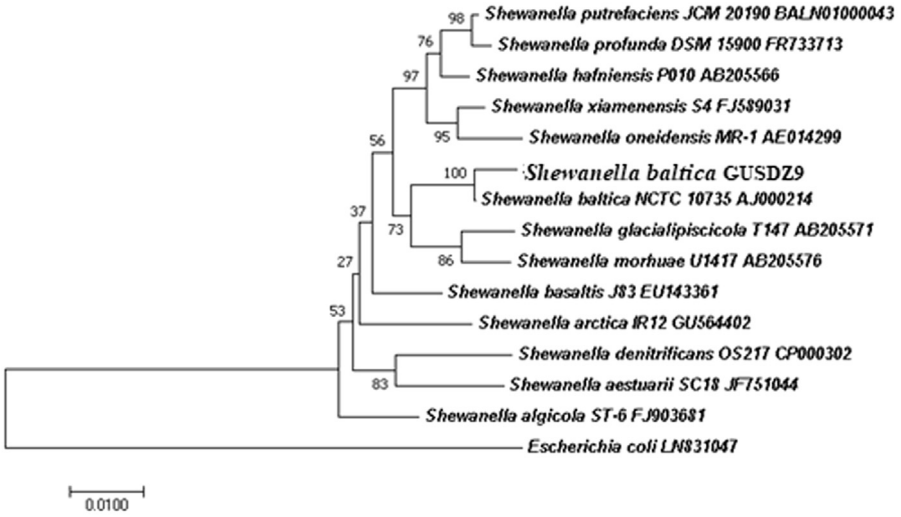

Fig. 1. Phylogenetic tree showing the relatedness of *Shewanella baltica* strain GUSDZ9 with other strains of *Shewanella* constructed using neighbor-joining method (Tamura et al., 2013). The bootstrap values are based on 1000 replicates.

phase at 4.0 and 5.5 mM K_2TeO_3 which is 6 h and 8 h respectively.

3.5. Uptake of tellurite by tellurite reducing Shewanella baltica strain GUSDZ9

Tellurite uptake by *Shewanella baltica* strain GUSDZ9 grown in ZMB with 2 mM K_2TeO_3 was observed during the early log phase of growth (2 h) with a steady increase during mid-log phase (Fig. 2). At mid-log phase (22 h), a 50% reduction of tellurite was observed. However, complete utilization of tellurite was achieved at the end of the stationary growth phase (38 h). The previous study on *Salinococcus* sp. showed a 75% reduction of tellurite after 72 h of bacterial growth supplemented with 0.4 mM K_2TeO_3 (Amoozegar et al., 2008). A similar reduction pattern was also reported in *Rhodococcus* sp. after 120 h while, *Bacillus* sp. BZ showed higher reduction rate (i.e. 80%) after 48 h of bacterial growth (Zare et al., 2012; Presentato et al., 2016). Although, most of the studies pertaining to *Shewanella* spp. on tellurite-reduction have been reported to be more effective under anaerobic conditions, our study showed a higher reduction of tellurite under aerobic conditions. This is in agreement with one recent study which has reported 70–80% tellurite removal under aerobic conditions efficiently (Soda et al., 2018). Knowing the fact that *Shewanella* spp. are facultative anaerobes the bacterial strain GUSDZ9 may also be used for tellurite-reduction under anaerobic conditions.

The present study holds considerable significance since a 100% reduction of 2 mM K_2TeO_3 was achieved at the end of the stationary growth phase (i.e. 38 h) which is the shortest time recorded so far.

3.6. TeNPs Biosynthesis using Shewanella baltica strain GUSDZ9

Reduction of tellurite to elemental tellurium which is tentatively indicated by metallic black colouration was observed in culture supplemented with 2 mM K_2TeO_3. Control flasks without K_2TeO_3 and that of culture supernatant with 2 mM of K_2TeO_3 did not show any black colouration indicting that nanoparticle synthesis is growth dependent and is intracellular (Supplementary fig. 4). Intracellular biosynthesis of

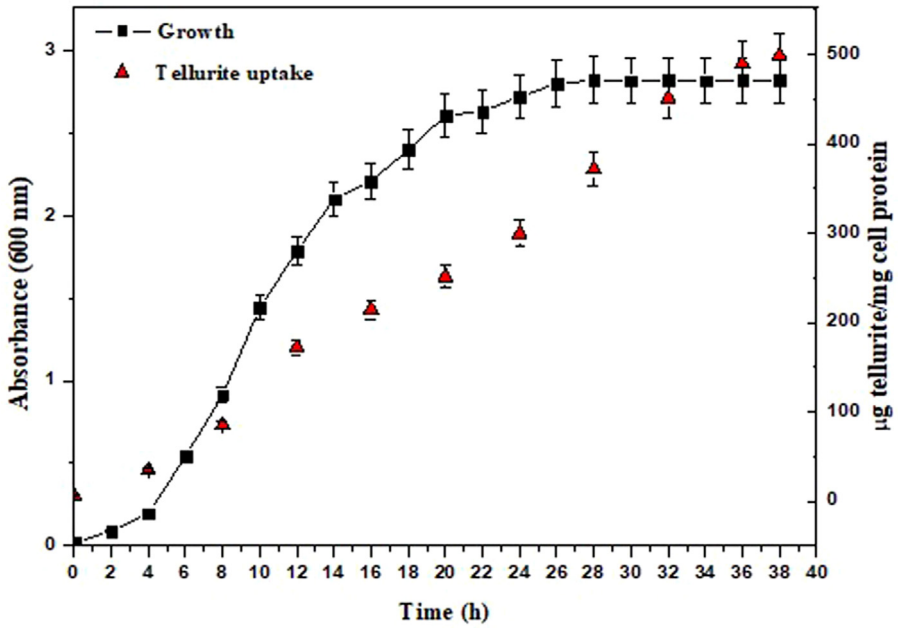

Fig. 2. Growth pattern and tellurite uptake shown by *Shewanella baltica* strain GUSDZ9 in **ZMB with 2 mM K_2TeO_3.**

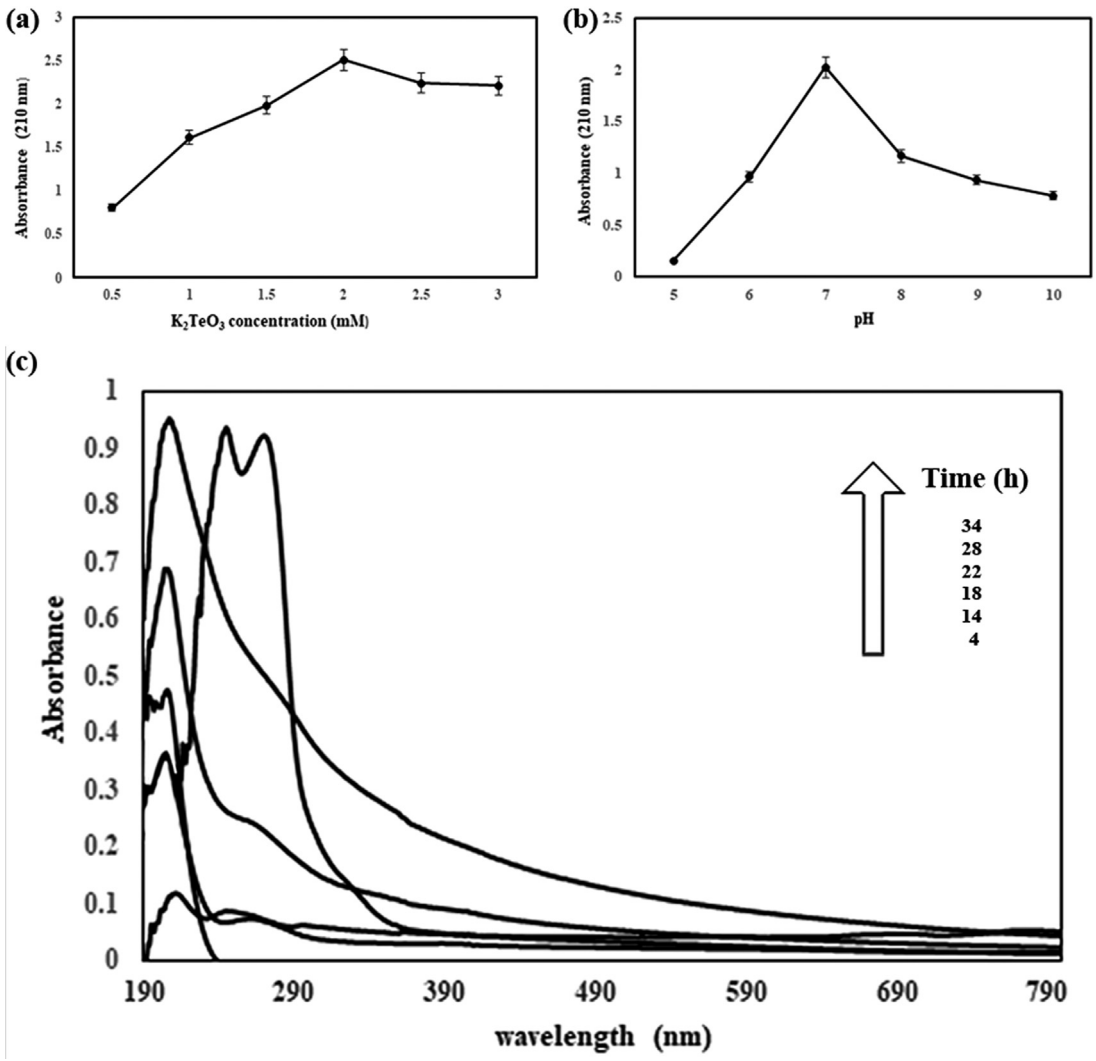

Fig. 3. TeNPs biosynthesis at different: K_2TeO_3 concentrations (a); pH (b); Time course study for TeNPs biosynthesis under optimized conditions (c).

TeNPs has been previously demonstrated in various bacteria viz. *Pseudomonas pseudoalcaligenes* KF707, *Shewanella oneidensis* and *Rhodococcus aetherivorans* (Di Tomaso et al., 2002; Kim et al., 2012; Presentato et al., 2016).

3.7. Optimization and time course study for TeNPs biosynthesis using *Shewanella baltica* strain GUSDZ9

Optimum K_2TeO_3 concentration and pH for TeNPs biosynthesis were found to be 2 mM and 7 respectively (Fig. 3a, b). It was interesting to note that the strain GUSDZ9 could synthesize TeNPs at broad pH range i.e. 6–10 and tellurite concentrations (0.5–3 mM). However, variation in the intensity of black colouration was observed indicating differences in the extent of TeNPs biosynthesis at different pH and K_2TeO_3 concentrations. Time course study of TeNPs interestingly revealed that the biosynthesis was initiated during early log phase (4 h) of bacterial growth which was evident by the change in colour of the media and a distinct peak at 210 nm. Although the reduction of tellurite was initiated during the second hour, no prominent peak was observed at 210 nm since threshold concentration for nanoparticle detection was not achieved. Biosynthesis of TeNPs was found to be time-dependent i.e. there was an increase in absorbance (210 nm) with time (Fig. 3c). However, nanoparticle synthesis was found to be maximum during mid-log to early stationary phase. The optimum time for maximum nanoparticle synthesis was found to 28 h. Even though complete reduction of tellurite was observed at the end of the stationary phase there was a shift in surface plasmon resonance for TeNPs after early stationary phase indicating the formation of TeNPs with a larger diameter. A similar shift in surface plasmon with the formation of larger diameter nanoparticles has been reported (Stoeva et al., 2002). Our strain synthesises TeNPs faster than the previously reported bacterial strain *Pseudomonas pseudoalcaligenes* KF707 (Di Tomaso et al., 2002) since the Te crystallites' synthesis began at the mid-exponential phase.

3.8. Characterization of TeNPs

3.8.1. UV–Vis analysis

An absorption peak at 210 nm by the black colloidal solution due to surface plasmon resonance clearly indicated the presence of TeNPs (Fig. 4a). Similar findings have already been published confirming synthesis of TeNPs (Gautam, Rao, 2004; Zare et al., 2012; Forootanfar et al., 2015).

3.8.2. XRD analysis

The XRD spectrum clearly illustrated characteristic Bragg's peaks at 23.02, 27.5, 38.2, 40.5, 47.0 and 49.65 which corresponds to [100, 101, 102, 110, 200] and [201] of hexagonal phase of Te nanocrystals respectively (Fig. 4b). The average grain size was found to be 57.7 nm. This was in accordance with a standard card of tellurium (ICDD card no. 36) and is also in agreement with the earlier reports (Yuan et al.,

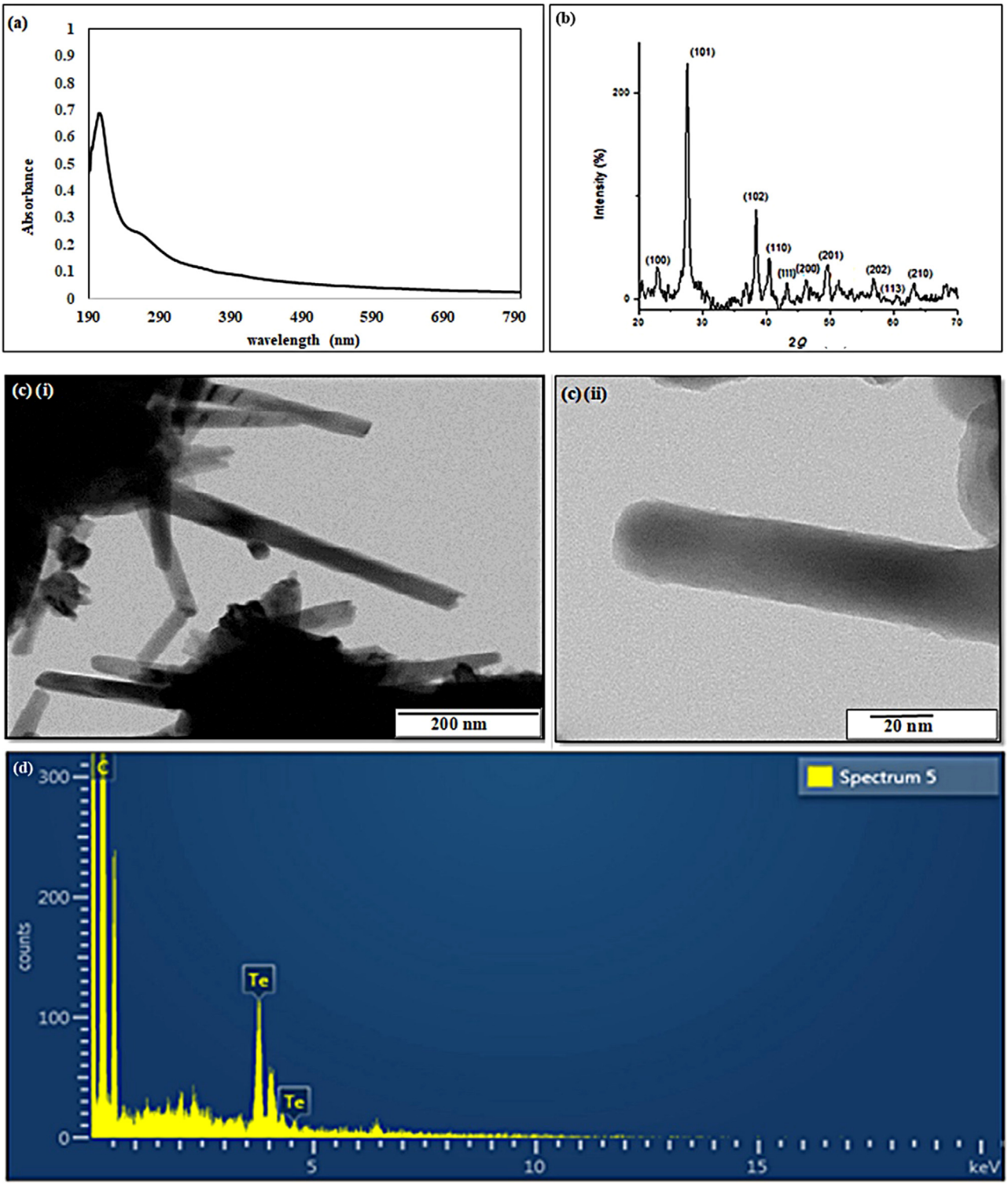

Fig. 4. Characterization of biogenic TeNPs: Absorbance maxima for biosynthesized TeNPs suspended in methanol: chloroform (2:1 v/v) at 210 nm (a); XRD pattern for biosynthesized TeNPs exhibiting characteristics Bragg's angles (b); TEM micrograph of biogenic TeNPs (c) (i) & (ii); EDAX spectrum showing characteristic peak of elemental tellurium at 3.6 keV(d).

2013; Manikandana et al., 2015; Srivastava et al., 2015).

3.8.3. TEM analysis

TEM analysis of nanoparticles revealed unique nano-rod morphology for TeNPs with a diameter in the range of 8–75 nm (Fig. 4c i, ii). Previously, various bacterial isolates have been reported to synthesise Te nano-rods viz. *Bacillus selenitireducens* (10 nm), *Shewanella oneidensis* MR-1 (10–20 nm), *Bacillus* sp. (20 nm), *Shewanella oneidensis* (10–20 nm) and *P. pseudoalcaligenes* (22 nm) (Baesman et al., 2007; Kim et al., 2012; Zare et al., 2012; Mohanty et al., 2014; Forootanfar et al., 2015). However, nano-sphere and needle-shaped TeNPs have also been reported (Di Tomaso et al., 2002; Klonowska et al., 2005). Interestingly, our study is the first evidence demonstrating TeNPs biosynthesis by *Shewanella baltica*.

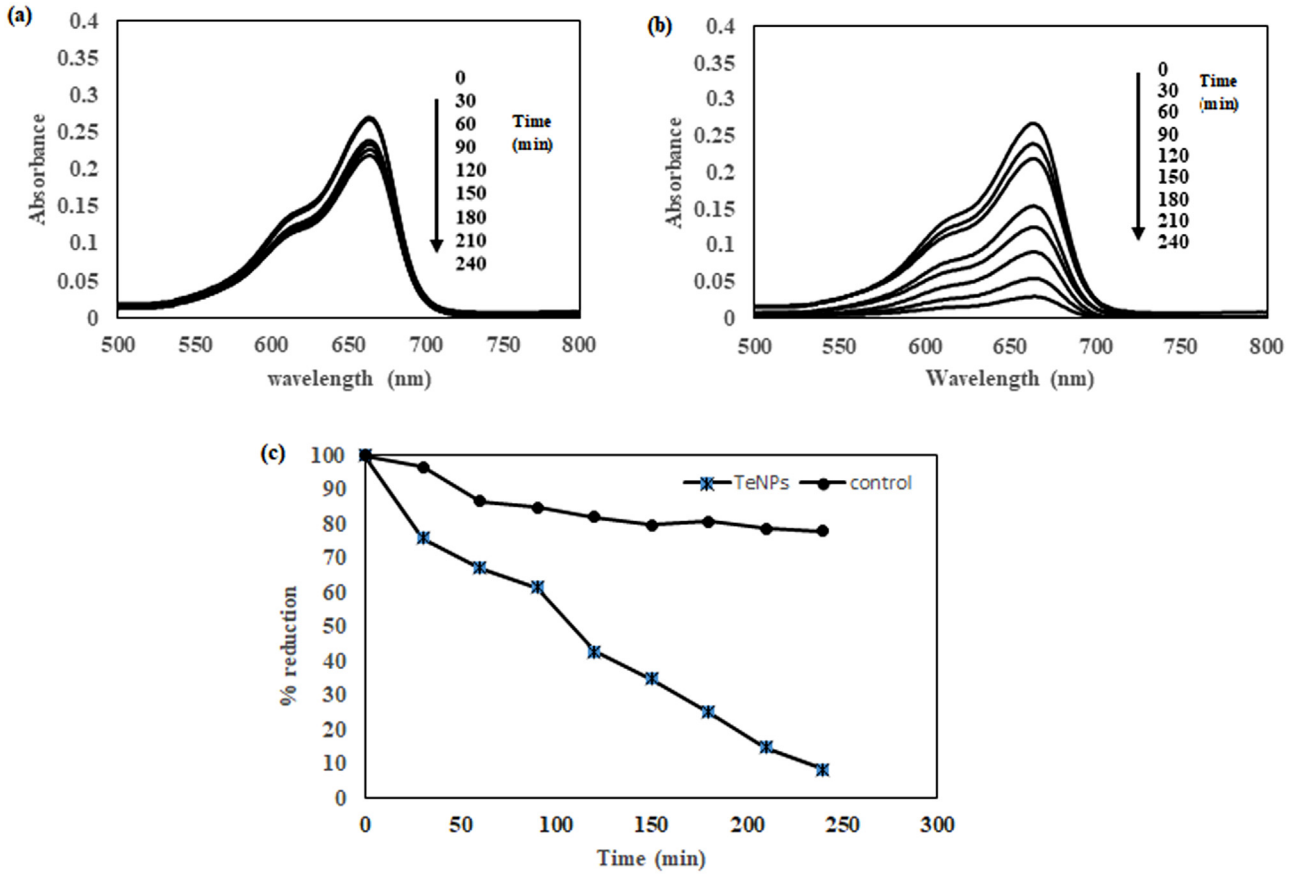

Fig. 5. UV–visible spectra of photo-catalytically degraded methylene blue dye: in absence of TeNPs (a); in presence of TeNPs (b); percent reduction of methylene blue (c).

3.8.4. Energy dispersive X-ray analysis

EDAX analysis of TeNPs clearly revealed a prominent peak of elemental tellurium at 3.6 keV (Fig. 4d). However, the peak due to carbon may be attributed to the carbon taped sample holder as well as coating with carbon.

3.8.5. Photo-catalytic activity of TeNPs

Methylene blue reduction under sunlight demonstrated a gradual change in colour from blue to pale blue. However, in presence of TeNPs as a catalyst, an enhanced decrease in absorbance was observed. In the control flask without Te nanorods, only 20% reduction of methylene blue was observed within 4 h. Whereas, in presence of TeNPs 90% reduction was observed which is very significant (Fig. 5a, b, c). There are various drawbacks associated with current physical and chemical methods employed for the degradation of organic pollutants. However, chemically synthesized TeNPs have already been reported for photocatalysis but there is no report on biogenic TeNPs-mediated photocatalysis (Shanmugam et al., 2015). The use of nanoparticles in photocatalytic degradation is advantageous since it is a reusable and recyclable process which does not require any additional step for disposal (Piella et al., 2013). Thus, biosynthesized TeNPs act as stable photocatalysts to reduce and bioremediate methylene blue dye which is present in the effluents of textile industries. This is the first report showing the photo-catalytic activity of biogenic TeNPs in methylene blue degradation through reduction.

3.9. Anti-biofilm activity assay using TeNPs

Anti-biofilm activity of biogenic TeNPs against clinically important microbial strains clearly demonstrated that these nanoparticles exhibited excellent anti-biofilm activity, which was dose-dependent. It was observed that TeNPs were very effective against *E. coli* wherein 92% of biofilm eradication was achieved at 15 µg/mL, whereas 64% was achieved at 10 µg/mL and 42% at 5 µg/mL concentration of TeNPs. *K. pneumoniae* showed a reduction in biofilm formation by 89%, 47% and 22% when treated with 15, 10 and 5 µg/mL TeNPs respectively. In the case of *S. aureus,* 81% biofilm removal was recorded at 15 µg/mL which was followed by 51% and 22% at 10 and 5 µg/mL of TeNPs respectively. A similar pattern was observed in case of *Streptococcus pyogenes* which recorded 63% biofilm removal at 15 µg/mL whereas, at 10 and 5 µg/mL concentrations, it was 20% and 9% respectively (Fig. 6). There are few reports on the antimicrobial activity of TeNPs (Lin et al., 2012; Zare et al., 2012; Mohanty et al., 2014; Pugin et al.,

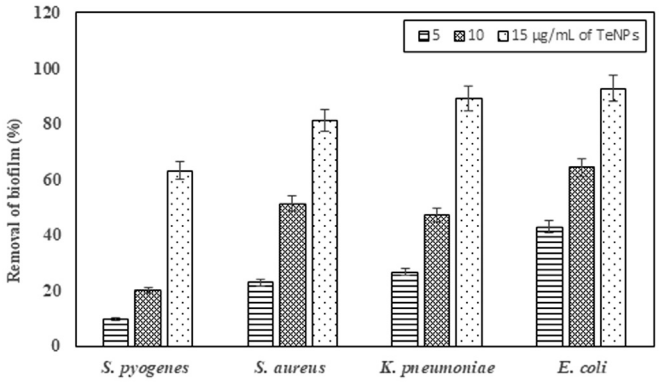

Fig. 6. Anti-biofilm activity of biosynthesized TeNPs against pathogenic clinical isolates.

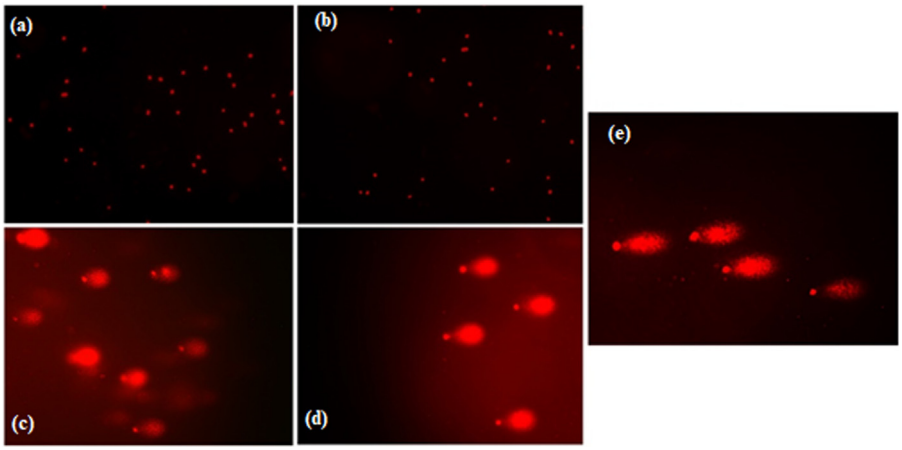

Fig. 7. Comet assay showing lymphocytes cells treated with: 0 μg/mL K_2TeO_3 (a); 15 μg/mL K_2TeO_3 (b); 20 μg/mL (c); 25 μg/mL (d); 50 μg/mL (e).

2014; Srivastava et al., 2015). However, removal of planktonic and biofilm forming bacteria by biogenic TeNPs have also been reported which ensured biofilm eradication at much higher concentrations of TeNPs (Zonaro et al., 2015). Therefore, TeNPs biosynthesised by *Shewanella baltica* strain GUSDZ9 are comparatively more effective in inhibiting potential biofilm forming Gram-positive and Gram-negative human pathogens at very low concentrations. This opens a new arena of applications for TeNPs as coating agents in medical and health-related devices in order to prevent bacterial infections. Furthermore, these TeNPs may also have promising applications in industrial sectors as potential tools to combat biofouling. Additionally, they can also serve as excellent candidates to eradicate biofilm formation in sewage tanks and other sewerage systems.

3.10. Genotoxicity of biogenic TeNPs

The percent (%) DNA damage induced by biogenic TeNPs at 15, 20, 25 and 50 μg/mL concentrations in the human lymphocytes at various time intervals (0, 1 and 2 h) are depicted in the Fig. 7. Interestingly, DNA damage observed at 15 μg/mL concentration of TeNPs with increasing time (1 and 2 h) was found to be insignificant compared to the control thus conferring that biogenic TeNPs do not induce any DNA damage in human cells at this concentration. However, a significant dose-dependent increase in the mean % tail DNA, with respect to the control was observed with time which was proved by the Student's *t*-test. Significant DNA damage was observed at 20 μg/mL (0 h) which increased in a time-dependent manner. A similar trend was also observed with 25 μg/mL concentration wherein 12.1% tail DNA damage was recorded, reaching maxima (30%) for 1 h whereas, at 2 h nearly 47% damage was observed. The highest DNA damage for lymphocytes was recorded at the 50 μg/mL concentration wherein significant % tail DNA recorded was 16%, 41% and 61% at 0, 1 and 2 h of treatments respectively (Fig. 8).

Increase in DNA damage at different concentrations of TeNPs (15, 20, 25 and 50 μg/mL) at all-time intervals (0, 1 and 2 h) was significant (except at 15 μg/mL) which was proved by one way ANOVA ($F = 499.4$, $p < 0.0001$).

Even though TeNPs have been studied for various applications majorly in the biomedical field but there are no reports as far as toxicity on human cells is concerned. Thus, these studies are of immense importance since this is the first ever report demonstrating the genotoxicity of biogenic TeNPs. Based on this study it is also advisable that utmost care must be taken in handling nano-wastes. Since insignificant DNA damage was observed at 15 μg/mL TeNPs, these nanorods can be effectively used to control biofilms inhabiting various medical as well as industrial appliances.

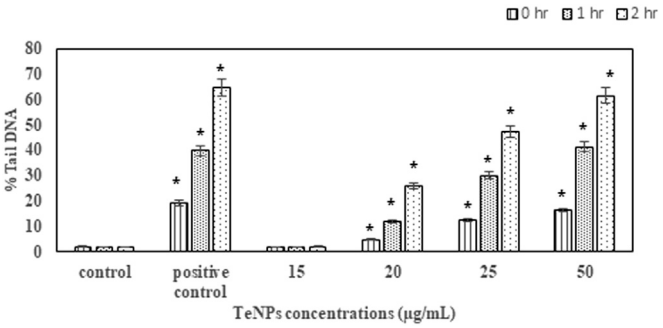

Fig. 8. Percent DNA damage in human lymphocytes exposed to different concentrations of TeNPs. Data are represented as mean ± SD (*$p < 0.0001$).

4. Conclusion

Tellurite-reducing *Shewanella baltica* strain GUSDZ9 isolated from Zuari estuary tolerated 5.5 mM K_2TeO_3 with a MIC of 6 mM in ZMB. Complete reduction of 2 mM K_2TeO_3 within 38 h of bacterial growth was observed using the diethyl-dithiocarbamate method. Interestingly, this strain successfully synthesized Te nanoparticles which was initiated at early log phase (4 h) and was found to be maximum during mid-log phase (28 h) to early stationary phase. A prominent peak of tellurium due to surface plasmon resonance at 210 nm assured the presence of TeNPs. XRD and TEM analysis confirmed the hexagonal tellurium nanocrystals exhibiting nanorod morphology with 8–75 nm average diameter. EDAX analysis further confirmed the elemental tellurium. These biogenic TeNPs also demonstrated 90% reductive degradation of methylene blue dye. TeNPs also exhibited anti-biofilm activity against potential human pathogens at even 5 μg/mL concentration. However, insignificant genotoxicity against human lymphocytes was also observed at 15 μg/mL. Thus, *Shewanella baltica* strain GUSDZ9 can be exploited simultaneously for bioremediation of toxic tellurite to elemental tellurium and TeNPs biosynthesis. We also report for the first time TeNPs biosynthesis by *Shewanella baltica* exhibiting photo-catalytic degradation of methylene blue dye, anti-biofilm activity against human pathogens and genotoxicity towards human lymphocytes.

Acknowledgment

Ms. Diviya Vaigankar is grateful to University Grants Commission, New Delhi for financial support as JRF (Ref. no. F./201718-NFO-2017-18-OBC-GOA-52491, F/2017-18(SA-III)). The authors gratefully acknowledge Mr. Areef Sardar and Mr. Girish Prabhu from CSIR-National Institute of Oceanography, Goa for EDAX and XRD analysis respectively. The authors are also obliged to Prof. Savio Rodriguez, Head,

Department of Microbiology at Goa Medical College, Goa for providing clinical pathogens. Ms. Diviya is also thankful to Prof. Sandeep Garg, Head, Department of Microbiology at Goa University, Goa for extending laboratory facilities. The authors also thank Dr. Milind Naik, Asst. Professor, Department of Microbiology at Goa University for his valuable suggestions.

Conflict of interest

The authors hereby declare no conflict of interest.

Appendix A. Supporting information

Supplementary data associated with this article can be found in the online version at doi:10.1016/j.ecoenv.2018.08.111.

References

Altschul, S.F., Gish, W., Miller, W., Myers, E.W., Lipman, D.J., 1990. Basic local alignment search tool. J. Mol. Biol. 215 (3), 403–410.

Amoozegar, M.A., Ashengroph, M., Malekzadeh, F., Razavi, M.R., Naddaf, S., Kabiri, M., 2008. Isolation and initial characterization of the tellurite reducing moderately halophilic bacterium, *Salinicoccus* sp. strain QW6. Microbiol. Res. 163 (4), 456–465. https://doi.org/10.1016/j.micres.2006.07.010.

Arenas, F.A., Pugin, B., Henríquez, N.A., Arenas-Salinas, M.A., Díaz-Vásquez, W.A., Pozo, M.F., Muñoz, C.M., Chasteen, T.G., Pérez-Donoso, J.M., Vásquez, C.C., 2014. Isolation, identification and characterization of highly tellurite-resistant, tellurite-reducing bacteria from Antarctica. Polar Sci. 8 (1), 40–52. https://doi.org/10.1016/j.polar.2014.01.001.

Baesman, S.M., Bullen, T.D., Dewald, J., Zhang, D., Curran, S., Islam, F.S., Beveridge, T.J., Oremland, R.S., 2007. Formation of tellurium nanocrystals during anaerobic growth of bacteria that use Te oxyanions as respiratory electron acceptors. Appl. Environ. Microbiol. 73 (7), 2135–2143. https://doi.org/10.1128/AEM.02558-06.

Bausinger, J., Speit, G., 2016. The impact of lymphocyte isolation on induced DNA damage in human blood samples measured by the comet assay. Mutagenesis 31 (5), 567–572.

Basnayake, R.S.T., Bius, J.H., Akpolat, O.M., Chasteen, T.G., 2001. Production of dimethyl telluride and elemental tellurium by bacteria amended with tellurite or tellurate. Appl. Organomet. Chem. 15 (6), 499–510. https://doi.org/10.1002/aoc.186.

Baygar, T., Ugur, A., 2017. In vitro evaluation of antimicrobial and antibiofilm potentials of silver nanoparticles biosynthesised by *Streptomyces griseorubens*. IET Nanobiotechnol. 677–681. https://doi.org/10.1049/iet-nbt.2016.0199.

Borghese, R., Baccolini, C., Francia, F., Sabatino, P., Turner, R.J., Zannoni, D., 2014. Reduction of chalcogen oxyanions and generation of nanoprecipitates by the photosynthetic bacterium *Rhodobacter capsulatus*. J. Hazard. Mater. 269, 24–30. https://doi.org/10.1016/j.jhazmat.2013.12.028.

Chasteen, T.G., Fuentes, D.E., Tantaleán, J.C., Vásquez, C.C., 2009. Tellurite: history, oxidative stress, and molecular mechanisms of resistance. FEMS Microbiol. Rev. 33 (4), 820–832. https://doi.org/10.1111/j.1574-6976.2009.00177.x.

Csotonyi, J.T., Stackebrandt, E., Yurkov, V., 2006. Anaerobic respiration on tellurate and other metalloids in bacteria from hydrothermal vent fields in the Eastern Pacific Ocean. Appl. Environ. Microbiol. 72 (7), 4950–4956. https://doi.org/10.1128/AEM.00223-06.

D'Costa, A., Shyama, S.K., Kumar, M.P., 2017. Bioaccumulation of trace metals and total petroleum and genotoxicity responses in an edible fish population as indicators of marine pollution. Ecotoxicol. Environ. Saf. 142, 22–28. https://doi.org/10.1016/j.ecoenv.2017.03.049.

Di Tomaso, G., Fedi, S., Carnevali, M., Manegatti, M., Taddei, C., Zannoni, D., 2002. The membrane-bound respiratory chain of *Pseudomonas pseudoalcaligenes* KF707 cells grown in the presence or absence of potassium tellurite. Microbiology 148 (6), 1699–1708.

De Lima, R., Oliveira, J.L., Murakami, P.S.K., Molina, M.A.M., Itri, R., Haddad, P., Seabra, A.B., 2013. Iron oxide nanoparticles show no toxicity in the comet assay in lymphocytes: a promising vehicle as a nitric oxide releasing nanocarrier in biomedical applications. J. Phys. Conf. Ser. 429. https://doi.org/10.1088/1742-6596/429/1/012021.

Foldbjerg, R., Dang, D.A., Autrup, H., 2011. Cytotoxicity and genotoxicity of silver nanoparticles in the human lung cancer cell line, A549. Arch. Toxicol. 85 (7), 743–750. https://doi.org/10.1007/s00204-010-0545-5.

Forootanfar, H., Amirpour-Rostami, S., Jafari, M., Forootanfar, A., Yousefizadeh, Z., Shakibaie, M., 2015. Microbial-assisted synthesis and evaluation the cytotoxic effect of tellurium nanorods. Mater. Sci. Eng. C 49, 183–189. https://doi.org/10.1016/j.msec.2014.12.078.

Fredrickson, J.K., Romine, M.F., Beliaev, A.S., Jennifer, M., Osterman, L., Pinchuk, G., Reed, J.L., Rodionov, D.A., Jorge, L.M., 2008. Towards environmental systems biology of *Shewanella*. Nat. Rev. Microbiol. 6 (8), 592. https://doi.org/10.1038/nrmicro1947.

Fuentes, D.E., Fuentes, E.L., Castro, M.E., Pérez, J.M., Araya, M.A., Chasteen, T.G., Pichuantes, S.E., Vâsquez, C.C., 2007. Cysteine metabolism-related genes and bacterial resistance to potassium tellurite. J. Bacteriol. 189 (24), 8953–8960. https://doi.org/10.1128/JB.01252-07.

Gautam, U.K., Rao, C.N.R., 2004. Controlled synthesis of crystalline tellurium nanorods, nanowires, nanobelts and related structures by a self-seeding solution process. J. Mater. Chem. 14 (16), 2530–2535.

Ghosh, M., Manivannan, J., Sinha, S., Chakraborty, A., Mallick, S.K., Bandyopadhyay, M., Mukherjee, A., 2012. In vitro and in vivo genotoxicity of silver nanoparticles. Mutat. Res. Gen. Toxicol. Environ. 749 (1), 60–69.

Gupta, A., Joia, J., Sood, A., Sood, R., Sidhu, C., Kaur, G., 2016. Microbes as potential tool for remediation of heavy metals: a review. J. Microb. Biochem. Technol. 8 (4), 364–372. https://doi.org/10.4172/1948-5948.1000310.

Kaushik, N., Thakkar, M.S., Snehit, S., Mhatre, M.S., Rasesh, Y., Parikh, M.S., 2010. Biological synthesis of metallic nanoparticles. Nanomedicine 6, 257–262.

Khalilian, M., Zolfaghari, M.R., Soleimani, M., 2015. High potential application in bioremediation of selenate by *Proteus hauseri* strain QW4. Iran. J. Microbiol. 7 (2), 94–102.

Khanolkar, D.S., Dubey, S.K., Naik, M.M., 2015. Biotransformation of tributyltin chloride to less toxic dibutyltin dichloride and monobutyltin trichloride by *Klebsiella pneumoniae* strain SD9. Int. Biodeterior. Biodegrad. 104, 212–218. https://doi.org/10.1016/j.ibiod.2015.04.030.

Kim, D.H., Kanaly, R.A., Hur, H.G., 2012. Biological accumulation of tellurium nanorod structures via reduction of tellurite by *Shewanella oneidensis* MR-1. Bioresour. Technol. 125, 127–131. https://doi.org/10.1016/j.biortech.2012.08.129.

Kim, D.H., Kim, M.G., Jiang, S., Lee, J.H., Hur, H.G., 2013. Promoted reduction of tellurite and formation of extracellular tellurium nanorods by concerted reaction between iron and *Shewanella oneidensis* MR-1. Environ. Sci. Technol. 47 (15), 8709–8715.

Kim, D.H., Park, S., Kim, M.G., Hur, H.G., 2014. Accumulation of amorphous Cr (III)-Te (IV) nanoparticles on the Surface of *Shewanella oneidensis* MR-1 through reduction of Cr (VI). Environ. Sci. Technol. 48 (24), 14599–14606.

Klonowska, A., Heulin, T., Vermeglio, A., 2005. Selenite and tellurite reduction by *Shewanella oneidensis*. Appl. Environ. Microbiol. 71 (9), 5607–5609. https://doi.org/10.1128/AEM.71.9.5607-5609.2005.

Kurimella, V.R., Kumar, K.R., Sanasi, P.D., 2013. A novel synthesis of tellurium nanoparticles using iron (II) as a reductant. Int. J. Nanosci. Nanotechnol. 4, 209–221.

Lebedová, J., Hedberg, Y.S., Odnevall Wallinder, I., Karlsson, H.L., 2017. Size-dependent genotoxicity of silver, gold and platinum nanoparticles studied using the mini-gel comet assay and micronucleus scoring with flow cytometry. Mutagenesis 33 (1), 77–85. https://doi.org/10.1093/mutage/gex027.

Li, X., Xu, H., Chen, Z.S., Chen, G., 2011. Biosynthesis of nanoparticles by microorganisms and their applications. J. Nanomater. https://doi.org/10.1155/2011/270974.

Li, Z., Sun, Q., Zhu, Y., Tan, B., Xu, Z.P., Dou, S.X., 2014. Ultra-small fluorescent inorganic nanoparticles for bioimaging. J. Mater. Chem. B 2 (19), 2793–2818. https://doi.org/10.1039/C3TB21760D.

Lin, Z.H., Lee, C.H., Chang, H.Y., Chang, H.T., 2012. Antibacterial activities of tellurium nanomaterials. Chem. Asian J. 7 (5), 930–934. https://doi.org/10.1002/asia.201101006.

Liu, Z., Hu, Z., Xie, Q., Yang, B., Qian, Y., 2003. Surfactant-assisted growth of uniform nanorods of crystalline tellurium. J. Mater. Chem. 13 (1), 159–162. https://doi.org/10.1039/b208420a.

Manikandana, M., Dhanuskodia, S., Mathewb, S., Nampoorib, V.P.N., 2015. Nonlinear Optical Property of Tellurium Nanoparticles (Conference paper).

Mohanty, A., Kathawala, M.H., Zhang, J., Chen, W.N., Loo, J.S.C., Kjelleberg, S., Yang, L., Cao, B., 2014. Biogenic tellurium nanorods as a novel antivirulence agent inhibiting pyoverdine production in *Pseudomonas aeruginosa*. Biotechnol. Bioeng. 111 (5), 858–865. https://doi.org/10.1002/bit.25147.

Naumov, A.V., 2010. Selenium and tellurium: state of the markets, the crisis, and its consequences. Metallurgist 54 (3), 197–200. https://doi.org/10.1007/s11015-010-9280-7.

Ollivier, P.R.L., Bahrou, A.S., Marcus, S., Cox, T., Church, T.M., Hanson, T.E., 2008. Volatilization and precipitation of tellurium by aerobic, tellurite-resistant marine microbes. Appl. Environ. Microbiol. 74 (23), 7163–7173. https://doi.org/10.1128/AEM.00733-08.

Pereira, F., 2017. Manganese-Tolerant Bacteria from the Estuarine Environment and their Importance in Bioremediation of Contaminated Estuarine Sites: In Marine Pollution and Microbial Remediation. Springer, Singapore, pp. 153–175. https://doi.org/10.1007/978-981-10-1044-6.

Piella, J., Bastús, N.G., Casals, E., Puntes, V., 2013. Characterizing nanoparticles reactivity: structure-photocatalytic activity relationship. J. Phys. Conf. Ser 429. IOP Publishing, pp. 012040. https://doi.org/10.1088/1742-6596/429/1/012040.

Presentato, A., Piacenza, E., Anikovskiy, M., Cappelletti, M., Zannoni, D., Turner, R.J., 2016. *Rhodococcus aetherivorans* BCP1 as cell factory for the production of intracellular tellurium nanorods under aerobic conditions. Microb. Cell Fact. 15 (1), 204. https://doi.org/10.1186/s12934-016-0602-8.

Pugin, B., Cornejo, F.A., Muñoz-Díaz, P., Muñoz-Villagrán, C.M., Vargas-Pérez, J.I., Arenas, F.A., Vásquez, C.C., 2014. Glutathione reductase-mediated synthesis of tellurium-containing nanostructures exhibiting antibacterial properties. Appl. Environ. Microbiol. 80, 7061–7070. https://doi.org/10.1128/AEM.02207-14.

Rathgeber, C., Yurkova, N., Stackebrandt, E., Beatty, J.T., Yurkov, V., 2002. Isolation of tellurite- and selenite-resistant bacteria from hydrothermal vents of the Juan de Fuca Ridge in the Pacific Ocean. Appl. Environ. Microbiol. 68 (9), 4613–4622. https://doi.org/10.1128/AEM.68.9.4613.

Satyanarayana, T., Johri, B.N., Prakash, A. (Eds.), 2012. Microorganisms in Environmental Management: Microbes and Environment. Springer Science & Business Media, Dordrecht.

Samant, S., Naik, M., Parulekar, K., Charya, L., Vaigankar, D., 2018. Selenium reducing

Citrobacter fruendii strain KP6 from Mandovi estuary and its potential application in selenium nanoparticle synthesis. Proc. Natl. Sci. India Sect. B Biol. Sci. 88 (2), 747–754.

Shanmugam, N., Suthakaran, S., Kannadasan, N., Sathishkumar, K., 2015. Synthesis and characterization of Te doped ZnO nanosheets for photocatalytic application. JO Heterocycl. 105, 15–20.

Srivastava, P., Nikhil, E.V.R., Bragança, J.M., Kowshik, M., 2015. Anti-bacterial TeNPs biosynthesized by haloarcheaon *Halococcus salifodinae* BK3. Extremophiles 19 (4), 875–884. https://doi.org/10.1007/s00792-015-0767-9.

Stoeva, S., Klabunde, K.J., Sorensen, C.M., 2002. Gram-scale synthesis of monodisperse gold colloids by the solvated metal atom dispersion method and digestive ripening and their organization into two- and three-dimensional structures. J. Am. Chem. Soc. 124 (10), 2305–2311.

Sunitha, M.S.L., Prashanth, S., Kishor, P.B.K., 2015. Characterization of arsenic-resistant bacteria and their ars genotype for metal bioremediation. IJSER 6 (2), 304–309.

Soda, S., Ma, W., Kuroda, M., Nishikawa, H., Zhang, Y., Ike, M., 2018. Characterization of moderately halotolerant selenate-and tellurite-reducing bacteria isolated from brackish areas in Osaka. Biosci. Biotech. Biochem. 82 (1), 173–181.

Taylor, D.E., 1999. Bacterial tellurite resistance. Trends Microbiol. 7 (3), 111–115.

Tamura, K., Stecher, G., Peterson, D., Filipski, A., Kumar, S., 2013. MEGA6: molecular evolutionary genetics analysis version 6.0. Mol. Biol. Evol. 30 (12), 2725–2729. https://doi.org/10.1093/molbev/mst197.

Tchounwou, P.B., Yedjou, C.G., Patlolla, A.K., Sutton, D.J., 2012. Heavy Metal Toxicity and the Environment: Molecular, Clinical and Environmental Toxicology. Basel, Springer, pp. 133–164.

Trutko, S.M., Akimenko, V.K., Suzina, N.E., Anisimova, L.A., Shlyapnikov, M.G., Baskunov, B.P., Duda, V.I., Boronin, A.M., 2000. Involvement of the respiratory chain of Gram-negative bacteria in the reduction of tellurite. Arch. Microbiol. 173 (3), 178–186. https://doi.org/10.1007/s002039900123.

Turner, R.J., Weiner, J.H., Taylor, D.E., 1992. Use of diethyldithiocarbamate for quantitative determination of tellurite uptake by bacteria. Anal. Biochem. 204 (2), 292–295. https://doi.org/10.1016/0003-2697(92)90240-8.

Valdivia-González, M.A., Díaz-Vásquez, W.A., Ruiz-León, D., Becerra, A.A., Aguayo, D.R., Pérez-Donoso, J.M., Vásquez, C.C., 2018. A comparative analysis of tellurite detoxification by members of the genus Shewanella. Arch. Microbiol. 200 (2), 267–273. https://doi.org/10.1007/s00203-017-1438-2.

Xi, G., Peng, Y., Yu, W., Qian, Y., 2005. Synthesis, characterization, and growth mechanism of tellurium nanotubes. Cryst. Growth Des. 5 (1), 325–328.

Yuan, Q.L., Yin, H.Y., Nie, Q.L., 2013. Nanostructured tellurium semiconductor: from nanoparticles to nanorods. J. Exp. Nanosci. 8 (7–8), 931–936. https://doi.org/10.1080/17458080.2011.620021.

Zare, B., Faramarzi, M.A., Sepehrizadeh, Z., Shakibaie, M., Rezaie, S., Shahverdi, A.R., 2012. Biosynthesis and recovery of rod-shaped tellurium nanoparticles and their bactericidal activities. Mater. Res. Bull. 47 (11), 3719–3725. https://doi.org/10.1016/j.materresbull.2012.06.034.

Zonaro, E., Lampis, S., Turner, R.J., Junaid, S., Vallini, G., 2015. Biogenic selenium and tellurium nanoparticles synthesized by environmental microbial isolates efficaciously inhibit bacterial planktonic cultures and biofilms. Front. Microbiol. 6, 584. https://doi.org/10.3389/fmicb.2015.00584.

Proc. Natl. Acad. Sci., India, Sect. B Biol. Sci. (Apr–June 2018) 88(2):747–754
https://doi.org/10.1007/s40011-016-0815-y

RESEARCH ARTICLE

Selenium reducing *Citrobacter fruendii* strain KP6 from Mandovi estuary and its potential application in selenium nanoparticle synthesis

Sanika Samant[1] · Milind Naik[1] · Karishma Parulekar[1] · Lakshangy Charya[1] · Divya Vaigankar[1]

Received: 10 May 2016 / Revised: 2 July 2016 / Accepted: 29 September 2016 / Published online: 7 October 2016

Abstract The present study foregrounds the isolation of selenium tolerant bacteria from Mandovi estuary of Goa, India, known to be contaminated with mining and industrial waste. The isolate was tentatively identified as *Citrobacter fruendii* strain KP6, which can tolerate up to 60 mM of Na_2SeO_3 in mineral salt medium (MSM). Bacterial strain KP6 when grown in 60 mM Na_2SeO_3 in MSM precipitated soluble toxic selenite (Se^{4+}) into colloidal elemental selenium (Se^0, red colored) using glucose as a sole source of carbon. Interestingly, scanning electron micrograph (SEM), transmission electron micrograph (TEM) and X-Ray diffraction (XRD) analysis also confirmed this bioconversion reaction in the formation of nano –sized material extracellularly with the size ranging from 45 to 70 nm. This bioconversion ability of strain KP6 can be exploited for eco-friendly bioremediation of selenite contaminated estuarine sites as well as for synthesis of Se^0 nanoparticles having its significance in nanobiotechnology.

Keywords Estuarine waters · *Citrobacter fruendii* strain KP6 · Biogenic selenium nanoparticles · Bioremediation

Introduction

In recent years industrialization and mining activities are accounted to release heavy metals and metalloids in terrestrial and marine environment exhibiting their toxic effects on micro and macro biota [1]. Metals and metalloids are persistent in nature and can cause toxicity for years to come. This further opens a gateway for extensive research opportunities in remediation of metal polluted regions along with significant metal conversion reactions carried out by diverse group of microorganisms [2].

Selenium is a metalloid, widely distributed in mining ores and aquatic zones on the earth, existing as reduced form (selenide, Se^{-2}), as an element form (Selenite, Se^0), and as water soluble form (Selenite, SeO_3^{-2}/Selenate SeO_4^{-2}). It is an important structural component of many enzymes such as thioredoxin reductase and glutathione peroxidase [3]. However, at higher concentration in drinking water it can negatively affect human health due to its bio-magnification [4, 5]. Conversely, dietary deficiency of selenium causes Keshan disease [6] but higher concentration of >400 μg ml^{-1} selenium/selenite in body causes selenosis [7]. Selenosis causes diffuse necrosis and hemorrhage resulting from capillary damage and chronic poisoning by degenerative and fibrotic changes in liver and skin [8]. WHO has recommended safe level of selenite in drinking water as 40 μg l^{-1} [9].

Industrial discharge from tanneries, glass production industry, plastic industry, paint and pigment industry, oil refineries and power sources are the main sources of water soluble selenium contamination in aquatic life forms [10] along with mining industry which releases selenium as a major contaminant in aqueous waste streams [11]. Direct discharge of selenium polluted effluent in marine environment may result in biomagnification of selenium in fishes and thus, ultimately reaching to humans [12]. Therefore, there is a pressing need to bioremediate selenium from marine sites polluted with selenite. Alternatively, cost effective and eco-friendly technologies should be employed since existing chemical methods themselves

✉ Sanika Samant
sanika2k4@gmail.com

[1] Department of Microbiology, Goa University, Taleigao-Plateau, Taleigao, Goa 403206, India

contribute to pollution. Besides being toxic to macro and micro biota some natural microbial strains can survive at very high concentration of selenite without having any impact on their growth and metabolism [13, 14].

Selenium reducing bacteria are ubiquitous occurring in diverse terrestrial and aquatic environments [15]. Moreover, microorganisms that have been well characterized for their ability to reduce selenate and selenite oxyions into non-toxic elemental form Se^0 under anaerobic conditions include *Thauera selenatis* [16], *Aeromonas salmonicida* [17], and *Shewanella oneidensis* MR-1 [18] and under aerobic conditions they show diverse species of *Rhizobium* sp. B1 [19], *Pseudomonas* sp. CA5 [20], *Duganella* sp. and *Agrobacterium* sp. [21] to list a few, respectively. Although these studies explored the terrestrial soils and aquatic waters, there are few reports on selenium reduction by a marine estuarine habitant microbe [22].

It is well known fact that Mandovi estuary is heavily contaminated with mining waste containing metals such as iron, manganese, cobalt, copper, zinc, lead and chromium [23] along with metalloid arsenic [24]. Moreover, it is also ascertained that the bacteria isolated from Mandovi estuary demonstrate cross resistance to multiple heavy metals such as lead, mercury, cadmium and organo-metal tributyltin [25]. In the view of this, the authors attempted to investigate the selenium reducing ability of an estuarine eubacteria isolated from Mandovi estuary contaminated with mining and industrial rejects.

Material and methods

Enrichment and isolation of selenite reducing bacteria from Mandovi estuary

Surface estuarine water sample was collected in sterile polycarbonate bottles from Mandovi estuary, Goa, India (Latitude: 15°09′ and 15°33′N, Longitude 73°45′ and 74°14′E, temperature 30 °C) and 1 ml of this water sample was added in 50 ml nutrient broth amended with 1 mM of sodium selenite (Na_2SeO_3) and kept at 30 °C on rotary shaker (150 rpm) for 48 h for enrichment. Nutrient broth (50 ml) with 1 ml of estuarine water sample without Na_2SeO_3 served as a control. This was followed by isolation of selenite reducing bacteria by dilution of enriched sample on MSM plates [26] incorporated with 2 mM Na_2SeO_3 and glucose as sole source of carbon. Red colored colonies that appeared on MSM plates were transferred on MSM plates with varying concentrations of Na_2SeO_3. Bacterial colony which appeared on MSM plate with highest concentration of Na_2SeO_3 was selected for further characterization study and designated as strain KP6. Bacterial strain KP6 was routinely subcultured on MSM plates with 1 mM of Na_2SeO_3 at 30 °C.

Determination of maximum tolerance concentration (MTC) and minimum inhibitory concentration

Maximum tolerance concentration of selenium reducing bacterial isolate was performed in MSM broth with varying concentrations of Na_2SeO_3 such as 10, 20, 30, 40, 50, 60,70 and 80 mM respectively, at 30 °C and pH 7.5 with constant shaking at 150 rpm. Stock solution of 1 M of sodium selenite was prepared by dissolving 172.95 g of Na_2SeO_3 in 1 l of sterile distilled water followed by filter sterilization. Hence, 100 ml of MSM broth in 250 ml of Erlenmayer flask with 0.2 % glucose as sole source of carbon with respective concentrations of Na_2SeO_3 was inoculated with 5 % v/v overnight grown culture and incubated for 24 h at 30 °C with constant shaking at 150 rpm. The growth was measured every 2 h for 24 h (stationary phase) by taking absorbance at 600 nm using UV–visible spectrophotometer (Shimadzu 2470). Un-inoculated MSM media with appropriate concentration of selenite served as a control. MTC was calculated as maximum concentration of Na_2SeO_3 at which growth was seen while MIC was calculated as minimum concentration of Na_2SeO_3 that inhibited the growth of KP6 completely.

Selenite reduction studies

MTC was selected to study selenite reduction by the estuarine bacterial isolate strain KP6. Here, the culture was grown in 1 l MSM medium with 0.2 % glucose as sole source of carbon amended with 60 mM of Na_2SeO_3 with constant shaking (150 rpm) at 30 °C for 24 h. After 24 h, the red colored reduced selenium formed aggregate that either got settled at the bottom or was collected by centrifuging at 2000 rpm for 5 min. The red precipitate layer was scooped off using clean and dry spatula and was collected on a clean watch glass. The red colored pellet was washed thrice with sterile distilled water to remove any media components and then centrifuged at 1000 rpm. This process was repeated five times to remove media components and cell impurities. The red pellet was then dried at 80 °C in an oven for 2 h till constant weight and then used for characterization study. The dry weight of red pellet was also used to calculate conversion efficiency of selenite to selenium.

Morphological characterization

Scanning electron microscopy (Zeiss EVO18) was used to examine morphological alterations in strain KP6 when exposed to 60 mM Na_2SeO_3 during exponential growth.

Strain KP6 was grown with 60 mM Na_2SeO_3 in MSM media with 0.2 % glucose as sole source of carbon while culture grown without selenium in MSM media served as control. The cell pellet was harvested at exponential growth phase followed by centrifugation at 10,000 rpm for 15 min at 4 °C. Thin smear was made on a glass coverslip and fixed with 3 % gluteraldehyde for 24 h at 4 °C followed by dehydrating the fixed bacterial cells with series of alcohol gradients (10, 30, 50, 70, 90 and 100 %, respectively.) and finally sputter coated with gold and examined using SEM.

Identification of selenite reducing bacteria

Identification of Na_2SeO_3 tolerant bacterial strain KP6 was done based on morphological characterization and biochemical test following Bergey's Manual of systematic bacteriology [27].

Characterization of red precipitate

TEM

TEM micrographs of mineral was obtained by drop coating of homogenous solution obtained by sonicating the red pellet in 200 µl of milliQ water for 5–10 min onto 2 mm carbon coated copper grids of 200–300 mesh followed by air drying. The grid was then placed in the sample chamber of the TEM (Philips CM200 Supertwin STEM) operated with the voltage of 200 keV and imaged.

SEM

SEM was performed of a thin smear of homogenous solution obtained by sonicating the red pellet in 200 µl of milliQ water for 5–10 min on glass coverslip. The air dried smear was then sputter coated with gold to a thickness of 10 nm approximately and examined under SEM (Zeiss EVO18) operating at 30 kV.

XRD

The dried red pellet was finely powdered and was analyzed by Rigaku Miniflex powder diffract meter equipped with a Ultima IV solid- state detector at a voltage of 40 kV and current of 20 mA using CuKα radiation ($\lambda = 1.5406$ A) in the range of $5° \leq 2\theta \leq 80°$ at 40 kV. The particle size (D) of the sample was calculated using the Scherrer's relationship ($D = 0.9\,\lambda/\beta\,\cos\theta$) which has been used, where λ is the wavelength of X-ray, β is the broadening of the diffraction line measured half of its maximum intensity in radians and θ is the Bragg's diffraction angle.

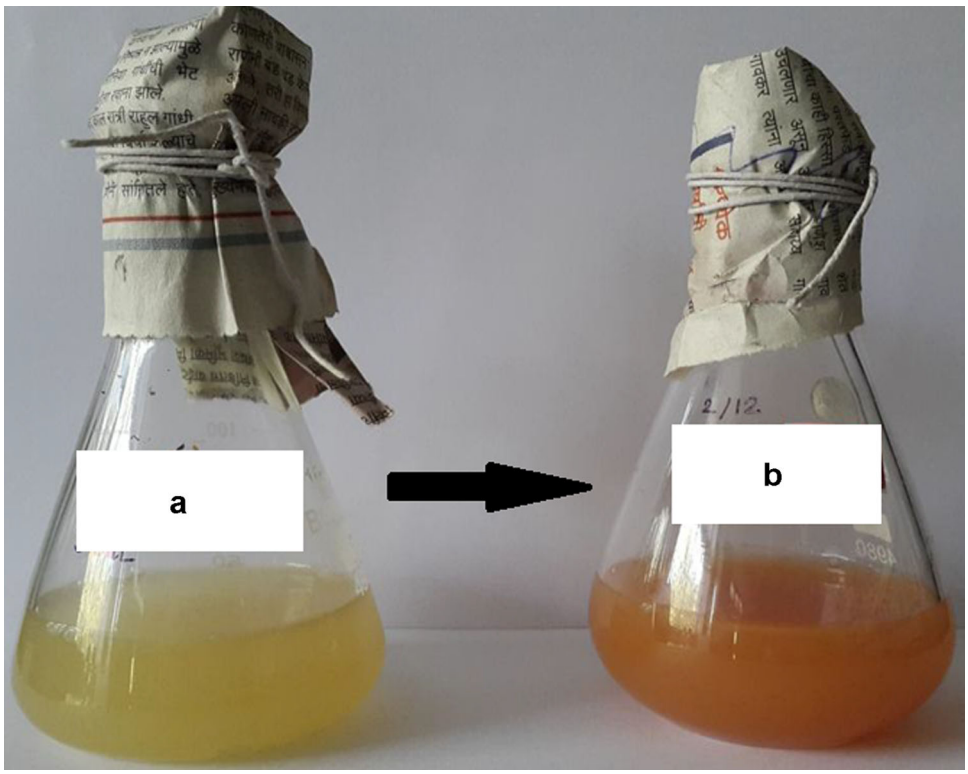

Fig. 1 Reduction of selenite (Se^{4+}, flask **a**) to elemental selenium ($Se^{0,}$ flask **b**) in nutrient broth amended with 1 mM Na_2SeO_3

Results and Discussion

Selenium is bio-essential element in trace amount but at higher concentrations of selenium it is toxic to the natural biota including humans [28]. Se exist in marine water in water soluble form (Selenite SeO_3^{2-}/selenate SeO_4^{2-}), and as an element form (Se^0). Although it exists in natural environment in trace quantity (0.09–2 ppm) anthropogenic activities such as mining and release of industrial effluents in water bodies have led to the increase in selenium concentration (0.15–19 ppm) causing chronic effect on flora and fauna of marine environment [29, 30]. Therefore, scientists around the world are looking for alternate eco-friendly and cost-effective method over chemical method which generates toxic chemical waste.

Appearance of reddish color in enrichment broth after 24 h indicated that selenite reducing bacteria has been enriched which converted soluble selenite (Na_2SeO_3) into red colored elemental selenium (Se^0) when compared to control flask which failed to show a change in color when incubated under same conditions (Fig. 1). After dilution plating of enriched broth on MSM agar plates amended with 1 mM of Na_2SeO_3, 20 morphologically distinct red colored selenite reducing bacterial colonies appeared (data not shown). These 20 bacterial isolates were then transferred to MSM agar plates with varying concentration of selenite (10, 20, 30, 40, 50, 60, 70 and 80 mM). Only one bacterial isolate that could grow on 60 mM Na_2SeO_3 was selected for further study and designated as bacterial strain KP6.

Moreover, the selenite reducing bacterial strain KP6 that could grow on MSM plate amended with 60 mM Na_2SeO_3 was found to be gram negative, short, rod shaped, motile and fermentative (Table 1). It showed the presence of enzyme such as catalase, urease, and nitrate reductase. Indole and VP tests were found to be negative, but bacterial isolate showed methyl red test positive and was able to utilize citrate. Based on the morphology and biochemical analyses followed by Bergey's Manual of Systematic Bacteriology, Volume I bacterial strain KP6 was tentatively identified as *Citrobacter fruendii*. The MTC of *Citrobacter fruendii* strain KP6 was found to be 60 mM in MSM broth and MIC was recorded as 61 mM (Fig. 2). Consequently, *Citrobacter fruendii* strain KP6 isolated from contaminated water sample from Mandovi estuary was able to tolerate 60 mM of selenite by reducing selenite (soluble) to insoluble elemental selenium as revealed by a change in color of MSM broth from white to red. Similar studies of bioconversion of selenite to selenium have been reported by Hunter and Manter [20] in *Pseudomonas* sp., *Bacillus cereus* [31] and *Bacillus* sp. MSh-1 [32]. Moreover, Dhanjal and Cameotra [31] also reported that aerobic bacterial reduction of selenite and selenate to elemental

Table 1 Biochemical tests for identification of bacterial strain KP6

Biochemical tests	Observed results
Morphology	Rod
Arrangement	Single
Pigments	−
Motility	+
Catalase	+
Oxidase	−
Indole	[−]
MR	+
VP	−
Citrate	+
Urease	D
PPA	−
Ornithine	D
Gelatinase	−
H_2S	+
Nitrate red	+
Starch	−
Glucose	+
Lactose	+
Sucrose	D
Gas	+
Mannitol	+
O/F	FA

FA, Facultative anaerobe; OA, obligate aerobe; +, 90 % or greater positive; −, 90 % or greater negative; D, 26−75 % strains positive; [+], 76–89 % positive; [−], 76−89 % negative

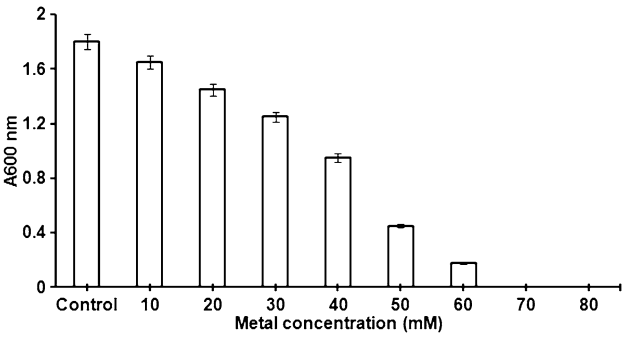

Fig. 2 Growth of bacterial strain KP6 at different concentrations of Na_2SeO_3 in MSM media

selenium is suggestive of a detoxification mechanism. Various detoxification mechanisms consisting of enzymatic systems have been proposed to catalyze the reduction of selenite in bacteria. According to Losi and Frankenberger [33], the selenite reduction in *Enterobacter cloacae* occurs close to the membrane as the result of membrane associated reductases followed by rapid expulsion of Se^0 particles expelled by the membrane efflux pump. Similar

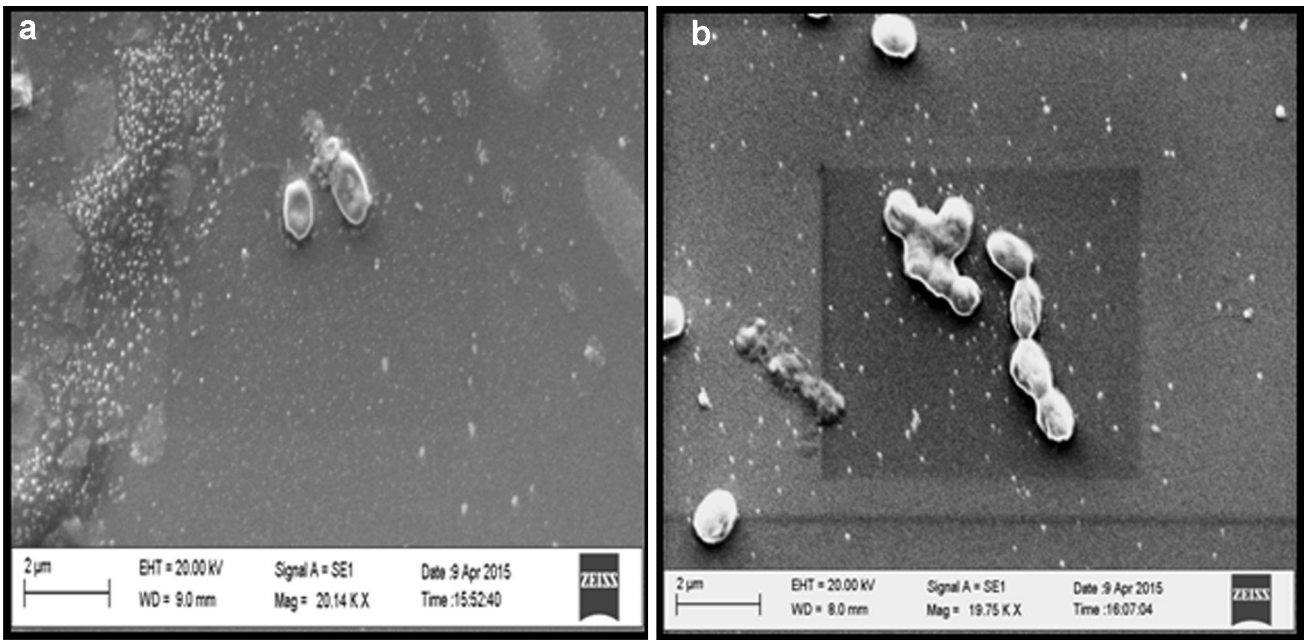

Fig. 3 Scanning electron micrograph of cells of bacterial strain KP6, **a** control cell grown without selenite, **b** cells grown in 60 mM selenite, in MSM broth with glucose as a sole carbon source

detoxification mechanism is also demonstrated in *Bacillus selenatarsenatis*, a facultative anaerobe that grows aerobically by oxidative respiration using arsenate, selenate or nitrate as electron acceptor [34]. It comprises of membrane bound selenate reductase complex (srdBCA) that couples quinone oxidation with selenate reduction. Thus, reducing the toxicity of selenium oxyions along with peroxiredoxin having its role in degrading the reactive oxygen species. Likewise, *Bacillus selenitireducens* is also reported to produce an enzyme capable of reversing the oxidation of selenate and arsenate ions to their less toxic "reduced" forms [35]. The key ingredient in these enzymes is the transition element molybdenum that grants the ability to reduce certain unusual elements. Moreover, as arsenate contamination and arsenate reducing bacteria are reported in Mandovi estuary [24], bacteria isolated from these estuarine waters will possibly have selenate reducing property. Also, there are electronic industries along the coastal belt of Mandovi estuary which may possibly be a responsible source of selenite contamination in Mandovi.

Further, the well separated and dried selenium nanoparticles weighed 3.6953 mg l^{-1}, therefore the bioconversion efficiency of selenium was found to be 77 %. Additionally, the SEM analysis revealed that *Citrobacter fruendii* strain KP6 is single short rod arrangement (Fig. 3a) but when exposed to 60 mM selenite cells it was found to form aggregate and produce exopolysaccharide like substance surrounding the bacterial cell (Fig. 3b) and hence was characterized as *Citrobacter* sp. The formation of cell aggregate and exopolysaccharide (EPS) production reveals the protection strategy of *Citrobacter fruendii* strain KP6 from toxic levels of selenite. This result corroborates to that reported by Naik et al. [36] which stated that *Enterobacter cloacae* in the presence of toxic levels of lead produced EPS and showed aggregation to withstand the metal stress.

Furthermore, the surface topology and morphological features of red precipitate obtained after bacterial reduction of soluble selenite to selenium was studied using SEM and particle size was analysed using TEM. The average particle size confirmed using TEM (Fig. 4a) was found to range from 45 to 70 nm while the SEM images revealed spherical shaped nanomaterials (Fig. 4b). Moreover, the powder XRD pattern (Fig. 5) of the red precipitate substantiated the formation of Se nanoparticles showing peaks with d values 3.30, 2.82, 1.99, 1.70 and 1.63 which are characteristic for nano selenium (JCPDS 27-601 and 27-1202) indicating that the Se particles were crystalline in nature [37, 38]. The nanocrystallites mean size analysis performed using Scherer's formula indicated the average size of mineral formed to be 40 nm. XRD thus confirmed the bioconversion of selenite by *Citrobacter fruendii* strain KP6 to red coloured elemental selenium. This is the first report of estuarine *Citrobacter* species isolated from Mandovi estuary of Goa, India, bioconverting selenite as elemental Se^0 nanomaterial. As compared to previous studies on aerobic bacterial reduction of selenite and selenate to elemental selenium [20, 31, 32] which lacks the detailed characterization of selenium nanoparticles.

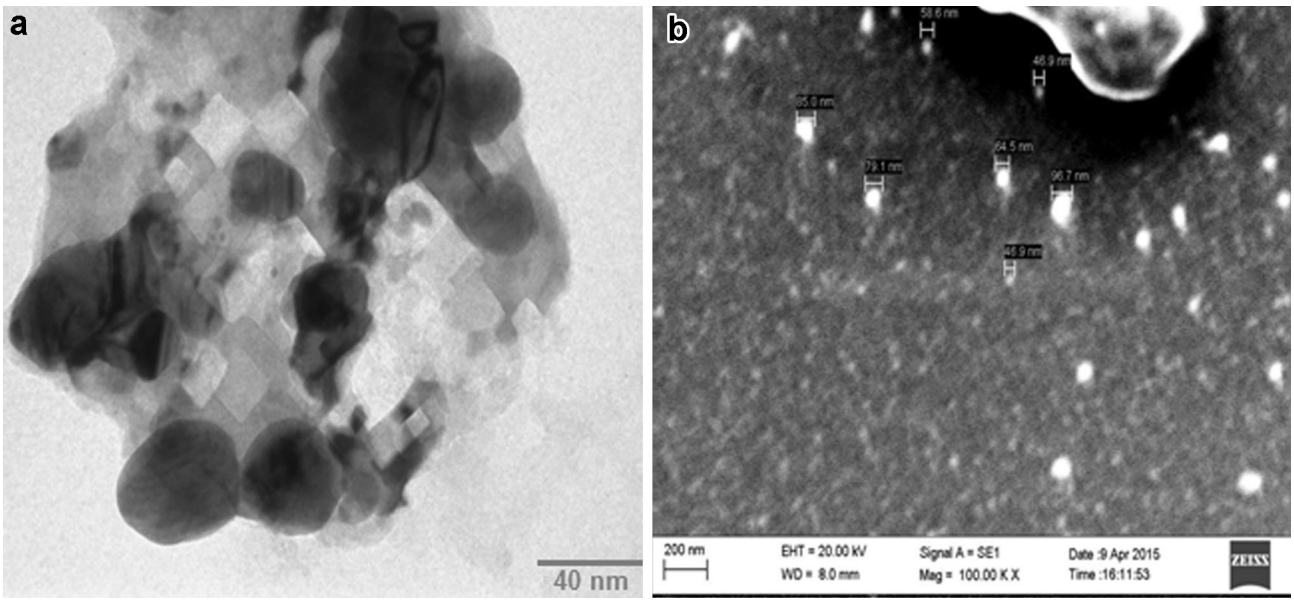

Fig. 4 TEM **a** and SEM **b** micrograph of selenium nanoparticles produced by bacterial strain KP6

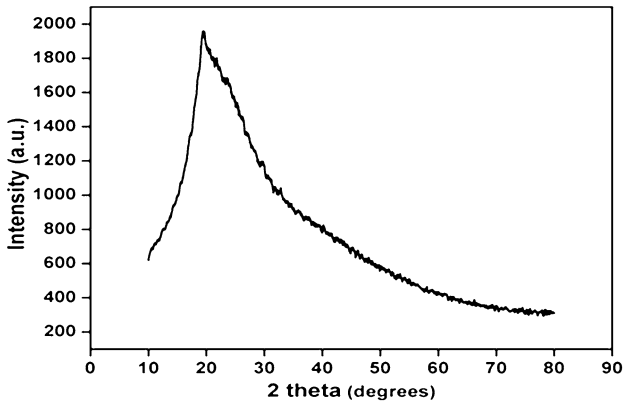

Fig. 5 X-ray diffraction pattern of selenium nanoparticles produced by bacterial strain KP6

The present study reported for the first time that the MIC and MTC of selenite as well as nanocrystallite size determination of selenium nanoparticles synthesized by an estuarine isolate can also be used for bioremediation of selenite contaminated sites. Moreover, the studies in an estuarine environment so far emphasized mainly on the anaerobic reduction of selenite and selenate to elemental selenium [15, 39] making the present study more advantageous for being carried out in aerobic environment at room temperature (30 °C) and easier separation of selenium nanoparticles which the former is deficient. The biologically synthesized selenium nanoparticles are recognized for their significant applications in electronics, optics, catalysis and sensors [40] as well as having biomedical applications [41].

Future prospective

Deducing the fundamental mechanism of selenite resistance in estuarine, *Citrobacter fruendii* strain KP6 by enzyme mediated detoxification of selenite (soluble and toxic) to selenium (insoluble and non toxic) would prove useful in designing bioremediation of estuarine polluted with toxic selenite in near future. The combination of genetic engineering of bacterial catalysts with judicious eco-engineering of polluted sites will be of paramount importance in future bioremediation strategies. Genetic engineering and high level expression of selenite reducing enzyme in estuarine bacteria has proved to be a very promising strategy in near future to deal with metalloid pollution. Ecological and environmental concerns and regulatory constrains are major obstacles for testing GEMs in the fields therefore their practical impact and delivery under field conditions need to be studied in details.

Conclusion

Citrobacter fruendii strain KP6 can be exploited for bioremediation of estuarine sites contaminated with selenite into non-toxic selenium while the green synthesis of Se nanoparticles could be further employed for its use in the field of nanotechnology and biotechnology which is more economical and eco-friendly solution to chemically synthesized Se nanoparticles.

Acknowledgments The authors acknowledge IIT, Bombay, Powaii for TEM analysis. They are also thankful to the help provided by Dr. Meghnath Prabhu and Dr. Bhanudas Naik, Bits Pilani, Goa Campus

for XRD analysis. Phd research scholar Madhavi Naik, Department of Chemistry, Goa University, India is also acknowledged for interpretation of XRD profile.

Compliance with ethical standards

Conflict of interest The authors declare no conflict of interest.

References

1. Tchounwou P B, Yedjou CG, Patlolla AK, Sutton DJ (2012) Heavy metals toxicity and the environment. In: Luch A (ed) Molecular, Clinical and Environmental Toxicology, Volume 3 Environmental Toxicology, Springer, pp 133-164
2. Gadd GM (2010) Metals, minerals and microbes: geomicrobiology and bioremediation. Microbiology 156:609–643
3. Liu X, Pietsch KE, Sturla SJ (2011) Susceptibility of the antioxidant selenoenyzmes thioredoxin reductase and glutathione peroxidase to alkylation-mediated inhibition by anticancer acylfulvenes. Chem Res Toxicol 24(5):726–736
4. Vinceti M, Bonvicini F, Bergomi M, Malagoli C (2010) Possible involvement of overexposure to environmental selenium in the etiology of amyotrophic lateral sclerosis: a short review. Ann Ist Super Sanita 46(3):279–283
5. Ouédraogo O, Chételat J, Amyot M (2015) Bioaccumulation and trophic transfer of mercury and selenium in African sub-tropical fluvial reservoirs food webs (Burkina Faso). PLoS ONE 10(4):e0123048
6. Chen J (2012) An original discovery: selenium deficiency and Keshan disease (an endemic heart disease). Asia Pac J Clin Nutr 21(3):320–326
7. Morris JS, Crane SB (2013) Selenium toxicity from a misformulated dietary supplement, adverse health effects, and the temporal response in the nail biologic monitor. Nutrients 5:1024–1057
8. Watts DL (1994) The nutritional relationships of selenium. J Orthomol Med. 9(2):111–117
9. World Health Organization (WHO) (2011) Guidelines for drinking-water quality, 4th edn. WHO, Geneva
10. Nissim WG, Hasbroucq S, Kadri H et al (2015) Potential of selected Canadian plant species for phytoextraction of trace elements from selenium-rich soil contaminated by industrial activity. Int J Phytorem 17:745–752
11. Sanders L, Moore LR, Durand JR (2013) Selenium removal from effluents in industrial mineral processes. In: Wolkersdorfer BF (ed) Reliable mine water technology. Golden Co, New York, pp 723–728
12. Lemlya AD (1999) Selenium impacts on fish: an insidious time bomb. Hum Ecol Risk Assess 5(6):1139–1151
13. Ghosh A, Mohod M, Paknikar KM, Jain RK (2008) Isolation and characterization of selenite- and selenate-tolerant microorganisms from selenium-contaminated sites. World J Microbiol Biotechnol 24(8):1607–1611
14. Umysová Vítová M, Doušková I, Bišová K, Hlavová M et al (2009) Bioaccumulation and toxicity of selenium compounds in the green alga *Scenedesmus quadricauda*. BMC Plant Biol 9:58–62
15. Narasingarao P, Haggblom MM (2007) Identification of anaerobic selenate respiring bacteria from aquatic sediments. Appl Environ Microbiol 73:3519–3527
16. DeMoll-Decker H, Macy JM (1993) The periplasmic nitrite reductase of *Thauera selenatis* may catalyze the reduction of selenite to elemental selenium. Arch Microbiol 160:241–247
17. Hunter WJ, Kuykendall LD (2006) Identification and characterization of an *Aeromonas salmonicida* (syn *Haemophilus piscium*) strain that reduces selenite to elemental red selenium. Curr Microbiol 52(4):305–309
18. Li DB, Cheng YY, Wu C, Li WW et al (2014) Selenite reduction by *Shewanella oneidensis* MR-1 is mediated by fumarate reductase in periplasm. Sci Rep 4:3735
19. Hunter WJ, Kuykendall LD (2007) Reduction of selenite to elemental red selenium by *Rhizobium* sp. strain B1. Curr Microbiol 55(4):344–349
20. Hunter WJ, Manter DK (2009) Reduction of selenite to elemental red selenium by *Pseudomonas* sp. strain CA5. Curr Microbiol 58:493–498
21. Bajaj M, Schmidt S, Winter J (2012) Formation of Se (0) nanoparticles by *Duganella* sp. and *Agrobacterium* sp. isolated from Se-laden soil of North-East Punjab, India. Microb Cell Fact 11(1):64
22. Siddique T, Zhang Y, Okeke BC, Frankenberger WT Jr (2006) Characterization of sediment bacteria involved in selenium reduction. Bioresour Technol 97(8):1041–1049
23. Alagarsamy R (2006) Distribution and seasonal variation of trace metals in surface sediments of the Mandovi estuary, west coast of India. Estuar Coast Shelf Sci 67(1–2):333–339
24. Nair M, Joseph T, Balachandran KK, Nair KKC, Paimpillii JS (2003) Arsenic enrichment in estuarine sediments-impact of iron and manganese mining. Fate of arsenic in the environment. In: Ahmed MF, Ali MA, Adeel Z (eds) International symposium on fate of arsenic in the environment, Dhaka; Feb 2003. International Training Network (ITN), Dhaka, pp 57–67
25. Naik MM, Pandey A, Dubey SK (2012) *Pseudomonas aeruginosa* strain WI-1 from Mandovi estuary possesses metallothionein to alleviate lead toxicity and promotes plant growth. Ecotoxicol Environ Saf 79:129–133
26. Mergeay M, Nies D, Schiegel HG et al (1985) *Alcaligenes eutrophus* CH34 is a facultative chemolithotroph with plasmid-bound resistance to heavy metals. J Bacteriol 162:38–334
27. Bergey DH, Kreig NR, Holt JG (1984) Bergey's manual of systematic bacteriology. Williams & Wilkins, Baltimore
28. Vinceti M, Wei ET, Malagoli C et al (2001) Adverse health effects of selenium in humans. Rev Environ Health 16(4):233–251
29. Lemly A, Dennis and Gregory J Smith (1987) Aquatic cycling of selenium: implications for fish and wildlife.US fish and wildlife services, Fish wildlife leaf let 12, p 10
30. Ogle RS, Knight AW (1996) Selenium bioaccumulation in aquatic ecosystems: effects of sulfate on the uptake and toxicity of selenate in *Daphnia magna*. Arch Environ Contam Toxicol 30(2):274–279
31. Dhanjal S, Cameotra SS (2010) Aerobic biogenesis of selenium nanospheres by *Bacillus cereus* isolated from coalmine. Microb Cell Fact 9:52
32. Shakibaie M, Mohazab NS, Mousavi SAA (2015) Antifungal activity of selenium nanoparticles synthesized by *Bacillus* species Msh-1 against *Aspergillus fumigatus* and *Candida albicans* Jundishapur. J Microbiol 8(9):e26381
33. Losi ME, Frankenberger WT Jr (1997) Reduction of selenium oxyanions by *Enterobacter cloacae* SLD1a-1: isolation and growth of the bacterium and its expulsion of selenium particles. Appl Environ Microbiol 63:3079–3084
34. Yamamura S, Yamashita M, Fujimoto N, Kuroda M, Kashiwa M, Sei K, Fujita M, Ike M (2007) *Bacillus selenatarsenatis* sp. nov., a selenate and arsenate-reducing bacterium isolated from the effluent drain of a glass-manufacturing plant. Int J Syst Evol Microbiol 57:1060–1064

35. Stolz JF, Basu P, Santini JM, Oremland RS (2006) Arsenic and selenium in microbial metabolism. Ann Rev Microbiol 60:107–130
36. Naik MM, Pandey A, Dubey S (2012) Biological characterization of lead-enhanced exopolysaccharide produced by a lead resistant *Enterobacter cloacae* strain P2B. Biodegradation 23(5):775–783
37. Mishra RR, Prajapati S, Das J et al (2011) Reduction of selenite to red elemental selenium by moderately halotolerant *Bacillus megaterium* strains isolated from Bhitarkanika mangrove soil and characterization of reduced product. Chemosphere 841:1231–1237
38. Li B, Liu N, Li Y et al (2014) Reduction of selenite to red elemental selenium by *Rhodopseudomonas palustris* strain N. PLoS ONE 9(4):e95955
39. Rauschenbach I, Narasingarao P, Haggblom M (2011) *Desulfurispirillum indicum* sp.nov., a selenate and selenite respiring bacterium isolated from an estuarine canal in southern India. Int J Syst Evol Microbiol 61:654–658
40. Chaudhary S, Mehta SK (2014) Selenium nanomaterials: applications in electronics, catalysis and sensors. J Nanosci Nanotechnol 14(2):1658–1674
41. Xia Y, You P, Xu F, Liu J, Xing F (2015) Novel functionalized selenium nanoparticles for enhanced anti-hepatocarcinoma activity in vitro. Nanoscale Res Lett 10:349–362

Proc. Natl. Acad. Sci., India, Sect. B Biol. Sci.
https://doi.org/10.1007/s40011-018-1034-5

RESEARCH ARTICLE

Application of Marine Bacteria Associated with Seaweed, *Ulva lactuca*, for Degradation of Algal Waste

Milind Mohan Naik[1] · Diksha Naik[1] · Lakshangy Charya[1] · Sajiya Y. Mujawar[1] · Diviya C. Vaingankar[1]

Received: 23 April 2018 / Revised: 14 June 2018 / Accepted: 15 September 2018

Abstract In the present study, three marine *Ulva lactuca*-associated bacteria capable of producing agarase, λ-carrageenase, amylase, cellulase and protease were isolated from rocky intertidal region of Anjuna beach, Goa, India, and designated as DM1, DM5 and DM15. Based on 16S rRNA sequence analysis and biochemical tests, bacteria were identified as *Vibrio brasiliensis*, *Bacillus subtilis* and *Pseudomonas aeruginosa*. Bacteria DM1, DM5 and DM 15 could able to utilize seaweed waste (*Sargassum* powder) in seawater-based media by releasing reducing sugars, 503.3 ± 17.5 µg/ml, 491.6 ± 20 µg/ml and 376.6 ± 16 µg/ml, respectively, which was confirmed through 3,5-dinitrosalicylic acid method. Therefore, the eco-friendly reuse of seaweed waste is possible by using marine bacteria for the production of reducing sugars in ethanol-producing industry. All three bacterial isolates were found to produce indole acetic acid (IAA) at concentration 98 ± 12 µg/ml, 113.6 ± 13 µg/ml and 121.6 ± 8.5 µg/ml, respectively. Nitrogen fixation by bacterial strains was confirmed when they showed growth on artificial seawater devoid of nitrogen and comprising of 5% carrageenan as a sole source of carbon and gelling agent. Photosynthetic seaweed, *Ulva lactuca,* provides organic carbon and O_2 for associated bacteria and associated bacteria fix atmospheric N_2 and provides iron by siderophore production and synthesize hormone IAA for algal growth during their cooperative association.

Keywords Seaweed · Associated bacteria · Polysaccharide · Enzymes · Cooperative association

Significance statement *Ulva lactuca*-associated marine bacteria were found capable of degrading algal waste and therefore can be used to bioremediate marine sites polluted with algal waste.

Electronic supplementary material The online version of this article (https://doi.org/10.1007/s40011-018-1034-5) contains supplementary material, which is available to authorized users.

✉ Milind Mohan Naik
milindnaik4@gmail.com

Diksha Naik
dikshanaik606@gmail.com

Lakshangy Charya
lakshangyscharya@gmail.com

Sajiya Y. Mujawar
sajiyamujawar@gmail.com

Diviya C. Vaingankar
vaingankardivya@gmail.com

[1] Department of Microbiology, Goa University, Goa, India

Introduction

Marine macroalgae are diverse photosynthetic eukaryotes and play an important ecological role in sustainable productivity of rocky intertidal coastal areas [1]. Marine macroalgal biomass is mainly composed of polysaccharides, and marine heterotrophic bacteria are primarily responsible for cycling of polysaccharide in marine environment [2]. Carrageenan and agar which are component of algal cell wall in marine ecosystem constitute a massive biomass and therefore a valuable carbon source for marine heterotrophic bacteria [2]. Extracellular substances released from marine macroalgae also serve as food for diverse associated bacteria in coastal ecosystems [3]. Macroalgae-associated marine bacteria benefit from organic compounds produced by a host macroalgae, and bacteria, in turn, provide CO_2, minerals, produce auxin and fix atmospheric N_2 and play a crucial role in algal health [2, 4]. Marine environment is a potential source of

Published online: 24 September 2018

microbial enzymes having novel biochemical and functional properties which are very important in industries [4]. Moreover, seaweed-associated bacteria also produce a variety of industrially important enzymes viz. carrageenase, agarases, esterases, cellulase, amylases, phosphatases, lipases, ureases and β-galactosidases inured to be able to assimilate macroalgal organic compounds and play important role in carbon, nitrogen and sulphur cycles [4–8]. Marine bacteria, and in particular those associated with macroalgae, are potential source of novel carbohydrate-active enzymes [5]. Therefore, multiple polysaccharide-degrading bacteria associated with macroalgae play a main role in recycling of carbon from algal complex polysaccharides (CPs) in marine environment [6–8].

Macroalgae contribute significantly to global primary production and are composed of agar and carrageenan, which find their application as constituents in food, personal care, laboratory experiments in microbiology and cosmetic industries owing to their gelling and emulsifying properties [2]. Agar is a polysaccharide and consists of mixture of agarose and agaropectin. In agar, structural repeats are D-galactose and 3,6-anhydro-L-galactose with alternate α-1,3- and β-1,4-linkages, with various residues such as hydroxyl, sulphate and methoxyl. Agar is obtained from the cell walls of Gelidium and Gracilaria [9] and has been extensively used in various laboratory and industrial applications, due to its jellifying properties [10]. There are two types of agarases: α-agarase and β-agarase depending on the cleavage site; α-agarases recognize and cleave α-1,3 linkages of agarose to yield agaro-oligosaccharides, whereas β-agarases identify and cleave β-1,4 linkages of agarose to produce neoagaro-oligosaccharides [5]. Cell walls of marine red seaweeds are also made up of sulphated galactans known as carrageenan, and depending on the number of sulphate ester groups and their position, carrageenans are classified [11]. The most sulphated carrageenan containing at least three sulphates per disaccharide unit is λ-carrageenan (most negatively charged and form highly viscous solutions) followed by *i-iota* (two SO_4 group) and *k*-kappa carrageenan (one SO_4 group). All three carrageenans are made up of linear chains of galactose with alternating α-(1 $\rightarrow$ 3) and β-(1 $\rightarrow$ 4) linkages. Seaweeds also comprise of polysaccharides like starch and cellulose, which are degraded by amylases and cellulases produced by bacteria. Among multiple polysaccharide-degrading (MPD) marine bacteria isolated in recent years which play a significant role in recycling of carbon from complex polysaccharide (CP), *Saccharophagus degradans* and *Microbulbifer* are dominant MPD bacteria [12]. There are ample of reports on marine bacteria producing agarases and carrageenases[13–19], but there are very few reports on marine macroalgae-associated bacteria producing agarases and carrageenases [12, 20]. Cell wall of seaweed comprises array of heterologous polysaccharides and promotes biofilm formation by complex polysaccharide (CP)-degrading bacteria by offering unique econiche [12]. But still the relationship between macroalgae and associated bacteria is poorly understood.

Modification of repeating units of algal polysaccharide with diverse functional groups such as sulphate, methoxy and hydroxyl makes them recalcitrant [12]. Domestic food waste, microbiology laboratory waste and industrial waste containing carrageenan and agar are directly discharged into marine water bodies which persist for long time and affect marine biota, and therefore, there is pressing need to remove these pollutants from marine-polluted sites or treated before discharging into marine environment. Therefore, isolation of multiple polysaccharide-degrading (MPD) marine bacteria is very crucial which serve as potential candidates for eco-friendly degradation of macroalgal waste. In the present study, the authors are investigating marine alga (*Ulva lactuca*)-associated potential agar, carrageenan, starch, cellulose and protein-degrading bacteria for bioremediation of marine environment polluted with algal waste and also to study cooperative association between seaweed *Ulva lactuca* and associated bacteria.

Material and Methods

Collection of Marine Macroalgae

Marine macroalgae (*Ulva lactuca*) [21] were collected from rocky intertidal zone of Anjuna Goa, India, using sterile forceps in sterile Petri plates. *Ulva lactuca* samples were immediately processed to isolate of macroalgae-associated bacteria.

Isolation of Agarase-Producing Marine *Ulva lactuca*-Associated Bacteria

For isolation of *Ulva lactuca*-associated agarase-producing bacteria, *Ulva lactuca* (approx 1 g) was gently rinsed with sterile seawater and then suspended in 50 ml sterile seawater in Erlenmeyer flask and kept on incubator shaker for 1 h at room temperature (RT) with constant shaking at 250 rpm. Algae are removed aseptically from flask, and resultant seawater suspension (0.1 ml) was spread plated on seawater-based agar medium (2% agar without any other added carbon source) and incubated at RT (28 $\pm$ 2 °C) for 24–48 h. Colonies, which showing proper depression in agar plates, were selected as potential agarase-producing marine bacteria. Agarase production was further confirmed by flooding plates with Lugol's iodine and observing zone of clearance around colony [12]. Best

agarase-producing bacteria were selected based on size of zone of clearance after adding Lugol's iodine.

λ-Carrageenase Production by *Ulva lactuca*-Associated Marine Bacteria

Carrageenase production by selected agarase-producing marine *Ulva lactuca*-associated bacteria was checked by spot inoculating bacterial isolates on seawater-based media plate (5% carrageenan as gelling agent without any other added carbon source) and incubated at RT (28 ± 2 °C) for 48 h. Then, agar plate was flooded with phenol red [12].

Production of Cellulase, Amylase and Protease by *Ulva lactuca*-Associated Bacteria

Amylase production by *Ulva lactuca*-associated bacteria was checked by spot inoculating on seawater-based starch agar plate (1.5% agar with 2% starch) and incubated at RT (28 ± 2 °C) for 24 h. After incubation, starch agar plate was flooded with iodine solution. Also, starch utilization was checked in sea water-based broth containing 2% starch as sole, a source of carbon and incubated at RT (28 ± 2 °C) for 24 h with constant shaking at 150 rpm. Cellulase production was checked by spot inoculating on seawater-based agar plates containing 1% carboxymethyl cellulose (CMC) and incubated at RT (28 ± 2 °C) for 48 h. Plates were flooded with 1% (w/v) congo red and allowed to stand for 15 min, and after pouring out excess congo red, plates were flooded with 1 M NaCl solution (decolourization). Excess NaCl solution was discarded after incubating for 15 min. This step was repeated three times to wash off excess unbound congo red. The zone of clearance around colony [22] was observed. Protease activity was checked by spot inoculating on skim milk agar and incubated at RT (28 ± 2 °C), and zone of clearance around bacterial colony was observed.

Identification of Seaweed-Associated Bacteria

Identification of seaweed-associated bacterial isolates was done based on biochemical tests and 16S rDNA sequencing. PCR amplification of 16S rDNA was done using following eubacterial primers: 27F (5′ AGA GTT TGA TCM TGG CTC AG 3′) and 1492R (5′ CGG TTA CCT TGT TAC GAC TT 3′). 16S rDNA sequencing was done at Eurofins Genomics Pvt. Ltd., Bangalore. 16S rDNA sequence was compared against GenBank database using NCBI BLAST search [23].

Nitrogen-Fixing Potential and Auxin-Producing Potential of *Ulva lactuca*-Associated Bacteria

Nitrogen fixation by *Ulva lactuca*-associated bacteria was tested by growing strains DM1, DM5 and DM15 on artificial seawater devoid of nitrogen and containing 5% carrageenan as a sole source of carbon and gelling agent and incubated at RT (28 ± 2 °C) for 48 h [24]. The appearance of colonies on artificial seawater-based media devoid of N_2 after 48 h was observed, which will confirm N_2-fixing ability of isolates, and then plates were flooded with 1% phenol red. See colour change around bacterial colony after flooding with phenol red. Indole acetic acid (IAA) production by seaweed-associated bacteria was tested by inoculating bacterial isolates in Zobell marine broth containing tryptophan and incubated at RT (28 ± 2 °C) for 24 h. After incubation, culture broth was centrifuged at 8000 rpm for 5 min and culture supernatant (1 ml) was mixed with 2 ml Salkowski's reagent (2% of 0.5 M $FeCl_3$ in 35% $HClO_4$ solution) and one drop of orthophosphoric acid and kept in the dark for 30 min. The optical density (OD) was recorded at 530 nm [25, 26]. The concentration of IAA was determined using standard calibration curve of pure IAA following linear regression analysis.

Siderophore Production

Siderophore production by *Ulva lactuca*-associated bacteria was checked by spot inoculating on chrome azurol S agar (CAS) plates and incubated at RT (28 ± 2 °C) for 48 h [27].

Seaweed Waste (*Sargassum* powder) Degradation by *Ulva lactuca*-Associated Bacteria

Sargassum algae were collected from Anjuna beach and sun-dried for 1 month. The dried *Sargassum* samples were ground using mortar and pestle/electronic mixer to make fine powder and used as algal waste. Seawater-based agar was prepared by using 2% ground *Sargassum* powder as carbon source, and 1.5% agar was added as gelling agent. Selected bacterial cultures were spot inoculated and incubated at RT (28 ± 2 °C) for 48 h. The plate was flooded with Lugol's iodine, and zone of clearance around bacterial colony was observed. Seawater-based broth was prepared by using 2% ground *Sargassum* powder as a sole carbon source and sterilized. Broth was inoculated with bacterial culture and incubated for 72 h with constant shaking at 150 rpm. After 72 h incubation, culture broth (5 ml) was centrifuged at 8000 rpm to pellet bacterial cells and supernatant was taken in another tube and reducing sugar was analysed by 3,5-dinitrosalicylic acid (DNSA) method [28], which measures the release of reduced sugar from

algal waste equivalents at 540 nm, with D-galactose as a standard. Appropriate control was kept, and all experiments were performed in triplicate.

Results and Discussion

Isolation of Agarase-Producing Marine *Ulva lactuca*-Associated Bacteria

Twenty-three bacterial colonies which showing proper depression in agar plates were selected as potential agarase-producing marine bacteria. Out of 23 agarase-producing bacteria, only three bacterial isolates which show the best (highest) depression in agar plates were selected for further study and designated as DM1, DM5 and DM15. Agarase production was further confirmed by zone of clearance around colonies, and rest of the plates stained dark brown when plates were flooded with Lugol's iodine. It was also observed that bacterial isolates DM1, DM5 and DM15 showed maximum zone of clearance among 23 isolates and hence selected (Fig. 1).

Carrageenase Production by Marine *Ulva lactuca*-Associated Bacteria

Growth of all three (DM1, DM5 and DM15) selected *Ulva lactuca*-associated bacterial isolates on seawater-based media plate (5% carrageenan as gelling agent without any other added carbon source) was observed after incubation at RT (28 ± 2 °C) for 48 h which confirms utilization (degradation) of carrageenase. This was further confirmed by production of yellow zone around colonies of DM1 and DM5 due to the production of acidic product during carrageenan degradation (Fig. 2) which changed the colour of phenol red from red to yellow. *Microbulbifer* strain CMC-5 showed similar results [12]. Interestingly, bacterial isolate DM15 showed pink colouration around colony when flooded with phenol red which indicate alkaline product formation during degradation of carrageenan which increase the pH and change colour of phenol red from red to dark pink (Fig. 2).

Production of Cellulase, Amylase Protease

All three *Ulva lactuca*-associated bacterial isolates produced amylase, protease and cellulase. Amylase production was confirmed when zone of clearance around bacterial colonies was seen after adding iodine solution, whereas rest of plate stained dark blue. Also, growth in sea water-based broth containing 1% starch as sole source of carbon confirmed amylase production. Cellulase production was detected when zone of clearance was observed around bacterial colonies and rest of plate stained dark red colour (Fig. 3a, b). Protease activity was confirmed when zone of clearance was seen around colonies spot inoculated on skim milk agar due to casein hydrolysis.

Identification of Seaweed-Associated Bacteria

The 16S rDNA sequence analysis was followed by NCBI BLAST search and biochemical tests (Supplementary data 1) by referring to Bergey's manual of systematic bacteriology [29]. The authors confirmed multiple polysaccharide-degrading *Ulva lactuca*-associated bacteria which were identified as *Vibrio brasiliensis* strain DM1, *Bacillus subtilis* strain DM5 and *Pseudomonas aeruginosa* strain

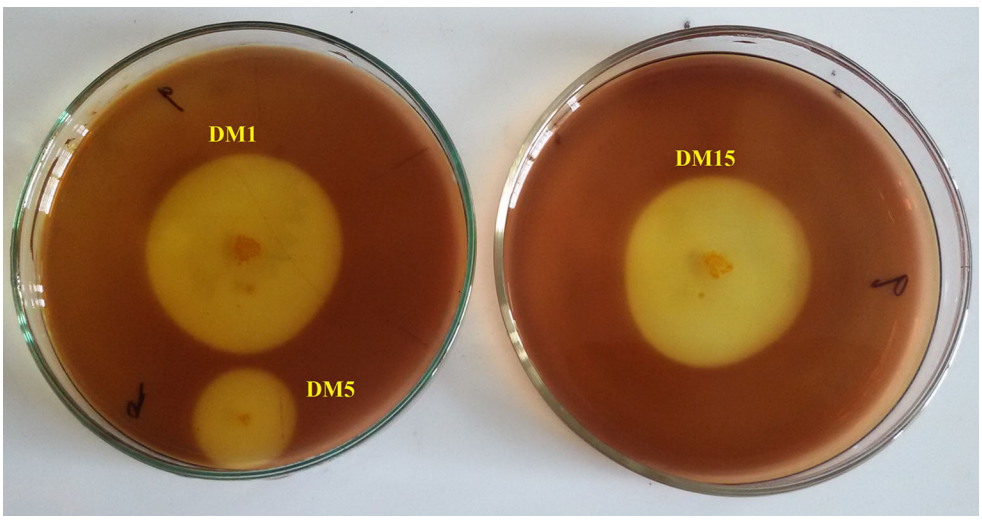

Fig. 1 Agarase production by bacterial strains DM1, DM5 and DM15 on seawater-based agar medium with 2% agar as sole source of carbon

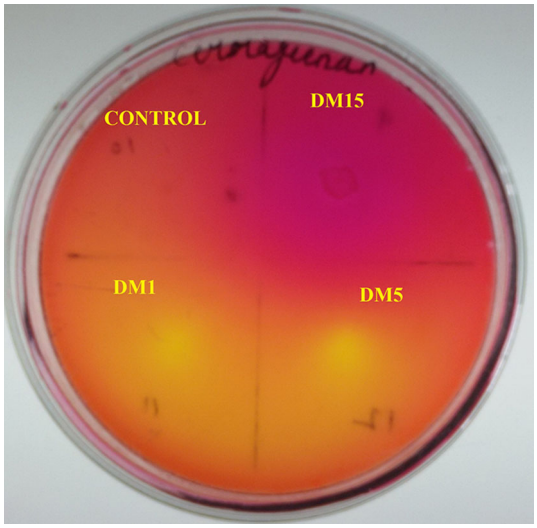

Fig. 2 Carrageenase production by marine *Ulva lactuca*-associated bacterial isolates DM1, DM5 and DM15 on seawater-based agar amended with 5% carrageenan as carbon source and gelling agent

DM15 (GenBank accession nos. MG971393, MG972930 and MG971397, respectively).

Nitrogen-Fixing and Auxin-Producing Potential of *Ulva*-Associated Bacteria

Nitrogen fixation by *Ulva lactuca*-associated bacterial strains DM1, DM5 and DM15 was confirmed when they showed growth on artificial seawater devoid of nitrogen and 5% carrageenan as sole source of carbon and gelling agent when incubated at RT (28 ± 2 °C) for 48 h. *Vibrio brasiliensis* strain DM1 and *Bacillus subtilis* strain DM5 showed yellow colouration around colonies when flooded with phenol red. This is due to breakdown of carrageenan into sugars and subsequently fermentation of sugars producing sufficient acids to which colour of phenol red changed to yellow. *Pseudomonas aeruginosa* strain DM15 showed pink colouration around colonies when flooded with phenol red. *Pseudomonas aeruginosa* strain DM15 breakdowns carrageenan into sugars, but *Psedomonas aeruginosa* DM15 is unable to ferment sugars (oxidative metabolism) and produce acids. Pink colour around DM15 colony is due to ammonium secretion by bacterial cells during nitrogen fixation which increases pH to alkaline and thus colour of phenol red changed from red to pink (Supplementary data 2). Nitrogen-fixing *Paenibacillus* strain and *Azotobacter vinelandii* are capable of secreting ammonium outside cell and changing the pH [30, 31]. Indole acetic acid (IAA) production by seaweed-associated bacteria was confirmed by getting pink colour after adding Salkowski's reagent along with one drop of orthophosphoric acid and keeping it in dark for 30 min. It was further confirmed by specific absorption by IAA at 530 nm. IAA concentration produced by DM1, DM5 and DM15 was determined as 98 ± 12, 113.6 ± 13 and 121.6 ± 8.5 µg/ml, respectively (Fig. 4).

Siderophore Production

All three bacterial isolates showed orange halo around colonies on CAS agar plates, thus confirming siderophore-producing potential of *Ulva lactuca*-associated bacterial isolates. *Ulva lactuca*-associated bacteria producing siderophores may be helping *Ulva lactuca* to uptake iron from seawater during iron-limiting conditions and thus promoting their growth (Fig. 5).

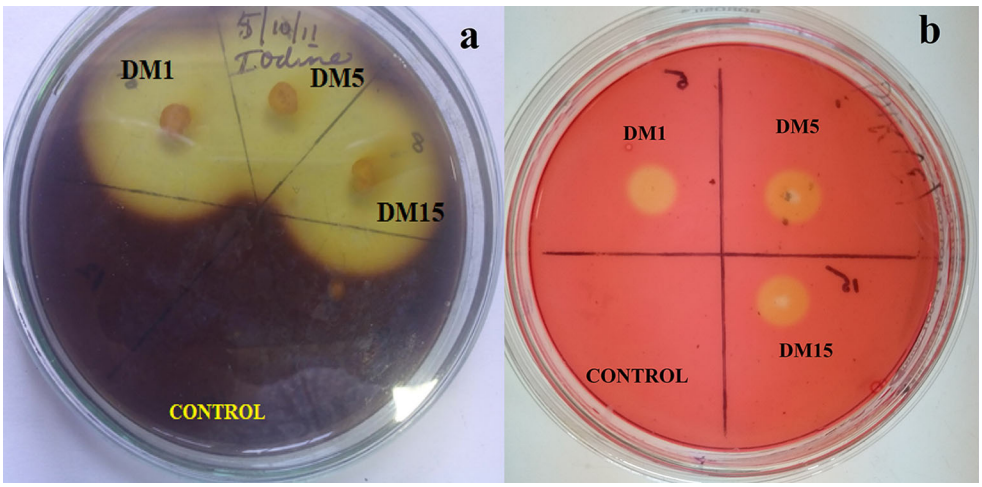

Fig. 3 **a**, **b** Amylase and cellulase production by marine *Ulva lactuca*-associated bacterial isolates DM1, DM5 and DM15 on casein agar, starch agar and CMC agar plates

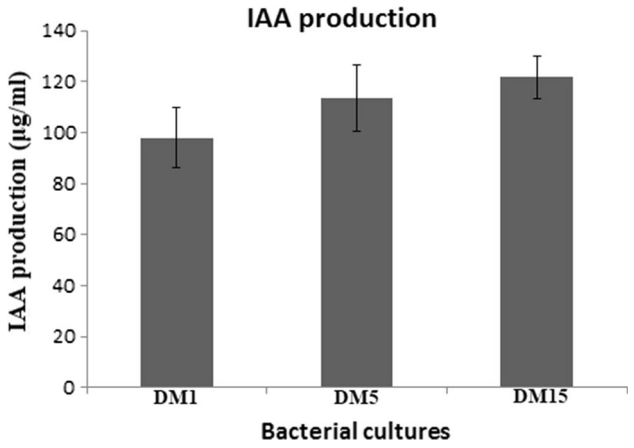

Fig. 4 IAA production by marine *Ulva lactuca*-associated bacterial isolates DM1, DM5 and DM15

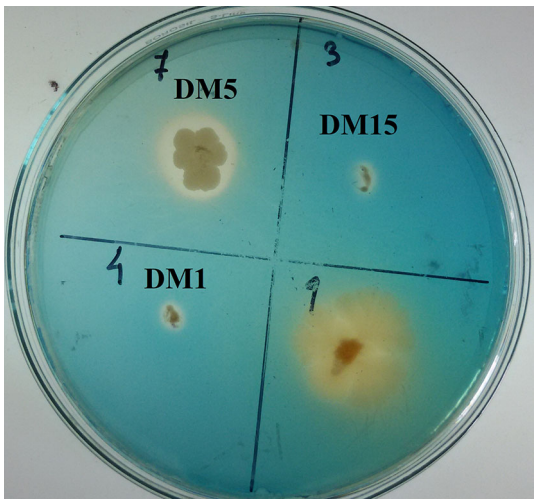

Fig. 5 Siderophore production by marine *Ulva lactuca*-associated bacterial isolates DM1, DM5 and DM15 on CAS agar plates

Seaweed Waste Degradation by Marine *Ulva lactuca*-Associated Bacteria

Potential of seaweed-associated bacteria *Vibrio brasiliensis* strain DM1, *Bacillus subtilis* strain DM5 and *Pseudomonas aeruginosa* strain DM15 for degradation of seaweed waste was confirmed when all three isolates grew on seawater-based agar containing 2% ground *Sargassum* powder as a carbon source and 1.5% agar as gelling agent. Zone of clearance around bacterial colonies after adding Lugol's iodine supported the results (Supplementary data 3). Furthermore, utilization of seaweed powder as a sole source of carbon in seawater-based broth by all three bacterial isolates was confirmed by analysing release of reducing sugar using DNSA method. Through DNSA method, it was confirmed that reducing sugar released after 72 h by DM1, DM5 and DM 15 was 503.3 ± 17.5, 491.6 ± 20 and 376.6 ± 16 µg/ml, respectively (Fig. 6) which is much higher than previous study on *Microbulbifer* Strain CMC-5, isolated from decomposing seaweed by Jonnadula et al. [6]. Jonnadula et al. [6] reported that *Microbulbifer* strain CMC-5 releases only 60 µg/ml reducing sugar from seaweed after 120 h. *Bacillus* sp. SYR4 possessing both agarase and carrageenase activities was studied for its application for reuse of red seaweed waste [17]. When the isolate was cultivated in red seaweed powder medium for 10 days, the reducing sugar released was 24 µg/ml which is much lower than the present report. This confirmed that the *Ulva lactuca*-associated bacterial isolates have better potential for agar waste degradation than previously reported bacterial isolates. Therefore, the eco-friendly reuse of red seaweed waste by these *Ulva lactuca*-associated bacterial isolates appears to be feasible for the production of reducing sugars and could be a valuable resource for ethanol-producing industry.

In recent years, seaweed waste has been increased tremendously owing to two reasons: one is rapid growth of macroalgae due to anthropogenic input of inorganic nutrients (eutrophication); another is culturing of seaweeds on large scale as an industrial resource [32]. Therefore, treatment of seaweed waste using marine bacteria is very crucial for preservation and sustainable development of marine environment. Therefore, *Ulva lactuca*-associated bacterial isolates *Vibrio brasiliensis* strain DM1, *Bacillus subtilis* strain DM5 and *Pseudomonas aeruginosa* strain DM15 can be exploited for degrading multiple polysaccharides or bioremediation of marine environment. Apart from bioremediation of algal waste from marine environments, DM1, DM5 and DM15 isolates producing agarase and carrageenase can be applied to recover DNA from agarose gel, prepare protoplasts, and produce agar/carrageenan-derived oligosaccharides having multiple applications such as improving food quality, antioxidation,

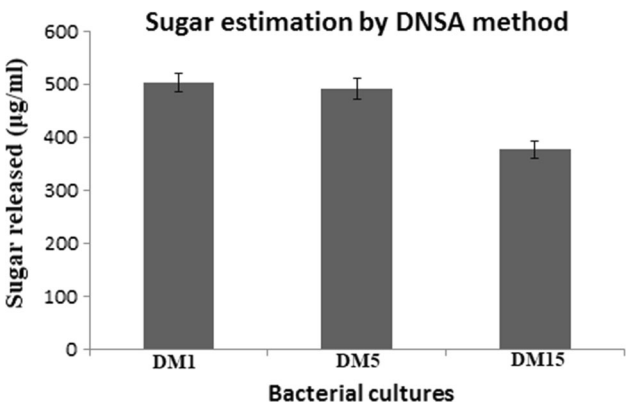

Fig. 6 Sugar released during degradation of algal waste (sargassum) by marine *Ulva lactuca*-associated bacterial isolates DM1, DM5 and DM15 in sea water-based broth

whitening and moisturization [2]. Using agarase and carrageenase enzyme, seaweed waste can also be used for bioethanol production, i.e. for initial hydrolysis of algal waste for reducing sugar production and then fermentation using *Saccharomyces cerevisiae*.

Marine macroalgae are known to hold a large number of associated heterotrophic bacteria which contribute to their survival processes. Macroalgae-bacterial relationship mainly depends on production of organic matter (food) and oxygen which are used by bacteria. Moreover, marine macroalgae-associated bacteria are reported to provide CO_2 and minerals [4]. Some bacteria excrete auxins, siderophores and fix atmospheric N_2 enhancing cell division and growth of macroalgae [1, 4]. Also, it has been reported that macroalgae-associated bacteria produce acyl homoserine lactone (AHL), which plays a great role in growth and development of *Gracilaria dura* [3]. The study also associated all three seaweed marine bacteria which produced a significant amount of algal growth-promoting substance—auxin, fixed atmospheric nitrogen and produced iron-chelating siderophores, whereas, seaweed (*Ulva lactuca*) provided polysaccharide as food for bacteria thus proved their cooperative association.

Conclusion

Three multiple polysaccharide-degrading seaweed (*Ulva lactuca*)-associated bacteria *Vibrio brasiliensis* strain DM1, *Bacillus subtilis* strain DM5 and *Pseudomonas aeruginosa* strain DM15 producing multiple enzymes viz. agarase, carrageenase, amylase, protease and cellulase were isolated. These bacterial strains were found to degrade algal waste and therefore can be used to bioremediate marine sites polluted with algal waste. All three bacterial isolates were found to have potential of fixing atmospheric nitrogen and siderophore production; therefore, the authors can use these bacteria to bioremediate marine sites polluted with algal waste without using biostimulation strategy (addition of NO_3 and Fe to enhance microbial bioremediation). Also, all three bacterial cultures were found positive for IAA, and therefore, the authors conclude that seaweed provides organic carbon and O_2 for bacteria and associated bacteria in turn fix atmospheric N_2 for seaweed in nitrogen-limiting ocean water and also provide hormone IAA and siderophores for algal growth during their cooperative association.

Acknowledgements The authors thank the Science and Engineering Research Board (SERB), Department of Science and Technology, Government of India, for financial support as Young Scientist Project (File Number: YSS/2014/000258). They are also thankful to Prof. S.K. Dubey, Prof. Sandeep Garg and Dr. Shyamalina Haldar (all from), Department of Microbiology, Goa University, Goa.

Compliance with Ethical Standards

Conflict of interest The authors declare that they have no conflict of interest to publish this manuscript.

References

1. Singh RP, Reddy CRK (2016) Unravelling the functions of the macroalgal microbiome. Front Microbiol. https://doi.org/10.3389/fmicb.2015.01488
2. Ficko-Blean E, Préchoux A, Thomas F, Rochat Larocque R, Zhu Y, Stam M, Génicot S, Jam M, Calteau A, Viart B, Ropartz D, Pérez-Pascual D, Correc G, Matard-Mann M, Stubbs KA, Rogniaux F, Jeudy A, Barbeyron T, Médigue C, Czjzek M, Vallenet D, McBride MJ, Duchaud E, Michel G (2017) Carrageenan catabolism is encoded by a complex regulon in marine heterotrophic bacteria. Nat Commun. https://doi.org/10.1038/s41467-017-01832-6
3. Singh RP, Baghel R, Reddy CRK, Jha B (2015) Effect of quorum sensing signals produced by seaweed-associated bacteria on carpospore liberation from *Gracilaria dura*. Front Plant Sci. https://doi.org/10.3389/fpls.2015.00117
4. Comba-González NB, Ruiz-Toquica JS, López-Kleine L, Montoya-Castaño D (2016) Epiphytic bacteria of macroalgae of the genus *Ulva* and their potential in producing enzymes having biotechnological interest. J Mar Biol Ocean. https://doi.org/10.4172/2324-8661.1000153
5. Alvarado R, Leiva S (2017) Agar-degrading bacteria isolated from Antarctic macroalgae. Folia Microbiol 62:409–4016
6. Jonnadula RC, Verma P, Shouche YS, Ghadi SC (2009) Characterization of *Microbulbifer* Strain CMC-5, a new biochemical variant of *Microbulbifer elongatus* type strain DSM6810T isolated from decomposing seaweeds. Curr Microbiol 59:600–607
7. Martin M, Portetelle D, Michel G, Vandenbol M (2014) Microorganisms living on macroalgae: diversity, interactions, and biotechnological applications. Appl Microbiol Biotechnol 98:2917–2935
8. Martin M, Barbeyron T, Martin R, Portetelle D, Michel G, Vandenbol M (2015) The cultivable surface microbiota of the brown Alga *Ascophyllum nodosumis* enriched in macroalgal-polysaccharide-degrading bacteria. Front Miocrobiol. https://doi.org/10.3389/fmicb.2015.01487
9. Song T, Zhang W, Wei C, Jiang T, Xu H, Cao Y, Cao Y (2015) Isolation and characterization of agar-degrading endophytic bacteria from plants. Curr Microbiol 70:275–281
10. Chi WJ, Chang YK, Hong SK (2012) Agar degradation by microorganisms and agar-degrading enzymes. Appl Microbiol Biotechnol 94:917–930
11. Guibet M, Colin S, Barbeyron T, Genicot S, Kloareg B, Michel G, Helbert W (2007) Degradation of λ-carrageenan by *Pseudoalteromonas carrageenovora* λ-carrageenase: a new family of glycoside hydrolases unrelated to κ- and ι-carrageenases. Biochem J 404:105–114
12. Imran Md, Poduval PB, Ghadi SC (2017) Bacterial degradation of algal polysaccharides in marine ecosystem. In: Naik MM, Dubey SK (eds) Marine pollution and microbial remediation. Springer, Berlin, pp 196–202
13. Shieh WY, Simidu U, Maruyama Y (1988) Nitrogen fixation by marine agar-degrading bacteria. J Gen Microbiol 134(1821–1): 825
14. Hu Z, Lin BK, Xu Y, Zhong MQ, Liu GM (2009) Production and purification of agarase from a marine agarolytic bacterium *Agarivorans* sp. HZ105. J Appl Microbiol 106:181–190

15. Vashist P, Nogi Y, Ghadi SC, Verma P, Shouche YS (2013) *Microbulbifer mangrovi* sp. nov., a polysaccharide-degrading bacterium isolated from an Indian mangrove. Int J Syst Evol Microbiol 63:2532–2537
16. Yao Z, Wang F, Gao Z, Jin L, Wu H (2013) Characterization of a κ-carrageenase from Marine *Cellulophaga lytica* strain N5-2 and analysis of Its degradation products. Int J Mol Sci 14:24592–24602
17. Kang S, Kim JK (2015) Reuse of red seaweed waste by a novel bacterium, *Bacillus* sp. SYR4 isolated from a sandbar. World J Microbiol Biotechnol 31:209–217
18. Liu G, Wu S, Jin W, Sun C (2016) Amy63, a novel type of marine bacterial multifunctional enzyme possessing amylase, agarase and carrageenase activities. Sci Rep. https://doi.org/10.1038/srep18726
19. Chauhan PS, Saxena A (2016) Bacterial carrageenases: an overview of production and biotechnological applications. 3 Biotech 6:146–163
20. Singh RP, Reddy CRK (2014) Seaweed–microbial interactions: key functions of seaweed-associated bacteria. FEMS Microbiol Ecol 88:213–230
21. Kerkar V (2004) Addition to the marine algal flora of Goa. Seaweed Res Util 26:19–21
22. Liang YL, Zhang Z, Wu M, Wu Y, Feng JX (2014) Isolation, screening, and identification of cellulolytic bacteria from natural reserves in the subtropical region of China and optimization of cellulase production by *Paenibacillus terrae* ME27-1. BioMed Res Int. https://doi.org/10.1155/2014/512497
23. Altchul SF, Madden TL, Schaffer AA, Zhang J, Zhang Z, Miller W, Lipman DJ (1997) Gapped BLAST and PSIBLAST: a new generation of protein database search programs. Nucleic Acids Res 25:3389–3402
24. Komives CF, Cheung LY, Pluschkell SB, Flickinger MC (2005) Growth of *Bacillus methanolicus* in seawater-based media. J Ind Microbiol Biotechnol 32:61–66
25. Bano N, Musarrat J (2003) Characterization of new *Pseudomonas aeruginosa* strain NJ-15 as a potential biocontrol agent. Curr Microbiol 46:324–328
26. Mohite B (2013) Isolation and characterization of indole acetic acid (IAA) producing bacteria from rhizospheric soil and its effect on plant growth. J Soil Sci Plant Nutr 13:638–649
27. Schwyn B, Neilands JB (1987) Universal chemical assay for the detection and determination of siderophores. Anal Biochem 160:47–56
28. Miller GL (1959) Use of dinitrosalicylic acid reagent for determination of reducing sugar. Anal Chem 31:426–428
29. Bergey DH, Kreig NR, Holt JG (1984) Bergey's manual of systematic bacteriology. Williams & Wilkins, Baltimore
30. Dariush S, Emtiazi G (2010) Ammonium production during the nitrogen-fixing process by wild *Paenibacillus* strains and cell-free extract adsorbed on nano TiO_2 particles. J Microbiol Biotechnol 20:1251–1258
31. Barney BM, Plunkett MH, Natarajan V, Mus F, Knutson CM, Peters JW (2017) Transcriptional analysis of an ammonium-excreting strain of *Azotobacter vinelandii* deregulated for nitrogen fixation. Appl Environ Microbiol. https://doi.org/10.1128/AEM.01534-17
32. Tang JC, Taniguchi H, Chu H, Zhou Q, Nagata S (2009) Isolation and characterization of alginate-degrading bacteria for disposal of seaweed wastes. Lett Appl Microbiol 48:38–43

Biometals
https://doi.org/10.1007/s10534-018-0158-7

Arsenite biotransformation and bioaccumulation by *Klebsiella pneumoniae* strain SSSW7 possessing arsenite oxidase (*aioA*) gene

Sajiya Yusuf Mujawar · Kashif Shamim · Diviya Chandrakant Vaigankar · Santosh Kumar Dubey

Received: 9 August 2018 / Accepted: 17 November 2018

Abstract Arsenite oxidizing *Klebsiella pneumoniae* strain SSSW7 isolated from shipyard waste Goa, India showed a minimum inhibitory concentration of 21 mM in mineral salts medium. The strain possessed a small supercoiled plasmid and PCR amplification of arsenite oxidase gene (*aioA*) was observed on plasmid as well as chromosomal DNA. It was confirmed that arsenite oxidase enzyme was a periplasmic protein with a 47% increase in arsenite oxidase activity at 1 mM sodium arsenite. Scanning electron microscopy coupled with electron dispersive X-ray spectroscopic (SEM–EDS) analysis of 15 mM arsenite exposed cells revealed long chains of cells with no surface adsorption of arsenic. Transmission electron microscopy combined with electron dispersive X-ray spectroscopic (TEM-EDS) analysis demonstrated plasma membrane disruption, cytoplasmic condensation and periplasmic accumulation of arsenic. The bacterial strain oxidized 10 mM of highly toxic arsenite to less toxic arsenate after 24 h of incubation. Fourier transformed infrared (FTIR) spectroscopy confirmed the interaction of arsenite with functional groups present on the bacterial cell surface. Sodium dodecyl sulfate-polyacrylamide gel electrophoresis (SDS-PAGE) analysis of 5 mM arsenite exposed cells demonstrated over-expression of 87 kDa and 14 kDa proteins of two subunits aioA and aioB of heterodimer arsenite oxidase enzyme as compared to control cells. Therefore, this bacterial strain might be employed as a potential candidate for bioremediation of arsenite contaminated environmental sites.

Keywords Arsenite · *AioA* gene · Bioremediation · Biotransformation

Introduction

Extensive anthropogenic activities such as mining, combustion of fossil fuels, arsenical pesticides, herbicides, paints, ceramic, glass and pharmaceutical industries have resulted in the release of highly toxic metalloid arsenic in the environment which poses serious threat to all living organisms (Welch et al. 2000; Smedley and Kinniburgh 2002; Cheng et al. 2009; Stolz et al. 2010). Although WHO (1993) has set the permissible limit of 10 µg/l arsenic in drinking

Electronic supplementary material The online version of this article (https://doi.org/10.1007/s10534-018-0158-7) contains supplementary material, which is available to authorized users.

S. Y. Mujawar · K. Shamim · D. C. Vaigankar
Laboratory of Bacterial Genetics and Environmental Biotechnology, Department of Microbiology, Goa University, Taleigao Plateau, Goa 403206, India

S. K. Dubey (✉)
Center of Advanced Study in Botany, Banaras Hindu University, Varanasi, U.P. 221005, India
e-mail: santoshdubey.gu@gmail.com; santosh.dubey@bhu.ac.in

Published online: 23 November 2018

water, many countries still exceed this permissible limit (Chowdhury et al. 2000; Anawar et al. 2002; Mitra et al. 2002; Smedley and Kinniburgh 2002; Mukherjee et al. 2006).

Arsenic usually exists in four oxidation states such as − 3 (arsine), 0 (elemental arsenic), + 3 (arsenite) and + 5 (arsenate) with arsenite and arsenate being the most common forms of arsenic in the environment (Oremland and Stolz 2005). Arsenite is 100 times more toxic than arsenate and acts by interacting with thiol groups of proteins and enzymes inhibiting their functions (Hughes 2002; Rosen 2002; Rai et al. 2011). Arsenic also causes mutagenic and genotoxic effects on humans (Mandal and Suzuki 2002; Chen et al. 2002).

The ubiquity of arsenic in the environment has led microorganisms to develop various transformation mechanisms such as arsenite oxidation, arsenate reduction and arsenite methylation governed by *aio*, *arr, arsC* and *arsM* genes respectively which are located either on chromosomal or plasmid DNA (Silver and Phung 1996; Páez-Espino et al. 2009; Arsene-Ploetze et al. 2010; Bahar et al. 2013; Goswami et al. 2015). These mechanisms are commonly employed by various microorganisms to carry out detoxification or energy generation for their cellular growth and metabolism. The oxidation of highly toxic arsenite to less toxic arsenate encoded by arsenite oxidase enzyme is a key step of detoxification mechanism by microorganisms (Qin et al. 2006; Andreoni et al. 2012; Rauschenbach et al. 2012).

In recent years various bacterial strains capable of arsenite oxidation by arsenite oxidase (*aioA*/*aoxB*) gene have been reported in the genomes of *Acinetobacter junii*, *Acinetobacter baumannii, Geobacillus stearothermophilus, Thiomonas* sp. 3As, *Herminiimonas arsenicoxydans* and *Pseudomonas stutzeri* strain GIST-BDan 2 (Muller et al. 2007; Arsene-Ploetze et al. 2010; Chang et al. 2010; Majumder et al. 2013). In case of *Acinetobacter calcoaceticus* and *Brevibacillus* sp. KUMAs2 the *aioA* gene was present only on plasmid DNA whereas in *Acinetobacter soli,* the *aoxB* gene was located on genomic as well as plasmid DNA (Mallick et al. 2014; Goswami et al. 2015). The *aoxAB/aioAB* genes encode an arsenite inducible periplasmic protein which catalyzes the oxidation of highly toxic arsenite to less toxic arsenate (Silver and Phung 2005; Branco et al. 2009). It consists of two subunits, a small iron-sulfur cluster containing subunit *aoxA/aioB* and a large molybdopterin containing catalytic subunit *aoxB/aioA* (Silver and Phung 2005; Oremland et al. 2009). The *aoxB/aioA* gene acts as a genetic marker for arsenite oxidation (Hamamura et al., 2008; Quemeneur et al. 2008). Two families of arsenite transporters (ArsB and Acr3p) are known in bacteria (Rosen 1999) and Acr3p is divided into two subsets, Acr3(1)p and Acr3(2)p (Achour et al. 2007). Although these transporters have similar sizes and functions, they differ in mechanisms, as well as have different metalloid specificity. ArsB confers resistance to arsenite and antimonite, however Acr3p is highly specific to arsenite (Rosen 1999).

Keeping in view the potential of arsenic toxicity in humans and other life forms it is imperative to remove arsenic present in the environment. The traditional methods to remove arsenic from contaminated environmental sites are expensive, time-consuming and hazardous (Mahimairaja et al. 2005). Therefore, bioremediation of arsenic holds a great potential since it is an eco-friendly method involving microorganisms.

In the present investigation, we characterized one potential arsenite oxidizing bacterial strain from shipyard waste of Goa, India with reference to presence of arsenite oxidase gene, enzyme activity, arsenite uptake, morphological changes, presence of arsenic deposits, protein expression induced by arsenite stress using PCR, SEM, TEM, EDS and SDS-PAGE analysis.

Materials and methods

Isolation of arsenite oxidizing bacteria

Environmental samples were collected from shipyard waste, from Bicholim, Goa, India, in sterile zip-lock bags. Appropriate dilutions of the soil samples were made in 0.85% saline and plated on mineral salt medium (MSM) agar (Mahtani and Mavinkurve 1979) supplemented with 10 mM of sodium (meta) arsenite along with 0.2% glucose as a carbon source. Plates were incubated at 28 °C for 24 h and morphologically distinct bacterial colonies were selected for further studies.

Determination of minimum inhibitory concentration (MIC) of arsenite

Bacterial isolates were spot inoculated on MSM agar plates amended with increasing concentrations of 0–46 mM sodium arsenite along with 0.2% glucose. The plates were checked for visible bacterial colonies after incubation at 28 °C for 24–48 h. The bacterial strains showing highest MIC values were selected for determining MIC in MSM broth. Selected bacterial strains were inoculated in MSM broth supplemented with different concentration of arsenite (0–25 mM) and flasks were incubated at 28 °C, 150 rpm for 24 h. Growth was monitored by recording the absorbance at 600 nm using Biospectrometer (Eppendorf, Germany). The lowest concentration of arsenite which completely inhibited bacterial growth was considered as its MIC value.

Growth behavior of the selected bacterial isolate in presence of sodium arsenite

The selected bacterial strain was inoculated in MSM broth amended with different concentrations of sodium arsenite viz. 5 mM, 10 mM, 15 mM, 20 mM and 21 mM, whereas flask without sodium arsenite was maintained throughout the experiment as control. The flasks were incubated at 28 °C, 150 rpm for 24–30 h and absorbance at 600 nm was recorded after every 2 h using Biospectrometer (Eppendorf, Germany).

Identification of arsenite oxidizing bacterial isolate

The identification of selected bacterial strain was performed by extracting its genomic DNA using Dneasy Blood and Tissue Kit (Qiagen, Hilden, Germany) followed by amplification of 16S rRNA gene using universal eubacterial primers: 27F and 1495R (Studholme et al. 1999). The PCR was carried out using Nexus Gradient Mastercycler (Eppendorf, Germany) and the resulting PCR product was analyzed on 1% agarose gel. The PCR product was purified using PCR clean-up kit (Promega, USA) and sequenced. The nucleotide sequence obtained was subjected to BLAST (tblastn) search analysis using National Center for Biotechnology Information (NCBI) database. The sequence was submitted to GenBank (accession number: MG430351) and its taxonomical relatedness to closely associated genera was determined using the neighbor-joining method with MEGA 7 package (Kumar et al. 2016).

Plasmid profile

The plasmid DNA of the selected bacterial strain was extracted using Gen Elute Plasmid Miniprep kit (Sigma-Aldrich, USA) and was analyzed using 0.8% agarose gel electrophoresis. After electrophoresis gel was visualized under G:BOX gel documentation system (Syngene, UK).

PCR amplification of arsenite oxidase (*aioA*) and transporter (ACR3) genes

The large molybdopterin containing catalytic subunit (aioA) and one of the arsenite transporter (ACR3) genes were PCR amplified with gene-specific primers (Supplementary Table S1) using chromosomal and plasmid DNA separately as templates. The thermal cycler program comprised of an initial denaturation of 5 min at 94 °C, followed by 30 cycles of denaturation at 94 °C for 1 min, annealing at 55 °C for 1 min, extension at 72 °C for 1 min and a final extension at 72 °C for 5 min. The PCR products were analyzed on 1% agarose gel and visualized under G: BOX gel documentation system (Syngene, UK).

Arsenite oxidase enzyme assay

Preparation of cell-free extract

The bacterial cells were grown in MSM broth in presence of 15 mM sodium arsenite. Late log phase cells were harvested by centrifugation at 8000 rpm at 4 °C for 10 min. The cell pellet was washed thrice with washing buffer (20 mM Tris–HCl, 0.1 mM phenylmethylsulfonyl fluoride (PMSF), 0.6 mM EDTA with pH 8.4 and 0.9% NaCl with pH 8.4) and the pellet was resuspended in 10 ml 20 mM Tris–HCl buffer (pH 8.0) containing 0.6 mM PMSF and 0.6 mM EDTA. The cell suspension was incubated with 1 mg ml^{-1} lysozyme at 28 °C for 2 h with occasional stirring. Magnesium sulfate (20 mM), magnesium acetate (100 mM), DNase (100 µg) and RNase (500 µg) (Bangalore GeNei) were added to the cell suspension and incubated at 28 °C for 30 min. The cell suspension was sonicated thrice with 2 min bursts

and 10 min cool-down intervals followed by incubation at 60 °C for 1 min in water bath. Subsequently, the suspension was cooled on ice, followed by centrifugation at 8000 rpm for 10 min and the pH of the clear supernatant was adjusted to 8.4 with 2 M NaOH (Prasad et al. 2009).

Preparation of periplasmic and spheroplast fractions

Bacterial cells grown in MSM broth were harvested by centrifugation at 8000 rpm for 10 min and cell pellets suspended in 20 mM Tris–HCl buffer, 0.1 mM PMSF, 10 mM EDTA pH 8.4 along with 20% sucrose. The outer membrane was lysed using lysozyme (0.5 mg ml^{-1}) at 28 °C for 40 min followed by centrifugation at 8000 rpm for 10 min. The supernatant was collected in a fresh centrifuge tube and cell pellet containing spheroplast was washed twice in buffer containing 20 mM Tris–HC1, 0.1 mM PMSF, 10 mM EDTA (pH 8.4), 20% sucrose and assayed for arsenite oxidase activity.

Enzyme assay

The arsenite oxidase enzyme activity was determined in cell free extract, periplasmic and spheroplast fractions following standard method (Anderson et al. 1992). The enzyme sample was mixed with 1 ml of assay buffer containing 60 µM 2,6-dichlorophenol-indophenol (DCIP), 200 µM sodium arsenite and 50 mM morpholino ethelene diol sulfonic acid (MES) buffer (pH 6.0). The change in absorbance due to reduction of DCIP per minute was monitored at 600 nm for 5 min using Biospectrometer (Eppendorf, Germany). The specific activity of the enzyme was expressed as µmol of DCIP reduced min^{-1} mg^{-1} of protein. Similarly, the effect of arsenite (0.5 and 1 mM) on periplasmic protein was also studied. The protein concentration in the supernatants was determined by Folin Lowry method (Lowry et al. 1951) using bovine serum albumin (Himedia, Mumbai, India) as standard.

Scanning electron microscopy coupled with energy dispersive X-ray spectroscopic (SEM-EDS) analysis

The bacterial isolate was grown in MSM broth supplemented with 15 mM sodium arsenite (test) and without sodium arsenite (control). The flasks were incubated at 28 °C, 150 rpm for 8–20 h and bacterial cells in exponential growth phase (8 and 20 h) were harvested from control and test samples by centrifugation at 8000 rpm, 4 °C for 10 min (Eppendorf, Germany). The pellet obtained was washed thrice with 0.1 M phosphate buffer saline (PBS) with pH 7.4. The washed bacterial cells were evenly spread on a clean grease-free cover slip and fixed overnight using 2.5% glutaraldehyde. After incubation, cells were washed with PBS and were subjected to ethanol gradient of 30%, 50%, 70%, 90% and 100% by incubating for 10 min at each concentration. The samples were analyzed by SEM–EDS (Carl-Ziess, Germany).

Transmission electron microscopy coupled with energy dispersive X-ray spectroscopic (TEM-EDS) analysis

The TEM analysis of the bacterial strain was carried out to evaluate intracellular morphological changes and metal uptake by the cells. Cells grown with 15 mM sodium arsenite were harvested in the exponential growth phase (8 and 20 h) by centrifugation at 8000 rpm for 10 min followed by washing with 0.1 M sodium phosphate buffer (pH 7.2). The pellets obtained were fixed in a mixture of 2.5% glutaraldehyde and 2% paraformaldehyde prepared in 0.1 M sodium phosphate buffer (pH 7.2) for 2–3 h at 4 °C. The fixed bacterial cells were further incubated for 1 h in 1% OsO_4 and propylene oxide followed by graded series of dehydration in ethanol. The samples were then embedded in Epon 812 resins and ultra-thin sectioning (60 nm) was performed. This was followed by examining the samples using transmission electron microscope (TEM-JEOL 2100F, Germany) which were further analyzed for elemental content by EDS. A control without arsenite exposure under similar conditions was also maintained.

Arsenic transformation assay

The arsenite oxidizing ability of bacterial strain was determined qualitatively by silver nitrate test with minor modifications (Lett et al. 2001). The bacterial cells were grown in MSM broth with 15 mM sodium arsenite (test) and without sodium arsenite (control) at 28 °C, 150 rpm for 24 h. One ml culture suspension

was mixed with one ml of 0.1 M $AgNO_3$ and observed for colour change from colourless to light brown.

Quantitative determination of oxidized arsenite (i.e. arsenate) was performed using molybdene blue method with some modifications (Lenoble et al. 2003; Cai et al. 2009). Cells were harvested at 8000 rpm for 10 min and resulting cell pellet was disrupted by sonication (three times for 2 min with 10 min cool-down intervals). The supernatant (0.3 ml) obtained after centrifugation was added to a mixture of 4 ml Milli Q water, 0.4 ml 50% H_2SO_4 (v/v), 0.4 ml of 3% Na_3MoO_4 (w/v) and 0.2 ml of 2% ascorbic acid (w/v). The tubes were incubated at 90 °C in water bath for 20 min. The samples were cooled and final volume was adjusted to 10 ml using Milli Q water. The same protocol was also followed for control sample and absorbance of the samples was measured at 838 nm using Biospectrometer (Eppendorf, Germany). The standard curve of arsenate was used to determine the concentration of arsenate in the test sample.

Fourier transformed infrared (FTIR) spectroscopy

The FTIR samples were prepared using bacterial cells grown with and without 15 mM sodium arsenite. The cell suspension was harvested at 8000 rpm for 10 min followed by washing with 0.1 M PBS (pH 7.4). The cell pellet was dried at 45 °C for 48 h. The dried pellet was subjected to fine grinding in presence of KBr. The IR spectrum was recorded on IR prestige-21 instrument (Shimadzu, Japan) in the region of 4000–400 cm^{-1}.

SDS-PAGE

The bacterial cells were grown with and without 5 mM sodium arsenite and protein profile of extracted protein was studied using standard protocol (Laemmli 1970). Whole cell proteins were extracted and analyzed on 15% sodium dodecyl sulfate-polyacrylamide gel (SDS-PAGE) at a constant voltage of 90 V using BIORAD Mini-PROTEAN Tetra System (BIO-RAD, USA). The gel was stained overnight using freshly prepared 0.05% (w/v) Coomassie Brilliant blue R250 and destained using destaining solution (Sambrook et al. 1989).

Statistical analysis

All the experiments were carried out in triplicates and their mean, as well as standard error were calculated and incorporated as ± in the manuscript.

Results

Isolation of arsenite resistant bacterial strain and determination of MIC of arsenite

Among ten morphologically different arsenite resistant bacterial isolates, strain SSSW7 showed the highest MIC of 46 mM and 21 mM on MSM agar and in MSM broth respectively. The growth pattern of the bacterial strain SSSW7 exposed to sodium arsenite interestingly revealed an extended lag phase at higher concentrations of arsenite. A prominent shift in lag phase with increasing concentrations of sodium arsenite (10, 15, 20 mM) was observed compared to control (Supplementary Fig. 1).

Identification of arsenite oxidizing bacterial isolate

Strain SSSW7 was Gram-negative, non-motile rod which showed oxidase negative and catalase positive reaction. Based on BLAST analysis of 16S rDNA sequence the bacterial strain SSSW7 has been identified as *Klebsiella pneumoniae* (Supplementary Fig. 2) and the sequence has been submitted to Genbank (accession number: MG430351).

Plasmid profile and PCR amplification of arsenite oxidase and arsenite transporter genes

Klebsiella pneumoniae strain SSSW7 possessed a plasmid of > 10 kb in size (Fig. 1a). PCR amplification of *aioA* gene using plasmid and chromosomal DNA as template clearly revealed the presence of arsenite oxidase gene with amplicon size of 1100 bps (Fig. 1b). There was no PCR amplification of ACR3 gene encoding arsenite transporter using genomic as well as plasmid DNA as a template.

Arsenite oxidase assay

Klebsiella pneumoniae strain SSSW7 exhibited highest specific arsenite oxidase activity in the periplasmic

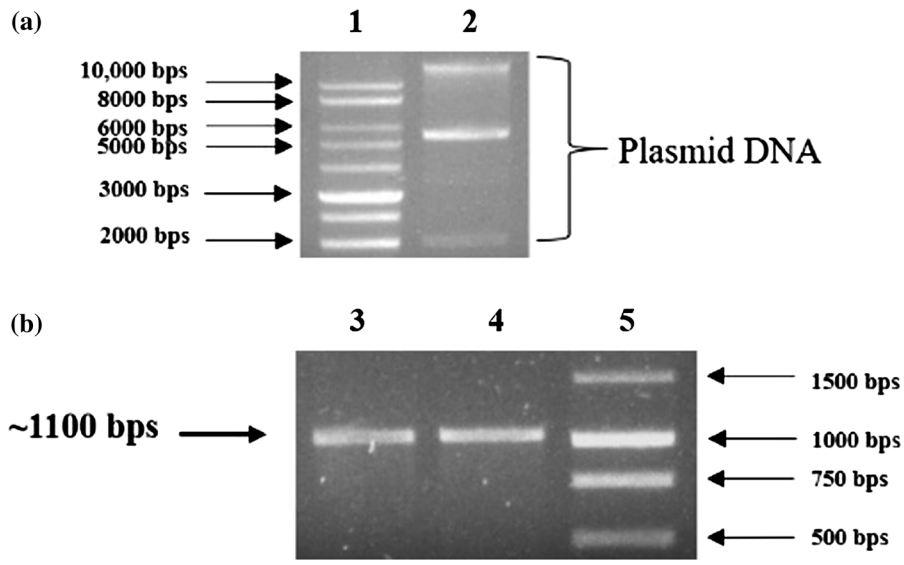

Fig. 1 Plasmid profile and PCR amplification of *aioA* gene of *Klebsiella pneumoniae* strain SSSW7. Lane 1a and 5b: 1 kb DNA markers. Lane 2a: Plasmid DNA of *K. pneumoniae* strain SSSW7. Lane 3b: PCR amplicon of *aioA* gene using chromosomal DNA as template. Lane 4b: PCR amplicon of *aioA* gene using plasmid DNA as template

fraction as the activity was recorded 1.328 µmol DCIP min^{-1} mg^{-1} protein, followed by cell free extract and spheroplast fraction with enzyme activity of 0.58 µmol DCIP min^{-1} mg^{-1} protein and 0.059 µmol DCIP min^{-1} mg^{-1} protein respectively. This clearly shows that arsenite oxidase enzyme is predominant in the periplasmic space. Interestingly, 12% and 47% increase in enzyme activity was observed in presence of 0.5 mM and 1 mM sodium arsenite indicating a high K_m.

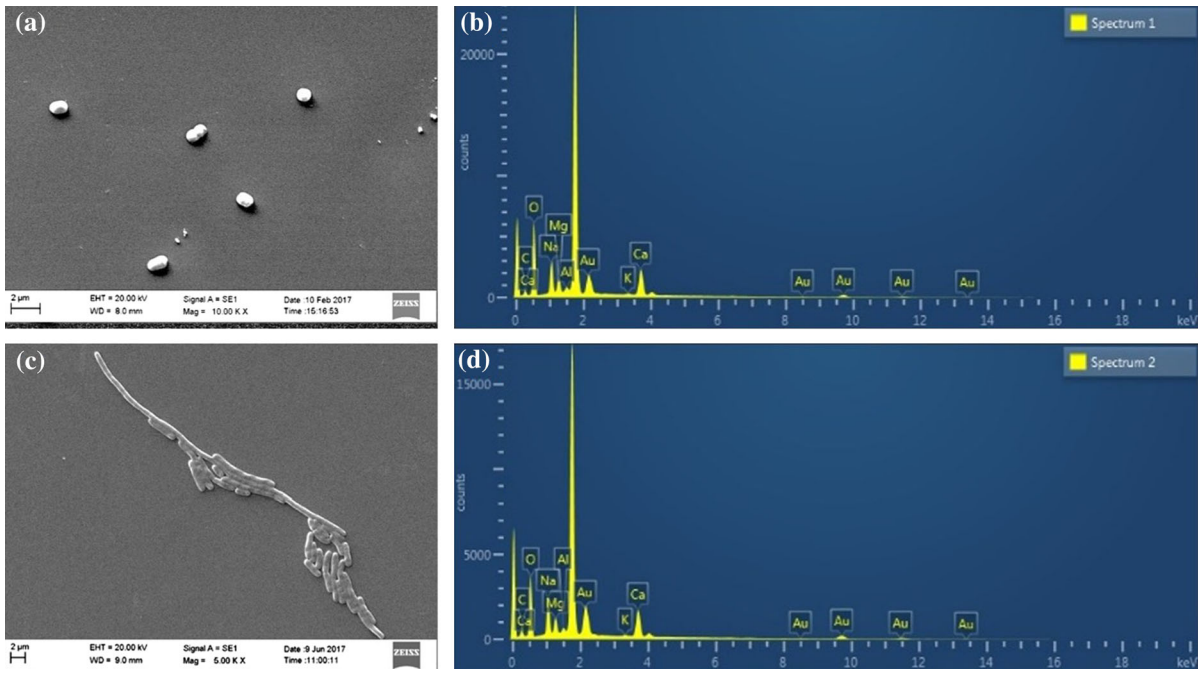

Fig. 2 SEM-EDS micrograph of *Klebsiella pneumoniae* strain SSSW7. **a** Bacterial cells in exponential growth phase (8 h) without exposure to arsenite showing rod shape morphology (control). **b** EDS micrograph of bacterial cells in exponential growth phase (8 h) without arsenite exposure (control). **c** Bacterial cells exposed to 15 mM arsenite in exponential growth phase (20 h) showing interconnected chains of cells. **d** EDS micrograph of bacterial cells in exponential growth phase (20 h) exposed to 15 mM arsenite

SEM-EDS analysis

The scanning electron micrograph of *K. pneumoniae* strain SSSW7 exposed to 15 mM arsenite demonstrated altered morphology from rods to interconnected chains of cells (Fig. 2a, c). The EDS spectrum of the cells exposed to 15 mM arsenite did not reveal any surface adsorption of arsenite (Fig. 2b, d).

TEM-EDS analysis

The intracellular structural analysis of *K. pneumoniae* strain SSSW7 by TEM clearly revealed that arsenite caused disruption of the plasma membrane, condensation of cytoplasm and presence of electron dense deposits throughout the periplasm (Fig. 3a, c). The presence of an arsenic peak in EDS spectrum of cells treated with 15 mM arsenite further confirmed intracellular accumulation of arsenic which was absent in control (Fig. 3b, d).

Arsenic transformation assay

The *K. pneumoniae* strain SSSW7 demonstrated arsenite oxidizing ability since a light brown coloured precipitate of silver-orthoarsenate was formed, indicating oxidation of arsenite to arsenate (Supplementary Fig. 3). Quantitative estimation of arsenate through molybdene blue method revealed that the bacterial strain SSSW7 internalized 10 mM of arsenate within 24 h.

Fourier transformed infrared (FTIR) spectroscopy

The FTIR spectrum analysis of 15 mM arsenite exposed bacterial cells of *K. pneumoniae* strain SSSW7 showed shifting as well as sharpening of many peaks which could be assigned to various functional groups responsible for arsenite accumulation (Fig. 4; Table 1). Arsenite exposed bacterial cells showed spectral changes in the region of

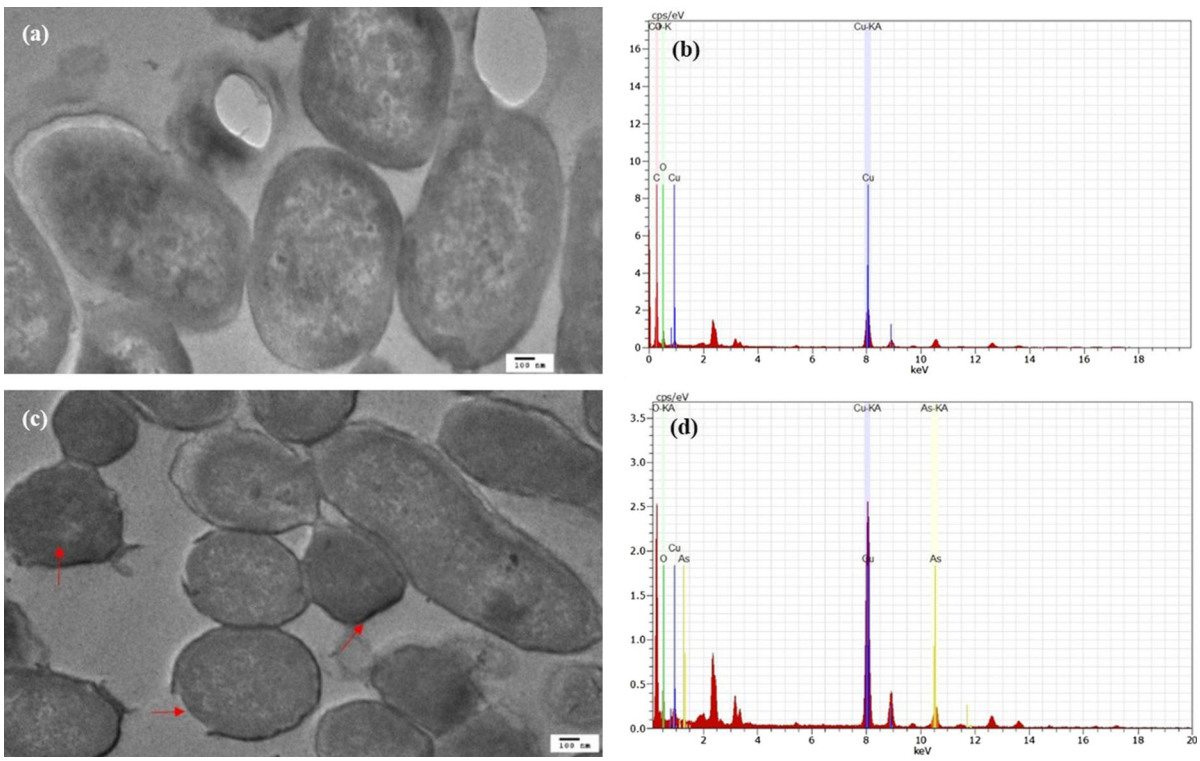

Fig. 3 TEM micrograph of *Klebsiella pneumoniae* strain SSSW7. **a** Bacterial cells in exponential growth phase (8 h) without arsenite exposure showing intact plasma membrane, clear cytoplasm and periplasm (control). **b** EDS micrograph of bacterial cells in exponential growth phase (8 h) without arsenite exposure (control). **c** Bacterial cells exposed to 15 mM sodium arsenite in exponential growth phase (20 h) showing disrupted plasma membrane, condensed cytoplasm and dark periplasm. **d** EDS micrograph of bacterial cells exposed to 15 mM arsenite in exponential growth phase (20 h)

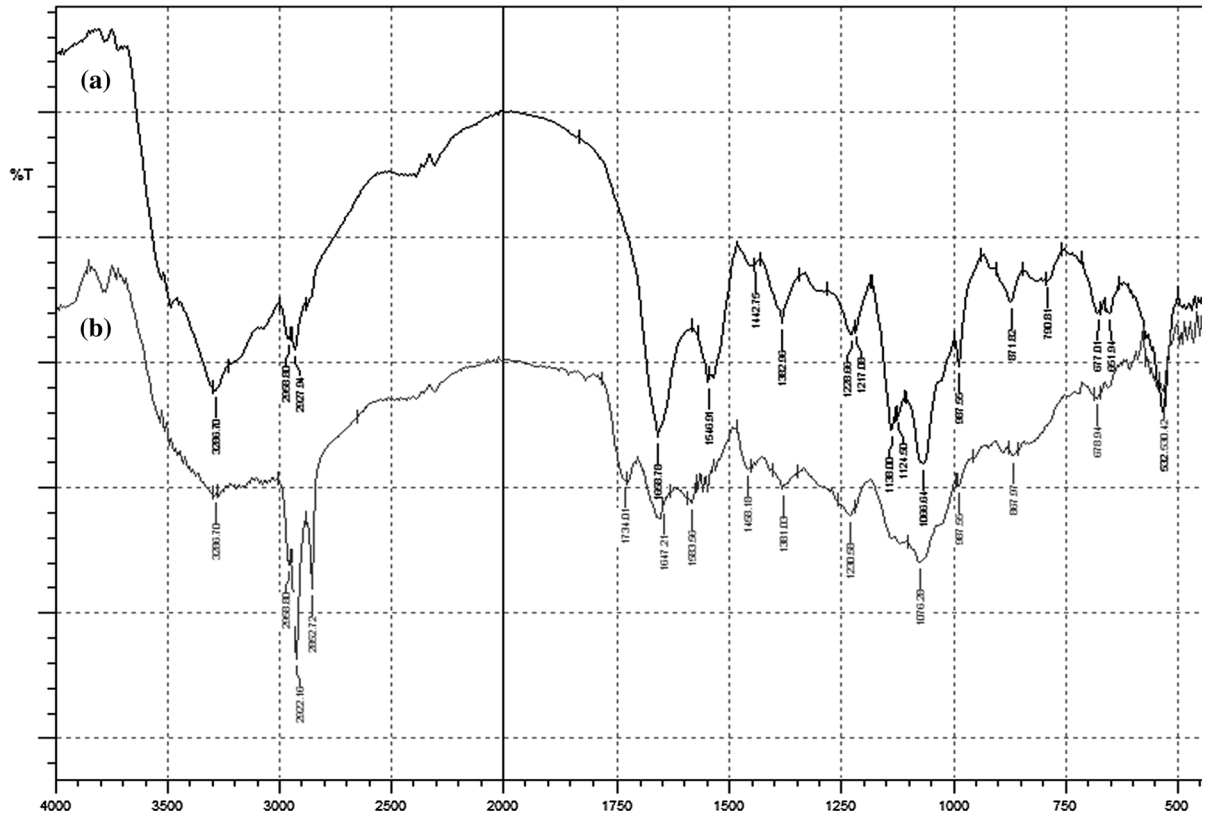

Fig. 4 FTIR spectrum of *Klebsiella pneumoniae* strain SSSW7. **a** Bacterial cells exposed to 15 mM arsenite. **b** Bacterial cells without exposure to arsenite (control)

3300–2800 cm^{-1} which may be attributed to stretching of amide and hydroxyl groups. Shifting of FTIR peaks was observed in the region spanning from 1750–1500 cm^{-1} and 1500–1200 cm^{-1} which showed the interaction of amide linkages from protein and peptides. The sharpening and peak shifts from 1200 to 1000 cm^{-1} was also observed in arsenite exposed cells which may be assigned to C–N stretching of an aliphatic amine and C–O stretching of alcohols, carboxylic acids, esters, and ethers.

SDS-PAGE

The SDS-PAGE analysis of whole-cell proteins of *K. pneumoniae* strain SSSW7 in presence of 5 mM arsenite clearly revealed up-regulation of several proteins as compared to control. Interestingly, two up-regulated proteins of molecular weight 87 kDa and 14 kDa were also observed (Supplementary Fig. 4) which may resemble the two subunits of arsenite oxidase enzyme aioA and aioB respectively.

Discussion

The arsenite resistant bacterial strain SSSW7 isolated from shipyard waste of Goa, India was identified as *K. pneumoniae*. It is interesting to note that *K. pneumoniae* strain SSSW7 exhibited the highest MIC of 21 mM in MSM broth as compared to previously reported bacterial strains. For instance, *K. pneumoniae* strains MNZ4 and MNZ6 tolerated up to 2.3 mM and 2.9 mM sodium arsenite in acetate minimal medium, whereas *K. pneumoniae* strain MR4 showed MIC of 5 mM in Luria–Bertani broth (Daware et al. 2012; Abbas et al. 2014). However, it would be inappropriate to compare the MIC values of present study with previous reports since the media composition alters availability of arsenite in the growth medium. Growth studies revealed extended lag and delayed log phases for this strain at increasing concentrations of arsenite in MSM broth. The slower growth of this bacterial strain exposed to arsenite may be attributed to ensuing

Table 1 Characteristic IR absorption peaks indicating functional groups on the surface of *K. pneumoniae* strain SSSW7

Control (frequency, cm^{-1})	Arsenite-exposed (frequency, cm^{-1})	Band assignment
3296.70	3296.70	N–H stretch of amides and O–H stretch of hydroxyl groups
2922.16	2927.94	C–H stretch of alkanes and O–H stretch of carboxyl acids
2852.72	–	C–H stretch of alkanes, O–H stretch of carboxyl acids
1734.01	1658.78	–C=C– stretch of alkenes
1647.21	1546.91	N–O asymmetric stretch of nitro compounds
1583.56	–	N–H bend of 1° amine
1458.10	1442.75	C–C stretch of aromatics
1381.03	1382.96	–C–H, bend of alkane
1230.58	1228.86	C–O stretch of alcohols, carboxylic acids, esters ethers
–	1138.00	C–N stretch of aliphatic amine and C–O stretch of alcohol carboxylic acids, esters, ethers
1076.28	1066.64	C–O stretch of alcohol carboxylic acids, esters, ethers
987.56	987.56	=C–H bend of alkenes
867.97	871.82	=C–H, bend of alkenes, C–H bend, aromatics
678.94	677.01	C–Br stretch of alkyl halide
651.94	651.94	C–Cl and C–Br stretch of alkyl halide
530.42	532.35	C–Br stretch of alkyl halide

physiological adaptation during extended lag phase leading to increase in doubling time (Paul et al. 2014).

PCR amplification using gene specific primers revealed that *K. pneumoniae* strain SSSW7 possessed *aioA* gene on both plasmid as well as chromosomal DNA. A similar study using *Acinetobacter soli* having *aioA* gene on both plasmid and chromosomal DNA has been reported (Goswami et al. 2015). Many arsenite transforming bacteria possessing arsenite oxidizing gene (*aoxB*) located only on chromosomal or plasmid DNA has been previously reported (Majumder et al. 2013; Mallick et al. 2014; Goswami et al. 2015). Interestingly, the absence of ACR3 gene from the plasmid and chromosomal genome of *K. pneumoniae* strain SSSW7 suggested an intracellular accumulation of arsenite since ACR3 protein has been reported to specifically transport arsenite in bacteria (Wysocki et al. 1997; Achour et al. 2007). Arsenite oxidase assay using different cell fractions further confirmed higher expression of arsenite oxidase enzyme in the periplasmic space. Similarly, arsenite oxidase enzyme is also reported in the periplasm of *Hydrogenophaga* sp strain NT-14, *Rhizobium* NT-26 and *Ochrobactrum triticii* SCII24 (Santini and Vanden Hoven 2004; Vanden Hoven and Santini 2004; Branco et al. 2009).

The exposure of bacterial cells to 15 mM arsenite demonstrated significant morphological alterations which were prominent as compared to control cells (Fig. 2a, c). This could be one of the strategies of bacterial cells to overcome arsenite toxicity since decrease in cell to volume ratio reduces toxicity. Similar morphological alterations have also been observed in arsenite exposed cells of *Acinetobacter lwoffii*, *Pseudomonas resinovorans* and *Acinetobacter calcoaceticus* (Banerjee et al. 2011). The EDS analysis revealed that there was no surface adsorption of arsenite and it may accumulate intracellularly. It was further substantiated by the absence of ACR3 gene which regulates transport of arsenite. Furthermore, TEM analysis of arsenite exposed cells evidently demonstrated structural changes which were similar to previous observations in *Microbacterium oleivorans* strain Ransu-1 and *Acinetobacter* sp. (Goswami et al. 2015). The TEM-EDS analysis of arsenite exposed cells also revealed intracellular accumulation of arsenic in the periplasm which is in agreement with the report of Banerjee et al. (2011). The bacterial strain SSSW7 could oxidize arsenite and showed intracellular accumulation of 10 mM arsenate which was higher than previous reports in bacterial strains (Jain et al. 2014; Naureen and Rehman 2016).

FTIR spectroscopic analysis further revealed interaction of functional groups such as carboxyl, hydroxyl and amino groups on bacterial cell surface with arsenite anions. Similar observations have also been reported in *E. coli* and *Bacillus aryabhattai* strain NBRI014 (Wu et al. 2010; Singh et al. 2016). SDS-PAGE analysis of whole cell proteins of strain SSSW7 exposed to 5 mM arsenite revealed over-expression of 87 kDa and 14 kDa proteins which may resemble with two subunits of arsenite oxidase enzyme. Therefore, it is clear that under stress of arsenite, over-expression of *aioA* gene facilitates transformation of arsenite to arsenate by bacterial cells in order to overcome the arsenite toxicity. This enzyme has been previously reported in *Rhizobium* NT-26 and *Hydrogenophaga* sp. strain NT-14 (Santini and Vanden Hoven 2004; Vanden Hoven and Santini 2004).

Conclusion

The *K. pneumoniae* strain SSSW7 isolated from shipyard waste demonstrated presence of arsenite oxidase gene and periplasmic arsenite oxidase enzyme. It showed high resistance to arsenite and could oxidize 10 mM arsenite to less toxic arsenate within 24 h which was found to be accumulated in the periplasmic space. Therefore, this bacterial strain SSSW7 has potential to bioremediate arsenite present in contaminated environmental sites.

Acknowledgements SM is grateful to University Grants Commission, New Delhi for financial support as Maulana Azad National Fellowship (SRF). The authors are thankful to Areef Sardar from CSIR- National Institute of Oceanography, Goa for EDX analysis; AIRF, Jawaharlal Nehru University, New Delhi for TEM–EDX analysis; B. R. Srinivasan, Head, Department of Chemistry and Rahul Kerkar from Department of Chemistry, Goa University for FTIR analysis. SM is also thankful to Sandeep Garg, Head, Department of Microbiology, Goa University for providing laboratory facilities.

Compliance with ethical standards

Conflict of interest The authors declare that there is no conflict of interest.

References

Abbas SZ, Riaz M, Ramzan N, Zahid MT, Shakoori FR, Rafatullah M (2014) Isolation and characterization of arsenic resistant bacteria from wastewater. Braz J Microbiol 45(4):1309–1315

Achour AR, Bauda P, Billard P (2007) Diversity of arsenite transporter genes from arsenic-resistant soil bacteria. Res Microbiol 158(2):128–137

Anawar HM, Akai J, Mostofa KMG, Safiullah S, Tareq SM (2002) Arsenic poisoning in groundwater: health risk and geochemical sources in Bangladesh. Environ Int 27(7):597–604

Anderson GL, Williams J, Hille R (1992) The purification and characterization of arsenite oxidase from *Alcaligenes faecalis*, a molybdenum-containing hydroxylase. J Biol Chem 267:23674–23682

Andreoni V, Zanchi R, Cavalca L, Corsini A, Romagnoli C (2012) Arsenite oxidation in *Ancylobacter dichloromethanicus* As3-1b strain: detection of genes involved in arsenite oxidation and CO_2 fixation. Curr Microbiol 65:212–218

Arsene-Ploetze F, Koechler S, Marchal M, Coppee JY, Chandler M, Bonnefoy V, Brochier-Armanet C, Barakat M, Barbe V, Battaglia-Brunet F, Bruneel O, Bryan CG, Cleiss-Arnold J, Cruveiller S, Erhardt M, Heinrich-Salmeron A et al (2010) Structure, function and evolution of the *Thiomonas* spp. genome. PLoS Genet 6(2):e1000859

Bahar MM, Megharaj M, Naidu R (2013) Kinetics of arsenite oxidation by *Variovorax* sp.MM-1 isolated from soil and identification of arsenite oxidase gene. J Hazard Mater 262:997–1003

Banerjee S, Datta S, Chattopadhyay D, Sarkar P (2011) Arsenic accumulating and transforming bacteria isolated from contaminated soil for potential use in bioremediation. J Environ Sci Health A 46:1736–1747

Branco R, Francisco R, Chung AP, Morais PV (2009) Identification of an *aox* system that requires cytochrome c in the highly arsenic resistant bacterium *Ochrobactrum tritici* SCII 24. Appl Environ Microbiol 75(5):5141–5147

Cai L, Rensing C, Li X, Wang G (2009) Novel gene clusters involved in arsenite oxidation and resistance in two arsenite oxidizers: *Achromobacter* sp. SY8 and *Pseudomonas* sp. TS44. Appl Microbiol Biotechnol 83:715–725

Chang J, Yoon I, Lee J, Kim K, An J, Kim K (2010) Arsenic detoxification potential of *aox* genes in arsenite oxidizing bacteria isolated from natural and constructed wetlands in the Republic of Korea. Environ Geochem Health 32:95–105

Chen M, Ma LQ, Harris WG (2002) Arsenic concentrations in Florida surface soils. Soil Sci Soc Am J 66(2):632–640

Cheng HF, Hu YN, Luo J, Xu B, Zhao JF (2009) Geochemical processes controlling fate and transport of arsenic in acid mine drainage (AMD) and natural systems. J Haz Mater 165:13–26

Chowdhury UK, Biswas BK, Chowdhury TR, Samanta G, Mandal BK, Basu GC, Chanda CR, Lodh D, Saha KC, Mukherjee SK, Roy S (2000) Groundwater arsenic contamination in Bangladesh and West Bengal, India. Environ health perspect 108(5):393–397

Daware V, Kesavan S, Patil R, Natu A, Kumar A, Kulkarni M, Gade W (2012) Effects of arsenite stress on growth and proteome of *Klebsiella pneumoniae*. J Biotechnol 158(1–2):8–16

Ghosh D, Bhadury P, Routh J (2014) Diversity of arsenite oxidizing bacterial communities in arsenic-rich deltaic aquifers in West Bengal, India. Front Microbiol 5:602

Goswami R, Mukherjee S, Rana VS, Saha DR, Raman R, Padhy PK, Mazumder S (2015) Isolation and characterization of arsenic-resistant bacteria from contaminated water-bodies in West Bengal, India. Geomicrobiol J 32:17–26

Hamamura N, Macur RE, Korf S, Ackerman G, Taylor WP, Kozubal M et al (2008) Linking microbial oxidation of arsenic with detection and phylogenetic analysis of As(III) oxidase genes in diverse geothermal environments. Environ Microbiol 11(2):421–431

Hughes MP (2002) Arsenic toxicity and potential mechanisms of action. Toxicol Lett 133:1–16

Jain R, Jha S, Adhikary H, Kumar P, Parekh V, Jha A, Mahanta MK, Kumar GN (2014) Isolation and molecular characterization of arsenite-tolerant *Alishewanella* sp. GIDC-5 originated from industrial effluents. Geomicrobiol J 31(1):82–90

Kumar S, Stecher G, Tamura K (2016) MEGA7: molecular evolutionary genetics analysis version 7.0 for bigger datasets. Mol Biol Evol 33:1870–1874

Laemmli UK (1970) Cleavage of structural proteins during the assembly of the head of bacteriophage T4. Nature 227:680–685

Lenoble V, Deluchat V, Serpaud B, Bollinger JC (2003) Arsenite oxidation and arsenate determination by the molybdene blue method. Talanta 61:267–276

Lett M, Paknikar K, Lievremont D (2001) A simple and rapid method for arsenite and arsenate speciation. Process Metall 11:541–546

Lowry OH, Rosebrough NJ, Farr AL, Randall RJ (1951) Protein measurement with the Folin phenol reagent. J Biol Chem 193(1):265–275

Mahimairaja S, Bolan NS, Adriano DC, Robinson B (2005) Arsenic contamination and its risk management in complex environmental settings. Adv Agron 86:1–82

Mahtani S, Mavinkurve S (1979) Microbial purification of longifolene: a sesquiterpene. J Ferment Technol 57:529–533

Majumder A, Bhattacharyya K, Bhattacharyya S, Kole SC (2013) Arsenic-tolerant, arsenite-oxidising bacterial strains in the contaminated soils of West Bengal, India. Sci Total Environ 463–464:1006–1014

Mallick I, Hossain SKT, Sinha S, Mukherjee SK (2014) *Brevibacillus* sp. KUMAs2 a bacterial isolate for possible bioremediation of arsenic in rhizosphere. Ecotoxicol Environ Saf 107:236–244

Mandal BK, Suzuki KT (2002) Arsenic round the world: a review. Talanta 58(1):201–235

Mitra AK, Bose BK, Kabir H, Das BK, Hussain M (2002) Arsenic-related health problems among hospital patients in southern Bangladesh. J Health Popul Nutr 20(3):198–204

Mukherjee A, Sengupta MK, Hossain MA, Ahamed S, Das B, Nayak B, Lodh D, Rahman MM, Chakraborti D (2006) Arsenic contamination in groundwater: a global perspective with emphasis on the Asian scenario. J Health Popul Nutr 24:142–163

Muller D, Medigue C, Koechler S, Barbe V, Barakat M, Talla E, Bonnefoy V, Krin E, Arsene-Ploetze F, Carapito C, Chandler M, Cournoyer Cruveiller S, Dossat C, Duval S, Heymann M, Leize E, Lieutaud A, Lievremont D et al (2007) A tale of two oxidation states: bacterial colonization of arsenic-rich environments. PLoS Genet 3(4):e53

Naureen A, Rehman A (2016) Arsenite oxidizing multiple metal resistant bacteria isolated from industrial effluent: their potential use in wastewater treatment. World J Microb Biotechnol 32(8):133

Oremland RS, Stolz JF (2005) Arsenic, microbes and contaminated aquifers. Trends Microbiol 13:45–49

Oremland RS, Saltikov CW, Wolfe-Simon F, Stolz JF (2009) Arsenic in the evolution of earth and extra-terrestrial ecosystems. Geomicrobiol J 26:522–536

Páez-Espino D, Tamames J, de Lorenzo V, Cánovas D (2009) Microbial responses to environmental arsenic. Biometals 22(1):117–130

Paul D, Poddar S, Sar P (2014) Characterization of arsenite-oxidizing bacteria isolated from arsenic-contaminated groundwater of West Bengal. J Environ Sci Health A 49(13):1481–1492

Prasad KS, Subramanian V, Paul J (2009) Purification and characterization of arsenite oxidase from *Arthrobacter* sp. Biometals 22:711–721

Qin J, Rosen BP, Zhang Y, Wang G, Franke S, Rensing C (2006) Arsenic detoxification and evolution of trimethylarsine gas by a microbial arsenite S-adenosyl methionine methyltransferase. Proc Natl Acad Sci USA 103(7):2075–2080

Quemeneur M, Sameron AH, Muller D, Lievremont D, Janzein M, Bertin PN, Garrido F, Joulian C (2008) Diversity surveys and evolutionary relationships of *aoxB* genes in aerobic arsenite oxidizing bacteria. Appl Environ Microbiol 74(14):4567–4573

Rai A, Tripathi P, Dwivedi S, Dubey S, Shri M, Kumar S, Tripathi PK, Dave R, Kumar A, Singh R, Adhikari B, Bag M, Tripathi RD, Trivedi PK, Chakrabarty D, Tuli R (2011) Arsenic tolerance in rice (Oryza sativa) have a predominant role in transcriptional regulation of a set of genes including sulphur assimilation pathway and antioxidant system. Chemosphere 82:986–995

Rauschenbach I, Bini E, Haggblom MM, Yee N (2012) Physiological response of *Desulfurispirillum indicum* S5 to arsenate and nitrate as terminal electron acceptors. FEMS Microbiol Ecol 81(1):156–162

Rosen BP (1999) Families of arsenic transporters. Trends Microbiol 7(5):207–212

Rosen BP (2002) Biochemistry of arsenic detoxification. FEBS Lett 529(1):86–92

Sambrook J, Fritsch EF, Maniatis T (1989) Molecular cloning: a laboratory manual. Cold Spring Harbor Laboratory Press, New York

Santini JM, Vanden Hoven RN (2004) Molybdenum-containing arsenite oxidase of the chemolithoautotrophic arsenite oxidizer NT-26. J Bacteriol 186(6):1614–1619

Silver S, Phung LT (1996) Bacterial heavy metal resistance: new surprises. Ann Rev Microbiol 50(1):753–789

Silver S, Phung LT (2005) Genes and enzymes involved in bacterial oxidation and reduction of inorganic arsenic. Appl Environ Microbiol 71:599–608

Singh N, Gupta S, Marwa N, Pandey V, Verma PC, Rathaur S, Singh N (2016) Arsenic mediated modifications in *Bacillus aryabhattai* and their biotechnological applications for arsenic bioremediation. Chemosphere 164:524–534

Smedley PL, Kinniburgh DG (2002) A review of the source, behaviour and distribution of arsenic in natural waters. Appl Geochem 17(5):517–568

Stolz JF, Basu P, Oremland RS (2010) Microbial arsenic metabolism: new twists on an old poison. Microbe 5:39–53

Studholme DJ, Jackson RA, Leak DJ (1999) Phylogenetic analysis of transformable strains of thermophilic *Bacillus* species. FEMS Microbiol Lett 172:85–90

Vanden Hoven RN, Santini JM (2004) Arsenite oxidation by the heterotroph *Hydrogenophaga* sp. str. NT-14: the arsenite oxidase and its physiological electron acceptor. Biochim Biophys Acta 1656(2–3):148–155

Welch AH, Westjohn DB, Helsel DR, Wanty RB (2000) Arsenic in ground water of the United States: occurrence and geochemistry. Groundwater 38(4):589–604

WHO (1993) Guidelines for drinking water quality. recommendations, 2nd edn. World Health Organization, Geneva

Wu YH, Feng SX, Li B, Mi XM (2010) The characteristics of *Escherichia coli* adsorption of arsenic (III) from aqueous solution. World J Microbiol Biotechnol 26(2):249–256

Wysocki R, Bobrowicz P, Ulaszewski S (1997) The *Saccharomyces cerevisiae ACR3* gene encodes a putative membrane protein involved in arsenite transport. J Biol Chem 272(48):30061–30066

Chapter 10

Biodegradation of seafood waste by seaweed-associated bacteria and application of seafood waste for ethanol production

Sanika Samant[1], Milind Mohan Naik[2,*], Diviya Chandrakant Vaingankar[2], Sajiya Yusuf Mujawar[4], Prachi Parab[2], Surya Nandan Meena[3]

[1]*Department of Biotechnology, Goa University, Goa, India;* [2]*Department of Microbiology, Goa University, Goa, India;* [3]*Biological Oceanography Division, National Institute of Oceanography, Dona Paula, Goa, India;* [4]*Laboratory of Bacterial Genetics and Environmental Biotechnology, Department of Microbiology, Goa University, Goa, India*

[*]*Corresponding author: milind@unigoa.ac.in; milindnaik4@gmail.com.*

10.1 Introduction

In recent years, seafood waste has increased tremendously, since during the processing of prawns, shrimps, and other shellfish mostly the meat is utilized while the shells, bones, and head portions are thrown as wastes into marine waters [1]. Fish production around the globe has increased tremendously and reached 174 million metric tons in 2017. India is the third largest producer of fishery around the globe and hence produces an enormous amount of fish waste [2]. India generates >2 metric million tons of waste during fish processing, of which 300,000 tons contribute to visceral waste alone [3]. Commercial processing of fish generates a significant amount of waste, which includes viscera, fins, scales, and bones [4]. This huge amount of discards (fishery waste) including solid wastes along with wastewater resulting from fishery processing are unutilized and usually disposed of in landfills, or dumped near shore and into the ocean without any pretreatment, causing environmental pollution, thus severely impacting aquatic biota health ailments [5,6]. Although these wastes are biodegradable, the process is very slow. This results in accumulation of fishery waste over time and pollutes coastal and marine environments due to bad odors and secretion of biogenic amines, thereby affecting marine life [7]. Due to

Advances in Biological Science Research. https://doi.org/10.1016/B978-0-12-817497-5.00010-0

foul odors, seafood waste in the marine environment attracts flies, insects, rodents, and other vermin, creating an unhygienic atmosphere. Fish waste is classified as certified waste because it is comprised of high organic content and is thus even more costly to dispose of [4]. In fish processing industries, acid, alkali, and heat treatments are used to degrade shell waste that is hazardous to the environment [8]. Hence, biodegradation of seafood waste using microorganisms is important as they can be used for polluted environment reclamation without harming natural biota. Bioremediation is ecofriendly and cost-effective as compared to physicochemical methods. Therefore, treatment of prawn shell, shellfish, and fish waste using marine bacteria is crucial for preservation and sustainable development of the marine environment.

The fish processing procedure involves removal of fish bones, scales, heads, and internal organs. Therefore, during the processing of seafood, a large amount of shell and scale waste is discarded from fish markets, seafood restaurants, fish-processing industries, and kitchens. Fish scales consist of protein, calcium phosphate, calcium carbonate, magnesium carbonate, chitin, and pigments [9]. Generally, crustacean shells consist mainly of 30%−50% calcium carbonate, 30%−40% protein, and 20%−30% chitin and calcium phosphate [4,10,11]. Shells also contain carotenoid pigments and a trace amount of lipids. The content of shell components varies with different species and seasons [12]. Therefore, to degrade seafood waste, bacteria possessing protease, chitinase activities, and phosphate and calcium carbonate solubilization properties will be of great importance. There are very few reports on the total degradation of seafood waste by bacteria. Microorganisms possessing proteolytic activity have been applied for the deproteinization of chemically demineralized shells [13]. Purification of chitin from shrimp wastes using microbial deproteination and decalcification activities has been demonstrated [7]. *Lactobacillus plantarum* and *Pseudomonas aeruginosa* were used for deproteinization and demineralization of crab shell and shrimp waste [1]. Two bacterial cultures, *Exiguobacterium acetylicum* and *Bacillus cereus*, were studied for their ability to decompose shrimp shell waste [14]. A *P. aeruginosa* strain, K-187, isolated from soil (in Taiwan) showing protease and chitinase activities when cultured in medium containing shrimp and crab shell wastes as sole carbon sources has been reported [15]. *Serratia marcescens* FS-3 strain exhibiting strong protease activity was isolated from soil toward the seaside of a southwestern region of Korea and was used for degradation of crab (*Chionoecetes opilio*) shell wastes [16].

Most of the above-mentioned studies demonstrate the use of chemicals in the seafood waste treatment process along with the use of microbial enzymes or microorganisms. Also, detail study on complete degradation of crab shell, prawn shell, and fish scale using bacteria has not yet been undertaken. Therefore, the current study focuses on isolation of seaweed-associated bacteria possessing the ability to degrade seafood waste such as scales, crab shell, and prawn shell waste by producing organic acids and hydrolytic enzymes and their

application in bioremediation of seafood waste. Here we also discuss studies on sustainable use of seafood waste for ethanol production.

10.2 Materials and methods

10.2.1 Collection of marine seaweed samples

Live and healthy seaweed samples (*Ulva* sp.) were collected from rocky intertidal regions of Anjuna Beach, Goa, India using sterile forceps in sterile petri plates. The samples were transported to the laboratory immediately under cool conditions for further analysis. *Ulva* sp. samples were processed for isolation of associated bacteria within 24 h.

10.2.2 Enrichment of *Ulva*-associated bacteria

For enrichment of *Ulva* sp.—associated bacteria, seaweed sample was rinsed gently two or three times with sterilized seawater to wash off sand particles and loosely bound bacteria. In order to isolate firmly associated bacteria, *Ulva* sp. was aseptically cut into 5-cm-long pieces and two pieces were inoculated into 50 mL sterile Zobell marine broth (ZMB) in 150-mL Erlenmeyer flask and incubated on shaker for 48 h at room temperature (RT, 28°C ± 2) with constant shaking at 150 rpm to enrich seaweed-associated bacteria.

10.2.3 Isolation of calcium carbonate solubilizing marine *Ulva*-associated bacteria

From enriched ZMB, seaweed pieces were removed aseptically and the broth was serially diluted up to 10^{-8} using sterile saline (2%) and spread plated (0.1 mL) on seawater-based agar containing 1% $CaCO_3$ and 0.4% glucose (pH 7). The plates were then incubated at room RT (28°C ± 2) for 48—72 h. Morphologically different calcium carbonate—solubilizing bacterial colonies showing a highest zone of clearance on agar were selected and purified for further study. These calcium carbonate—solubilizing bacterial cultures were maintained by regular subculturing on Zobell marine agar (HiMedia Laboratories) and stored at 4°C.

10.2.4 Investigating seafood waste (fish, crab, prawn waste) utilizing potential of selected calcium carbonate—solubilizing bacteria

10.2.4.1 Preparation of crab/prawn shell and fish scale powder

Crab shells, prawn shells, and fish scales were obtained from local markets. They were washed with distilled water, sun-dried for 1 week, and ground into a fine powder using an electronic mixer. This powder was then used as fish/crab/prawn waste for degradation studies.

10.2.4.2 Microbial utilization of seafood waste as a sole source of carbon

Seawater-based media was prepared in three different 50 mL conical flasks and 1% sterile crab shell, prawn shell, fish scale powder was added separately into three flasks as a sole carbon and nitrogen source (1.5% agar was added). Media was sterilized and poured into plates. Bacterial isolates were streaked on plates and incubated at RT (28°C ± 2) for 10 days. Plates were observed for bacterial growth.

Calcium-solubilizing bacterial isolates, which also showed the ability to utilize seafood waste as a sole carbon source, were further tested for their potential to produce protease, cellulase, chitinase, agarase, and phosphate-solubilizing activities.

10.2.5 Agarase production by marine *Ulva* sp.—associated bacteria

Bacterial isolates were plated on seawater-based agar medium (2% agar without any other added carbon source) and incubated at RT (28°C ± 2) for 24—48 h. Colonies were observed for depression in agar plates. Agarase production was also tested by flooding plates with Lugol's iodine and observing zone of clearance around colony [17]. Agarase activity was tested to rule out agar utilization by bacteria. The absence of agarase activity confirms the ability of organisms to utilize seafood waste as a sole carbon source.

10.2.6 Production of protease by *Ulva* sp.—associated bacteria

Ulva sp.—associated bacteria, which were found to be utilizing seafood waste as a sole source of carbon, were streaked on skim milk agar (HiMedia Laboratories) plates and incubated for 4 days at RT (28°C ± 2). Positive protease activity was indicated by a clear zone surrounding the bacterial streak/growth.

10.2.7 Phosphate solubilization by acid-producing *Ulva* sp.—associated bacteria

Bacterial isolates were streaked on seawater-based Pikovskaya's agar plates containing 0.05% bromothymol blue (Merck) and incubated at RT (28°C ± 2) for 72 h. Zone of clearance and yellow coloration around bacterial streak indicates phosphate solubilization due to acid production [18].

10.2.8 Cellulase production by *Ulva* sp.—associated bacteria

Bacterial isolates were streaked on seawater-based carboxymethyl cellulose agar (HiMedia Laboratories) and incubated at RT (28°C ± 2). After 4 days of incubation, plates were flooded with 1% Congo red solution (w/v) and allowed

to stand for 10 min. Excess stain was poured out gently and plates were flooded with 1M NaCl solution (destaining). After incubating for 10 min, excess NaCl solution was poured out. This step was repeated two times to wash off excess Congo red stain. Cellulase activity was indicated by a zone of clearance along the bacterial streak [19], whereas the rest of the plate stained dark red.

10.2.9 Production of chitinase by *Ulva* sp.–associated bacteria

Chitinase production by *Ulva* sp.–associated bacteria was checked by streaking on seawater-based agar plates containing 1% colloidal chitin as a sole carbon source and incubated at RT (28°C ± 2) for 4 days. Plates were flooded with 1% Congo red solution (w/v) and were allowed to stand for 10 min. Excess Congo red was discarded gently and plates were flooded with 1M NaCl solution (destaining). Excess NaCl solution was poured out gently after incubating for 15 min. This step was repeated twice to wash off excess Congo red stain. Chitinase activity was indicated by a zone of clearance along streak [20], whereas the rest of the plate stained dark red.

Bacterial isolates exhibiting calcium carbonate solubilizing, protease, chitinase, and cellulase activities were selected for the treatment of fish and shellfish waste by preparing consortia.

10.2.10 Degradation of fish/crab/prawn waste using microbial consortia developed using *Ulva* sp.–associated bacteria

Development of microbial consortia for seafood waste degradation is of utmost importance since improved degradation is achieved using microbial consortia as compared to individual isolates. Before using selected bacterial isolates as consortia for seafood degradation study, these isolates were tested by the cross-inhibition test. Test isolates were inoculated as a line in the center on the surface of Zobell marine agar and incubated at RT (28°C ± 2) for 20 h. Other isolates were inoculated as a perpendicular line to the test isolates, and plates were incubated at RT (28°C ± 2) for 48 h. Positive results were indicated by a zone of inhibition of growth of other isolates. This test was repeated for all the isolates. If bacterial isolates inhibit each other, then they cannot be used in consortia for degradation of seafood waste.

Three selected bacterial isolates were inoculated separately into 50 mL seawater-based broth containing 1% crab shell powder as a sole source of carbon for 4 days at RT (28°C ± 2) with shaking at 150 rpm. Then, 0.1 mL culture broth from each flask was added as inoculum into 100 mL seawater-based media in Erlenmeyer flask (250 mL) containing 2% crab shell powder and incubated at RT (28°C ± 2) with constant shaking at 150 rpm for 4 days. The test was performed in triplicate. Control was maintained containing seawater-based broth supplemented with 2% crab shell powder without

inoculum. After 4 days of incubation, 2 mL culture broth was collected under the aseptic condition and centrifuged at 8000 rpm for 10 min. The supernatant was taken in another tube and used for determining reducing sugars by DNSA method released during degradation of seafood waste [21]. Similar degradation study by consortia was repeated with prawn shell and fish scales in triplicate.

10.2.11 Identification of seaweed-associated bacteria

Three selected seaweed-associated bacteria having the potential of degrading seafood waste were identified by performing biochemical tests and referring to *Bergey's Manual of Systematic Bacteriology* [22] and also by using 16S rDNA gene sequence. Gene coding for 16S rRNA was amplified with universal eubacterial primers: 27F (5′ AGAGTTTGATCMTGGCTCAG 3′) and 1492R (5′ TACGGYTACCTTGTTACGACTT 3′). 16S rRNA sequence data were compared with GenBank database using BLAST.

10.3 Results and discussion

Nine morphologically different calcium carbonate—solubilizing seaweed-associated bacterial isolates showing a highest zone of clearance on agar were selected and purified for further studies. These nine bacterial isolates were designated as PM1, PM2, PM3, PM4, PM5, PM6, PM7, PM8, and PM9 (Fig. 10.1). Only three out of nine bacterial isolates—PM1, PM6, and PM9—were able to utilize crab shells, prawn shells, and fish scale powder as a sole carbon source in seawater-based agar after 10 days of incubation. Also, all three bacterial isolates didn't show growth on seawater-based agar media (agar

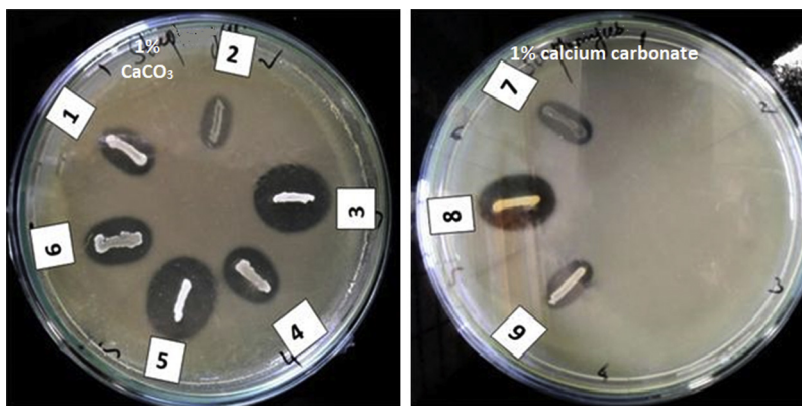

FIGURE 10.1 Calcium carbonate—solubilizing seaweed-associated bacterial isolates showing zone of clearance around colonies when streaked on seawater-based agar comprising 1% $CaCO_3$ and 0.4% glucose.

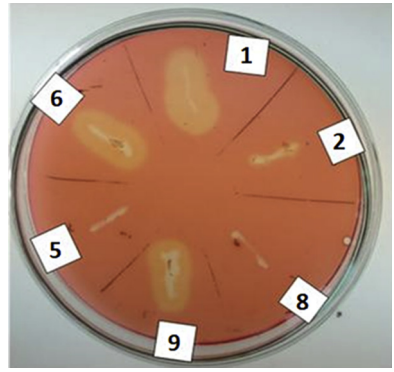

FIGURE 10.2 Seaweed-associated bacteria showing cellulase activity on seawater-based agar plates comprising 1% carboxymethyl cellulose (CMC) as a sole source of carbon.

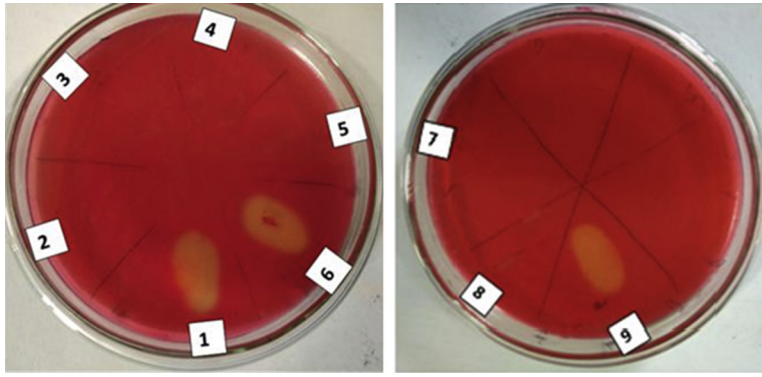

FIGURE 10.3 Seaweed-associated bacteria showing chitinase activity on seawater-based agar plates containing 1% colloidal chitin as a sole carbon source.

as the sole source of carbon), therefore, bacterial isolates PM1, PM6, and PM9 were selected for further studies since the absence of agarase activity confirms that organisms only utilize seafood waste as a sole source of carbon.

All three isolates PM1, PM6, and PM9 were found to be positive for protease, cellulase (Fig. 10.2), and chitinase (Fig. 10.3) activity and also could solubilize phosphate (Fig. 10.4) in seawater-based agar. Crustacean shells consist mainly of 30%−40% protein, 30%−50% calcium carbonate, and 20%−30% chitin and calcium phosphate [9−11]. They also contain carotenoid pigments and a trace amount of lipid resides. Seafood wastes are rich in organic contents such as protein, bioactive peptides, collagen, gelatin, calcium carbonate, and lipid, making the disposal process more complicated and expensive [4]. The content of shell components varies with different species

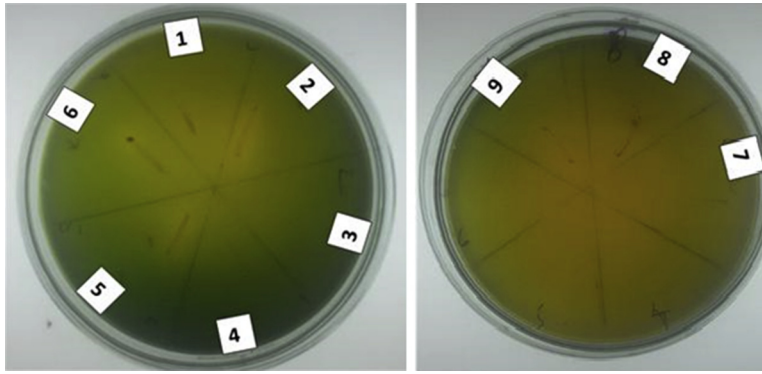

FIGURE 10.4 Seaweed-associated bacteria showing phosphate-solubilizing activity on seawater-based Pikovskaya's agar plates containing 0.05% bromothymol blue.

and seasons [12]. Therefore, to degrade seafood waste bacteria (PM1, PM6, and PM9), which have protease, chitinase activities, phosphate solubilizing and calcium carbonate solubilization properties are of great importance.

Seaweed-associated selected bacterial isolates didn't show any cross-inhibition activity with each other therefore were selected to develop microbial consortia to degrade seafood waste. Microbial consortia (PM1, PM6, and PM9) was developed to enhance degradation of seafood waste, which was evident from the amount of reducing sugars released from crab shell/prawn and fish scales (Fig. 10.5) and was found to be 310 ± 8 μg/mL, 245 ± 14 μg/mL, and 180 ± 15 μg/mL, respectively, after 4 days of incubation. These results confirmed that bacterial consortia have very high seafood waste degradation activity and can be used for bioremediation of seafood waste before discharging into marine waters and also marine sites already polluted with seafood waste. Based on morphology and biochemical tests, bacterial

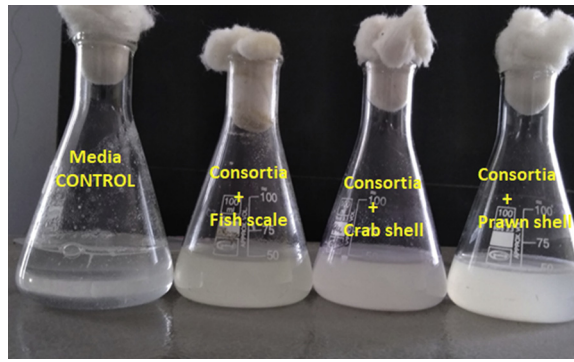

FIGURE 10.5 Seaweed-associated bacteria, when used as microbial consortia (PM1, PM6, and PM9), showed degradation of seafood waste (crab shell, prawn shell, and fish scales).

isolates PM1, PM6, and PM9 were identified as *Bacillus* sp. *Brevibacterium* sp. and *Vibrio* sp., respectively, and through 16S rRNA sequencing, bacterial isolate PM6 was further confirmed as *Brevibacterium iodinum* (accession number MG971400).

Fish production generates a huge amount of solid waste in the form of whole fish waste, fish heads, tails, skin, viscera, bones, blood liver, guts, and some muscle tissue along with wastewater composed of liquid waste produced during fish processing [6]. Improper disposal of seafood wastes generated by fishery-processing industries signifies an increasing environmental and health problem [8]. The intertidal region is exposed to fish, prawn, and crab waste as they get washed toward the shoreline when dumped in the sea during the wave currents. Biodegradation of waste is perhaps the most lucrative and environmentally friendly procedure for waste utilization since chemical treatment method can, in turn, add harmful chemicals (HCl, HNO_3, H_2SO_4, CH_3COOH, and HCOOH) to the environment [9,23]. Fishery waste being collected is in mixed type form near/along the shoreline inhabited by seaweeds, and bacteria associated with seaweeds are adapted to possess enzymes protease, chitinase, phosphate solubilization, and calcium solubilization activity. These properties make them efficient in biodegradation and treatment of fisheries waste containing a mixture of proteins, cellulose, chitin, and minerals, etc. In this study, we have reported for the first time isolation of seaweed-associated bacteria (*Bacillus* sp., *Brevibacterium* sp., *Vibrio* sp.) from the intertidal region of Goa, India, to degrade fish waste efficiently without using any chemical degradation step. Also, first-time detailed studies regarding enzymes (protease, chitinase, and cellulase) and organic acids (demineralization) produced by seafood waste degrading marine bacteria are now underway. Use of marine bacterial consortia for degradation of seafood waste is an ecofriendly and cost-effective method as compared to chemical method. In the near future, genes encoding protease, cellulase, and chitinase from these seaweed-associated bacteria will be used to genetically modify *Escherichia coli* for enhanced degradation of crab shell/prawn shell and fish scale waste as an advance in seafood waste management.

10.4 Application of seafood waste for bioethanol production

The main aim of waste management is to develop advanced biotechnology to biodegrade waste and for sustainable production of biofuel without harming the environment [24]. Application of seafood waste for bioethanol (biofuel) production is a very innovative and ecofriendly concept. The present biotechnology-based concept uses marine bacteria to break down crab shell/fish scales/prawn shell by utilizing them as the sole source of carbon and nutrients and break them down into monomer sugars. The sugars thus produced during degradation of seafood waste can be used to produce bioethanol

in the future, using *Saccharomyces cerevisiae* in a profitable, sustainable, and environmentally friendly manner. Biofuels (ethanol) do not contribute much toward environmental pollution and thus are beneficial over current fuels.

The rapid decline in the world's oil reserves is the main reason behind increasing interest in biofuels as a substitute for fossil fuels. Also, at present ethanol production is mainly done by yeast fermentation (*S. cerevisiae*) by using plant raw material containing very high levels of sugar. Use of plant raw material for biofuel production is economically costly, environmentally damaging, and requires a large cultivable area, therefore, we need an alternative source of raw material [24]. Since a large amount of seafood waste is generated every day, we can use this waste for biofuel production. Here the seafood waste can be first degraded using bacteria possessing calcium carbonate solubilization, cellulase, protease, and chitinase activity to release sugars. The sugars thus released can be used for bioethanol production by fermentation using *S. cerevisiae*. Sugar *N*-acetyl-D-glucosamine (GlcNAc) is the monomer of chitin and released during degradation of seafood waste. Inokuma et al. (2016) used *Scheffersomyces* (*Pichia*) *stipitis* strains for ethanol production by using GlcNAc as the sole carbon source [25]. *S. stipitis* NBRC1687, 10007 and 10063 strains gave 81%, 75% and 82% ethanol yield, respectively, after consuming 50 g/L GlcNAc at 30°C for 96 h. Not much research work has been done in this area to date, and therefore there is great potential for researchers to develop advanced biotechnological methods/processes to efficiently use seafood waste for ethanol (biofuel) production in a sustainable way without damaging the environment.

Acknowledgments

Dr. Milind Naik thanks SERB-DST project (File Number: YSS/2014/000258) and Dr. Shyamalina Haldar, postdoctoral fellow, Department of Microbiology, Goa University.

References

[1] Pal J, Verma HM, Munka VK, Maurya SK, Roy D, Kumar J. Biological method of chitin extraction from shrimp waste an eco-friendly low-cost technology and its advanced application. Int J Fish and Aquat 2014;1(6):104–7.

[2] Varun TK, Senani S, Jayapal N, Chikkerur J, Roy S, Tekulapally VB, et al. Extraction of chitosan and its oligomers from shrimp shell waste, their characterization and antimicrobial effect. Vet World 2017;10(2):170.

[3] Mahendrakar NS. Aqua feeds and meat quality of cultured fish. New Delhi: Biotech Consort India Ltd.; 2000. p. 26–30.

[4] Kumaran E, Mahalakshmipriya A, Rajan S. Effect of fish waste based Bacillus protease in silver recovery from waste X-ray films. Int J Curr Microb Appl Sci 2013;2(3):49–56.

[5] Bozzano A, Sardà F. Fishery discard consumption rate and scavenging activity in the Northwestern Mediterranean Sea. ICES J Mar Sci 2002;59(1):15–28.

[6] Rebah FB, Miled N. Fish processing wastes for microbial enzyme production: a review. 3 Biotech 2013;3(4):255−65.
[7] Xu Y, Gallert C, Winter J. Chitin purification from shrimp wastes by microbial deproteination and decalcification. Appl Microbiol Biotechnol 2008;79(4):687−97.
[8] Arvanitoyannis IS, Kassaveti A. Fish industry waste: treatments, environmental impacts, current and potential uses. Int J Food Sci Technol 2008;43(4):726−45.
[9] Younes I, Rinaudo M. Chitin and chitosan preparation from marine sources. Structure, properties and applications. Mar Drugs 2015;13(3):1133−74.
[10] Knorr D. Use of chitinous polymers in food: a challenge for food research and development. Food Technol 1984;38:85−97.
[11] Arbia W, Arbia L, Adour L, Amrane A. Chitin extraction from crustacean shells using biological methods-a review. Food Technol Biotechnol 2013;51(1):12−25.
[12] Cho YI, No HK, Meyers SP. Physicochemical characteristics and functional properties of various commercial chitin and chitosan products. J Agric Food Chem 1998;46(9):3839−43.
[13] Jung WJ, Jo GH, Kuk JH, Kim KY, Park RD. Extraction of chitin from red crab shell waste by co fermentation with *Lactobacillus paracasei* subsp. *tolerans* KCTC-3074 and *Serratia marcescens* FS-3. Appl Microbiol Biotechnol 2006;71(2):234.
[14] Sorokulova I, Krumnow A, Globa L, Vodyanoy V. Efficient decomposition of shrimp shell waste using *Bacillus cereus* and *Exiguobacterium acetylicum*. J Ind Microbiol Biotechnol 2009;36(8):1123−6.
[15] Wang SL, Chio SH. Deproteinization of shrimp and crab shell with the protease of *Pseudomonas aeruginosa* K-187. Enzym Microb Technol 1998;22(7):629−33.
[16] Jo GH, Jung WJ, Kuk JH, Oh KT, Kim YJ, Park RD. Screening of protease-producing *Serratia marcescens* FS-3 and its application to deproteinization of crab shell waste for chitin extraction. Carbohydr Polym 2008;74(3):504−8.
[17] Imran Md, Poduval PB, Ghadi SC. Bacterial degradation of algal polysaccharides in marine ecosystem. In: Naik MM, Dubey SK, editors. Marine poll microb remed; 2017. p. 196−202.
[18] Mondal D, Islam MS, Hoque MF, Hossain MK, Islam MK, Hossin MS, Ahsan SM. Isolation and screening of potential phosphate solubilizing bacteria (Psb) from tidal saline soils of Bangladesh. Octa J Environ Res 2016;4(3).
[19] Kasana RC, Salwan R, Dhar H, Dutt S, Gulati A. A rapid and easy method for the detection of microbial cellulases on agar plates using Gram's iodine. Curr Microbiol 2008;57(5):503−7.
[20] Krithika S, Chellaram C. Isolation, screening, and characterization of chitinase producing bacteria from marine wastes. Int J Pharm Pharmaceut Sci 2016;8(5):34−6.
[21] Monreal J, Reese ET. The chitinase of *Serratia marcescens*. Can J Microbiol 1969;15(7):689−96.
[22] Garrity GM, Brenner DJ, Kreig NR, Staley JT. Bergey's manual of systematic bacteriology, vol. 2. New York, Berlin, Heidelberg: Springer-Verlag; 2005. p. 685−93.
[23] Kumari S, Rath PK. Extraction and characterization of chitin and chitosan from (Labeo rohit) fish scales. Procedia Mater Sci 2014;6:482−9.
[24] Lozano VMP. Sustainable production of biofuel (bioethanol) from shellfish waste. Universidad de Alicante; 2015. p. 1−8.
[25] Inokuma K, Hasunuma T, Kondo A. Ethanol production from *N*-acetyl-d-glucosamine by *Scheffersomyces stipitis* strains. Amb Express 2016;6:83. https://doi.org/10.1186/s13568-016-0267-z.